DECAY OF THE ACTIVE DEPOSIT OF THE ACTINIUM SERIES

A Thesis

Submitted to

the Faculty of Graduate Studies

University of Manitoba

In Partial Fulfillment

of the Requirements for the Degree

DOCTOR OF PHILOSOPHY

by

Charles Richard Cothern

September 1964

TO MY WIFE, LINDA.

ABSTRACT

The objective of this work was to determine what radiations were emitted from the active deposit of the actinium series, their energies, relative intensities, and to which isotope they belonged. As an integral part of the decay scheme, spins and parities of excited states were determined through angular correlation and internal conversion measurements.

The following is an outline of how the above information was determined.

1. Alpha, beta, and gamma ray spectra showed the predominant radiations present and gave their energies and relative intensities. Weaker transitions were brought to light when they appeared in the coincidence spectra. From the alpha particle relative intensities the branching ratios to the ground and first excited state of Tl^{207} were obtained as well as the alpha to beta branching ratio in the decay of Bi^{211}.

2. Internal conversion measurements determined the kind and multipolarity of the gamma radiations and were essential in determining the spins and parities of the excited states. By knowing the K internal conversion coefficient of the 350 keV

transition in Tl^{207} and the alpha branching ratio to Tl^{207}, the internal conversion coefficients and the absolute gamma ray intensities could be determined. This information led to the determination of the log ft values for the beta transitions in the decay of Pb^{211}.

3. Coincidence experiments were used to determine where each radiation fitted into the decay schemes of the various isotopes present. Gamma-gamma and alpha-gamma coincidence measurements were made. Alpha and gamma transitions not seen in the spectra of part (1) above were found. Also a double recoil experiment was performed to collect Tl^{207} in a pure state. This determined which gamma rays belonged to Pb^{207}.

4. Gamma-gamma and alpha-gamma angular correlations allowed spin and parity assignments to be made to some excited states.

5. Should there be other radiations present in these decays which were not detected, their intensities must be very small and upper limits for these intensities were calculated.

PREFACE

The work to be described was carried out at the University of Manitoba during 1962, 1963 and 1964.

The author wishes to express sincere thanks to his advisor, Dean R. D. Connor, for his guidance and encouragement throughout this work.

Professors H. R. Coish and K. G. Standing provided insight in helpful discussions. Mr. R. H. Batten constructed several pieces of apparatus. Dr. K. I. Roulston and Mr. R. Foulds gave assistance in the design, building and servicing of the electronics equipment. Mr. T. White and Mr. A. Heinicke helped in computer programming. Thanks to President H. H. Saunderson and the National Research Council of Canada for financial support of the project.

CONTENTS

continued,

NOMENCLATURE

1. Chapters will be indicated by arabic numbers, 1, 2, 3, 4, 5, 6 and sections of chapters will be designed 1.1, 2.3 ... to mean chapter 1 section 1, chapter 2-section 3, etc.

2. Equations will be listed as equation 2-1 (to be read as chapter 2-equation 1) for the chapters and equation I-2 (to be read as appendix I-equation 2) for the appendix.

3. The appendices will be listed by Roman Numeral I, II.

4. References will be listed by the first letter of the last name of the first author, an arabic numeral to locate them in the reference list and usually the date, (e.g. R-12, 1959).

Chapter 1

INTRODUCTION

1.1 Actinium radioactive series

The actinium series of radioactive elements (sometimes called the 4n + 3 series) has been studied ever since 1899 when a Frenchman Debierne (D-1, 1899) discovered actinium. This material was independently discovered by Giesel (G-1, 1902) in Germany in 1901. By 1904 Debierne and Giesel realized that they were working on the same element and much was known concerning the actinium series (D-2, 1904; B-4, 1904; G-2, 1904). Debierne used uranium residues obtained from M. and Mme. Curie and with great difficulty was able to separate the actinium from the thorium and rare earths (R-2, 1904). Giesel performed a similar but equally difficult separation on pitchblende. The emanation of actinium was discovered in 1903 by A. Debierne (D-3). The emanation was found to behave like an ordinary gas in all respects, and was even capable of being liquified at low temperatures, its radioactivity remaining unaffected. The decay of the activity of the emanation was accompanied by the development of an 'induced' activity in the vicinity. This was later shown by Rutherford to be due to what he called an active deposit, left by the emanation as it decayed.

The active deposit was collected by recoil from the gas actinon. Po^{215} (AcA) was the material collected but its half life was so short (0.0018 sec) that the active deposit essentially consisted of Pb^{211} (AcB) and its daughters. Hahn and his co-workers (H-3, 1905-8) were the original identifiers of many of the members of the actinium series (see Fig. 1-1). The parent of the actinium series was not, as was originally supposed, the element actinium, the first member of the series to be discovered, but rather a much longer lived element sometimes referred to as actinouranium (U^{235}) with a half life of 7.1×10^8 yrs.(G-3, 1958). That this might be so was first suggested by Aston and Rutherford (R-3, 1930) and later confirmed mass spectrographically by Dempster (D-4, 1935). The precursers of actinouranium (U^{235}), Pu^{239} and Am^{243} have been identified only recently (H-2, 1956 and S-2, 1955).

Informative discussions of the varied types of experimental evidence which have helped to unravel the upper end of the actinium series (above AcB) have been given by Rutherford (R-4, 1913) and Sargent (S-3, 1947).

Work on the active deposit since Hahn and Meitner's original work (H-4, 1908) and prior to the commencement of the present work has been far from extensive. The only known work on the beta radiations

Figure 1 - 1

The actinium series below Ac^{227}.

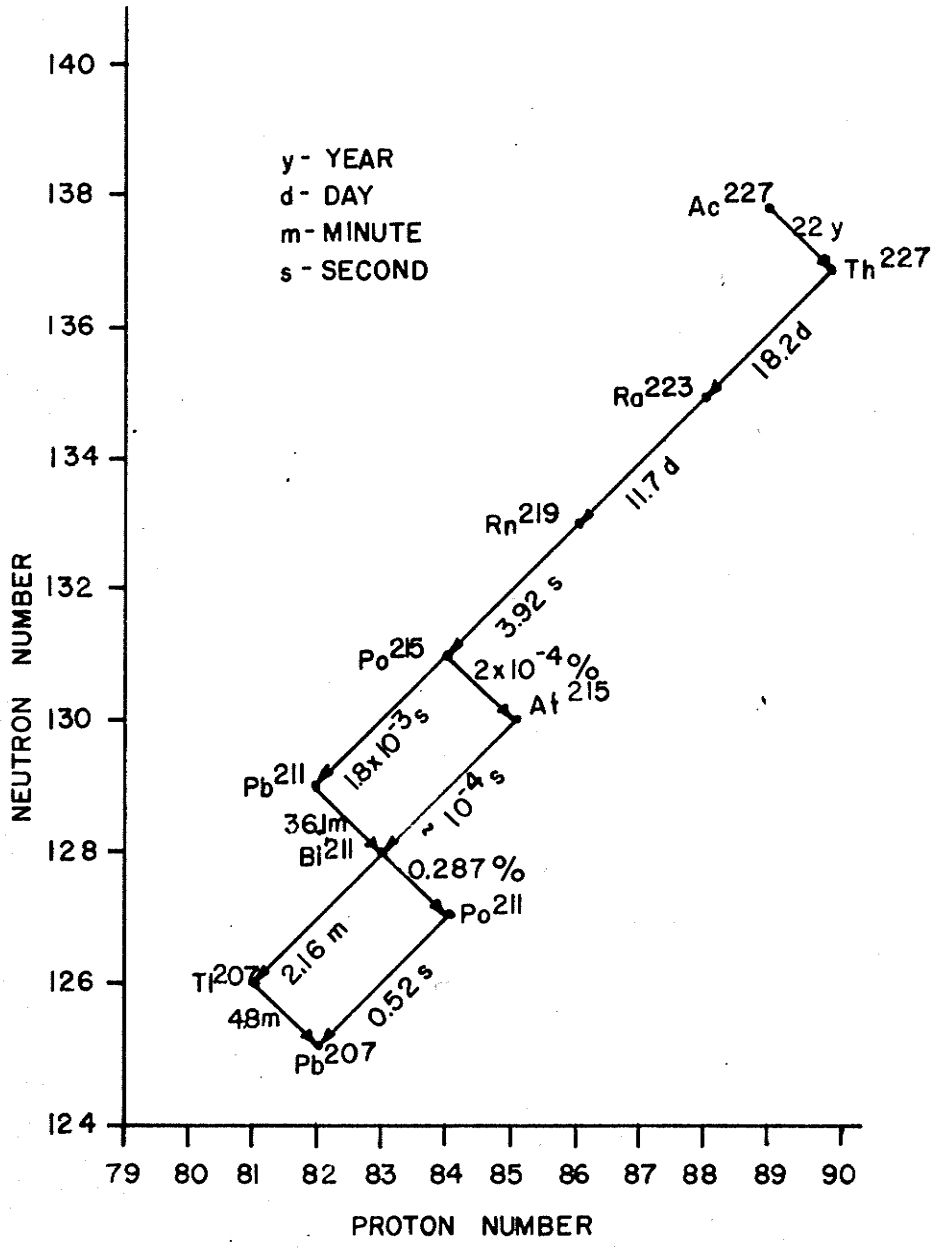
y - YEAR
d - DAY
m - MINUTE
s - SECOND
Ac227
22 y
Th227
18.2d
Ra223
11.7 d
Rn219
3.92 s
Po215
2x10-4 %
At215
1.8x10-3s
Pb211
36.1m
Bi211
~10-4 s
0.287 %
Po211
2.16 m
Tl207
4.8m
0.52 s
Pb207
NEUTRON NUMBER
PROTON NUMBER
140
138
136
134
132
130
128
126
124
79
80
81
82
83
84
85
86
87
88
89
90

Fig 1

of the active deposit was due to several authors between 1929 and 1939. Sargent (S-15, 1929; S-16, 1933, and S-4, 1939) used absorber foils, however only the 1939 work seems to be experimentally convincing. Lecoin (L-3, 1936 and L-4, 1938) used a cloud chamber and a magnet and Sanielevici (S-17, 1936) used heating measurements with a micro-calorimeter. Li (L-1, 1937) used a combination of a magnet and photographic plates to determine the beta continuum. Except for Sargent's 1939 work these experiments were not very convincing either because of the weakness of the source, the experimental method used or the theoretical analysis employed (Konopinski-Uhlenbeck plot). The only known alpha particle experiments were those by Rutherford and Wynn-Williams (R-9, 1931) and Pilger (P-3, 1957). Rutherford had weak sources, and equipment that would be crude by todays standards. Pilger's work using a large magnet was very accurate but limited to the strongest radiations. The only experimenter to measure the gamma radiation from the active deposit was Surugue who published several papers between 1936 and 1946 (S-18, 1936; S-19, 1936; S-20, 1937; S-14, 1941, S-13, 1946 and C-2, 1938). His work seems convincing enough, but he too was hindered by weak sources and crude techniques. Another measurement made more recently on the active deposit was to determine the internal conversion coefficient of the 350 keV gamma ray in Tl^{207}

(G-6, 1961 and F-5, 1954). This measurement was popular since that gamma ray was by far the strongest and the most heavily converted in the active deposit. The only other measurement known concerning the active deposit of the actinium series was the determination of the alpha-gamma angular correlation of Bi^{211} (G-7, 1953 and G-8, 1962). During the course of the present work two more papers appeared (V-1, 1963 and G-5, 1962); and as they were in disagreement on some aspects of the decay, the need for further detailed evaluation became more pressing.

A complete and thorough discussion of all the past work pertaining to the decay of the active deposit of the actinium series will be given in Chapter 5 where the information obtained by the present experiments can be compared to it.

1.2 The single particle models

Nuclear physics today has as its main goal the comprehension of the structure of the nucleus. This includes all results of the motion of nucleons: their paths in space, their momenta, the correlations between them, and the energies binding them to each other. The complete theoretical account of nuclear structure would be described by the total wave function of the nucleus.

If one considers all the possible degrees of freedom possessed by such a complex system as a heavy nucleus, the difficulties that would arise in their determination appear enormous. Even if these difficulties could be overcome the number of parameters that would be necessary would be beyond human comprehension. However there needs to be a sufficient number of parameters to describe at least the more prominent nuclear features. Because of present limited knowledge and inability to think abstractly, conceptual or theoretical models are invented in an attempt to explain the actions of the nucleons. Calculations based on a nuclear model must predict the various observable properties. The accuracy of these predictions determines the extent of the validity of the model.

The simplest kind of model is one in which the motion of only one nucleon need be studied, i.e., where the rest of the nucleus is considered to act as a single body providing a potential in which the extra nucleon moves. The nuclear shell model (or single particle model), being such a model, pairs off the nucleons in such a way that a single unpaired nucleon by itself determines many of the properties of the nucleus (e.g. the ground state spin of an odd A nucleus would be given by the spin of the single unpaired nucleon). The nuclear shell model was arrived at simultaneously but

independently by M. G. Mayer (M-1, 1949) acting on a suggestion by E. Fermi, and by O. Haxel, J. H. D. Jensen and H. E. Suess (H-1, 1949). By the inclusion of the spin-orbit interaction in the interaction between the single body (core) and the extra nucleon the model showed good agreement with the well known closed shells. As can be seen from Fig. 1-3 the shell model predicts closed shells for 82 protons and 126 neutrons among others. Thus 82 protons or 126 neutrons are the 'magic' combinations of nucleons which the shell model considers as one body (thus Pb^{208} would be doubly magic with both its neutron and proton shells closed). If more than one nucleon exists outside these shells, it may be necessary to consider their interaction with each other. The table below shows the number of neutrons and protons (or neutron and proton holes) outside these closed shells for the nuclei in the present work.

	Protons outside the 82 closed shell	Neutrons outside the 126 closed shell
Pb^{211}	0	3
Bi^{211}	1	2
Po^{211}	2	1
Tl^{207}	-1(hole)	0
Pb^{207}	0	-1(hole)

Because they only have a few nucleons (or holes) outside the closed shells these nuclei would be expected to be described well by the shell model. In a nucleus such as

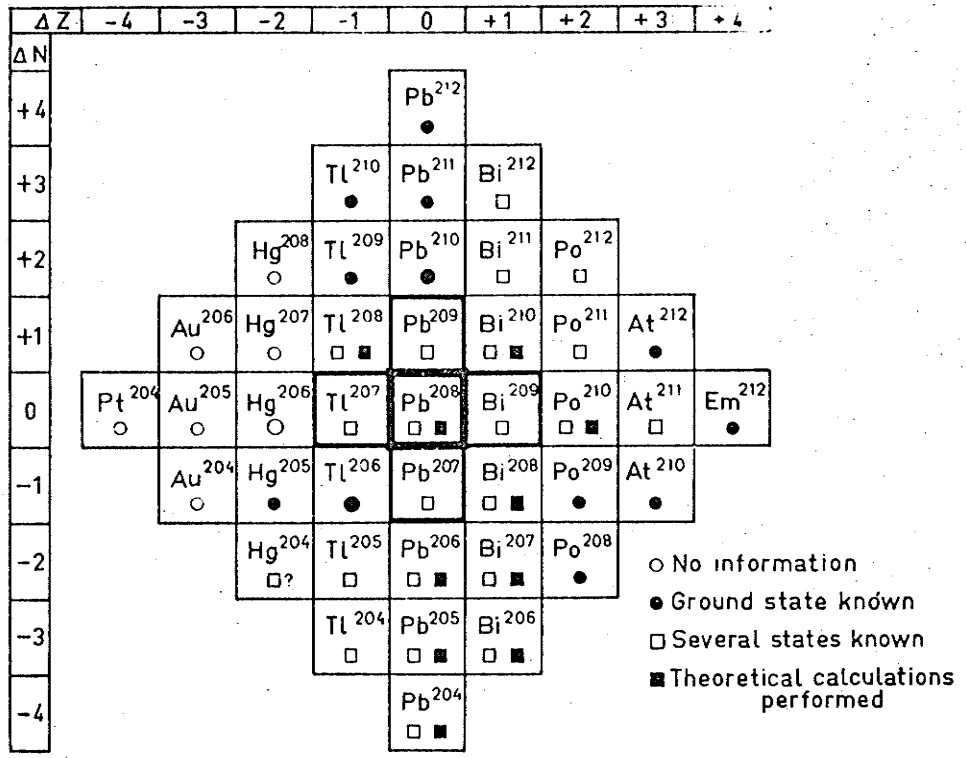

Nuclei in the Pb^{208} region for which calculations of levels based on the shell model have been performed or may be performed, when more experimental information is available. A filled circle means that only the ground state has been observed. An unfilled square means that in addition to the ground state at least one excited state is known.

Fig. 1-2 (from Bloomqvist and Wahlborn, B-2,1960)

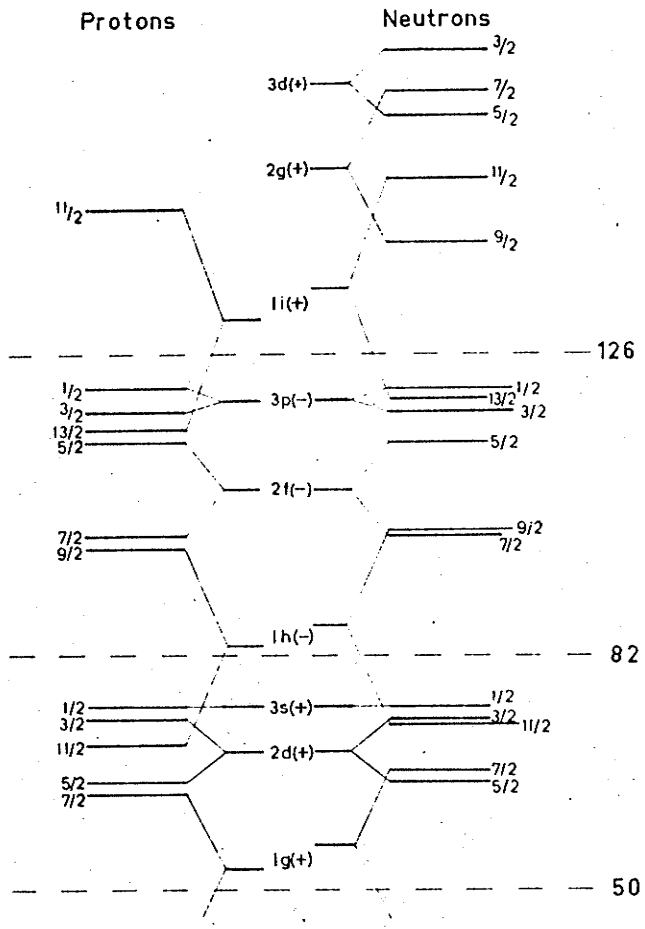

Single-particle levels for protons and neutrons (N and $Z > 50$).

Fig. 1-3 (from K-6,1952)

Bi^{211} the shell model would pair the two extra neutrons together and leave only the extra proton to determine the physical properties of the nucleus.

When experimentally observed levels are compared with the predictions of the shell model it must be kept in mind that excited states can be obtained either by promoting the last particle to a higher shell or by exciting a particle from an inner shell to a vacancy in a higher shell.

In view of the severe restrictions of the shell model, one is not surprised that its predictions are limited to only a few nuclear phenomena. One of the shell model's most striking failures is its inability to predict electric quadrupole moments of anything like the observed magnitude (P-1, 1962).

Because the shell model pairs off neutrons and protons the discussions of alpha decay, binding energy and clusters of nucleons are not usually attempted. When such calculations are attempted (M-2, 1960) the interpretation is not altogether clear.

In the shell model all different states which can be formed by particles with the same (n,l,j) possess the same energy. When the interaction between particles is added this degeneracy is eliminated. This interaction must be strong enough to remove the degeneracies but not

so strong, compared to the spin-orbit interactions, that j ceases to be a good quantum number for each nucleon. If a superposition of the wave functions of two or three (n,l,j) states whose energies are close to one another is used to represent a state, the shell particle model language may be retained. This form of calculation is called configuration mixing.

Some shell particle model calculations have been made in the Pb^{208} regions (see Fig. 1-2) e.g. Pb^{206} (T-1, 1958; T-3, 1957 and K-4, 1957), Pb^{207} (P-2, 1952 and B-2, 1960), Pb^{208} (C-1, 1960), Tl^{207} (B-2, 1960), Po^{211} and Bi^{211} (M-2, 1960 and M-3, 1957). The Po^{211} and Bi^{211} calculations are only for alpha decay probabilities. However the lack of success of the calculations in the Pb^{208} region leads one to suspect the applicability of the single particle model for Pb^{211} and its daughter products.

The term individual particle model is used to describe the single particle model method for determining nuclear wave functions. If one has some complete and orthogonal set (S-1, 1949) of functions it is possible to determine wave functions and energies of the physical quantum mechanical system. The functions used must have several parameters which eventually will be called quantum numbers. For simplicity, write the functions as ϕ_i where i may stand for a large number of these. These wave

functions need not resemble in any way the actual wave functions of the system. The first step in the procedure is to form a matrix $(\phi_i \mid H \mid \phi_j)$ where H is the Hamiltonian of the system. When this matrix is diagonalized the energies of the actual system appear as the diagonal elements and their corresponding eigenvectors α_{ik} give the actual wave functions $\psi_k = \sum_i \alpha_{ik} \phi_i$ of the system. It is a requirement of quantum mechanical statistics that the wave functions ψ_k be anti-symmetric. This procedure is not unique to the individual particle model as it is one of the fundamental techniques of the quantum mechanics. It is difficult to find a complete, orthogonal set with a finite number of functions ϕ_i; however this is necessary if the calculation is to be possible. The easiest solution to this problem is to find initially wave functions that are close to the actual ones. Then part of the matrix will already be diagonalized hopefully leaving total diagonalization as a reasonable calculation. To find such a set requires some physical insight.

The main feature of the individual particle model is that it constructs the wave functions ψ_k from products of single particle states, the single particle states being those of some reasonable central potential, e.g. the harmonic oscillator potential.

The calculations of the levels of nuclei which differ from Pb^{208} only by a few particles are similar to the perturbation calculations of the atomic levels in helium. In the two particle case the energy is given by

$$E_{total} = E_1 + E_2 + E_{int}$$

In the zero order approximation the total energy is simply the sum of the individual particle energies giving levels which are in general degenerate (E_1 and E_2). This degeneracy is removed by the introduction of an interaction energy (E_{int}). In the helium case this is, in principle, simple because the interaction between the electrons as well as between the nucleus and the electrons is the well known Coulomb interaction. The one particle levels (hydrogen levels) and the interaction energy in this case can be accurately calculated.

In the Pb^{208} region the calculation is much more involved than for the two particle problem of helium. First of all, the nuclear potential is not sufficiently well known to be able to calculate even one nucleon or one hole states. An idea of the absolute value of the level spacing of the one nucleon levels can be obtained from schemes such as that of Bleuler and Terraux (B-5, 1957). This scheme gives reasonable agreement for levels in stable nuclei but is too approximate to be used for the calculation of levels for unstable nuclei where the level

spacings may be reasonably predicted but the energy of the ground state with respect to neighboring nuclei is in error. However it is possible to use experimentally known one nucleon level spacings to calculate level spacings when several nucleons are involved. For a complete knowledge of the levels of the isotopes in the Pb^{208} region (see Fig. 1-2) it is necessary to know, to a high degree of accuracy, the excited states in Pb^{207}, Tl^{207} and Bi^{209}. Only the levels of Pb^{207} are known well enough to be useful. Another difficulty with this method of calculation is the insufficient knowledge of the (n,p), (n,n) and (p,p) interactions. For simplicity Pryce (P-2, 1952) assumed that this interaction could be described by a delta function. With this assumption it is possible to write the n,p interaction, ignoring configuration mixing, as

$$E_{np} = a_s A_s R + a_t A_t R = R A_s (a_s + 1.5 a_t)$$

where s and t refer to singlet and triplet states, with a_s and a_t as calculable constants depending on the configuration of the two particles and on total spin. A_s and A_t are the strengths of the singlet and triplet interactions respectively and from scattering experiments it is known that A_t/A_s is approximately 1.5. R, an integral involving the total radial wave function, is dependent on the quantum

numbers (n,l,j) of the two particles. Pryce did not calculate R but obtained RA_s by comparison with experimentally known two particle levels. Harmonic wave functions and Yukawa potentials for the nucleon interaction have been used for Pb^{206} (T-1, 1958 and K-4, 1957).

A calculation with some success similar to those described above in which a quadrupole potential and a strong pairing force (an extra force when two neutrons or protons are in the same shell) were assumed (K-3, 1963) has been made for isotopes below Pb^{208}. Only one calculation has been made (B-2, 1960) for nonstable isotopes in the actinium series (other than Pb^{207}), the correspondence to the experimental value for the first excited state of Tl^{207} being successfully shown. From the present literature Pb^{211} and its daughters would be expected to be described reasonably well by the single particle model (B-3, 1957, review).

1.3 Why investigate the actinium series ?

The present investigation of Pb^{211} and its daughter products (AcB-AcD) was undertaken for three reasons:

1) At the start of the project there existed only a very meager knowledge of the properties of the nuclei in this region (see section 1.1). It was felt that because of better equipment

(see chapter 3) not only could the past experiments (alpha, beta, and gamma ray spectroscopy) be improved upon but also new experiments could be performed (coincidence and angular correlation measurements).

2) Since the isotopes in question were near double magic Pb^{208} the information gained might well demonstrate the applicability of the shell model to Pb^{211} and its daughters.

3) The stronger sources needed for the high accuracy and coincidence experiments contemplated were now available thanks to the supply of actinium being no longer dependent on natural sources. The advent of nuclear reactors enabled the production of Ac^{227} in previously unheard of quantities by irradiating radium (Ra^{226}) with neutrons according to the reaction $_{88}Ra^{226} + _{0}n^{1} \rightarrow {}_{88}Ra^{227}$; the Ra^{227} then decays with a half life of 41 min. by beta emission to $_{89}Ac^{227}$. The general lack of information and work in this area stemmed very much from the lack of available source material. Even though reactor time is relatively inexpensive the elimination of contaminations (notably Ra^{226}) from the Ac^{227} was a difficult and expensive procedure.

1.4 Short outline of experiments performed.

The information required about the active deposit (Pb^{211} and its daughters) was:

1) the relative intensities and energies of the alpha, beta and gamma radiations including the estimation of lower limits on any other possible transitions,

2) the internal conversion coefficients of the gamma ray transitions,

3) the information necessary to determine which radiation belonged to which isotope,

4) the spins of levels and the angular momentum of the radiations involved.

This information was gathered by the following list of experiments:-

1) To determine the relative intensities and energies of the alpha and gamma radiations, the relevant spectra were collected (3.1, 3.3, 4.2 and 4.3). The alpha particle spectra yielded the relative intensities and energies directly; however the gamma ray spectra measured by scintillation counters had to be 'unpeeled' to determine the energies and relative intensities (4.3).

2) To determine the relative intensities and energies of the beta radiations, the beta momentum distribution was measured (3.2 and 4.4) and a Fermi plot constructed (4.4).

3) To measure the internal conversion coefficients the peak to background spectrum (P.B.S.) method was used (4.4 and 4.5). A knowledge of the alpha particle branching ratios was necessary to calculate the conversion coefficients (4.5).

4) To determine which radiation belonged to which isotope, alpha-gamma and gamma-gamma coincidence measurements were made (4.6 and 4.7). Also Tl^{207} was collected by recoil to determine which gamma rays belonged to transitions in Pb^{207} (4.3).

5) To determine the level spins and angular momentum of the radiations involved, alpha-gamma and gamma-gamma angular correlation measurements were made (4.10 and 4.11). Because high accuracy was needed for unique angular momentum assignments, only the strong radiations could be investigated by coincidence methods. The internal conversion coefficients were also needed to determine uniquely the spins involved.

Chapter 2

SOURCE

2.1 Source preparation technique

Sources of the active deposit of the actinium series were prepared by the classical technique of collecting the decay product of a gaseous alpha emitter by electrostatic attraction onto a metal (foil) held at a negative potential. The gas (sometimes called emanation) in the present case was actinon (Rn^{219}, see Fig. 1-1) whose daughter Po^{215} (AcA) has such a short half life (.0018 sec) that the sources collected consisted essentially of Pb^{211} (AcB - 36 min)(daughter of Po^{215}) and its daughter products. The sources being only a few atoms thick, were for all practical purposes weightless. This eliminated any problem of energy absorption for a particle leaving the source.

The parent material Ac^{227} was supplied by The Radiochemical Center, Amersham, England. It was produced artifically by pile neutron irradiation of Ra^{226} through the reaction Ra^{226} (n, gamma) $Ra^{227} \xrightarrow[\text{decay}]{\text{Beta}} Ac^{227}$. After a primary separation, the Ac^{227} was purified as follows (description by the supplier).

''Th^{228} was removed by anion exchange and the Ac^{227} was precipitated on Th^{232} carrier using barium as hold back for Ra^{226}. After two further precipitations, thorium isotopes were removed by anion exchange and the Ac^{227} precipitated on iron carrier using barium as hold back carrier for Ra^{226}. The emanation source was then prepared by the Hahn method (Chapter X Applied Radiochemistry)''.

The suppliers estimated that the 5 mc. of purified Ac^{227} contained no more than 1 microcurie of Th^{228} and Ra^{226} combined.

The investigation of alpha particle emission from the active deposit revealed the only observable impurities in the source. The well known 8.78 MeV alpha particle from the decay of Bi^{212} (ThC) was seen with an intensity of one part in 50,000 compared to the main alpha particle group in the decay of Bi^{211} (AcC).

The activity of the Ac^{227} was 5 mc. and the gas emanated quite well allowing sources of up to 1 mc. to be collected.

2.2 Source activation apparatus

To eliminate the possibility of the experimenter inhaling the radioactive gas and the possibility of the long lived parent Ac^{227} (half life 22 yr) contaminating

the source preparation area or being carried to the experimental room, the sources were prepared in a separate, ventilated room inside a closed glove box (see Fig. 2-3). The ventilated room was within the radiochemistry laboratory which itself is ventilated separately from the rest of the building. The source activation apparatus consisted of two stainless steel bricks located one on top of the other (see Fig. 2-1). The lower brick was fixed and contained the Ac^{227} in a recessed chamber in a platinum dish. The upper brick was moveable and held a plastic plug which contained the source backing (aluminum) to be exposed to the gas (see Fig. 2-2). The intensity of the source was determined by the length of exposure to the gas and by the size of hole in the bottom of the plastic plug. A 720 volt potential difference was used to collect the decay product of the emanation. However the collection efficiency was only slightly greater than that obtained when a potential difference of 450 volts was used. If the polarity of the voltage used was reversed (foil normally negative) the activity collected was seemingly unaffected. This effect has been observed previously for an activation apparatus using thorium (C-15, 1949), and is unexplained in terms of present knowledge. However if no voltage was used only a little activity is collected by diffusion. The source activation apparatus was located inside the glove box (see Fig. 2-3) and sources were removed through the double doors at the front.

Figure 2 - 1

Source activation apparatus.

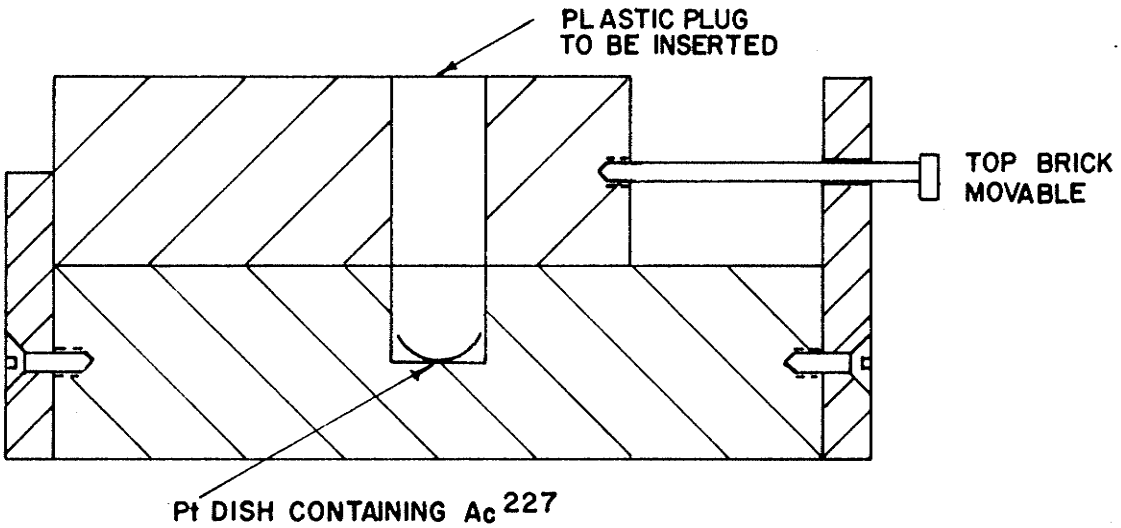
PLASTIC PLUG
TO BE INSERTED
TOP BRICK
MOVABLE
Pt DISH CONTAINING Ac^{227}

Figure 2 - 2

Source activation plug.
The source backing is the aluminum
foil supported on an aluminum ring.

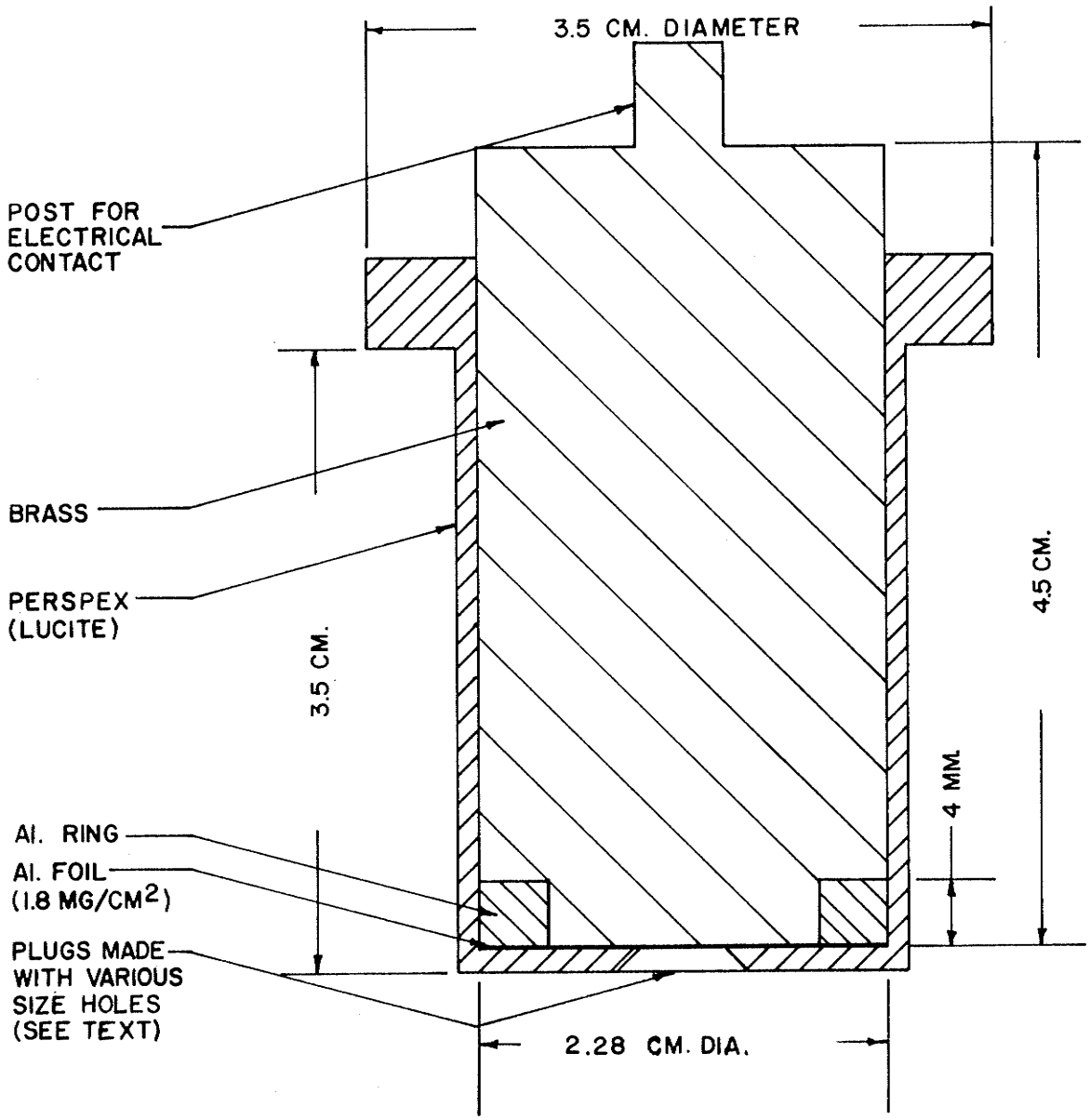
3.5 CM. DIAMETER
POST FOR ELECTRICAL CONTACT
BRASS
PERSPEX (LUCITE)
3.5 CM.
4.5 CM.
4 MM
Al. RING
Al. FOIL (1.8 MG/CM2)
PLUGS MADE WITH VARIOUS SIZE HOLES (SEE TEXT)
2.28 CM. DIA.

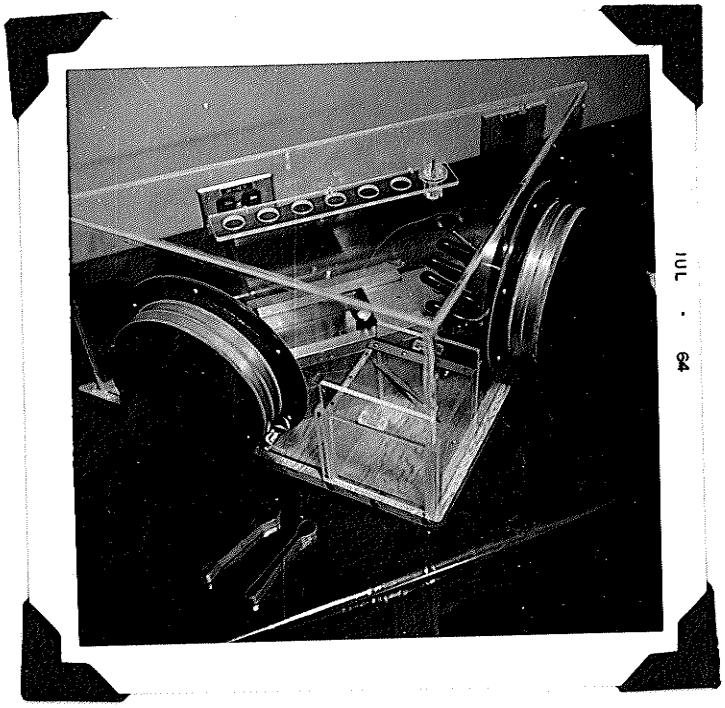

Fig. 2-3 Glove box used for source activation.

2.3 Physical nature of sources

Most of the sources were prepared on 1.8 mg./cm.^{2} aluminum foil. The actual area of the foil exposed varied from 1 mm. diameter for the beta and gamma spectrum measurements to 3 mm. diameter for the alpha-gamma angular correlation to 3/8 in. diameter for other experiments. A wire (1/3 mm. in diameter) was activated at one end (rounded) and used for the high energy beta measurements since it had a collection efficiency about ten times greater than the 1 mm. diameter foil sources. The wire was supported in the plastic plug (Fig. 2-2) by a cylindrical piece of plastic with a hole through the center and held in position by an aligator clip. The cylindrical piece of plastic replaced the brass plug. Only the tip (rounded end) of the wire was exposed to the gas, and the high electric field in the vicinity of the tip gave the greater collecting power. A highly polished stainless steel disc was used to collect the activity for the alpha spectra measurement. The stainless steel was polished with a fine diamond dust. Even though the surface had a mirror finish, small microscopic (approximately 10^{-3} mm.) scratches were left in the surface. A liquid source was used for part of the gamma-gamma angular correlation measurement. It was prepared by disolving the aluminum foil in a saturated NaOH solution. (HCl would not dissolve the aluminum foil well because of the thick oxide layer.) Approximately 600 sources of the various kinds described above were needed for the experiments described here.

2.4 The nature of the equilibrium

Since measurements were made to determine the relative intensities of alpha, beta and gamma radiations from more than one isotope, it was necessary to determine how the decay rates of the isotopes were related. In particular the time (t) necessary for the Pb^{211} and its daughter products to achieve transient equilibrium after being exposed to the emanation for a time T was calculated (see appendix I, a and b).

The equations I-11 (appendix I) for the populations of Pb^{211} (N_1), Bi^{211}(N_2) and Tl^{207} (N_3) were programmed on the Bendix G15-D computer at the University of Manitoba. The supply of actinon was assumed to be constant during activation, and since Po^{215} (AcA) has such a short half life it may be assumed that Pb^{211}(AcB) is collected on the foil at a constant rate (i.e., n_0 is a constant). This was verified experimentally since sources prepared under the same conditions had very close to the same strength (intensity). For purposes of calculation n_0 was taken as 1 atom/sec. Fig. 2-4 shows the resulting graphs of population vs. time (t) for four exposure times T = 20 min, 30 min, 1 hr, and 2 hr. Equilibrium existed when the decay of all isotopes was exponential (indicated by a straight line on the semi-log plots) and followed the decay of the longest lived component, Pb^{211}

(36 min half life). As can be seen from the graphs, all three isotopes were in equilibrium after about twenty minutes if the exposure time was 1 hr. The 1 hr exposure time was generally used because the sources could then be produced and used one after another giving little loss in actual data collection time. Also exposures for longer than two half lives (72 min) did not add much to the activity.

The relationship between the decay rates of the three isotopes is derived in Appendix I-c. Equation I-13 shows that Bi^{211} emits alpha particles 6.3% faster than Pb^{211} emits beta particles and that Tl^{207} emits beta particles 22.6% faster than Pb^{211} emits beta particles.

Figure 2 - 4

Activity of Pb^{211}, Bi^{211} and Tl^{207}
As a function of the time (t) for four
exposure times (T).

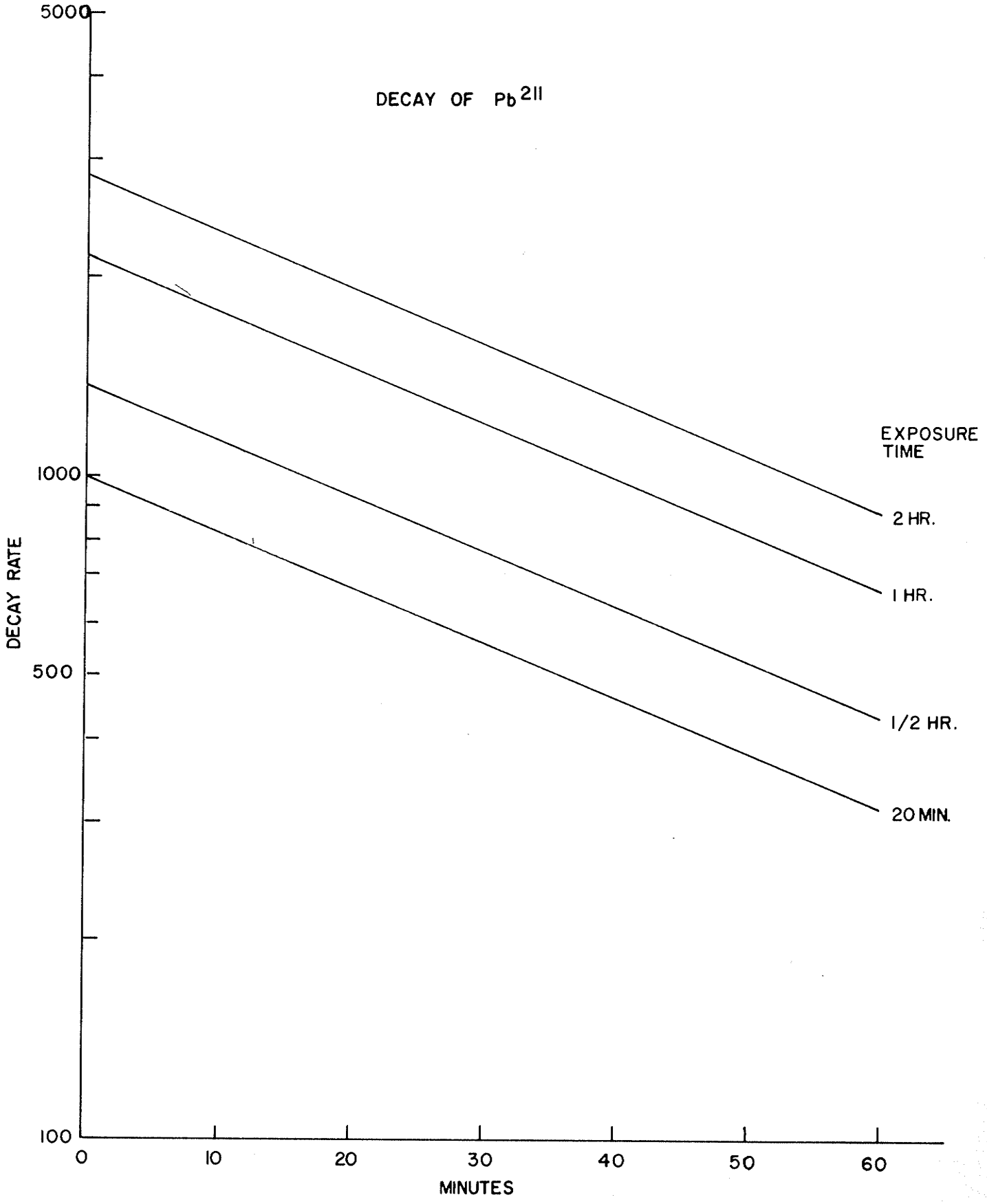
DECAY OF Pb 211
5000
1000
500
100
DECAY RATE
EXPOSURE TIME
2 HR.
1 HR.
1/2 HR.
20 MIN.
0
10
20
30
40
50
60
MINUTES

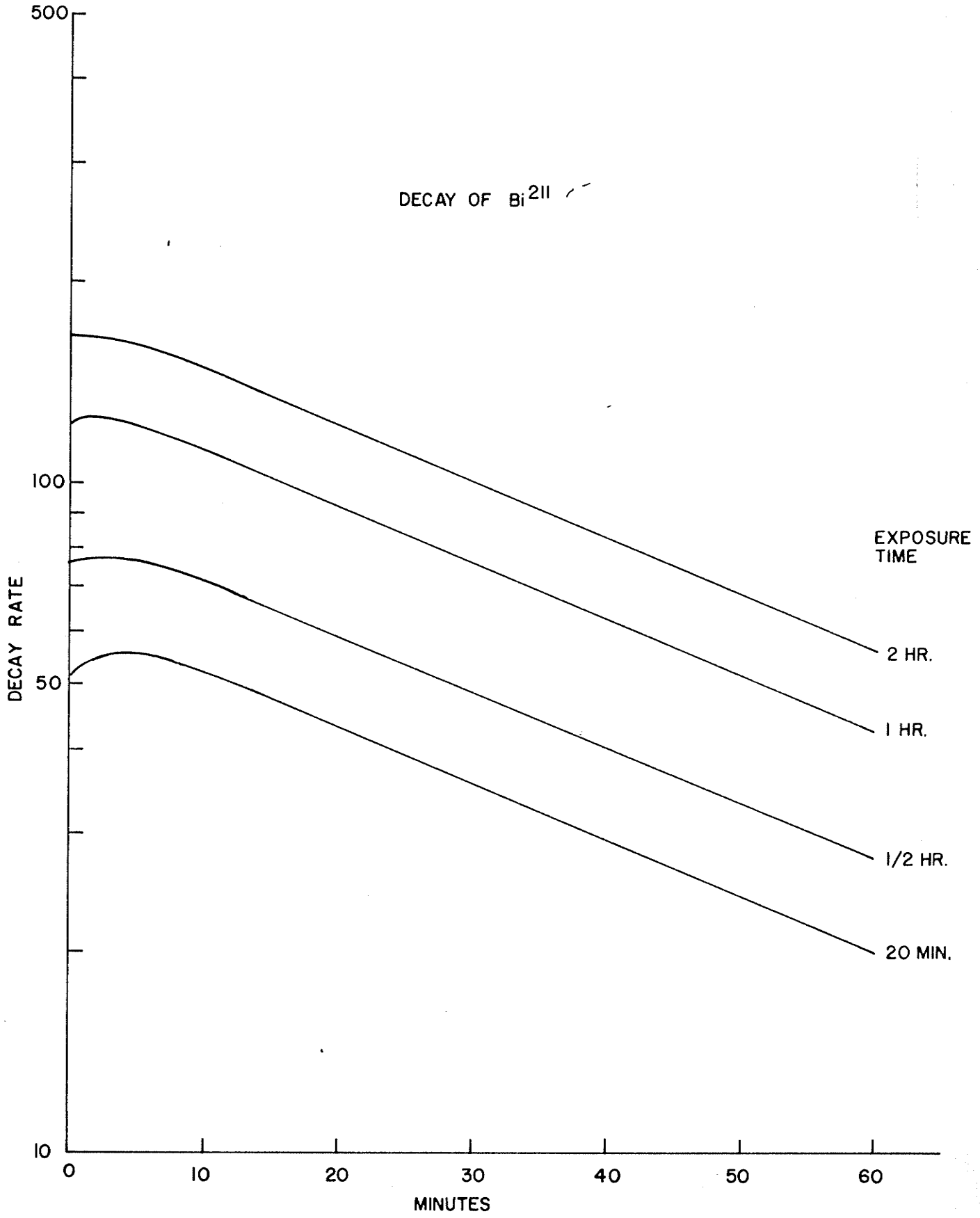
DECAY OF Bi 211
500
100
50
10
DECAY RATE
EXPOSURE TIME
2 HR.
1 HR.
1/2 HR.
20 MIN.
0
10
20
30
40
50
60
MINUTES

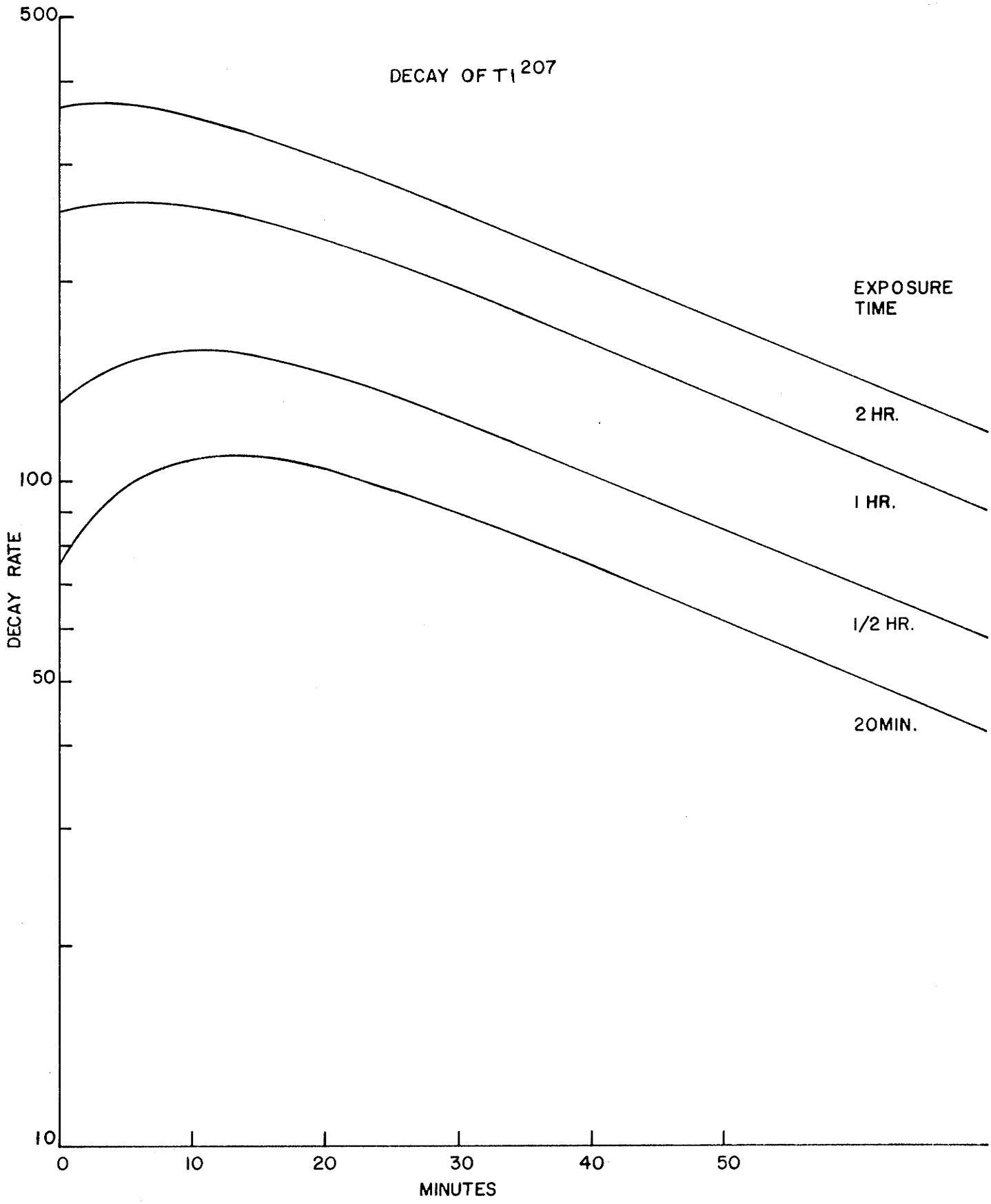
DECAY OF Tl 207
500
100
50
10
DECAY RATE
EXPOSURE TIME
2 HR.
1 HR.
1/2 HR.
20MIN.
0
10
20
30
40
50
MINUTES

Chapter 3

EQUIPMENT

3.1 Alpha particle detection apparatus

The detector used for alpha particles was a p-n junction diode consisting of an extremely thin p type layer on the sensitive side of a high purity n type silicon wafer. A voltage (bias) was placed across the silicon wafer to collect the ions created by the alpha particle. The two electrical contacts to this diode were made:

1. to the p type surface through an evaporated gold film approximately a hundred and fifty angstroms thick,

2. through an 'ohmic' contact to the n type silicon on the back.

The gold layer interfered with absolute energy measurements because of the energy loss it caused. However all energy measurements made in this work were relative (relative to a known source e.g., thorium active deposit or Am^{241}) and hence were unaffected by the gold barrier. The counter discussed above is sometimes called a surface barrier detector and in the simplest analogy is just an ionization chamber where the usual gas has been replaced with a semi-conducting solid.

The advantages of a surface barrier detector (as compared to scintillation methods or ionization chambers) are:

1. a relatively short collection time (of the order of a few, nano-seconds (10^{-9} sec.),
2. a sensitive depth which can be easily changed (simply by changing the bias),
3. a linear energy response,
4. a resolution which is independent of energy and is of the order of 20 keV (full width at half maximum),
5. small physical size,
6. long term stability.

The one disadvantage of the surface barrier detector used was that it is easily corroded and destroyed by vacuum pump oils. This necessitated using a liquid nitrogen trap in the pumping line.

The counter used for the alpha spectra measurements was supplied by Oak Ridge Technical Enterprises (Ortec), Oak Ridge, Tennessee. (Model number SBDJ-300). It had a nominal active area of 300 square mm, a depletion depth of 310 microns at 125 volts bias, and a nominal resistivity of 300 ohm-cm. This allowed alpha particles with energies up to 25.4 MeV to be totally absorbed. A useful discussion

of properties of surface barrier detectors may be found in the Ortec ''Instruction Manual for Semiconductor Devices''. General discussions of solid state counters, their properties, and uses also exist (G-4, 1964).

To examine the output of the detector a charge sensitive preamplifier and a highly stable amplifer (Ortec 103 and 203 respectively) were used with a 100 channel pulse height analyzer (Computing Devices of Canada Ltd., CDC). The amplifier contained a pulse generator which after calibration with the alpha particles from the thorium active deposit (6.086, 6.047, 5.765, 5.622 and 5.603 Mev(H-5, 1959)) was itself used as the calibration. It was discovered that the first tube in the preamplifier (6922) contributed approximately 90% of the noise in the system and when used for high counting rates (approximately 50,000 counts/sec) became very noisy after a few days operation. Hence it was replaced at least once a week as a standard practice.

It should be noted that because of the good resolution of the detector used, standard amplifiers could not be employed since they are too noisy and their gains are not sufficiently constant. Solid state counters in general have very high resolutions and thus need highly sensitive and stable preamplifiers and amplifiers (such as the Ortec 103 and 203). All measurements of alpha

particle energies were conducted in a vacuum of approximately 0.01 - 0.1 mm. Hg. This vacuum was provided by a Balzers rotary pump. The dewar for the liquid nitrogen, the trap and the pumping system can be seen in Fig. 3-1.

3.2 The beta ray spectrometer

The Siegbahn-Slatis intermediate image beta ray spectrometer was first conceived in 1949 (S-7). The commercial model (manufactured by LKB, Stockholm, Sweden, See fig. 3-2) contains many improvements on the original design. The beta particles were detected by a piece of NE102 scintillating plastic placed at the focal point of the electron trajectories and optically coupled via a light pipe to a selected low noise one inch photomultiplier (EMI type 9524SA) placed outside the instrument. The photomultiplier was further protected from strong magnetic fields by a mu-metal shield. The pulses were passed by an emitter follower circuit to a low gain amplifer and then into an automatic scaler. Although the spectrometer could achieve a 0.25% resolution (full width at half maximum) the measurements were made with a resolution of approximately 1% so that reasonable statistics could be obtained with the sources available (±3% for the continuum).

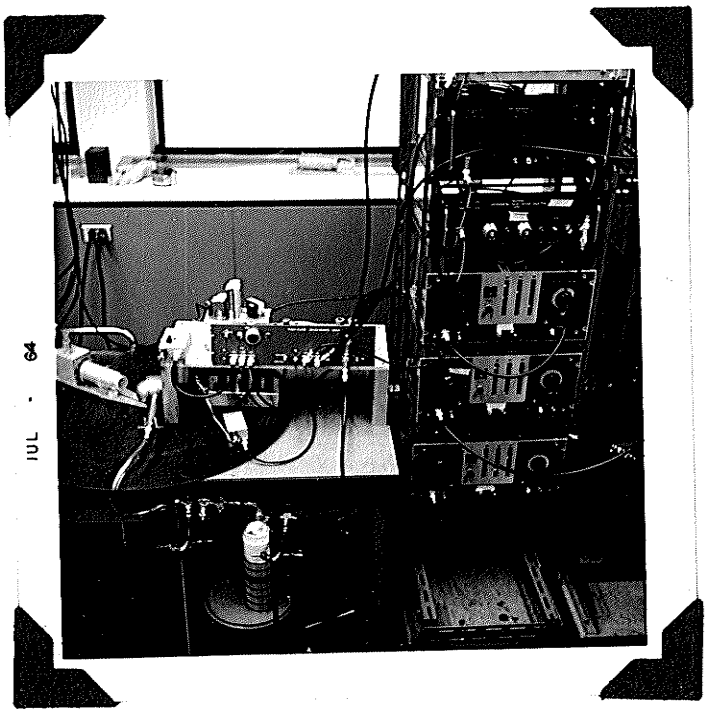

Fig. 3-1 The experimental arrangement for alpha particle spectroscopy(including alpha particle spectra, alpha-gamma coincidence and angular correlation). The liquid nitrogen trap is in front of the table and the rotary pump can be seen under the table. The charge sensitive preamplifier is shown on the table under the fast-slow coincidence unit.

The operation of the spectrometer was fully automatic (K-5, 1963). The number of counts accumulated in a preset time, together with a number proportional to the electron momentum was printed out on paper tape, the spectrometer current was then advanced one step and the count recommenced. The automation was extremely useful in that it allowed the experimenter time to prepare sources and calculate the momentum distribution as the data was being collected. The fastest counting rate achieved was approximately 1,000 counts/min. Near the end point counting rates were approximately 50 counts/min. Slower rates could not be tolerated because of the short half life of the source.

3.3 Gamma ray detection apparatus

Gamma rays were detected by a 1-1/2 in. (diam.) x 1 in. NaI(Tl) crystal which was incorporated with a photomultiplier tube in a Harshaw integral line assembly (Harshaw 6S4). The resolution of the unit was approximately 8% for the 662 keV gamma ray of Cs^{137}. A lead brick with a 1/2 in. hole was used as a collimator (see Fig. 3-3). To investigate high energy gamma rays, lead absorbers were inserted between the source and counter as shown in Fig. 3-3. The absorbers consisted of approximately 4 gm./cm.^{2} lead sheets. Experiments were conducted with 1, 2, 3, and 5 of

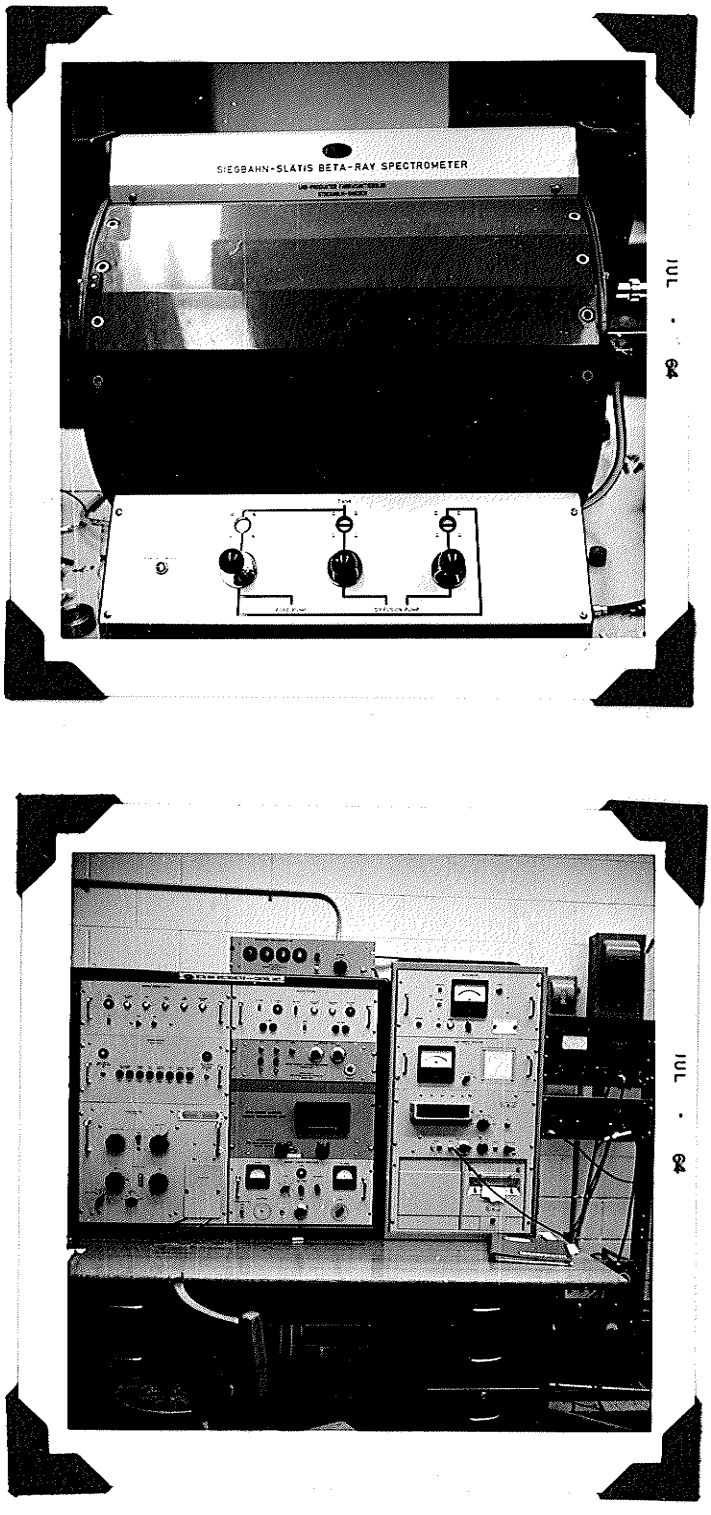

Fig. 3-2 Above is shown the Siegbahn-Slatis beta ray spectrometer built by LKB, Stockholm, Sweden. Below is the control panel for the spectrometer including the automation.

these sheets as absorbers. The photomultipler output was fed through a cathode follower to a Nuclear Enterprises 5202 (double delay line) amplifier and then to the CDC 100 channel pulse height analyser. Care was taken to maintain a uniform dead time throughout the taking of data for the actinium active deposit and the calibration sources (Cr^{51}, Au^{198}, Na^{22}, Cs^{137}, and Mn^{54}). This precaution was taken because the pulse height corresponding to a photopeak was known to be a function of the counting rate for NaI crystal-photomultiplier assemblies (C-16, 1960). Low counting rates of approximately 200 counts/sec were used to avoid gain shifts and possible pile up of pulses in the electronic system.

The efficiency of a NaI(Tl) crystal is a function of the energy of the gamma ray being detected, the physical size of the crystal and the source to crystal distance. Tables of theoretical efficiencies are available in the literature (M-13, 1958). These efficiencies (ϵ_t) are calculated for all interactions (photoelectric, compton, and pair production) of a gamma ray of a particlar energy. However a more accurate determination of the relative gamma ray intensity may be found by comparing only the photo peak areas. Thus the photo-electric efficiency (ϵ_p) is needed. The photoelectric efficiency may be found by the equation $\epsilon_p = R\epsilon_t$ where R is the ratio of the

Figure 3 - 1

Geometrical arrangement of
the gamma ray detector,
source and absorbers.

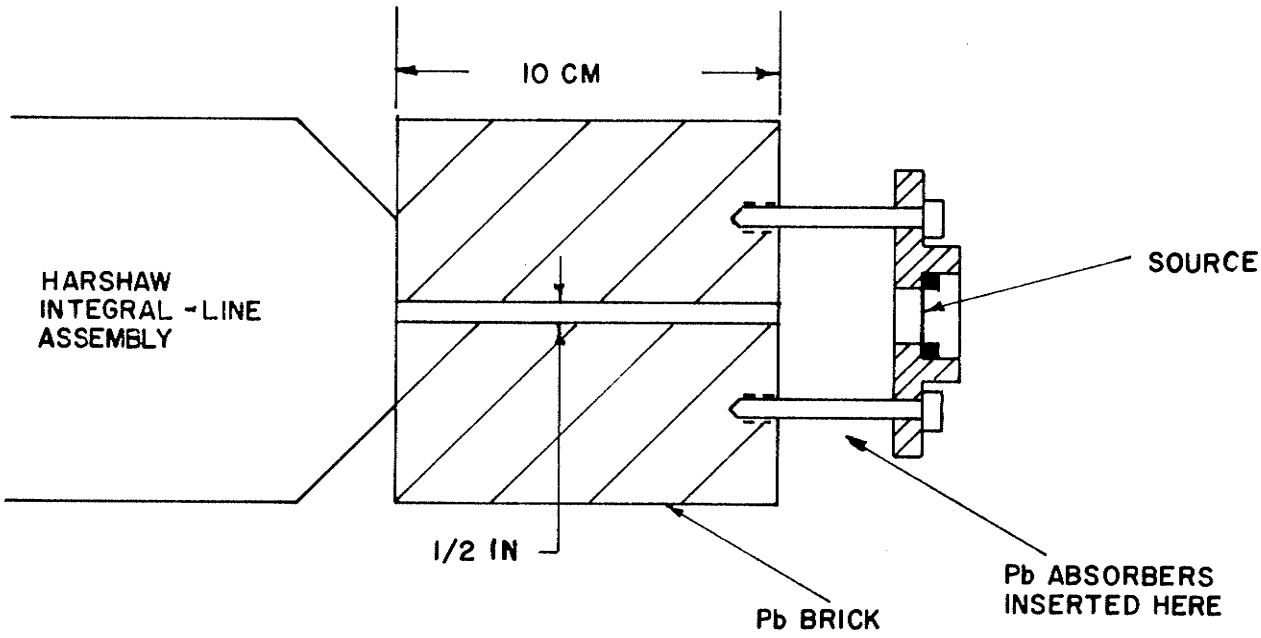
10 CM
HARSHAW
INTEGRAL - LINE
ASSEMBLY
SOURCE
1/2 IN
Pb BRICK
Pb ABSORBERS
INSERTED HERE

probability of a gamma ray being photo-electrically converted to the probability of its being compton scattered. Graphs of R vs. energy are available (see M-13, 1958).

3.4 Gamma-gamma coincidence apparatus

A block diagram of the gamma-gamma coincidence apparatus is shown in Fig. 3-4. The two amplifiers shown are of the double delay line type. Each gamma detector generated two electronic pulses. The pulse appearing at the eighth dynode of the photomultiplier was proportional to the energy of the gamma ray detected while the sharply rising pulse appearing at the collector was used to indicate that a gamma ray was detected but not to determine its energy. The first pulse had a rise time of a few microseconds and was called the slow pulse. The pulse from the collector was limited giving a pulse whose rise time was a few nanoseconds and was called the fast pulse. The two fast pulses were examined electronically for coincidence and the two slow pulses were examined electronically for simultaneously coincidence. If both fast and slow coincidence existed, the gate on the CDC 100 channel analyser was opened allowing the slow (energy) pulse to be analysed. This technique is a well known one (B-9, 1952).

The quantity which determines the overall performance of the system is the resolving time (t) which is defined by

$$N_{chance} = 2tN_1N_2$$

where N_{chance} is the accidental counting rate and N_1 and N_2 are uncorrelated single channel counting rates. The resolving time can be determined experimentally by placing a different monoenergetic source in front of each detector. The coincidence counting rate would then be the N_{chance} shown above. A lead brick should be placed between the two detectors so that no photons can be counted in one and then be scattered into the other.

The photomultipliers were operated at approximately 1750 volts so as to obtain a sharply rising pulse at the collector. This pulse effectively cuts off the 6688 high gm pentode used as the limiter. Pulses due to gamma rays whose energies were approximately 100 keV or greater were limited.

The pulses out of the limiter were approximately 1 volt high and approximately 25 n.sec.wide. These pulses were fed to the fast input on the coincidence unit (see Fig. 3-5) where they were clipped by the clipping line (approximately 2 ft of RG59U cable shorted at one end) and added, appearing at the output of the diode which was biased to reject single pulses. This output was then fed to an

Figure 3 - 4

Block diagram of gamma-gamma coincidence apparatus.

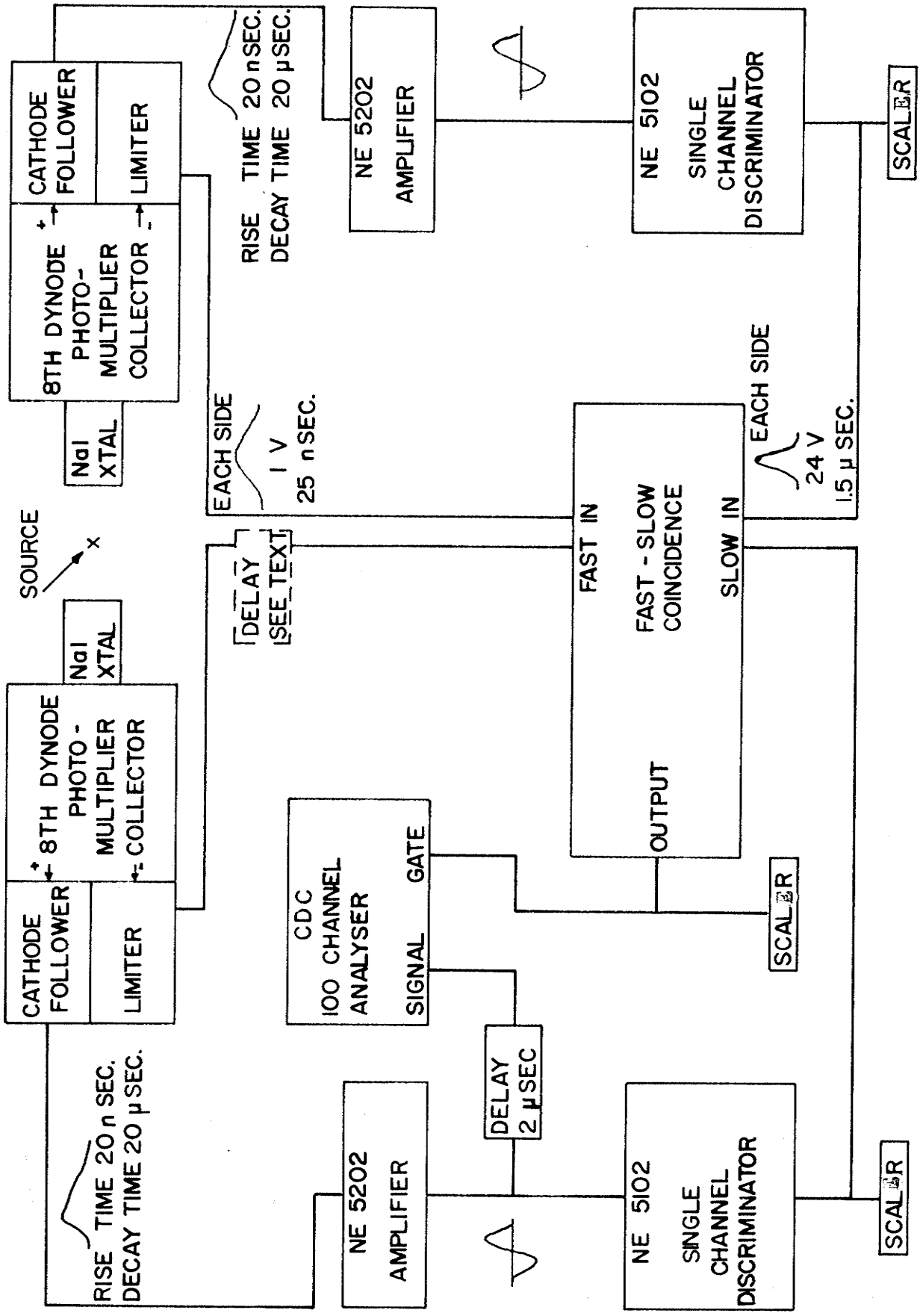
8TH DYNODE PHOTO-MULTIPLIER COLLECTOR
CATHODE FOLLOWER
LIMITER
NaI XTAL
RISE TIME 20 nSEC.
DECAY TIME 20 μSEC.
NE 5202 AMPLIFIER
NE 5102 SINGLE CHANNEL DISCRIMINATOR
SCALER
EACH SIDE
1 V
25 nSEC.
SOURCE
DELAY (SEE TEXT)
FAST IN
FAST - SLOW COINCIDENCE
SLOW IN
OUTPUT
EACH SIDE
24 V
1.5 μ SEC.
CDC 100 CHANNEL ANALYSER
SIGNAL
GATE
DELAY 2 μSEC

Figure 3 - 5

Schematic diagram of the fast-slow coincidence unit.

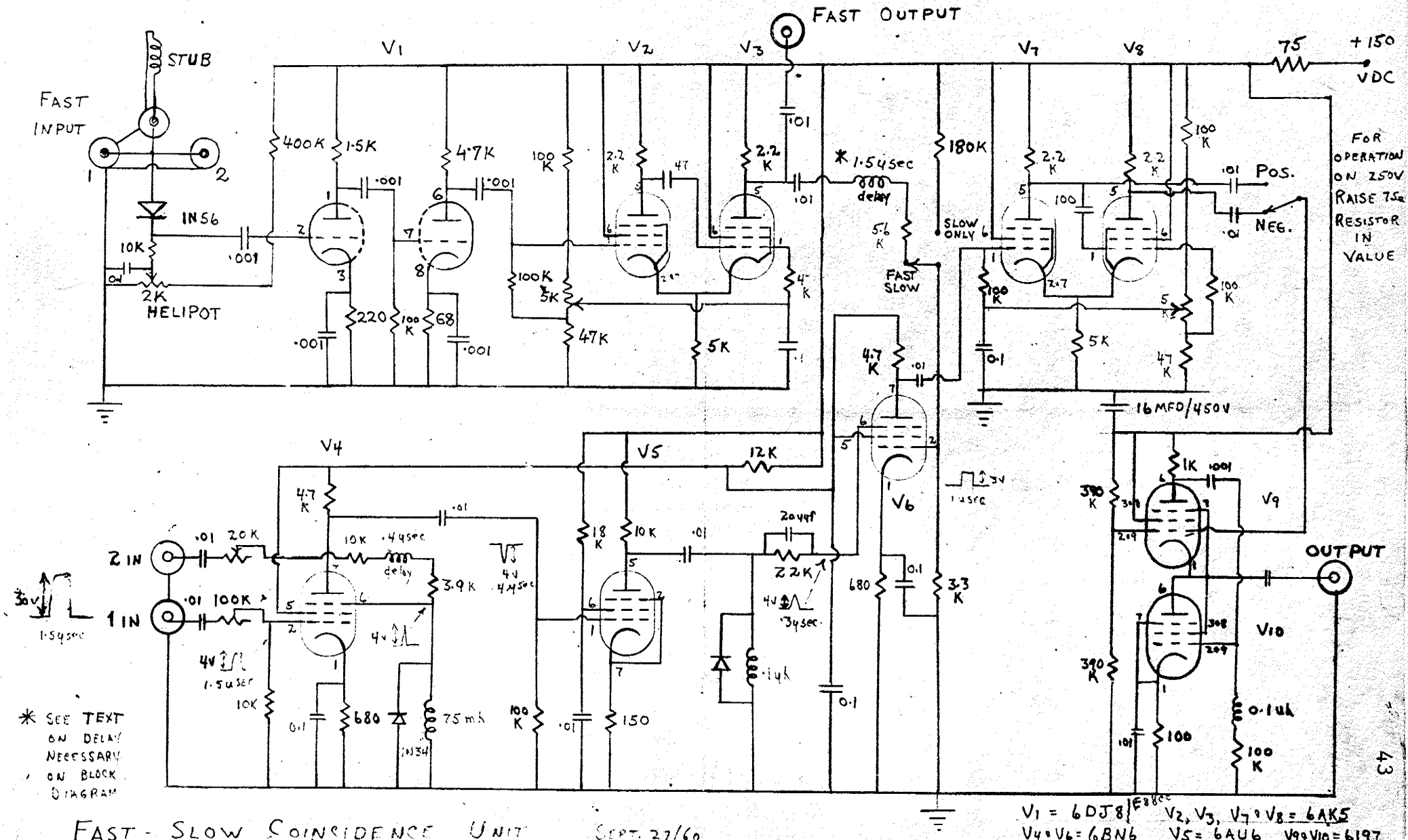
FAST INPUT
STUB
1
2
IN56
10K
.001
2K HELIPOT
400K
1.5K
.001
4.7K
.001
100K
220
100K
68
.001
.001
100K 5K
47K
V1
V2
V3
FAST OUTPUT
2.2K
47
2.2K
.01
* 1.54sec delay
5.6K
FAST SLOW
5K
4K
.1
180K
SLOW ONLY
V7
V8
2.2K
100
2.2K
100K
.01 Pos.
.01 NEG.
100K
5K
47K
5K
0.1
16 MFD/450V
75
+150 VDC
FOR OPERATION ON 250V RAISE 75Ω RESISTOR IN VALUE
V4
V5
12K
4.7K
.01
20K
10K .4usec delay
3.9K
4V .4usec
2 IN
1 IN
.01 100K
4V 1.5usec
10K
0.1
680
75 ma
1N34
100K
.01
150
18K
10K
.01
20 uuf
22K
4V .3usec
.1μh
0.1
680
0.1
3.3K
V6
3V 1usec
1K .001
390K
V9
OUTPUT
V10
390K
0.1μh
100
.01
100K
3V 1.54sec
* SEE TEXT ON DELAY NEEESSARY ON BLOCK DIAGRAM
FAST - SLOW COINCIDENCE UNIT
SEPT. 27/60
V1 = 6DJ8 E88CC
V2, V3, V7, V8 = 6AK5
V4 = V6 = 6BN6
V5 = 6AU6
V9 = V10 = 6197
43

amplifier to provide a large enough pulse to trigger a univibrator which in turn provided a fast output monitor pulse as well as a coincidence pulse for the resultant of the two slow coincidence pulses. Since the single channel analysers worked on the trailing edge of the positive going pulse they introduced approximately 3 microseconds delay. This can be seen from the pulse shape entering the single channel analyser (see Fig. 3-4). This was compensated for by introducing a 3 microsecond delay between the fast and slow sections of the coincidence unit (see Fig. 3-5). The single channel analyser on the right had side of Fig. 3-4 was used to select one gamma ray while the single channel analyser on the left had side allowed some wide range of gamma rays through (usually virtually all those appearing at its input). The CDC 100 channel pulse height analyser then displayed all gamma rays in coincidence with the gamma ray selected by the right hand single channel analyser. The relative intensities of the coincident gamma rays could be taken directly from the multichannel pulse height analyser. To check the stability of the single channel pulse height analysers and indeed much of the electronic system, systematic tests were conducted at intervals throughout the course of the experiment. The tests consisted of feeding the output of one single channel analyser into both inputs of the slow coincidence unit, the

output of which was used to gate a 100 channel pulse height analyser. The input to the single channel analyser was also fed to the input of the 100 channel pulse height analyser. Hence the display in the latter unit revealed the pulse height limits allowed through the single channel analyser and the position of the peak relative to these limits. At no time during the course of this work was any variation detected in the performance of the system.

Once the voltage pulses had been checked and the single channel analysers adjusted, it remained to select a fast bias setting. The bias setting should be high enough to reject single pulses, i.e. only accepting added pulses. To determine an acceptable region the number of fast monitor pulses was examined for different bias settings (see Fig. 3-6). As the bias setting was increased the number of coincidence pulses was decreased and the ratio of the real coincidence to chance coincidences was increased. Since it was desirable to have a high coincidence counting rate and a high real to chance ratio a compromise was necessary. In general a real to chance ratio was 50:1 or better was achieved. However a ratio of 3 or 4:1 was tolerated when necessary. The chance coincidence rate was obtained by inserting approximately 30 n. sec. of delay (RG59U cable) in one of the fast inputs. (See fig. 3-4). There was no effect on the amplitude of the signal when the cable was inserted (to 1%). Once the

system was known to be working it was useful to use a known source (e.g. the 400-430 keV cascade in the actinium active deposit) and find the real to chance ratio and the resolving time for a particular set of system parameters (fast bias, photomultiplier high voltage, amplifer gains, etc.) This provides a quick and complete check of the equipment during the run.

The experimental arrangement is shown in Fig. 3-7. As can be seen a lead brick was placed between the detectors so that scattering between the crystals could not occur.

3.5 Alpha-gamma coincidence apparatus

The block diagram of the alpha-gamma coincidence equipment is shown in Fig. 3-8. The operation was similar to that of the gamma-gamma coincidence apparatus (Section 3.4). The single channel analysers introduced a 1.5 microsecond delay because of acting on the trailing edge of the positive amplifier pulses. This can be seen from the pulse shape entering the single channel analyser (see Fig. 3-8). This necessitated a 1.5 microsecond delay between the fast and slow sections of the coincidence unit (see Fig. 3-5). Also, since the alpha and gamma detectors gave different polarities on the slow side, a pulse [illegible] inverting transformer was inserted in the gamma slow side to bring the pulses into correct time relationship.

Figure 3 - 6

Typical curve for number of fast coincidence output pulses vs. the bias setting on the fast input. The center of the 'plateau' was used for operating conditions.

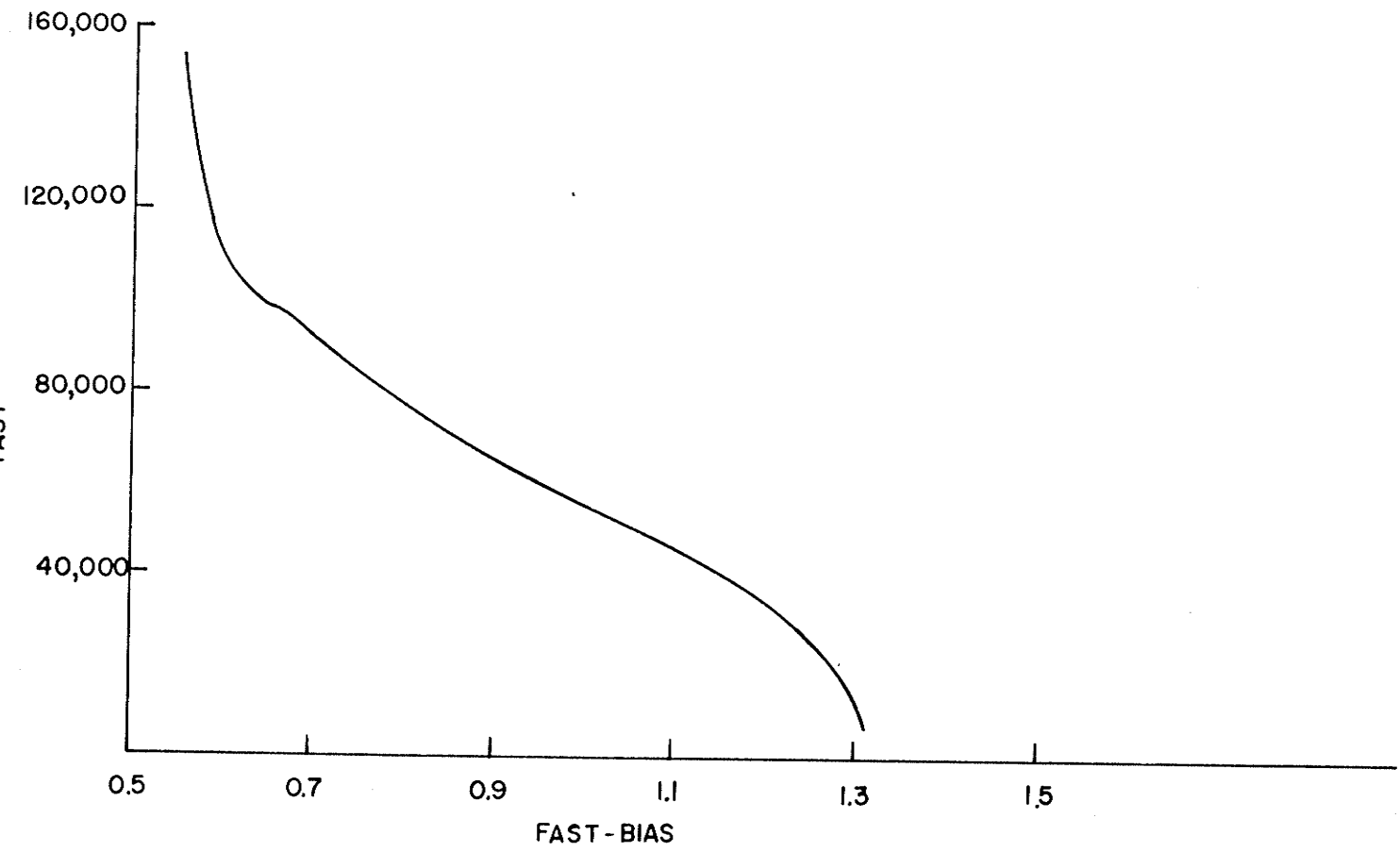
160,000
120,000
80,000
40,000
0.5
0.7
0.9
1.1
1.3
1.5
FAST - BIAS

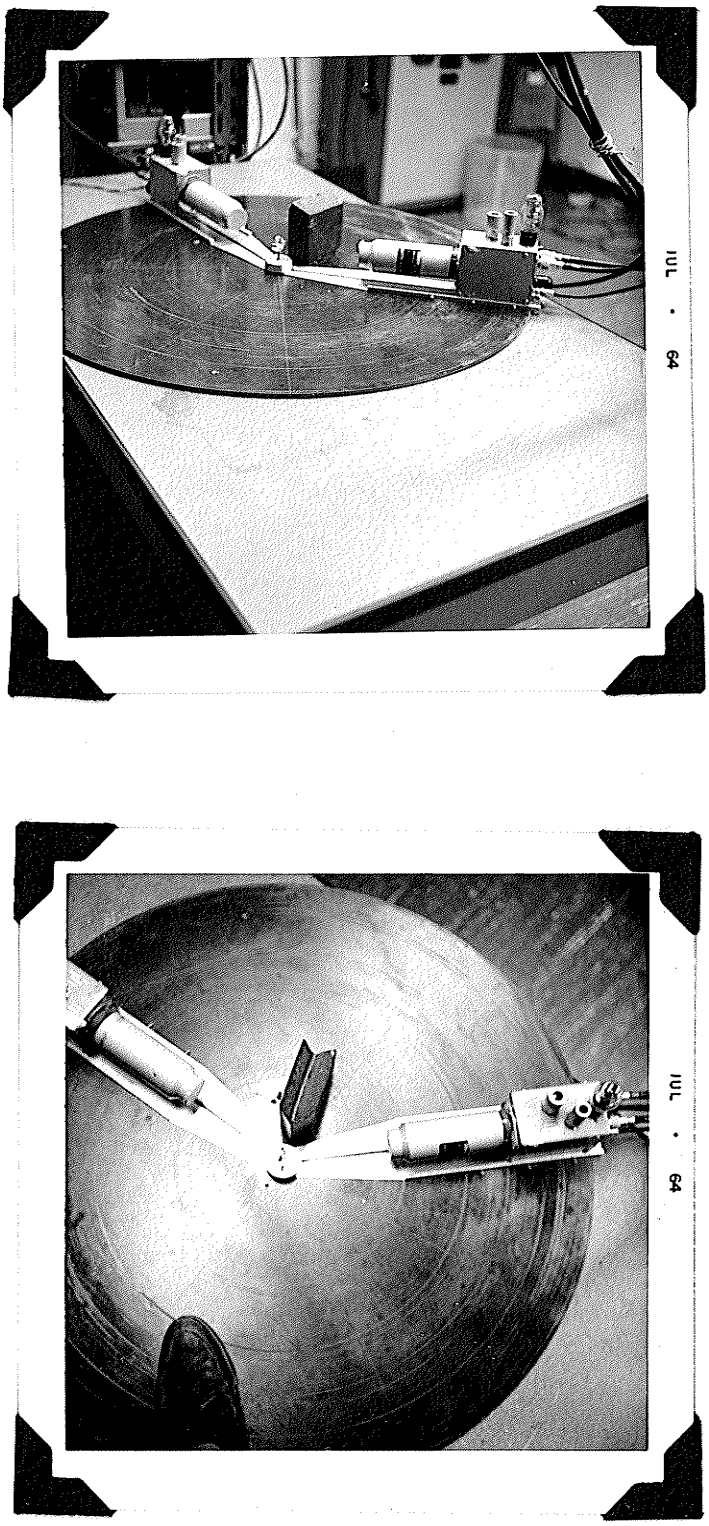

Fig. 3-7 Experimental arrangement of counters for gamma-gamma coincidence studies.

An internal connection was made to the Tennelec preamplifier (Fig. 3-8) to obtain an alpha particle pulse for the fast coincidence circuit. This was fed to a transistorized amplifier (Fig. 3-9) which gave an output of 5 volts into 100 ohms for any pulse of 50 millivolts or greater appearing at the input (this corresponds to alpha particles with energies of approximately 500 keV or more). The limiter circuit was a slight modification of a circuit due to Fraser and Tomlinson (F-8, 1962). This positive pulse from the alpha limiter was attenuated to be compatible with the gamma limiter pulse and fed to the fast coincidence circuit (see Fig. 3-5). The limiter pulse from the gamma side was found to be 20 nanoseconds earlier than the corresponding output from the alpha detector. Thus a delay was necessary in the gamma side. An electronic delay was used since it would not attenuate the signal and also because it could be easily varied. The limiter pulse was fed to a transistorized trigger circuit and the width of the pulse thus obtained was made variable by a small variable ceramic capacitor between the trigger pairs. The positive pulse obtained from the trigger pair was inverted giving a negative pulse approximately 35 n. sec. wide. This pulse was differentiated hard, passed through an emitter follower, and clipped by a diode to give a positive output. The time delay circuit was designed by K. I. Roulston (R-14) (see Fig. 3-10). The delay in the gamma side was

Figure 3 - 8

Block diagram of alpha-gamma coincidence apparatus.

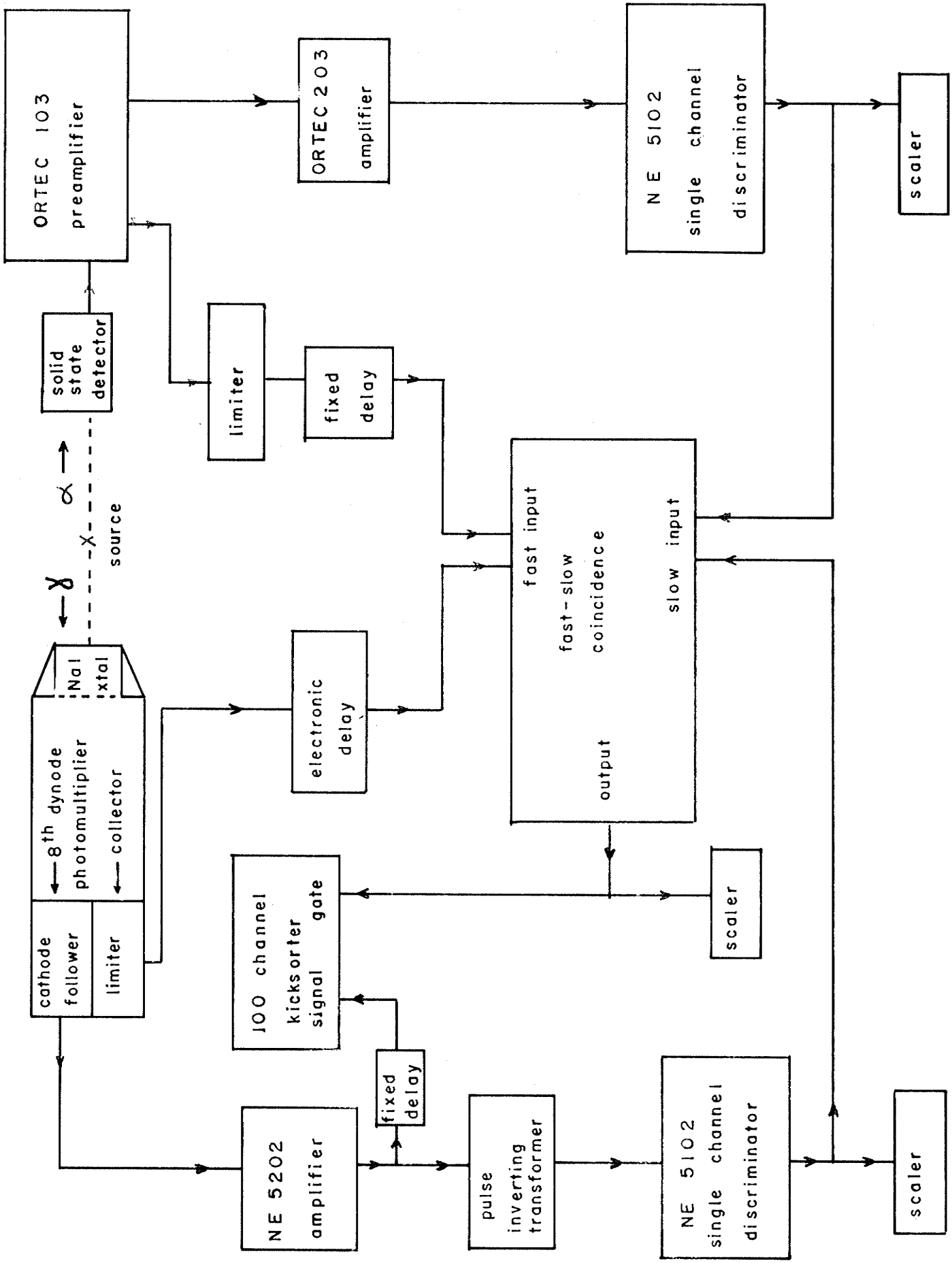
ORTEC 103
preamplifier
ORTEC 203
amplifier
NE 5102
single channel
discriminator
scaler
solid state detector
limiter
fixed delay
α
γ
X
source
fast input
fast-slow coincidence
slow input
output
electronic delay
Nal xtal
8th dynode photomultiplier
collector
cathode follower
limiter
100 channel kicksorter signal gate
scaler
fixed delay
NE 5202
amplifier
pulse inverting transformer
NE 5102
single channel
discriminator
scaler

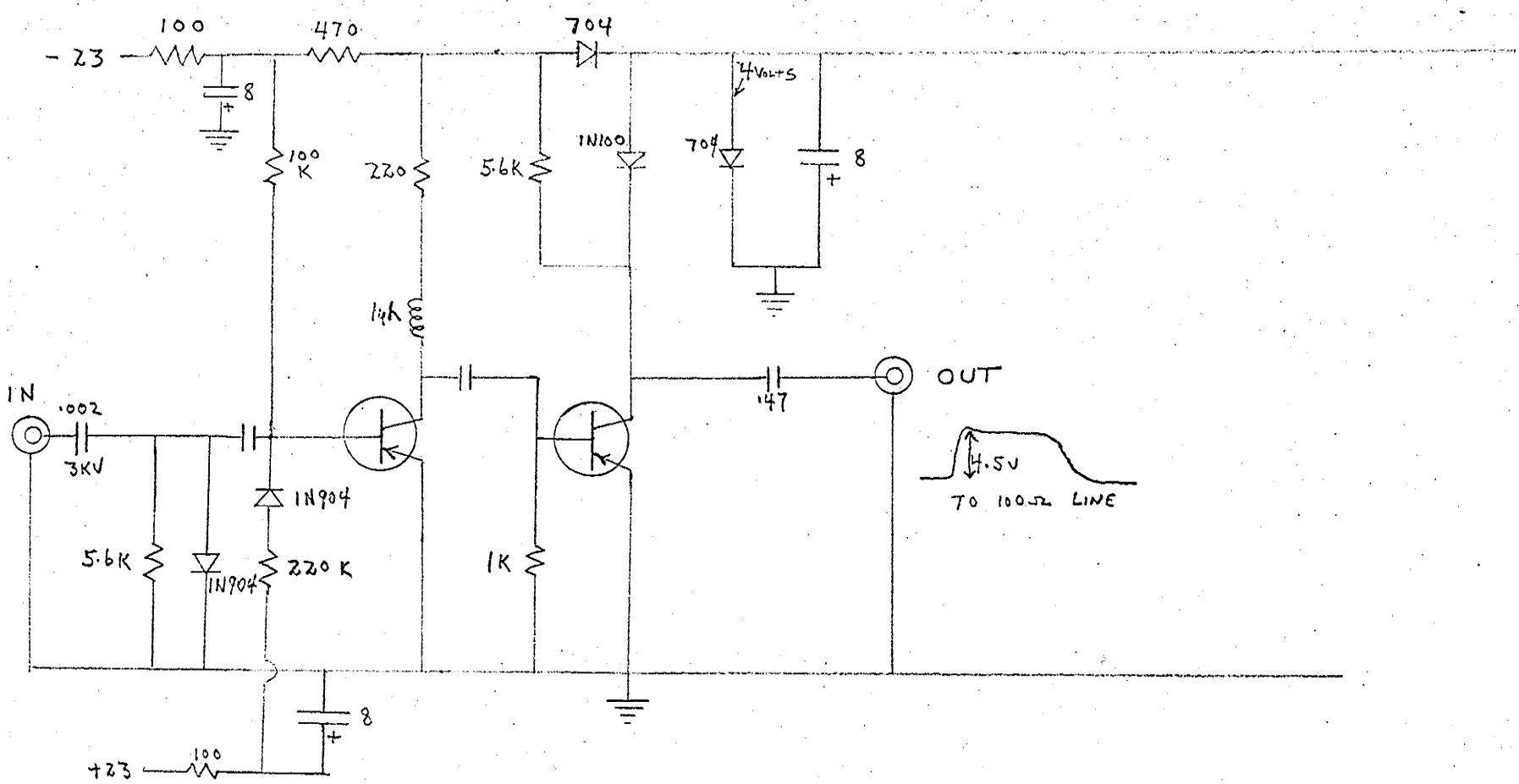

LIMITER — HIGH SENSITIVITY SATURATED AMPLIFIER

INPUT AMPLITUDE FOR SATURATION - 50 MILLIVOLTS

PULSE HEIGHT AT INPUT CLIPPED AT 700 MV MAXIMUM

TRANSISTORS 2N1500

APRIL 24/63

Fig. 3-9 Schematic diagram for the limiter used for fast alpha pulses in alpha-gamma coincidence and angular correlation studies.

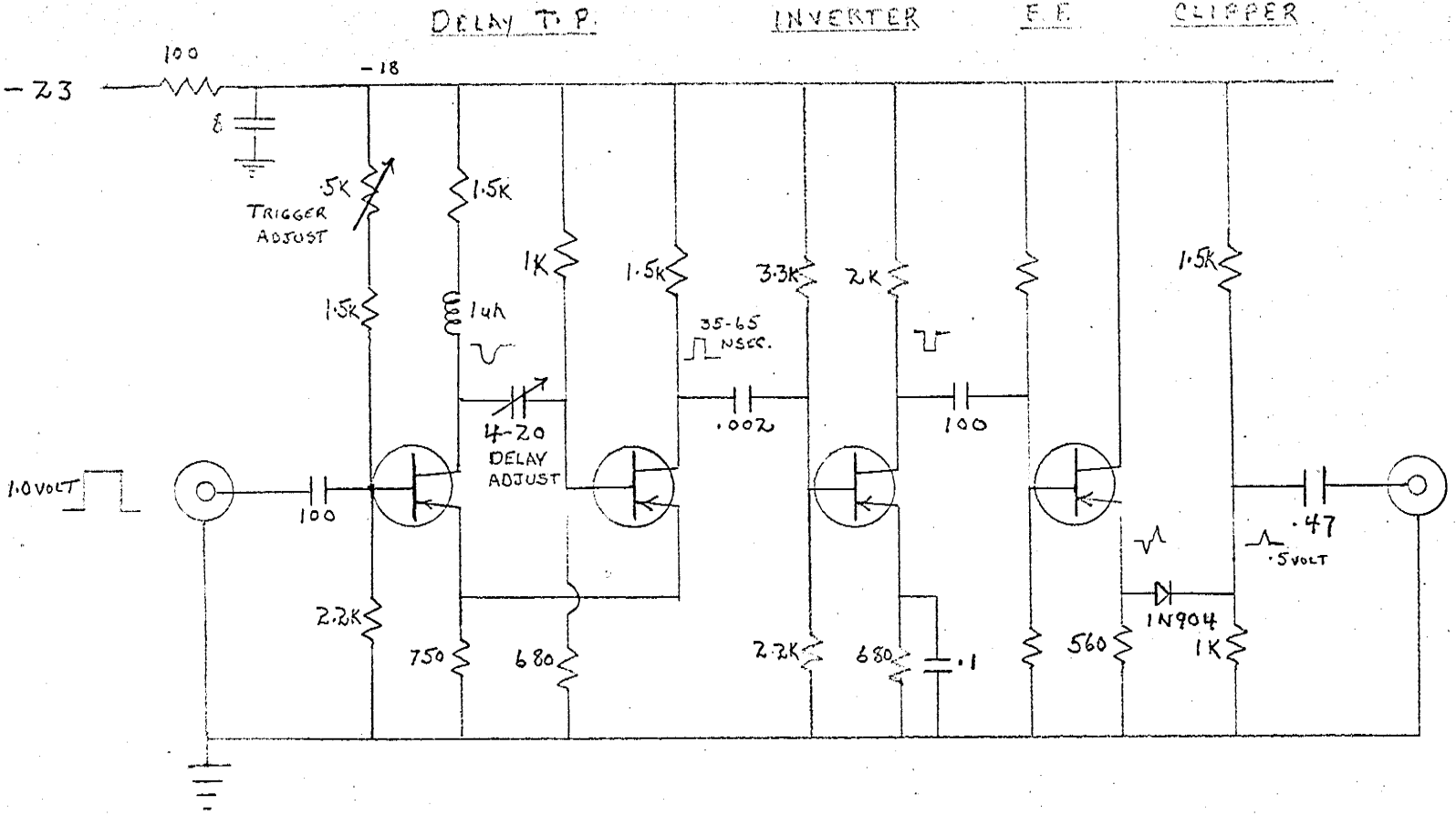

VARIABLE TIME-DELAY CIRCUIT —— APPROX. 35-65 NANOSEC.

Fig. 3-10 Schematic diagram for the electronic time delay used in alpha-gamma coincidence and angular correlation studies.

TRANSISTORS - 2N1500

APRIL 26/63

now slightly too great. However instability was encountered when the time constant in the trigger pair was reduced below 35 n.sec. Thus a 15 ft. length of RG59U cable was inserted in the alpha side following the limiter. The inserted cable did not cause any attenuation on the alpha side as it did on the gamma side. A large range of the variable capacitor gave true coincidence (approximately 150° of rotation). A variation in the true to accidental rate could be noticed when this delay time was varied over its range. However once set up the accidental rate was determined during operation by removing the 15 ft. of RG59U cable. It was found also that a difference existed in the timing of the two pulses if the system was set up using a radioactive source as compared with a pulse obtained from a pulse generator. This was not surprising since they would be expected to have different rise times, however it necessitated using the short lived actinium source to set up the apparatus. The bias setting on the fast side was chosen in a way similar to that described in section 3.4. That is a compromise was found between high counting rate and high real to chance coincidence ratios. Again the fast output was monitored for different bias settings. Again a wise procedure was to determine what the real to chance ratio and resolving time were for correct operation with a known source (e.g. the 6.280 MeV

alpha particle - 350 keV gamma ray coincidence) and to use this as a check throughout the run. The setting of the single channel analysers could be checked by the method described in section 3.4.

Fig. 3-11 shows the physical arrangement of the counters for the alpha-gamma coincidence experiment.

3.6 Angular correlation apparatus

To measure angular correlations (gamma-gamma and alpha-gamma) one counter remained fixed while the other one was moved at a constant distance from the source, in the same plane as the source and fixed counter, to determine the coincidence counting rate at various angles. The coincidence counting rate was determined by the apparatus described in sections 3.4 and 3.5. For the correlation measurements both single channel analysers were set on a single energy, be it alpha or gamma ray.

The physical arrangement for the gamma-gamma angular correlation measurement is shown in Fig. 3-12. The metal holder was used for foil sources and the plastic one for liquid sources (see section 2.3). Liquid sources were necessary because the gamma rays from the 400-430 keV peak which were compton scattered by the aluminum ring supporting the foil could enter the wide window of the single channel pulse height analyser. The window had to be made so wide

Figure 3 - 11

Physical arrangement of counters for alpha-gamma coincidence studies.

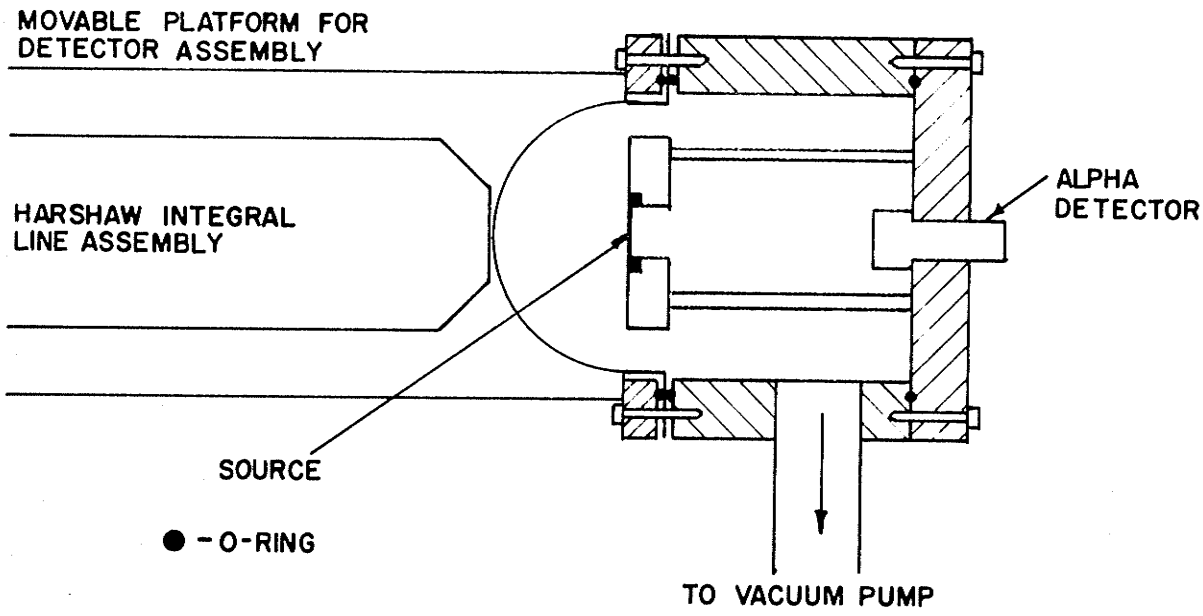
MOVABLE PLATFORM FOR
DETECTOR ASSEMBLY
HARSHAW INTEGRAL
LINE ASSEMBLY
ALPHA
DETECTOR
SOURCE
● - O-RING
TO VACUUM PUMP

because it had to include the intense 350 keV gamma ray. If the 350 keV gamma ray were not included in the window, slight shifts in the window position due to instabilities in the electronics could cause large changes in the single channel counting rates. These counting rates were used for normalization and hence had to be as accurate as possible. The position of the single channel pulse height windows (gates) is shown in Fig. 3-14. The liquid sources were weaker than the foil sources by a factor of 2 to 3. The 400 keV - 700 keV gamma-gamma angular correlation was examined with the stronger foil sources. Both source holders fit snugly on the center post so that the source was centered. The detectors used were the same as used for the gamma ray spectrum (see section 3.1) and were placed 10 cm. from the source. Both gamma detectors and pre-amplifiers were mounted on moveable trays centered at the source. Cylinders of iron were placed around the integral line units to eliminate gain shifts in the photomultiplier from the earth's magnetic field. Separate high voltage supplies were used for the photomultiplier tubes to eliminate interference between them. The performance of the system was checked by using a Co^{60} source whose gamma-gamma angular correlation is well known (S-26, 1955). The agreement was well within the experimental error.

The physical arrangement for the alpha-gamma angular correlation is shown in Figs. 3-13 and 3-13(a). The vacuum chamber consisted of a hollow brass cylinder closed at one end by a lucite plate at the center of which the alpha counter was mounted. The alpha detector was an Ortec SBBJ025-60 solid state detector which had a nominal active area of 25 sq. mm, a depletion depth of 105 microns at 50 volts bias, and a nominal resistivity of 850 ohm-cm. This allowed alpha particles with energies up to 14.25 MeV to be totally absorbed. The other end of the brass cylinder was closed by a hemispherical aluminum spinning and provision was made for mounting the activated foil supported on an aluminum ring at the center of the spinning. The gamma detector has been described previously (see section 3.1) and was mounted on a tray which was centered at the source. Because of scattering of gamma rays from the brass chamber the range through which the gamma ray counter could be moved was restricted to 108° - 252°. The gamma counter being the moveable one was surrounded by an iron cylinder to eliminate gain shifts in the photomultiplier tube from the earth's magnetic field. The gamma detector was placed 24 cm. from the source; however it still subtended a larger solid angle at the source than did the alpha counter.

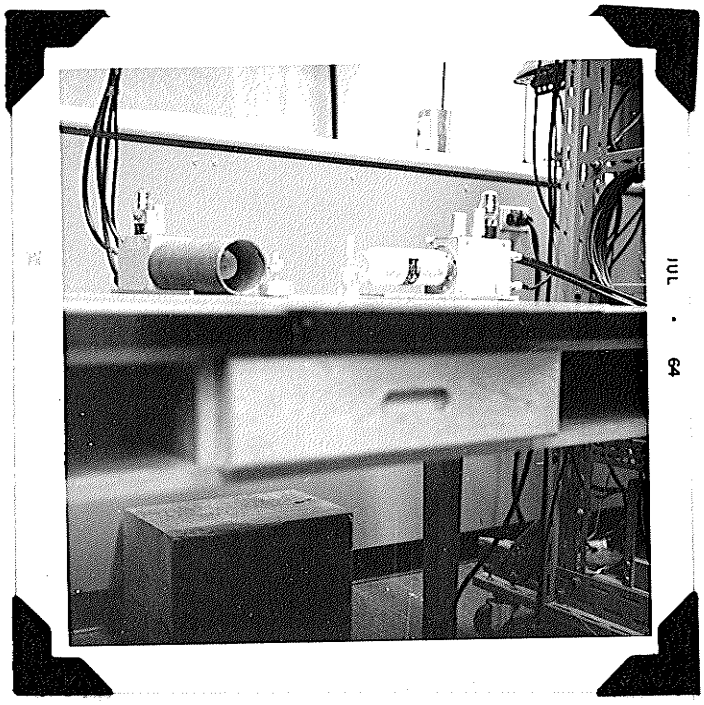

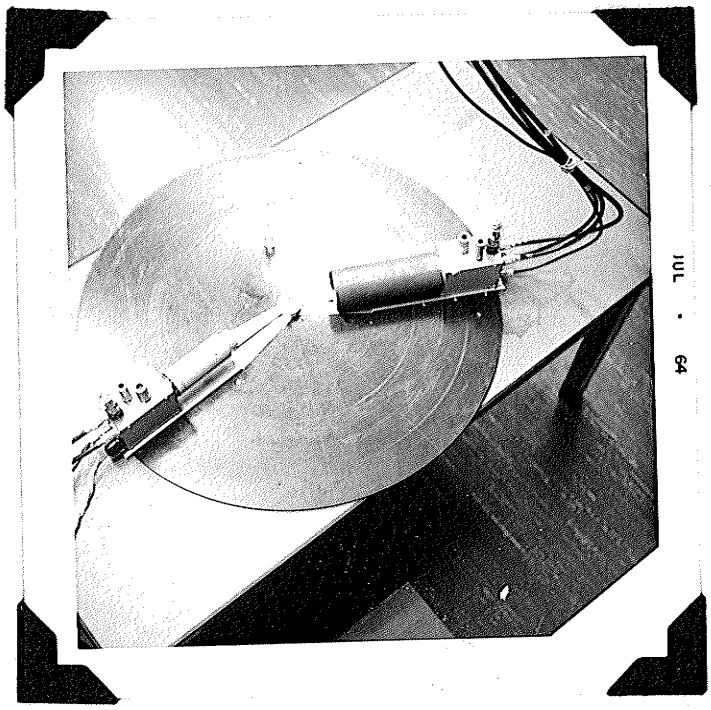

Fig. 3-12 Physical arrangement of the detectors for gamma-gamma angular correlations. The metal holder supported the foil sources and the plastic plug held a glass vial containing the liquid sources.

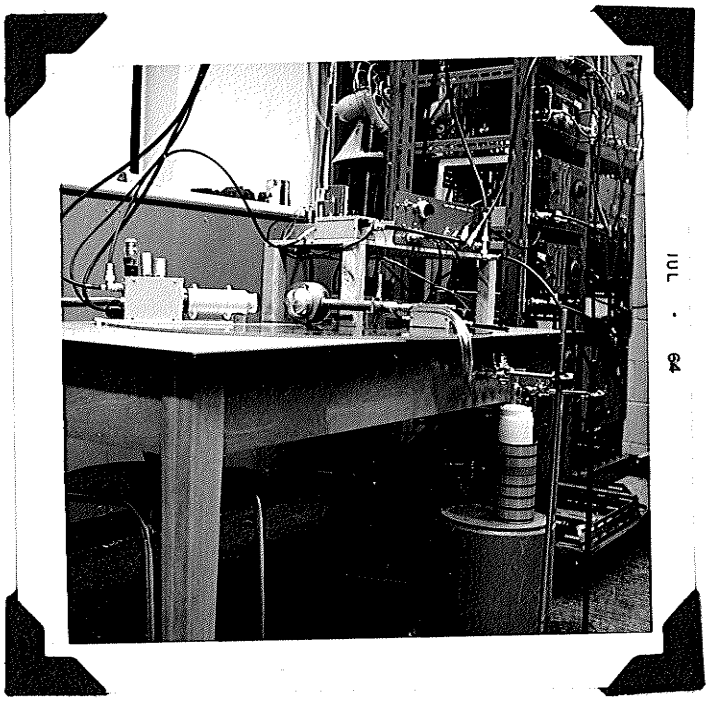

Fig. 3-13 Physical arrangement for the alpha-gamma angular correlation.

Figure 3 - 13(a)

Physical arrangement of the counters
for the alph-gamma angular correlation.

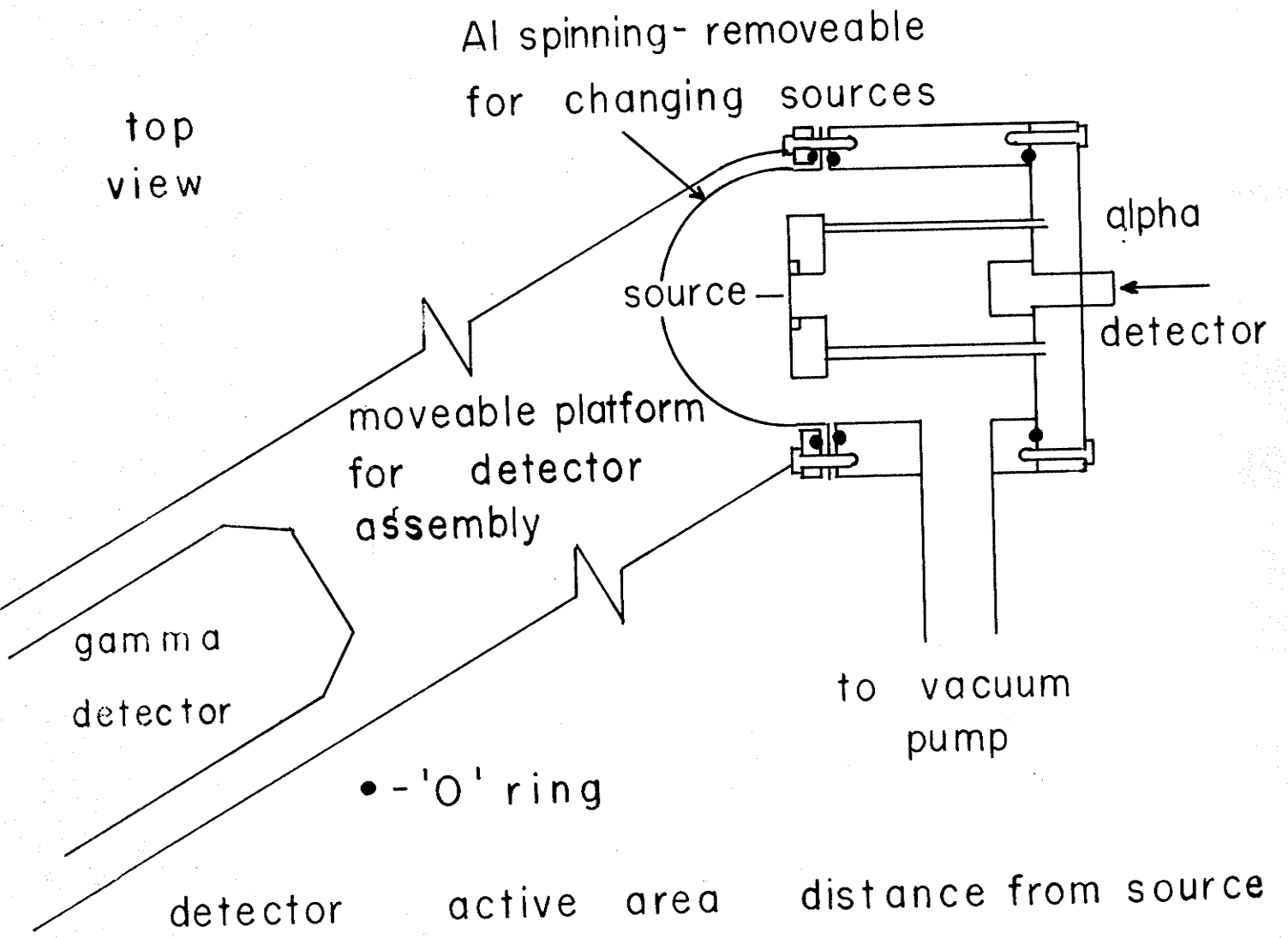

detector	active area	distance from source
alpha	25 mm^2	4.4 cm
gamma	1 1/2 in. diam	24 cm

Figure 3 - 14.

Typical gamma ray spectrum of the active deposit showing the position of the gates for the gamma-gamma angular correlation studies.

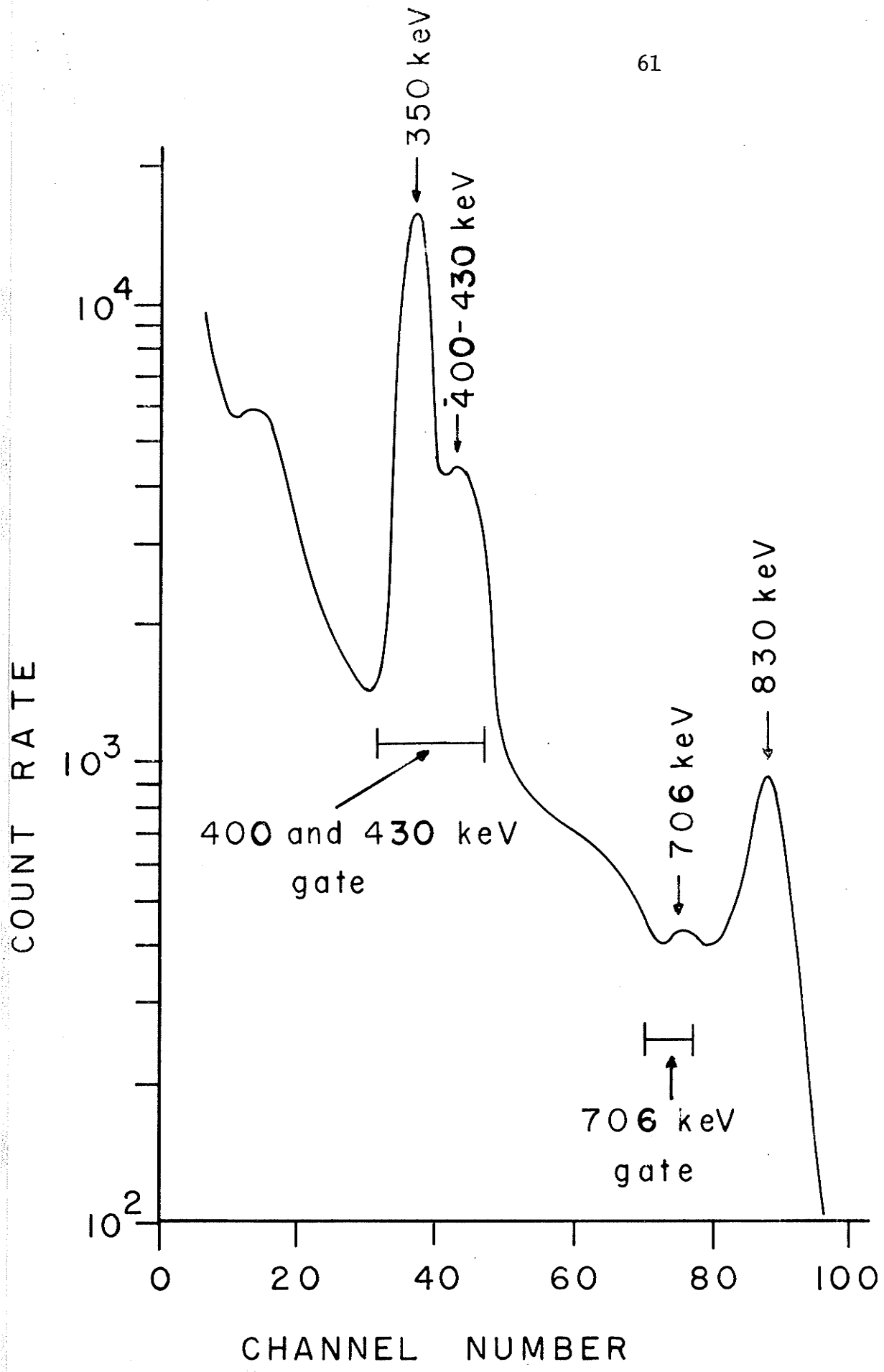
350 keV
400-430 keV
830 keV
706 keV
400 and 430 keV gate
706 keV gate
COUNT RATE
10^4
10^3
10^2
0
20
40
60
80
100
CHANNEL NUMBER

Chapter 4

EXPERIMENTAL RESULTS AND ANALYSIS

4.1 Introduction

The object of this work was to determine what radiations were emitted from the active deposit of the actinium series, their energies, relative intensities, and to which isotope they belonged. As an integral part of the decay scheme, spins and parities of excited states were determined through angular correlation and internal conversion measurements.

The following is an outline of how the above information was determined.

1) Alpha, beta, and gamma ray spectra showed the predominant radiations present and gave their energies and relative intensities. Weaker transitions were brought to light when they appeared in the coincidence spectra (see below). From the alpha particle relative intensities the branching ratios to the ground and first excited state of Tl^{207} were obtained as well as the alpha to beta branching ratio in the decay of Bi^{211} (see Fig. 4-1, S-21, 1958).

2) Internal conversion measurements determined the kind and multipolarity of the gamma radiations and were essential in determining the spins and parities of the

excited states. By knowing the K internal conversion coefficient of the 350 keV transition in Tl^{207} and the alpha branching ratio to Tl^{207}, all other internal conversion coefficients and absolute gamma ray intensities could be determined. This information led to the determination of the relative intensities and log ft values for the beta transitions in the decay of Pb^{211}.

3) Coincidence experiments were used to determine where each radiation fitted into the decay schemes of the various isotopes present. Gamma-gamma and alpha-gamma coincidence measurements were made. Alpha and gamma transitions not seen in the spectra of part (1) above were found. Also a double recoil experiment was performed to collect Tl^{207} in a pure state. This determined which gamma rays belonged to Pb^{207}.

4) Gamma-gamma and alpha-gamma angular correlations allowed spin and parity assignments to be made to some excited states.

5) Should there be other radiations present in these decays which were not detected, their intensities must be very small and upper limits for these intensities were calculated.

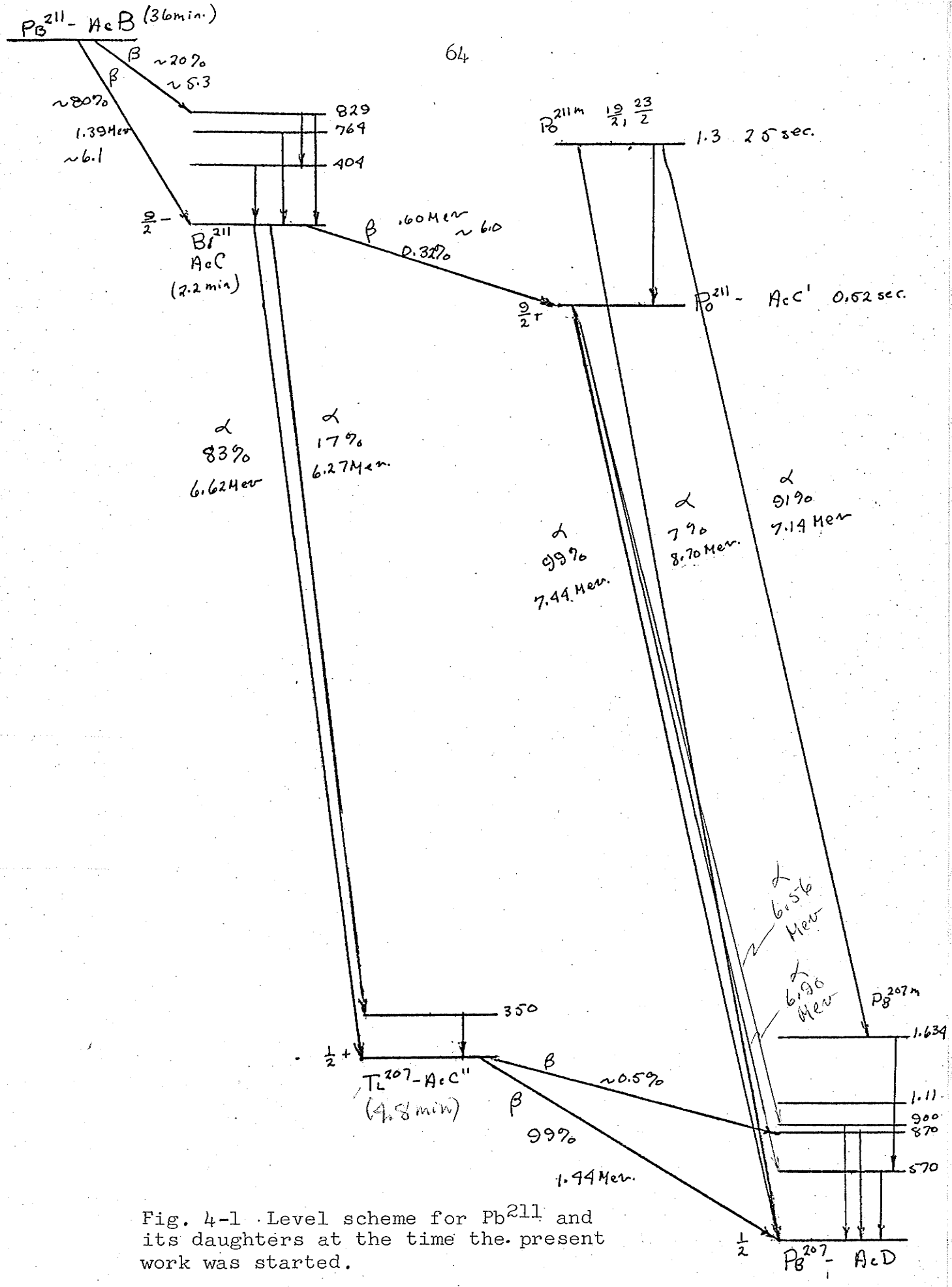

Fig. 4-1 Level scheme for Pb^{211} and its daughters at the time the present work was started.

4.2 Alpha particle spectra

The two alpha groups in the decay of Bi^{211} were the most dominant features of the alpha particle spectra. Using the thorium active deposit alpha particles as calibration, their energies were 6.618 ± 0.005 and 6.280 ± 0.005 MeV. One other alpha particle at 7.455 ± 0.005 MeV was easily observable. It was involved in the decay of Po^{211}. The alpha particle spectrum in the region of these groups is shown in Fig. 4-2. The search for any other possible alpha particles was done in two parts; the spectrum below the Bi^{211} alpha particle energies and the spectrum above them. All the work on the alpha particle spectra was done with highly polished stainless steel backings. Approximately 100 sources were used in the search for alpha groups. Each source backing was exposed to the actinon gas for 1 hr., left unexposed for 20 min. and then counted for 1 hr. The active area of the sources was 3/8 in. in diameter.

The energy range 3.00-5.72 MeV was searched carefully using several different stainless steel backings. (It was felt that no reasonable decay mechanism would yield an alpha particle with less than 3 MeV and the tail of the Bi^{211} alpha particles extended to approximately 5.7 MeV . The low energy tail of the strong alpha groups was in general four orders of magnitude down from the peaks.) This region was examined in eight parts, each of which spanned an energy range of about 350 keV. Thus each channel on the multichannel pulse height

Figure 4 - 2

Alpha particle spectrum showing the three main alpha groups in the active deposit of actinium.

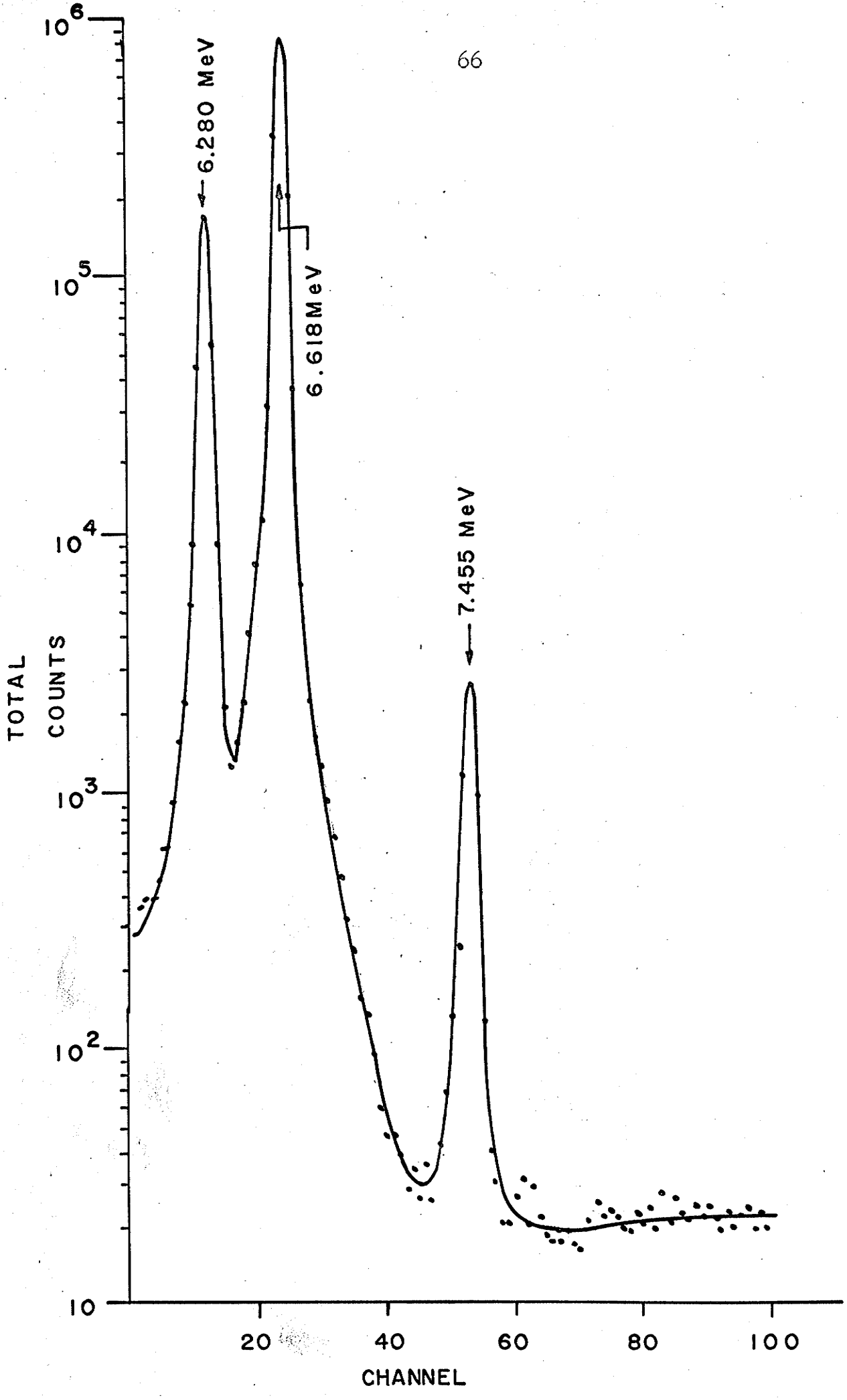
6.280 MeV
6.618 MeV
7.455 MeV
TOTAL COUNTS
CHANNEL
10
10^2
10^3
10^4
10^5
10^6
20
40
60
80
100

analyser represented about 3.5 keV. The pulse generator in the Ortec 203 amplifier was calibrated with the thorium active deposit alpha particles whose energies are well known and accepted standards, and then used as the calibration, because the spectrum had to be examined in segments containing no available alpha calibration energies. Since the resolution of the detecting system (counter and amplifiers) was approximately 45 keV a peak would span approximately 12 channels. A typical spectrum is shown in Fig. 4-3. The increase in counts in the high channels is attributed to the strong Bi^{211} alpha peaks (approximately 2×10^7 counts in that peak per channel for Fig. 4-3) and the increase at low channel number was attributed to backscattering from the stainless steel. It was expected that the backscattering of alpha particles would come from two places: (1) the source backing and (2) the counter. The source backing gave rise to a long gentle slope on the low energy side of a peak and alpha particles bouncing back out of the counter (approximately 100-200 micron depletion depth in the counter) gave rise to the increase at lower energies. The counting rates for these experiments was approximately 10^5 count/sec. The small peaks (see arrows on Fig. 4-3) occured at different energies for different source backings and were attributed to imperfections in the stainless steel.

There are some indications of peaks but these peaks were within the statistical error of the continuum on which they were sitting. Using the small peaks as a limit there were no alpha particles detected in the region 3.00-5.72 MeV with intensities greater than one part in 5×10^5 compared to the Bi^{211} alpha particles.

Figure 4 - 3

Typical low energy alpha particle spectra.

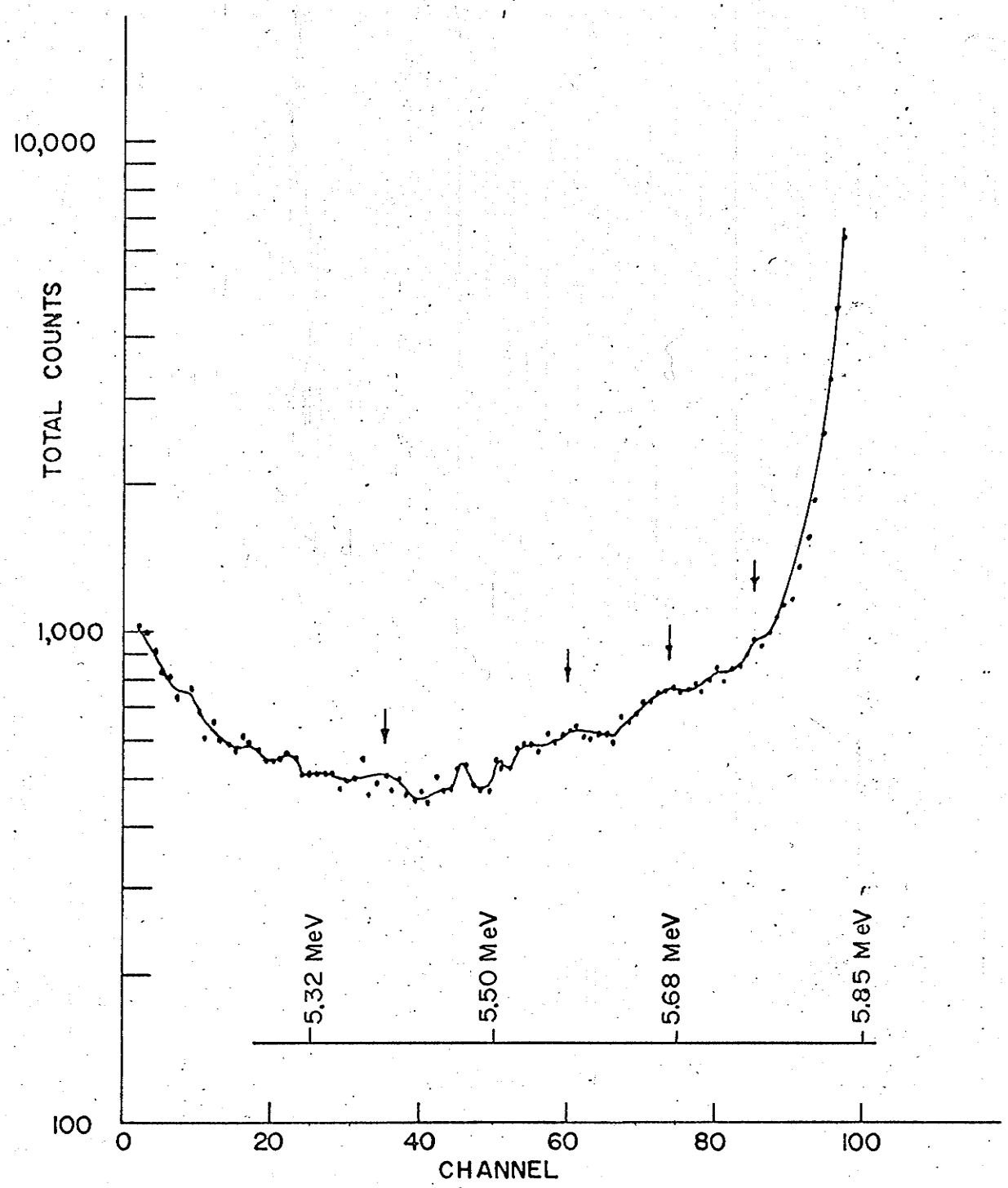
10,000
1,000
100
TOTAL COUNTS
0
20
40
60
80
100
CHANNEL
5.32 MeV
5.50 MeV
5.68 MeV
5.85 MeV

In checking for long lived contamination, four very weak peaks were observed (see Fig. 4-4) with approximately a 15 day half life. The spectrum shown in Fig. 4-4 is for an approximately 24 hr. period and thus would not contribute noticeably to the active deposit spectra in this energy region. These alpha particles were from AcX in the source which had entered by recoil due to the alpha decay of RaAc in the activation apparatus.

The 7.2 - 13.0 MeV energy range was also examined carefully with different stainless steel backings. The Bi^{211} alpha peaks extended to approximately 7.2 MeV. Not enough energy was available for the decay of an alpha particle with energy in excess of 8 MeV but the higher energies were included to look for electronic pileup. Because of the difficulty of calibration (the Ortec pulser did not go up that high in energy) the region could not be examined in small energy segments as in the lower energies. Three problems were encountered in this region.

1) In order to spread the energy range over the 100 channels either the signal had to be biased electronically or the alpha particle energies had to be degraded by the use of absorbers.

2) Electronic pileup, (two 6 MeV pulses coming so close in time that they look like one 12 MeV pulse), was significant at the high counting rates used (5×10^5 counts/sec.).

3) Contaminations were present in the source in the form of traces of thoron gas. It coated the chamber and counter with its active deposit.

Electronic biasing was rejected because it did not improve the pile up problem, leaving the use of absorbers as the best solution to the above problems. The following absorbers were used: 9.0 and 10.8 mg./cm.^{2} aluminum, 17.9 mg./cm.^{2} tin, and 7.45 and 8.05 mg./cm.^{2} of mica. A typical spectrum using absorbers is shown in Fig. 4-5. The peaks at 7.455 MeV and 8.78 MeV were identified as alpha particles because of their width and their shift in channel number upon the insertion of a thicker absorber. The 8.78 MeV alpha particle was due to traces of thorium active deposit in the source.

The other peaks in Fig. 4-5, here referred to as 'contamination peaks', are about 1/3 as wide as the true alpha particle peaks. (It should be noted that internal conversion lines show up roughly 1/3 as wide as alpha particle lines in the counter used.) However these 'contamination peaks' bear no resemblance to the internal conversion spectrum of the active deposit and cannot be due to alpha contamination on the foil because they are two narrow. Although the origin of these peaks has not been determined it seems reasonable to conclude from the following properties that they were not directly due to alpha, beta or gamma rays from the active deposit of the actinium series.

Figure 4 - 4

AcX(Ra^{223}) alpha particle spectrum seen as a long lived contamination in the active deposit sources. The spectrum was collected over about a 12 hour period.

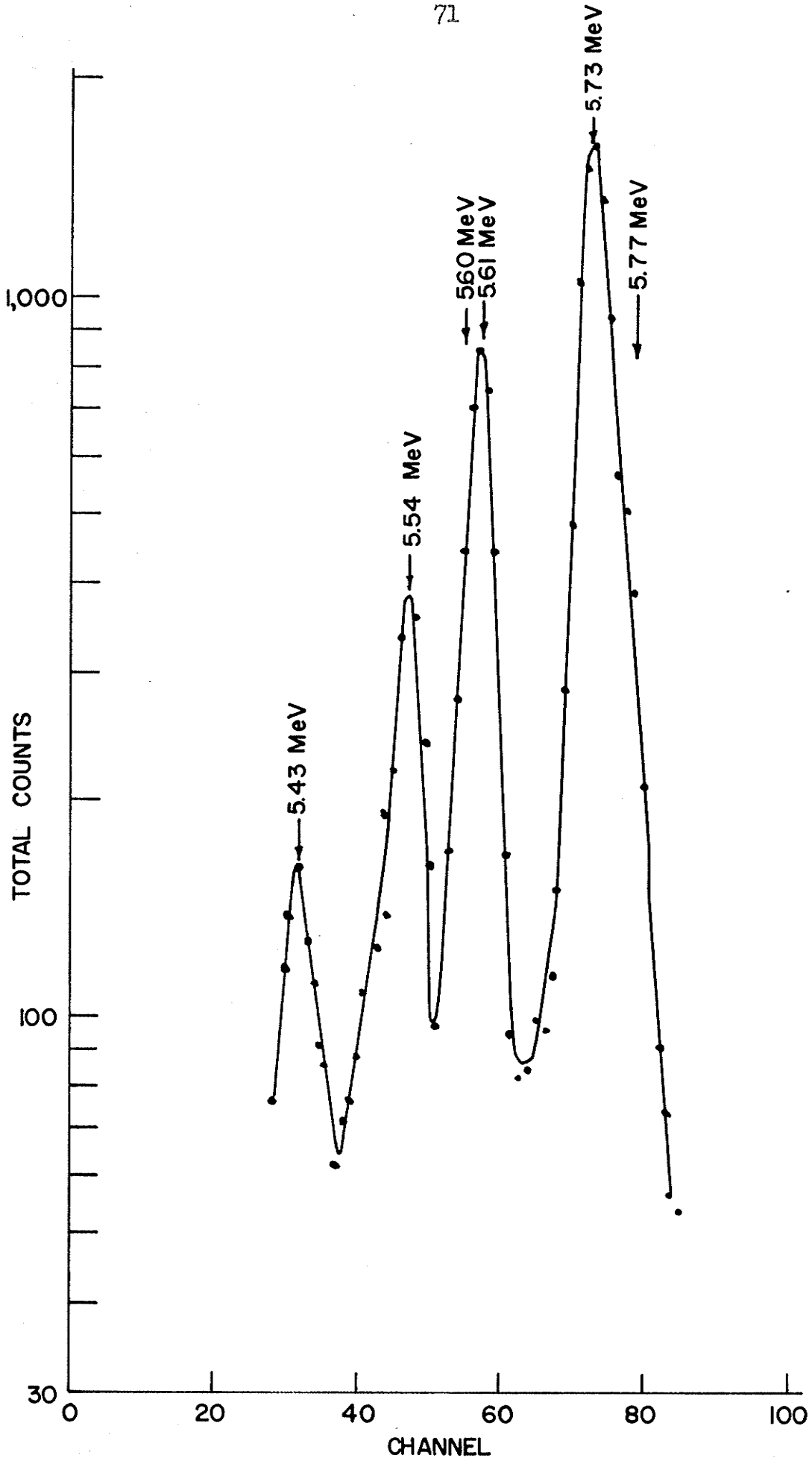
5.43 MeV
5.54 MeV
5.60 MeV
5.61 MeV
5.73 MeV
5.77 MeV
TOTAL COUNTS
1,000
100
30
0
20
40
60
80
100
CHANNEL

1) The half life of the 9.85 and 10.05 MeV peaks was approximately 1 hr. while that of the 10.5 and 11 MeV peaks was of the order of days and possibly longer (the energy assignment to these peaks was that of an alpha particle at that channel).

2) The four peaks fall at the same channel number regardless of which absorber or thickness was used.

3) The peaks remained when the source was removed but disappeared when the absorbers were removed.

This matter was not pursued further as the present investigation was concerned only with the active deposit of the actinium series.

Except for the 'contamination peaks', the 'thorium peak' at 8.78 MeV and the peak at 7.45 MeV no other peaks occur in the region 7.2 - 13.0 MeV with intensities greater than one part in 5×10^6 compared to the Bi^{211} alpha particle peaks.

Figure 4 - 5

Alpha particle spectrum of energies above 7 MeV for the active deposit.

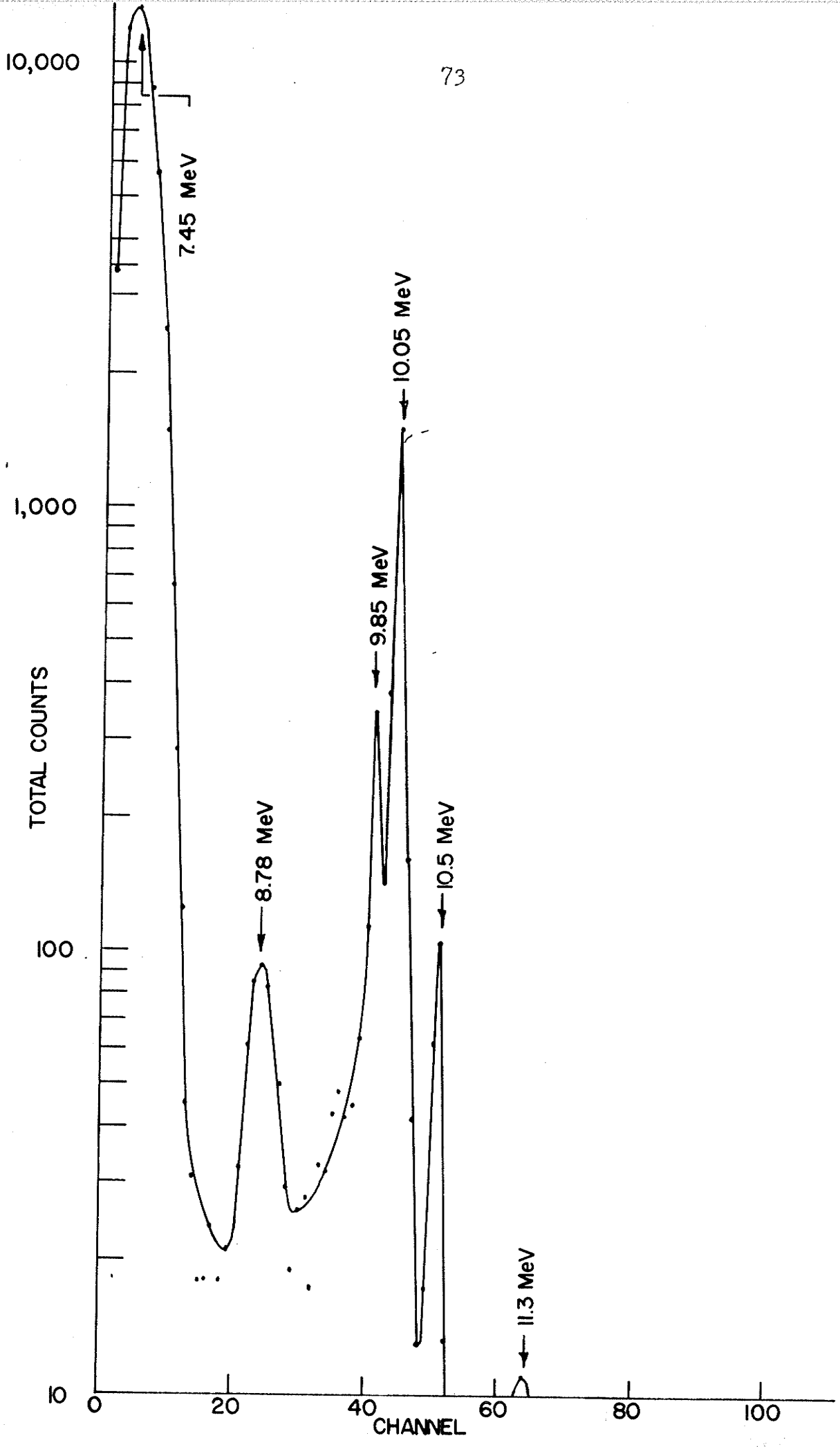
10,000
1,000
100
10
TOTAL COUNTS
7.45 MeV
8.78 MeV
9.85 MeV
10.05 MeV
10.5 MeV
11.3 MeV
0
20
40
60
80
100
CHANNEL

The energy range 6 - 8 MeV was displayed on the multichannel pulse height analyser to determine the relative intensities of the three main alpha particles. Since the resolution of the counter and amplifier was about 45 keV, the peaks spanned only two channels at half height. To get the total number of counts in each peak the number of counts in the six channels centered at the peak were added together. The only significant error (besides the statistical error) involved in this procedure was due to the additional counts on the low energy side of the peak from backscattered alpha particles, both from the peak being analysed and the higher energy peaks. (The contribution of the backscattering was about four orders of magnitude down from the peak height). This error was determined by assuming the shape of the alpha particle peaks to be symmetrical and observing the number of counts that fall outside the peak. The total number of counts in each peak are shown below

Energy (MeV)	Counts
6.618	1,379,515
6.280	266,550
7.455	4,687
total	,1,650,752

Therefore the relative intensities for the two alpha particles involved in the decay of Bi^{211} were 83.8 ± 0.2% (6.618 MeV) and 16.2 ± 0.2% (6.280 MeV). The relative intensity of the 7.455 MeV alpha particle in the decay of Po^{211} compared to the total intensity of all three alpha particles (6.618, 6.280 and 7.455 MeV) was (0.284 ± 0.005)%. The error for this calculation was smaller because the backscattering was not as serious (the strong alpha intensities are lower in energy). However it was known that the 7.455 MeV alpha particle represents 99% of the decay of Po^{211} (J-1, 1954) and thus the branching ratio is 1% larger than the relative intensity above. That is the beta branching ratio of Bi^{211} was (0.286 ± 0.005)%.

4.3 Gamma ray spectra of the active deposit and Tl^{207} - Determination of relative intensities.

(a) Active deposit.

The highest energy peak immediately visible in the gamma ray spectrum of the active deposit of the actinium series was one at 830 keV. The investigation, using the equipment discussed in section 3.3, involved taking the gamma spectra without absorbers and then with three different thicknesses of lead absorbers (3.958 gm./cm.^{2}, 7.937 gm./cm.^{2} and 11.911 gm./cm.^{2})(see Fig. 4-6). After correcting for the attenuation caused by the lead, one has four independent determinations for the relative intensities of the gamma rays.

The sources used for gamma ray spectra were collected on aluminum foil and were a few millimeters in diameter. The foil was exposed to the actinon gas for approximately 30 minutes, and then left unexposed for 20 minutes to allow transient equilibrium to develop. Data was usually taken for one hour at a time with each lead absorber.

Counting rates were deliberately kept low ($\sim$200 counts/sec.) to reduce the probability of electronic pileup (e.g. two 400 keV pulses coming so close in time that they appear as one 800 keV pulse). As a general rule data was taken until approximately 10^4 counts had piled up at the 830 keV peak making the statistical error $\pm 1\%$ or better for the spectrum.

Figure 4 - 6

Gamma ray spectrum of the active deposit of actinium up to 830 keV for three different lead absorbers. The method for determining the position of the constituent peaks is given in Section 4.3.

(a) no lead.

(b) 3.958 gm./cm.^{2} lead.

(c) 7.937 gm./cm.^{2} lead.

(d) 11.911 gm./cm.^{2} lead.

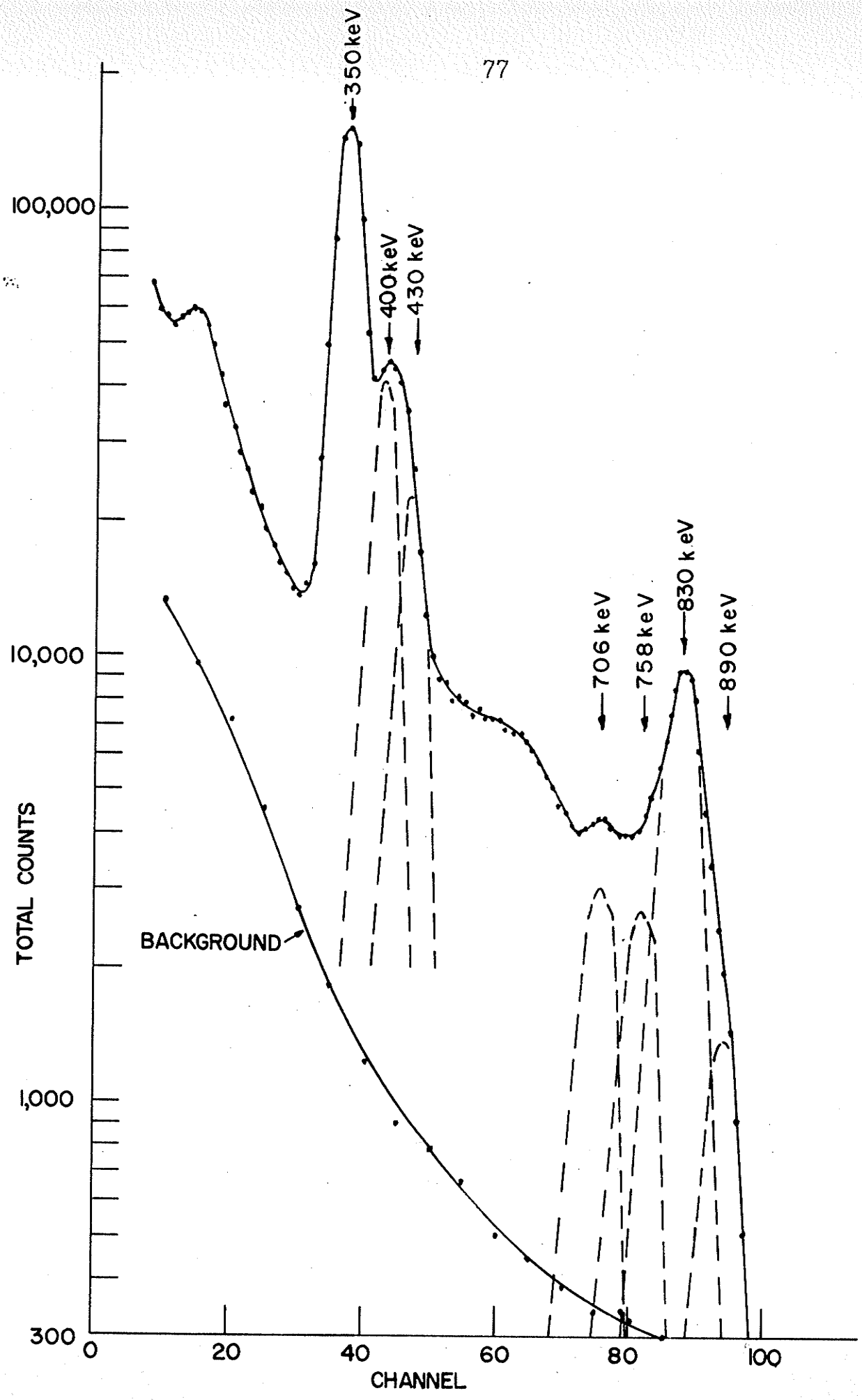
350 keV
400 keV
430 keV
706 keV
758 keV
830 keV
890 keV
BACKGROUND
100,000
10,000
1,000
300
TOTAL COUNTS
0
20
40
60
80
100
CHANNEL

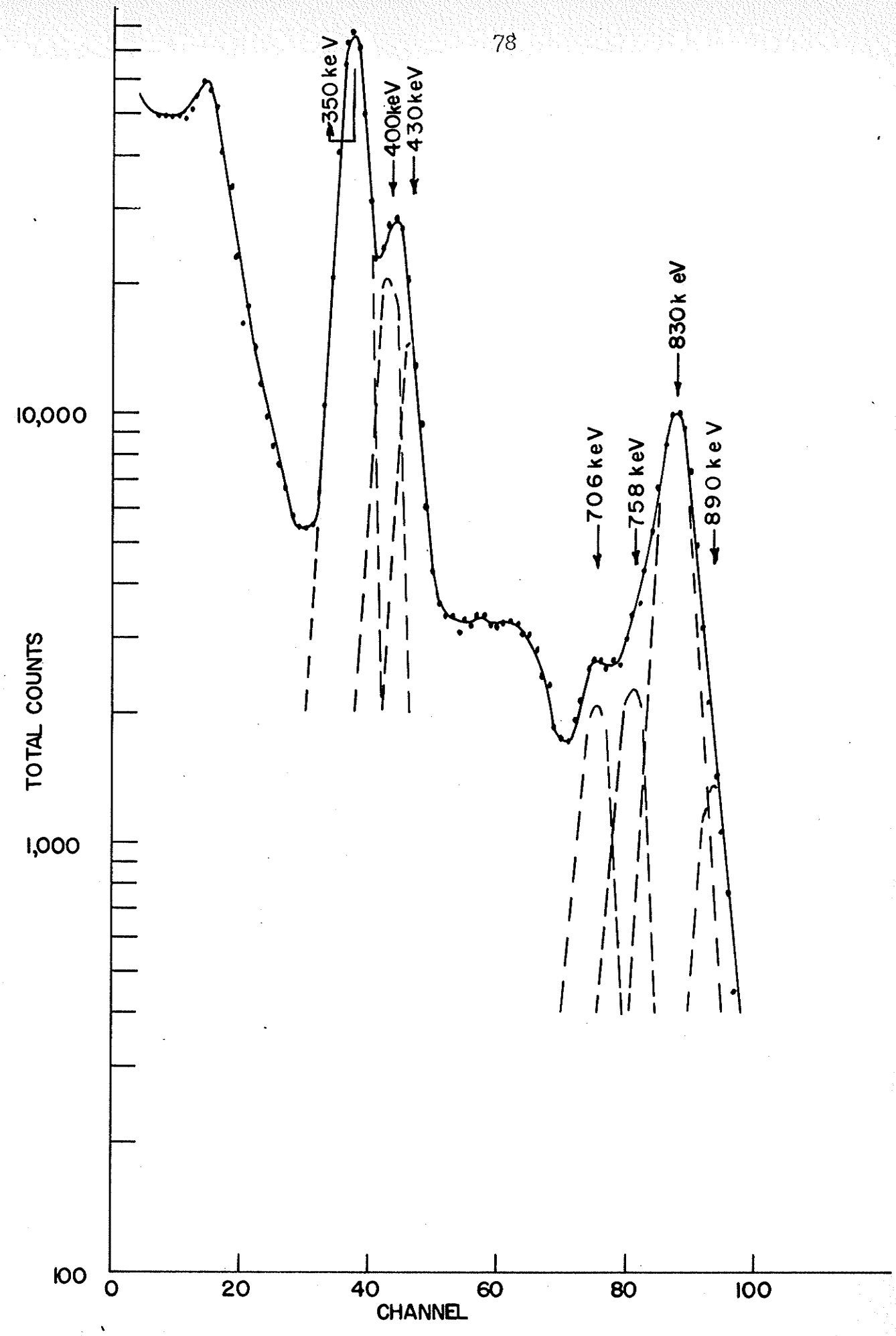
350 keV
400keV
430keV
706 keV
758 keV
830k eV
890 keV
10,000
1,000
100
TOTAL COUNTS
0
20
40
60
80
100
CHANNEL

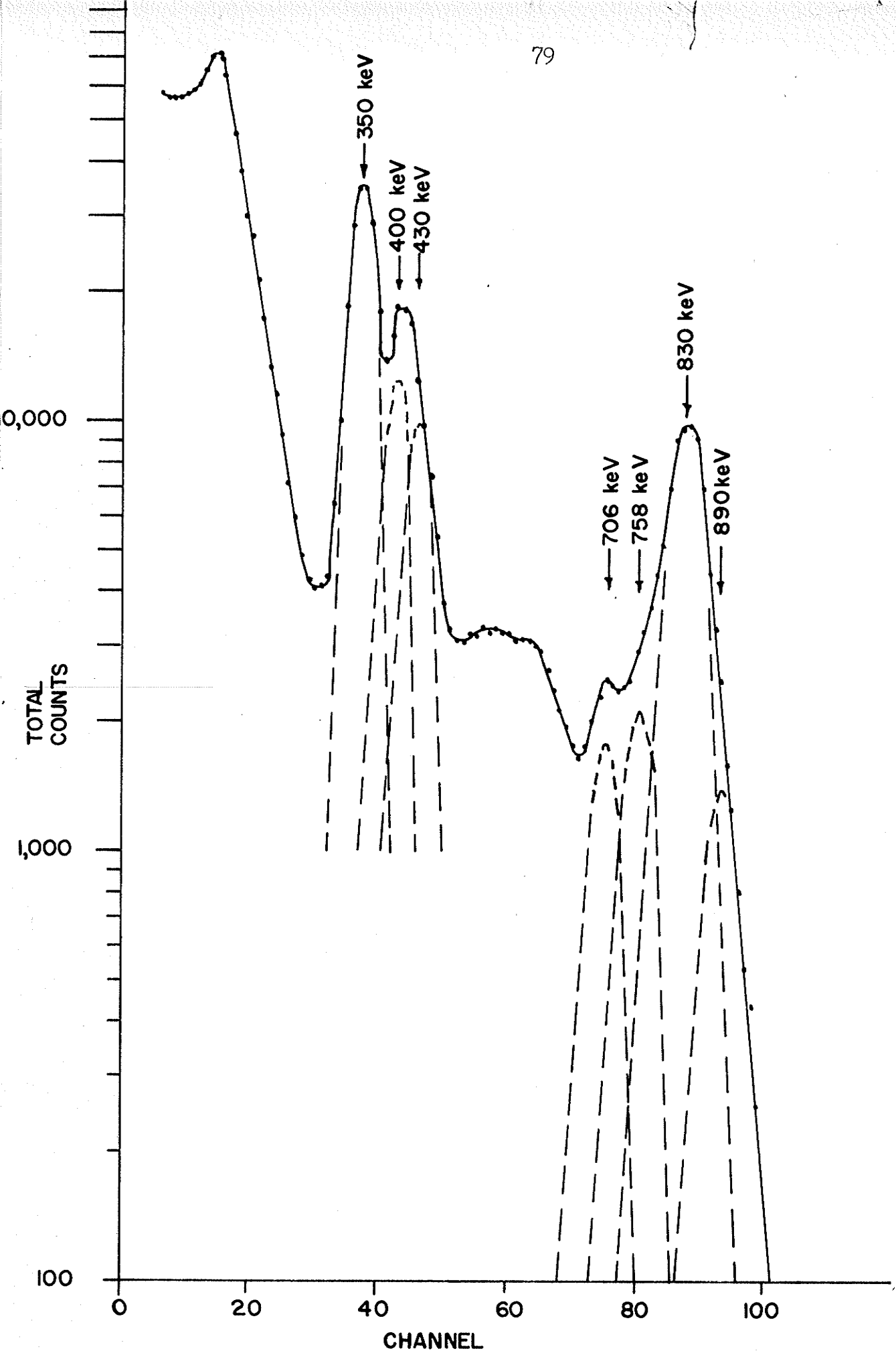
350 keV
400 keV
430 keV
830 keV
706 keV
758 keV
890keV
0,000
1,000
100
TOTAL COUNTS
0
20
40
60
80
100
CHANNEL

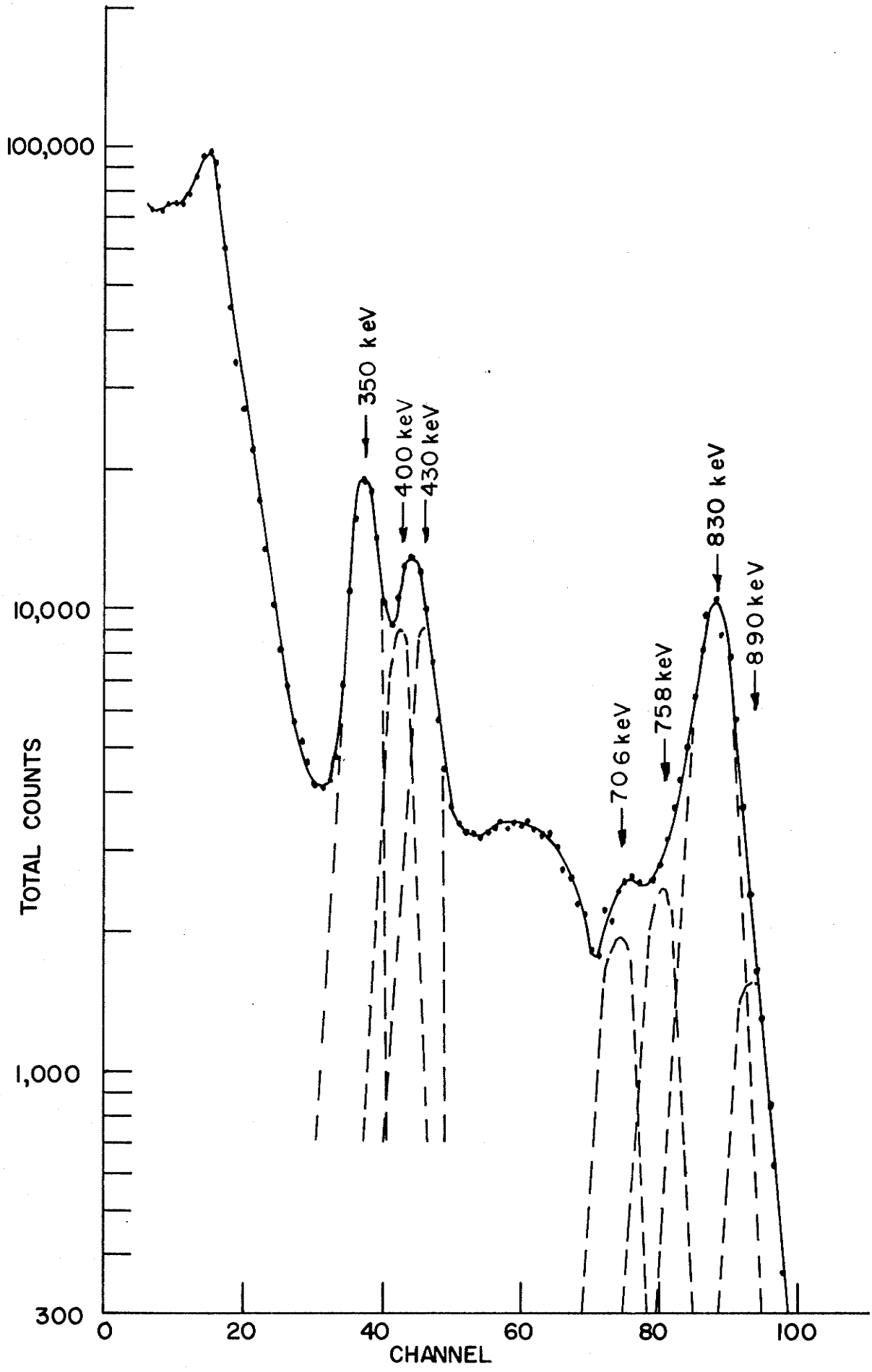
100,000
10,000
1,000
300
TOTAL COUNTS
0
20
40
60
80
100
CHANNEL
350 keV
400 keV
430 keV
706 keV
758 keV
830 keV
890 keV

Approximately 100 sources were used to obtain the gamma ray data presented in this section. Background data was collected in overnight runs (approximately 12 hr.) and have already been subtracted from the spectra presented here.

The region from 890 keV to approximately 2.5 MeV was carefully examined for any new gamma rays. Here the use of lead absorbers has an additional advantage. As the absorbers are made thicker higher energy gamma rays become more intense relative to lower energy gamma rays. When 19.821 gm./cm.^{2} of lead absorbers was used, two new gamma rays at approximately 1.1 MeV appeared (see Fig. 4-7). No peak was seen in the region 1200 keV to 2500 keV with intensity greater than 40 counts in 1000 compared to the composite peak at 1100 keV (or greater than 1 part in 10^3 compared to 350 keV gamma ray) (see Fig. 4-8 which shows the result of background subtraction for the region from about 1200 keV to 2200 keV corresponding to Fig. 4-7.)

The gamma ray calibration isotopes use in this experiment were Cr^{51} - 325 keV, Au^{198} - 411 KeV, Na^{22} -511 and 1280 keV, Cs^{137} -662 keV and Mn^{54} -840 keV. The energies of the gamma rays found directly in the active deposit of the actinium series were 1100 ± 18, 1060 ± 18, 890 ± 7, 758 ± 7, 706 ± 7, 430 ± 7, 400 ± 7 and 350 ± 7 keV.

Figure A - 7

Gamma ray spectrum of the active deposit
of actinium (energy range 830-2500 kev).
The absorber used was 19.821 gm./cm.^{2} of lead.

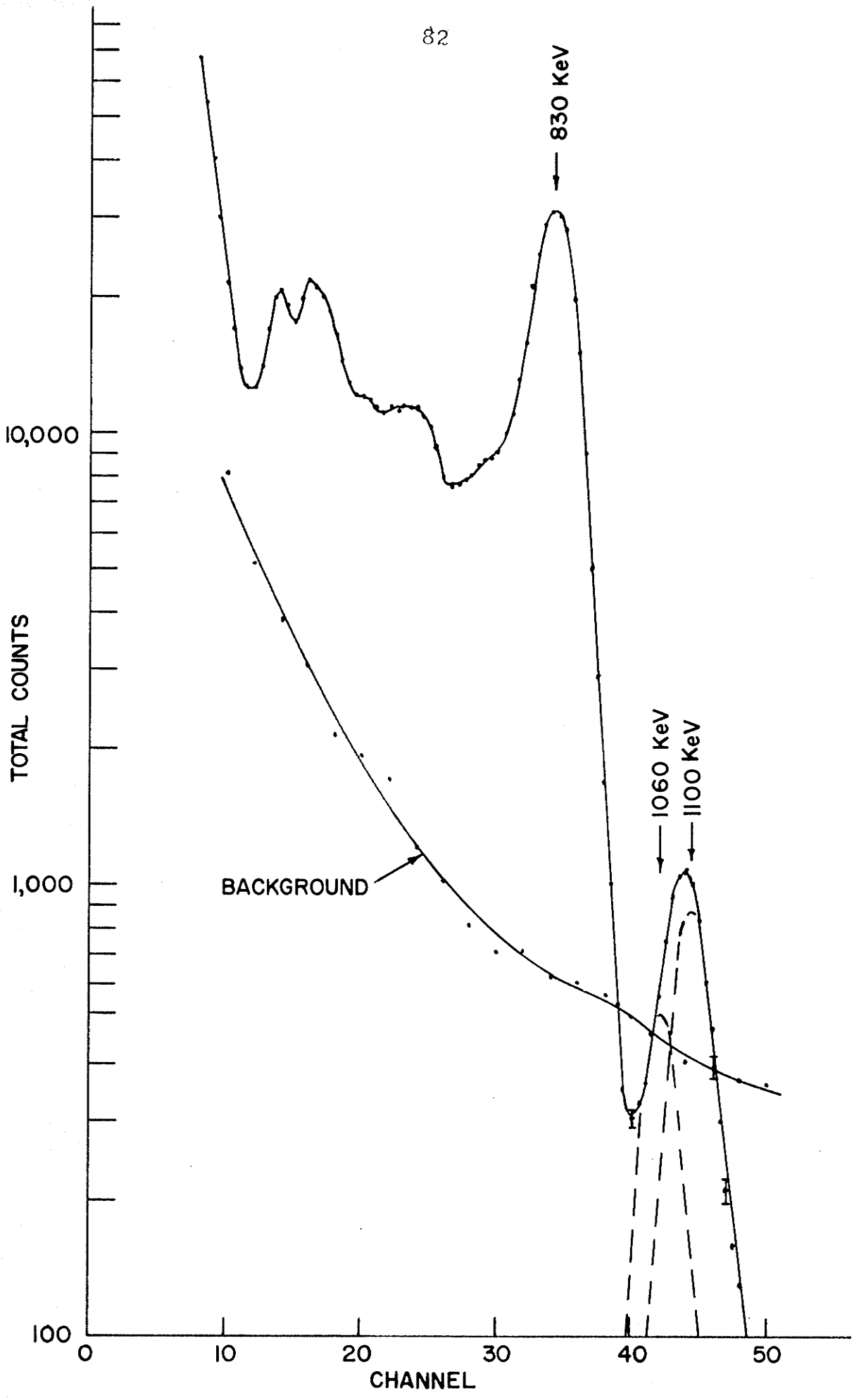
830 KeV
1060 KeV
1100 KeV
BACKGROUND
10,000
1,000
100
TOTAL COUNTS
0
10
20
30
40
50
CHANNEL

Figure 4 - 8

Difference between the spectrum and background for the region above the composite peak at 1100 keV in Fig. 4-7.

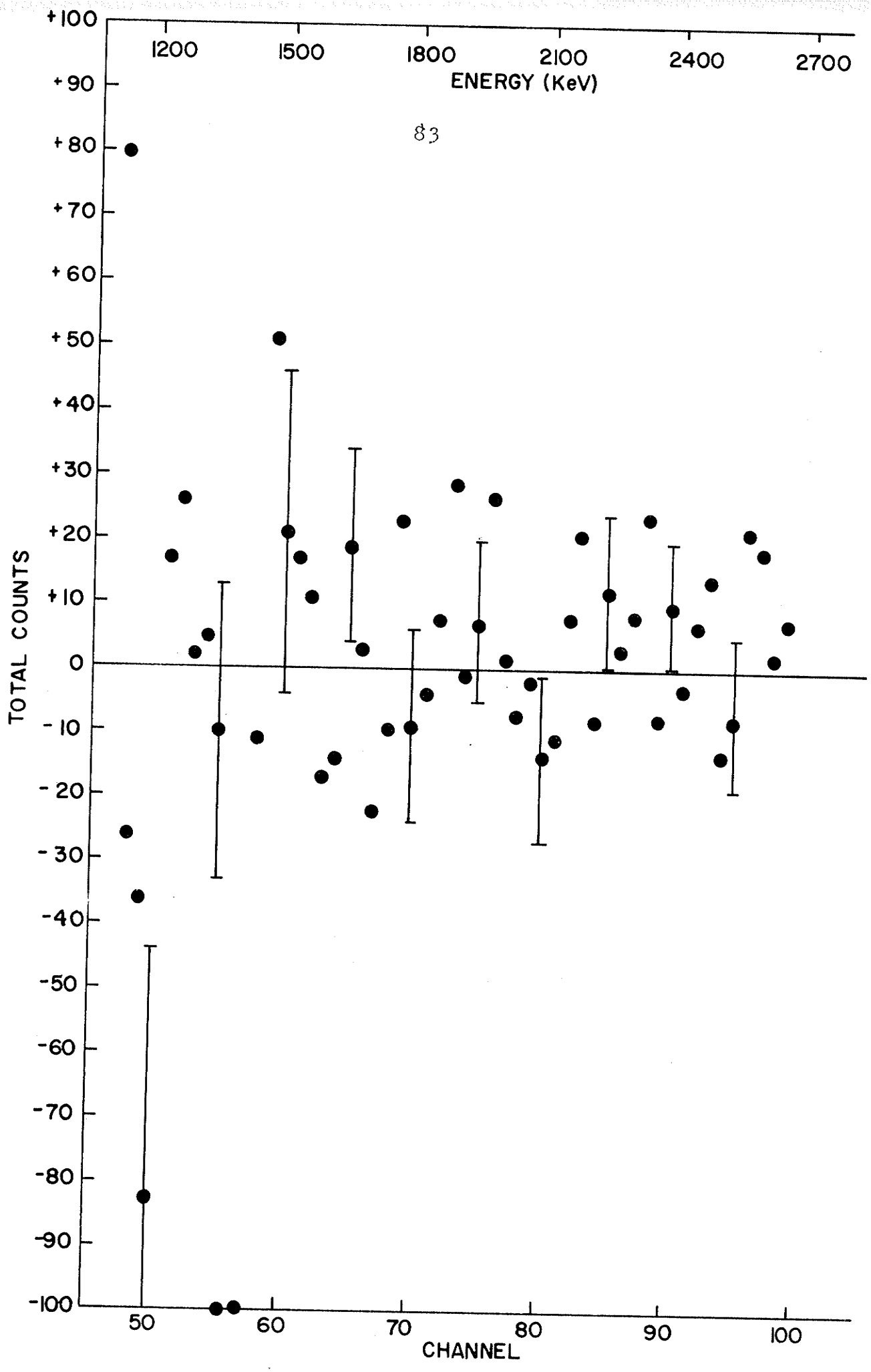
+100
+90
+80
+70
+60
+50
+40
+30
+20
+10
0
-10
-20
-30
-40
-50
-60
-70
-80
-90
-100
TOTAL COUNTS
1200
1500
1800
2100
2400
2700
ENERGY (KeV)
50
60
70
80
90
100
CHANNEL

The gamma ray scintillation spectra shown in Fig. 4-6 indicate that the spectrum of the actinium active deposit, hereafter called the complex spectrum, was made up of several gamma rays. This section shows how the number and relative intensities of the constituent gamma rays were determined.

After the background was subtracted, the complex spectra (for each lead absorber used) and the calibration gamma ray spectra were plotted on separate sheets of semi-log graph paper. A large box lit from the interior and having a translucent sheet of glass on the top was used to visually compare the complex spectra with the spectra of the various calibration sources. The procedure starts with the highest energy gamma ray, which for the present work was the 1060-1100 keV combined peak. To determine whether the peak was due to one or more than one gamma ray, the complex spectrum peak was compared to a calibration peak, known to be due to only one gamma ray (monoenergetic) and nearby in energy. If the peak in the complex spectrum was wider than the calibration peak, it must have been composed

of more than one gamma ray. If the highest energy gamma ray in the complex spectrum was a single transition the curve from the calibration source was drawn to fit exactly on the peak in the complex spectrum. Point by point (channel by channel) the entire calibration spectrum (including Compton distribution) was subtracted from the complex spectrum ('peeled off'). This procedure was then carried out for the next lowest energy gamma ray in the complex spectrum using a monoenergetic calibration gamma ray whose energy was near the peak in the complex spectrum that was being analysed. The procedure was continued until all counts in the spectrum had been accounted for. However, if two or more gamma rays made up a peak in the complex spectrum the analysis became more difficult. Trial and error must determine whether two or more of the calibration peaks could give rise to the peak in the complex spectrum (it was not unusual for such a result to be unique). When the number of single peaks fitting under the compound peak in the complex spectrum and their relative positions (intensities) were determined, each one was subtracted from the complex spectrum. When the above procedure had been carried out, all the spectrum was accounted for (including the Compton distribution). If counts were left in the spectrum, the relative intensities of the gamma rays were

incorrect. The above procedure was carried out for the gamma ray spectrum of the actinium series active deposit for the different lead absorbers. The 'peeling off' procedure is demonstrated in Fig. 4-9. The photopeaks of the unpeeled gamma rays were plotted on linear graph paper and their relative areas found by a planimeter. These areas were corrected for efficiency of the detector, peak to total area ratio (see section 3.3) and for the absorption due to lead. In table 4-1 ϵ is the relative efficiency and r the relative ratio of the number of counts in the photopeak to the number of counts in the total spectra (photopeak plus Compton distribution). These quantities are thoroughly tabulated (M-13, 1958). In the table (4-1) μ is the x ray absorption coefficient (N-6, 195) and x the thickness of lead absorber used.

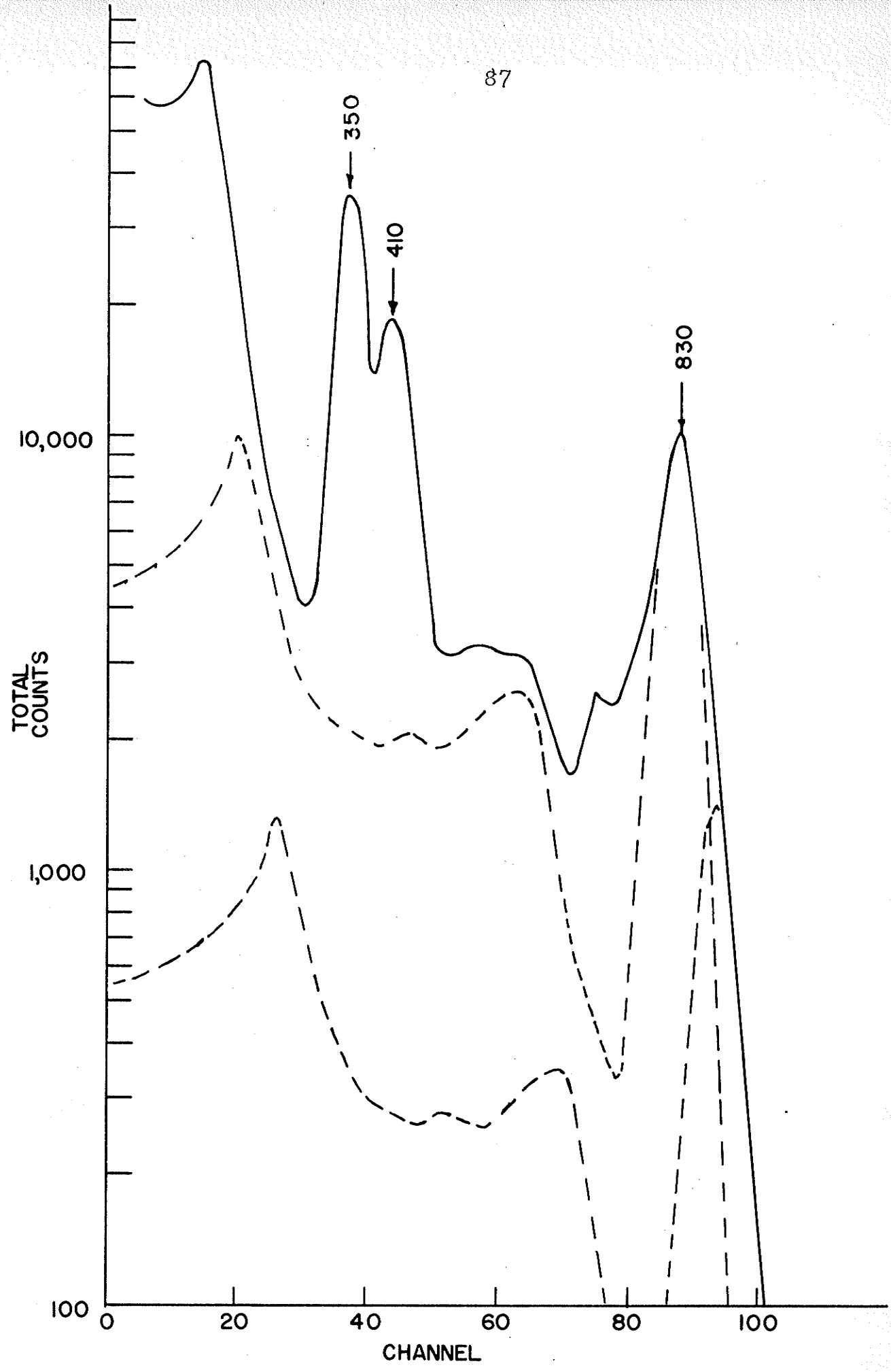
350
410
830
10,000
1,000
100
TOTAL COUNTS
0
20
40
60
80
100
CHANNEL

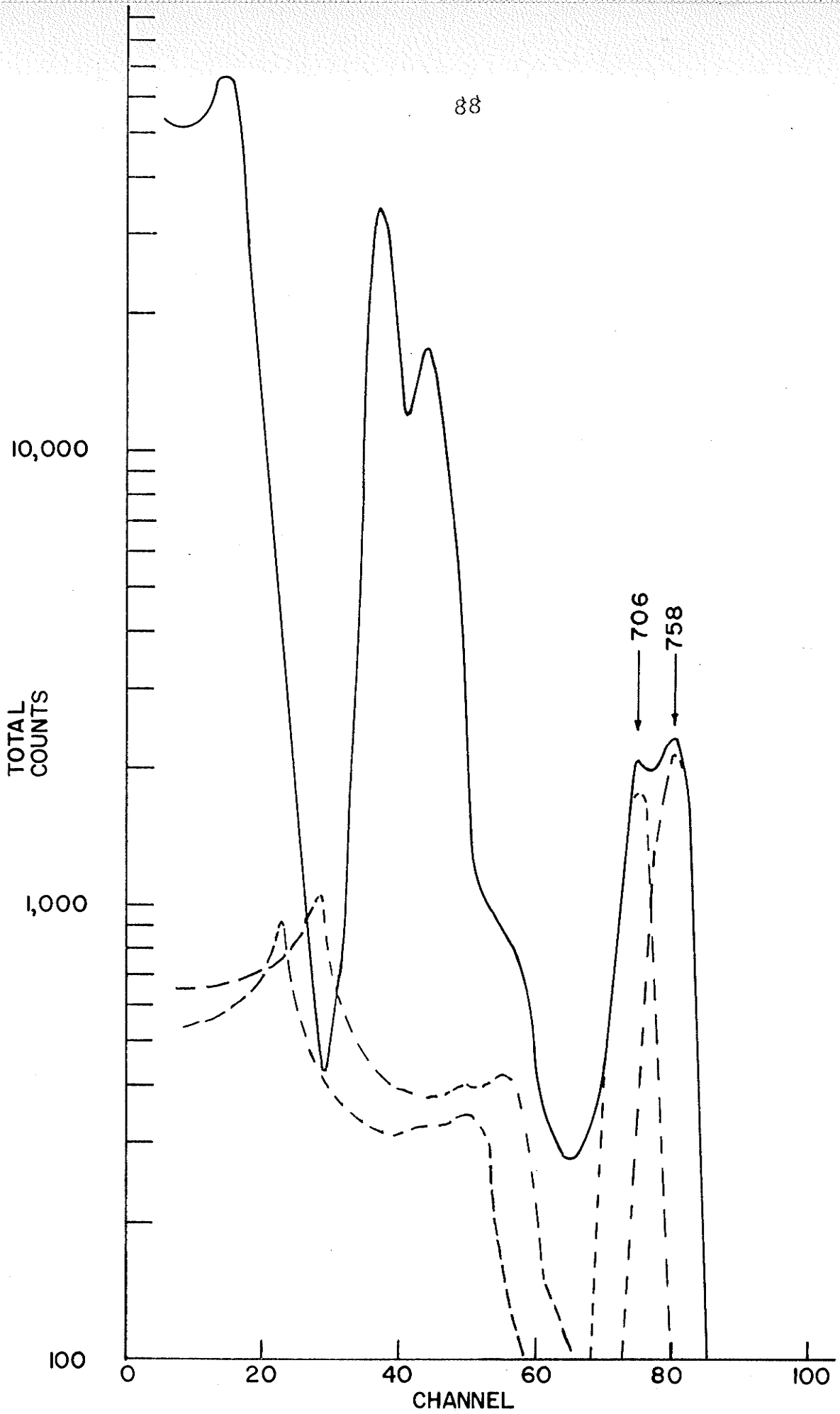
10,000
1,000
100
TOTAL COUNTS
706
758
0
20
40
60
80
100
CHANNEL

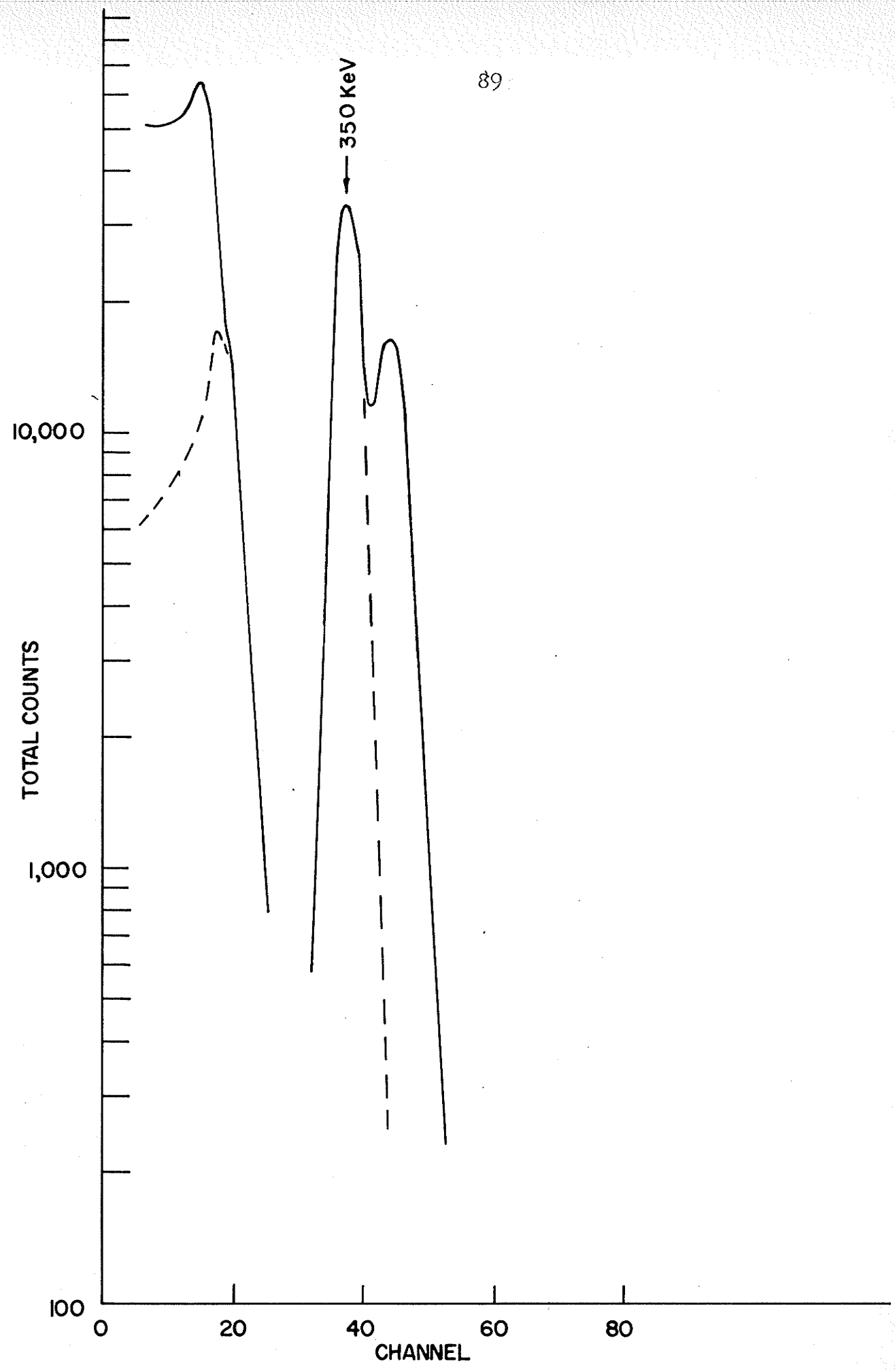
350 KeV
10,000
1,000
100
TOTAL COUNTS
0
20
40
60
80
CHANNEL

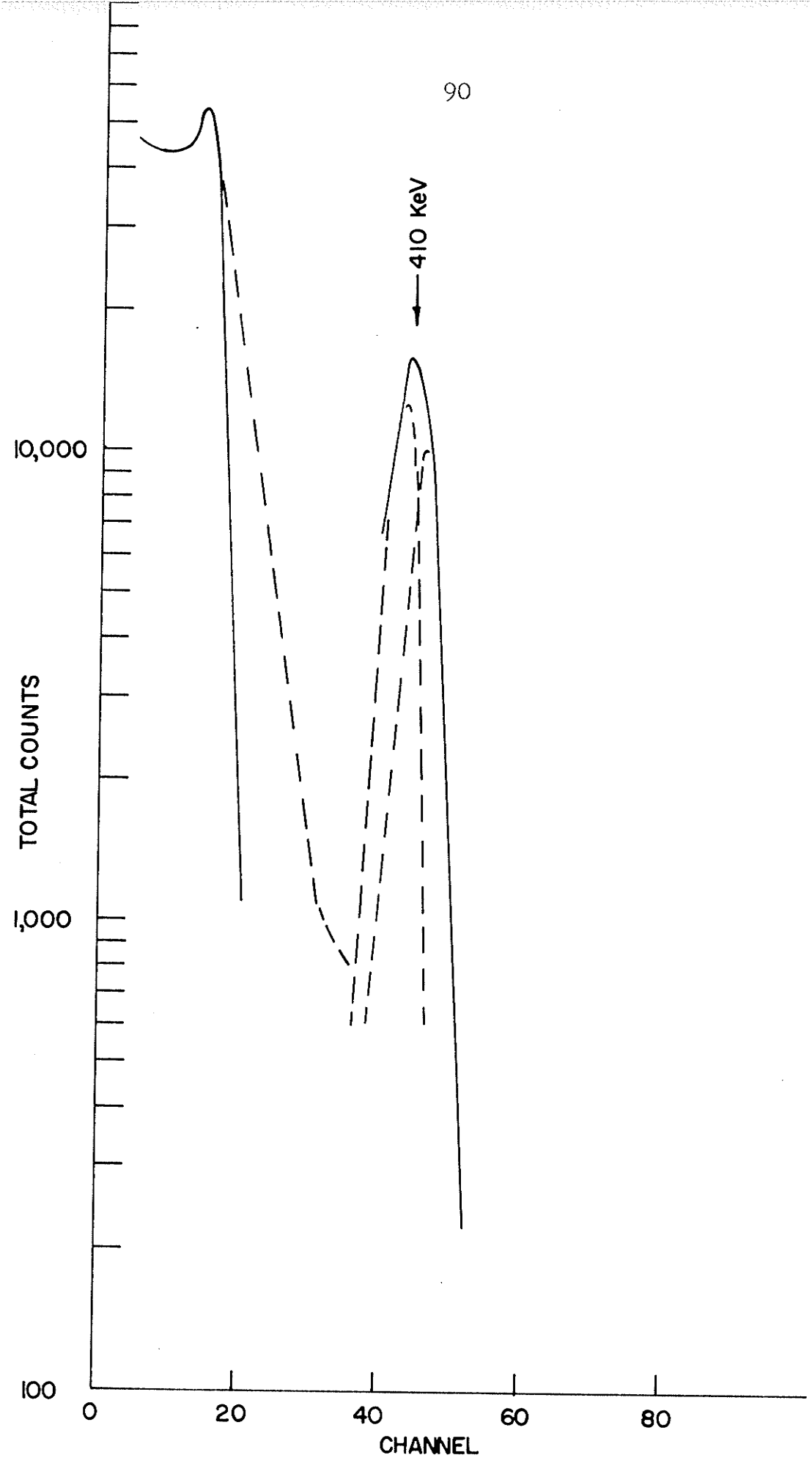
410 KeV
10,000
1,000
100
TOTAL COUNTS
0
20
40
60
80
CHANNEL

TABLE 4-1

Pb absorber (gm./cm2)	Energy (keV)	ϵ_r	Relative area	$\left(\frac{\text{rel. area}}{\epsilon_r}\right) e^{\mu x} \times 10$	Normalized to 350 keV intensity
none	350	.350	254.0	72.45	1.000
	400	.286	71.6	25.03	0.345
	430	.255	37.2	14.62	0.202
	706	.122	6.0	4.92	0.068
	758	.110	5.52	5.02	0.069
	830	. 955	18.9	19.47	0.269
	890	.0860	3.3	3.82	0.053
3.96	350	.350	121.0	102.4	1.000
	400	.286	36.0	28.35	0.277
	430	.255	25.0	20.64	0.202
	706	.122	4.86	5.83	0.057
	758	.110	5.42	6.98	0.068
	830	.0955	19.6	27.41	0.268
	890	.0860	2.72	4.28	0.042
7.94	350	.350	50.6	127.4	1.000
	400	.286	20.8	36.99	0.290
	430	.255	16.5	28.95	0.227
	706	.122	3.55	6.23	0.049
	758	.110	4.2	7.65	0.060
	830	.0955	20.0	39.88	0.313
	890	.0860	3.0	6.49	0.051

TABLE 4-1

Pb absorber ($gm./cm.^2$)	Energy (keV)	ϵr	Relative area	$\left(\frac{\text{rel.area}}{\epsilon r}\right) e^{\mu x} \times 10$	Normalized to 350 keV intensity
11.91	350	.350	30.4	228.1	1.000
	400	.286	19.4	78.08	0.342
	430	.255	14.9	54.77	0.240
	706	.122	4.20	10.80	0.047
	758	.110	5.16	13.39	0.059
	830	0.0955	20.9	57.46	0.252
	890	.0860	3.34	9.93	0.044
19.82	830	.0955	124.0	649.0	0.276
	1060	.0660	2.28	12.50	0.0053
	1100	.0625	3.84	20.82	0.0088

To obtain relative intensities for the gamma ray energies up to 890 keV a simple average was taken of the relative intensities determined for the four absorber situations: 1) no lead, 2) 3.958 gm./cm.^{2} lead, 3) 7.937 gm./cm.^{2} lead and 4) 11.911 gm./cm.^{2} lead. It will be noticed that the relative intensities determined using different absorbers are in excellent agreement with one another. The greatest divergence from the mean values shown below is 12% so conservatively it can be said that the relative intensities of the γ-rays are known to ±10%. An approximate error value of ±20% was put on the relative intensities of the 1060 and 1100 keV gamma rays. The results of averaging the values in table 4-1 is shown below.

Energy	Intensity (relative to the 350 keV gamma ray)
400	0.31
430	0.22
706	0.055
758	0.064
830	0.28
890	0.048
1060	0.0053
1100	0.0088

(b) $\underline{Tl^{207}}$

Tl^{207} was collected as a recoil product from the decay of Bi^{211} in the active deposit. A collection foil (standard 1.8 mg/cm.^{2} aluminum) was mounted close (approximately 1 cm.) to a foil containing the active deposit and given a potential of -1600 volts with respect to the active deposit foil. This allowed the preparation of foils containing Tl^{207} with an activity of approximately 40% compared to the active deposit itself. After the Tl^{207} had been collected in this way for approximately 10 minutes it was exposed to the NaI(Tl) crystal (with photomultiplier tube, amplifier and multichannel pulse height analyser as described in section 3.3) for about two half lives (approximately 10 min.) during which time another Tl^{207} foil was being prepared. After 10 min. the Tl^{207} foils were interchanged. Data could be collected in this way for about 1 hr. after which time the active deposit foil was down in activity by two half lifes and was replaced by a fresh one. One gamma ray

was detected in the decay of Tl^{207} at 900 keV(see Fig. 4-10). It decayed with approximately a 5 minute half life(the half life of Tl^{207} is 4.8 minutes). Great care was taken in determining the energy of this gamma ray as an 890 keV gamma ray had already been seen in the active deposit. The value of the gamma ray energy and error was 900±7 keV determined on five separate runs. About 20 sources were needed to conduct this investigation. The spectra of Figs. 4-7 were taken with uncovered sources and it is known by direct observation that 30% of the Tl^{207} is lost by recoil from such sources. Hence any peaks in the gross spectrum due to the decay of Tl^{207} are that much weaker than they would have been had the source been covered. There is no evidence which leaves one to believe other than that the 890±7 keV transition seen in the total active deposit spectrum is the same transition as that which was assigned the energy 900±7 keV in the decay of Tl^{207}.

Figure 4 - 10

Gamma ray spectrum of a separated source of Tl^{207}.

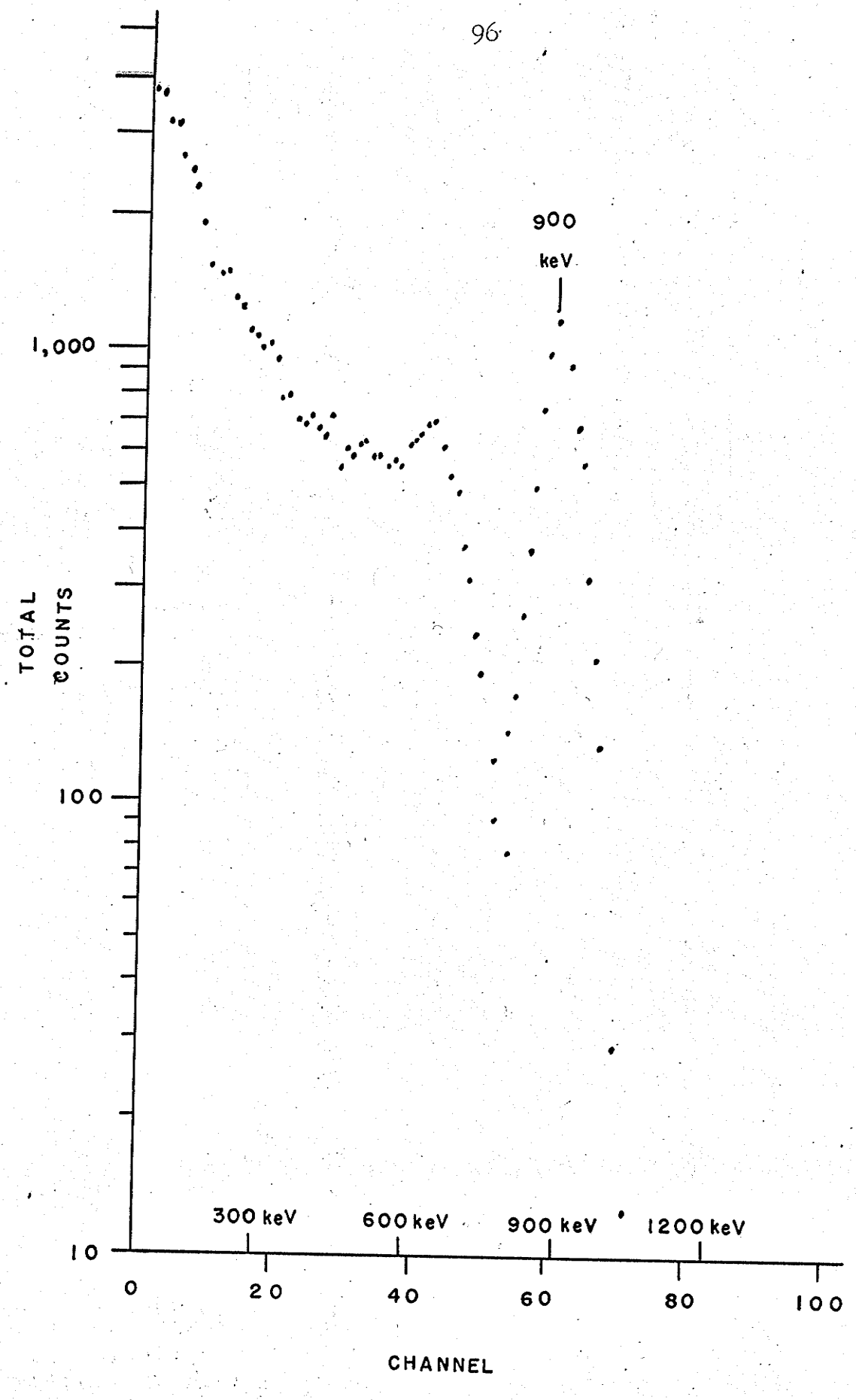
900
keV
1,000
100
10
TOTAL
COUNTS
300 keV
600 keV
900 keV
1200 keV
0
20
40
60
80
100
CHANNEL

4.4 Beta Ray spectra

Because of the short half life of Pb^{211} (36 min.) the entire beta continuum could not be recorded with the use of just one source. In fact 60 sources were needed to determine the continuum. To obtain reasonable statistics, the spectrometer baffles were opened to give 1% resolution. A minimum of 10^3 counts were taken at each momentum setting giving an overall statistical accuracy of at least±3%. The continuum was examined in approximately 20 adjacent segments each approximately 60 keV wide and was recorded. The continuum was recorded twice in order to overlap the segments. The raw data was corrected for background and decay (by multiplying by $e^{\lambda t}$ where λ was the decay constant of Pb^{211}) and then the data from each segment was plotted on a separate sheet of semi-log graph paper. The segments could then be fitted together visually. The entire spectrum was taken in large steps with a single source to determine the overall shape and to reduce the possibility of error in the fitting procedure.

Sources were prepared on aluminum foil (active area approximately 1 mm. in diameter) and on the end of a rounded wire (approximately 1/4 mm. in diameter). The wire source was about ten times more active than the foil source. This was not unreasonable since in the activation apparatus the electric field lines all pointed to the tip of the wire source while they were spread out over the entire foil source (the perspex mask limited the active region of the foil)(See Fig. 2-2). Because of the low counting rate of the foil sources, wire sources were used at high energies. However below 800 keV the backscattering was appreciable from the wire sources and foil sources had to be used. The distortion of the spectrum was found to be quite small above 800 keV when several representative points obtained with a foil were compared with the spectrum obtained with the wire. The source backings were exposed to actinon gas for approximately 1 hr., left unexposed for 20 min. and then counted for 30-40 min.

For a fixed geometry spectrometer as used here (see section 3.2) the increment of momentum Δp allowed through the baffles increases with increasing momentum p. Thus the ratio $\Delta p/p$ is a constant. To correct the data for this, the raw counting rate (n) was normalized by dividing it by a quantity which was proportional to the corresponding momentum (the voltage across the precision resistor in series with the magnet coils) giving the normalized counting rate N.

To analyze the continuum and determine its end-point, a Fermi plot was constructed. The Fermi plot is based on the well-known relationship (N-7, 1952) for an allowed spectrum.

$$\left[\frac{N}{f(Z,p)}\right]^{\frac{1}{2}} = (\text{constant})(\epsilon_o - \epsilon)$$

where f(Z,p) is the Fermi function, which gives the statistical shape of the momentum distribution of the beta particle and is tabulated (N-7, 1952), ϵ was the energy and ϵ_o the end-point energy (both expressed in units of $m_o c^2$). Thus plotting $(N/f)^{\frac{1}{2}}$ against $\epsilon_o - \epsilon$ gives a straight line.

The strength of the magnetic field was indicated by the voltage drop across a precision resistor in series with the field coils. The raw data from the spectrometer gave

the counting rate and the number of millivolts across the resistor. If B is the magnetic field in gauss, ρ the radius of curvature in cm. and η the momentum in units of mc, the following equations show the relationship between them.

$$B\rho = k \times (\text{number of millivolts})$$
$$= (B\rho)/(1704.4)$$
$$= (1 + \eta^2)^{1/2}$$

From calibrations using the well known standard, the thorium F line, k was determined to be 20.80. Corrections were made to the Fermi function f(Z,p) for relativistic effects (R-15, 1953) and the screening effect due to the extra nuclear electrons (N-7, 1952). Since beta decays to two isotopes (Bi^{211} - Z = 83 and Pb^{207} - Z = 82) were present in the continuum, the momentum distribution was analysed with a function which was an average of the Fermi functions for Z = 82 and Z = 83. To examine the error involved in this procedure, Fermi plots were calculated using the Fermi function for Z = 82 and Z = 83. It was found that the error introduced was much less than the statistical error of the continuum (±3%). The Bendix G15-D computer was programed to calculate ϵ , N, and $(N/f)^{1/2}$ and the results were put both on paper tape and the computer typewriter output. The paper tape was produced to be used in the partial beta ray spectrum analysis.

The partial beta ray spectra (those distributions due to beta rays leaving the nucleus in different excited states) where 'unpeeled' starting with that one resulting from the largest disintegration energy (i.e., highest end point energy). Assuming all the beta decays were allowed, each partial spectrum would give a straight line on the Fermi plot. After the computer output $(N/f)^{1/2}$ vs. ϵ had been plotted, the points belonging to the first partial (highest endpoint) were easily seen. The computer was then programmed to obtain a least square fit to these points, to calculate the endpoint energy and to subtract the partial spectrum from the composite spectrum. The true contribution of the partial spectrum was given by its momentum distribution (this was obtained by squaring the value on the Fermi plot and multiplying by the corresponding f(Z,p)). This information had been put on paper tape as a result of the computer Fermi analysis to facilitate the unpeeling of partial spectra. The Fermi plot showing the partial spectra is shown in Fig. 4-12. The endpoints calculated by the computer were: 1.431 ± 0.008, 1.378 ± 0.008 MeV, 470 ± 100, and 200 ± 100 keV. The intensity of the last two feeds compared to the 1.378 MeV feed was 6 ± 3% and 2 ± 1% respectively. These three feeds are consistent with the known level scheme of Bi^{211} (see Fig. 4-1 and Section 4.1). The calculation of relative intensities has suffered considerably by the removal of the 1.431 meV feed since it represents about one half of the beta continuum. Better values for the relative beta feeds will be determined from the absolute gamma ray intensities and internal conversion coefficients (see section 4.5).

Figure 4 - 12

The Fermi plot for the beta continuum of the active deposit. The lower four lines represent the partial beta continua. The highest end point is due to the beta decay of Tl^{207} and the other three are due to the beta decay of Pb^{211}.

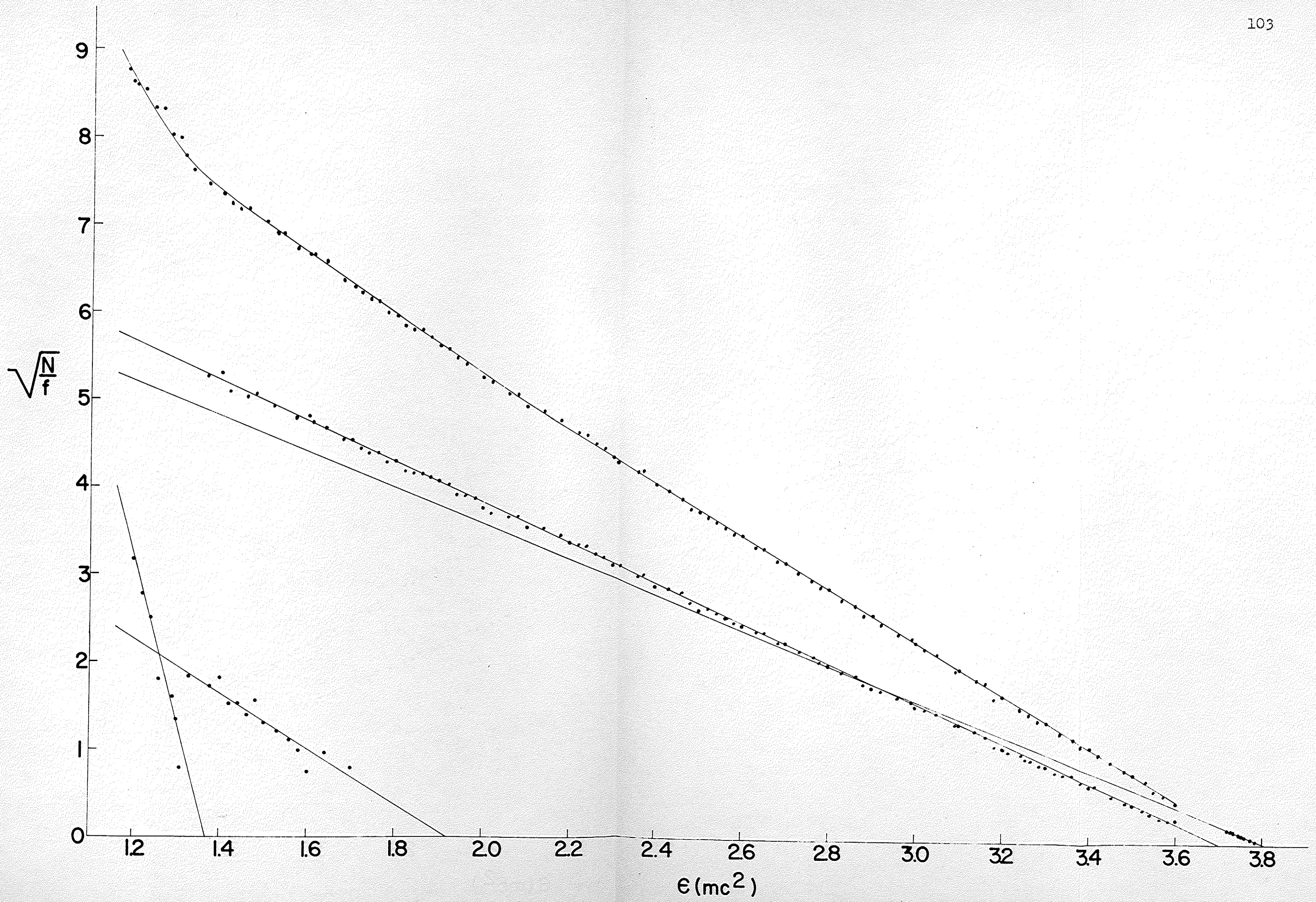
9
8
7
6
5
4
3
2
1
0
$\sqrt{\frac{N}{f}}$
1.2
1.4
1.6
1.8
2.0
2.2
2.4
2.6
2.8
3.0
3.2
3.4
3.6
3.8
$\epsilon (mc^2)$

4.5 Internal conversion lines

The internal conversion data was collected using both a wire and foil source. The 350 keV K and 400 K conversion lines were examined with a foil source and fitted to the continuum (by plotting the lines on semi-log graph paper). The foil source was covered with a 1.8 mg./cm.^{2} aluminum foil to prevent the loss of the beta emitting Tl^{207} by alpha recoil. Failure to observed this would have resulted in too large a line/continuum ratio. The wire source was then used to collect data on the 350 keV K, 400 keV K, 430 keV K, 400 keV L, and 430 keV L internal conversion lines. The wire source was used because of its higher activity. Using the thorium F line as the calibration standard, the energies of the corresponding gamma rays were 349.8 ± 0.5 keV, 403.3 ± 0.5 keV and 426.5 ± 0.5 keV.

Unfortunately the 350 keV L conversion line could not be resolved from the 430 keV K conversion line, but this did not prevent calculation of the conversion coefficients and K/L ratios (see section 4.4). By normalizing the wire source data to the foil source data (for the 350 and 400 keV K conversion lines) the areas under the conversion lines were determined relative to the foil source continuum. The wire source continuum would be false in this low energy region because of the backscattered electrons. The statistical error for the points on the K conversion lines was ±1% and for the L conversion lines was ±3%. However an error of a few percent (5-7%) was involved in fitting the K conversion lines to the continuum and an error of 15-20% was involved in fitting the L conversion lines to the the continuum. Approximately 50 sources were needed to determine the internal conversion lines with the accuracy discussed above.

The procedure used to determine the internal conversion coefficients was as follows:

1) From the ratio of the area under the 350 keV K conversion peak to the continuum area, after correction for transient equilibrium and the fact that the continuum represents two consecutive beta decays, the number of 350 keV K conversion electrons/Pb^{211} decay was determined.

2) Using (1) and the alpha branching ratio of Tl^{207}, the internal conversion coefficient for the 350 keV gamma ray was determined.

3) Using (2), the peak areas for the other converted gamma rays relative to the 350 keV K conversion peak, and their relative gamma ray intensities, internal conversion coefficients were determined for the 400 and 430 keV transitions.

The source was covered with a 1.8 mg./cm.^{2} aluminum foil for part 1 above to prevent the loss of Tl^{207} by alpha recoil from the alpha decay of Bi^{211}. The possibility of recoil was investigated by comparing the 350 keV K conversion line to continuum area ratio for the two situations (a) without the covering aluminum foil and (b) with the covering aluminum foil. It was found that

the (a) value was approximately 15% lower than the (b) value which means that approximately 30% of the Tl^{207} nuclei were lost by recoil from the alpha decay of Bi^{211} if the source was not covered.

The beta continuum was almost entirely (approximately 95%) due to the ground state transitions of Pb^{211} to Bi^{211} and Tl^{207} to Pb^{207}. Since these decays were sequential (ignoring the 0.3% branch to Po^{211}, see Fig. 4-1) each transition was represented by one half the area under the continuum (momentum distribution). As shown in Appendix I, Bi^{211} was emitting alpha particles 6.3% faster than Pb^{211} was emitting beta particles. Thus the total continuum represents 2.226 disintegrations of Pb^{211} while the conversion lines for Tl^{207} would be 1.063 times larger than they would be if secular equilibrium existed.

By definition the internal conversion coefficient is

$$\alpha = N_e/N\gamma$$

where N_e is the number of electrons (from the K, L, M, ... shells) and $N\gamma$ is the corresponding number of gamma rays. The coefficient for each shell is given by

$$\alpha_K = N_{ek}/N_\gamma, \text{ etc.}$$

so that

$$\alpha = \alpha_K + \alpha_L + \ldots \qquad 4\text{-}1$$

Let A be the area under the whole continuum and a the area under the K conversion peak due to the 350 keV gamma ray. Then

$$\frac{N_{ek}}{\text{number of } Pb^{211} \text{ disintegrations}} = \left(\frac{a}{1.063}\right)\left(\frac{2.226}{A}\right) \qquad 4\text{-}2$$

and from the known alpha branching ratio

$$\frac{N_\gamma + N_e}{\text{number of } Pb^{211} \text{ disintegrations}} = (0.162)(1.063)$$

thus

$$\frac{N_\gamma}{\text{number of } Pb^{211} \text{ disintegrations}} = \frac{(0.162)(1.063)N_\gamma}{N_\gamma + N_e}$$

$$= \frac{(0.162)(1.063)}{1 + \alpha} \qquad 4\text{-}3$$

Substituting the experimental values obtained for the areas a and A into equation 4-2 the number of 350 keV K conversion electrons per Pb^{211} decay was found to be .245 ± 0.0024.

Dividing equation 4-2 by equation 4-3 one gets

$$\frac{N_{ek}}{N_\gamma} = \left(\frac{a}{1.063}\right)\left(\frac{2.226}{A}\right)\frac{1 + \alpha}{(1.063)(0.162)}$$

$$= \alpha_K$$

or using the experimental values for a and A

$$\alpha_K = (0.142)(1 + \alpha_K + \alpha_L + \alpha_M + \ldots)$$

Assuming $\alpha_N + \alpha_O + \ldots$ to be negligible compared to

$\alpha_K + \alpha_L + \alpha_M$ then

$$\alpha_K = (0.142)(1 + \alpha_K + \alpha_L + \alpha_M) \qquad 4\text{-}4$$

To find a value for α_K the nature and multipolarity of the 350 keV gamma ray must be determined. The only combination that satisfied the above equation (4-4) was a mixed M1 plus E2 transition. Let x be the fraction of M1 radiation, $\alpha_K(M1)$ the K internal conversion coefficient for M1 radiation for the 350 keV transition, $\alpha_K(E2)$ the K internal conversion coefficient for E2 radiation for the 350 keV transition, etc. Then

$$\alpha_K = x[\alpha_K(M_1)] + (1 - x)[\alpha_K(E_2)], \text{ etc.} \qquad 4\text{-}5$$

Substituting equation 4-5 into equation 4-4 one gets

$$x[\alpha_K(M1)] + (1-x)[\alpha_K(E_2)] = \{1 + x[\alpha_K(M1)] + (1-x)\,\alpha_K(E2)$$

$$+ x[\alpha_L(M1)] + (1-x)[\alpha_L(E2)] + x[\alpha_M(M1)] + (1-x)[\alpha_M(E2)]\}\,(0.142)$$

Using the theoretical values for the internal conversion coefficients from Sliv and Band (S-24, 1958) as shown in Table 42, $\alpha_K = 0.175 \pm 0.017$ showing a 76 ± 10% M1 admixture for the 350 keV gamma ray in Tl^{207}. Unfortunately the L conversion peak for the 350 keV transition fell on top of the 430 keV K peak and hence no K/L ratio could be determined for the 350 keV transition directly. However since the a_K (350 keV) and the M1 admixture was known, the contribution of the

L peak (350 keV) to the total area could be calculated and subtracted, leaving only that area due to the 430 keV K conversion.

To determine the coefficient for the 400 and 430 keV transitions the following sample relations were used

$$\alpha_K(400) = \frac{N_{eK}(400)}{N_\gamma(400)} = \frac{N_{eK}(350)\ \dfrac{N_{eK}(400)}{N_{eK}(350)}}{N_\gamma(350)\ \dfrac{N_\gamma(400)}{N_\gamma(350)}}$$

$$= \alpha_K(350)\ \frac{\dfrac{N_{eK}(400)}{N_{ek}(350)}}{\dfrac{N_\gamma(400)}{N_\gamma(350)}} \qquad 4\text{-}6$$

The ratios in the numerator and denominator of equation 4-6 were determined experimentally, and the resulting values for the conversion coefficients are shown in table 4-2 together with the experimentally determined K/L ratios. The internal conversion coefficients for the 400 and 430 keV transitions are shown as M1 plus E2 mixtures. From the theoretical internal conversion coefficients shown in table 4-2, these transitions cannot be E2 plus M3, however the experimental coefficients were not inconsistent with a E1 plus M2 mixture. The latter mixture was considered improbable since it implies a parity change. In the Pb^{208} region parity changes are present only in the de-excitation of isomeric

states and none of the levels here involved are isomeric. The K internal conversion coefficient for the 706 keV transition in table 4-2 was determined by normalizing to the work in a previous paper (V-1, 1963) and making the required adjustment. The peak in the previous work was seen by beta-gamma coincidence and hence was not visible in the data obtained from the equipment used here.

Since there are 0.162 6.280 MeV alpha particles for each Bi^{211} decay (see section 4.2) and since α_K(350 keV) = 0.175 the number of 350 keV gamma rays/Bi^{211} decay was 0.162 (1 - .175) = 0.134 350 keV gamma rays/Bi^{211} decay.

Table 4-2

	M1	E2	M3	E1	M2	Present Work	% M1
α_K(330)	.216	.044				0.175 ± 0.017	76 ± 10%
α_L(330)	.037	.022					
α_M(330)	.017	.009					
K/L 330	5.84	2.00					
α_K(400)	.170	.034	1.20	.012	.530	.091 ± .018	42 ± 13%
α_L(400)	.030	.015	.446	.0022	.127		
K/L(400)	5.66	2.27	2.69	5.45	4.17	4 ± 1	
α_K(430)	.150	.031	1.02	.011	.470	.117 ± .024	72 ± 20%
α_L(430)	.026	.012	.368	.0019	.108		
K/L(430)	5.76	2.58	2.77	5.79	4.35	7 ± 2	
α_K(706)	.042	.011	.210			.025 ± .005	45 ± 50%

4.6 Alpha-gamma coincidence

Using the apparatus described in section 3.4 the coincidences between alpha particles and gamma rays were investigated with the two counters at 180^{o} to each other and with the gamma counter directly against the aluminum spinning (see Fig. 3-11). Sources were prepared on aluminum foil and were 3/8 in. diameter in active area. Source backings were exposed to the actinon gas for 1 hr., left unexposed for 20 min. to allow for transient equilibrium to be established and then counted for 1 hr. The single channel counting rate on both the alpha and the gamma side was approximately 5×10^{4} counts/sec., and the coincidence counting rate was approximately 5×10^{4} counts/hr. for the 6.280 MeV alpha particle with the 350 keV gamma ray.

Since extremely low intensities had been put on any possible alpha particles with energies in the range 3.0 - 5.72 MeV and 7.2 - 13.0 MeV (see section 4.2), the region investigated by alpha-gamma coincidences was limited to examining alpha energies in the region 5.1 - 8.1 MeV gated by gamma rays of energy greater than 500 keV (to avoid swamping the multichannel pulse height analyser with the 350 keV gamma ray) and, for completeness, by examining gamma energies from approximately 100 keV to 1.3 MeV gated by alpha energies in the range 2 MeV to 13 MeV. Figure 4-13 shows the real plus chance coincidences (solid line) and the chance coincidences (dotted line) when the gamma rays were analysed (latter situation). When the two curves were subtracted it was seen that the 350 keV gamma ray was in coincidence with an alpha particle. The peak at 970 keV is contained in both the real plus chance coincidences and the chance coincidences (no combination of known gamma ray energies gives an energy near 970 keV). The two peaks found at 560 and 700 keV after subtraction were analysed using the method described in section 4.3 (see table 4-3 and Fig.4-14). The peak at 700 keV was attributed to the adding (pileup) of two 350 keV pulses because of the high counting rate.

Figure 4 - 13

Gamma ray spectrum in coincidence with alpha particles of energy 2-13 MeV.

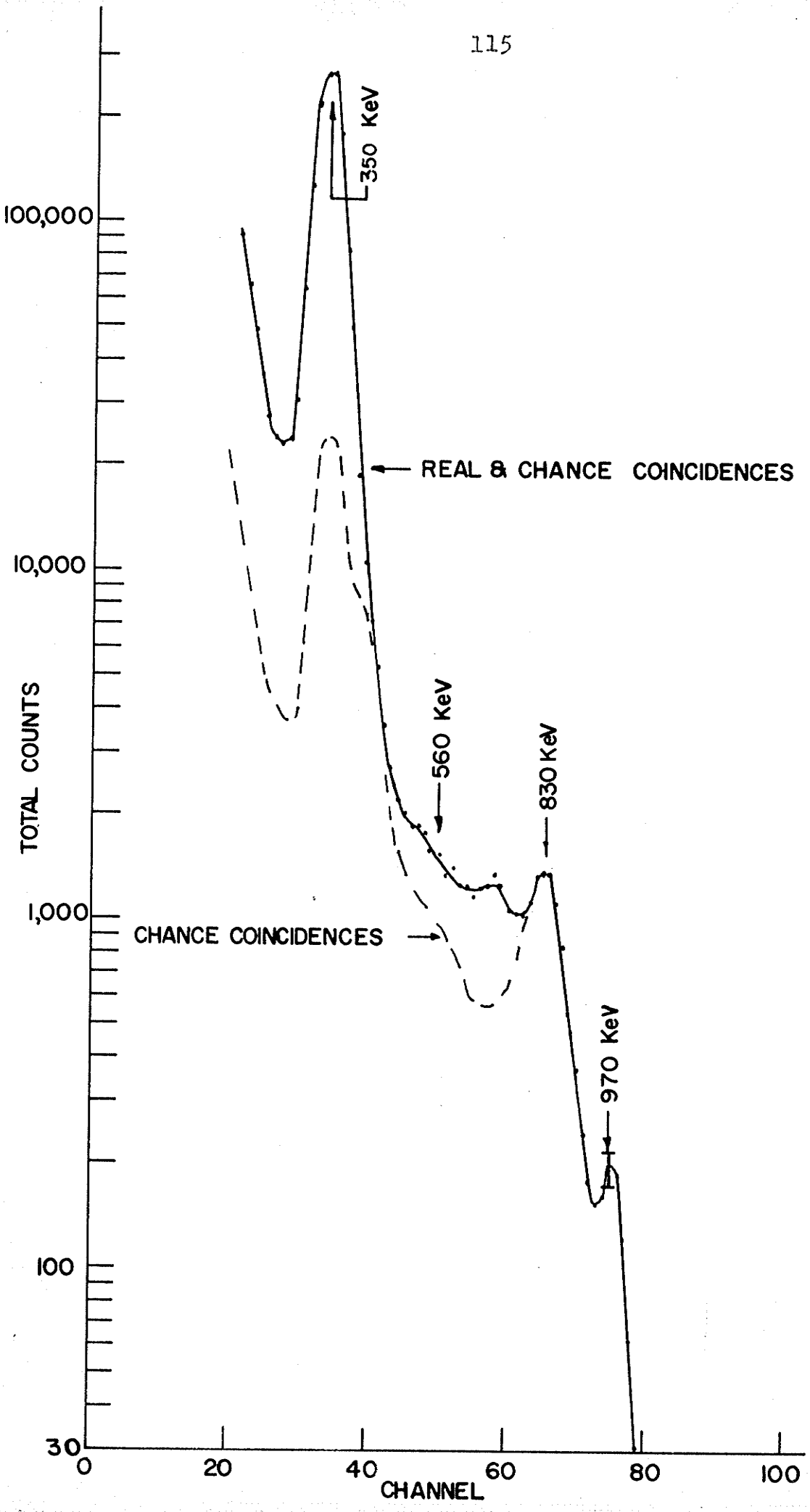
350 KeV
100,000
REAL & CHANCE COINCIDENCES
10,000
560 KeV
830 KeV
TOTAL COUNTS
1,000
CHANCE COINCIDENCES
970 KeV
100
30
0
20
40
60
80
100
CHANNEL

Figure 4 - 14

Result of subtraction of chance coincidences from real + chance coincidences in Fig. 4-13.

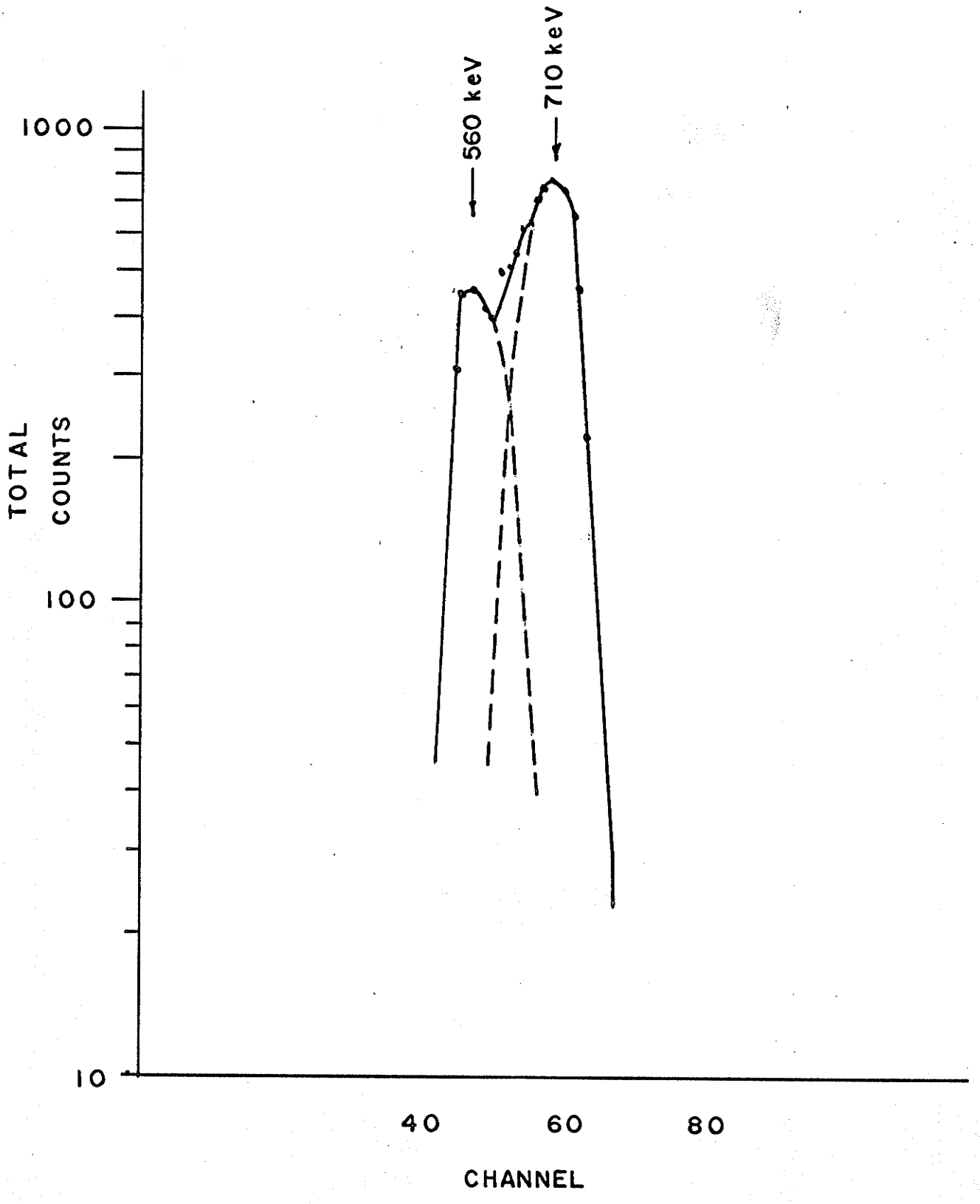
560 keV
710 keV
1000
100
10
TOTAL COUNTS
40
60
80
CHANNEL

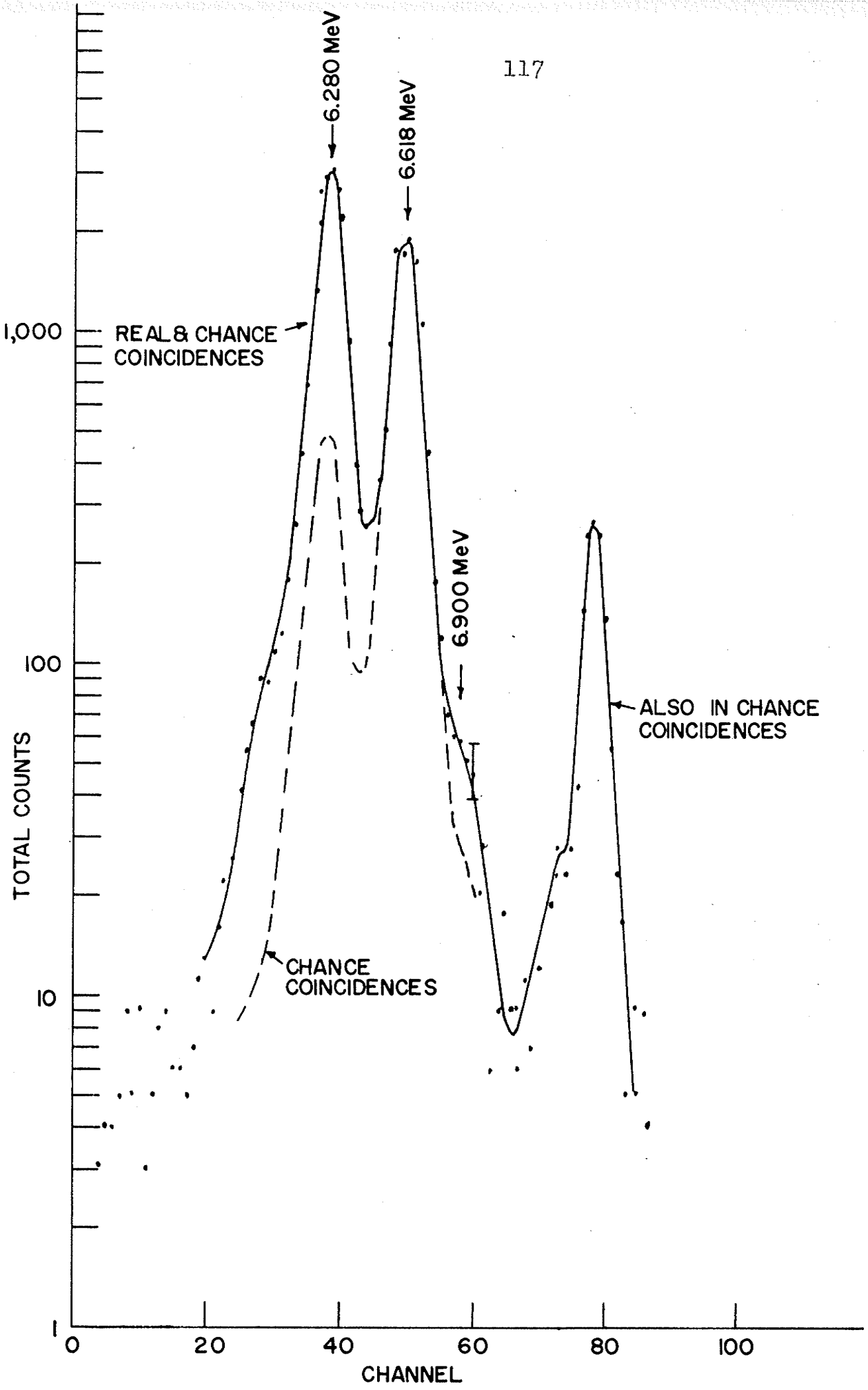
6.280 MeV
6.618 MeV
6.900 MeV
REAL & CHANCE COINCIDENCES
CHANCE COINCIDENCES
ALSO IN CHANCE COINCIDENCES
TOTAL COUNTS
1,000
100
10
1
0
20
40
60
80
100
CHANNEL

This view was further substantiated because when only gamma ray energies greater than 500 keV were allowed through the single channel pulse height analyser, alpha particles in coincidence with the 350 keV gamma ray were allowed into the multichannel pulse height analyser by the electronics (see Fig. 4-15), indicating the presence of a significant amount of pileup. The peak at 560 keV was due to a gamma ray in Pb^{207} (it was in coincidence with a 6.90 MeV alpha particle as seen in Fig. 4-15). Approximately 70 sources were needed for the alpha-gamma coincidence studies.

Figure 4-13 shows the coincidence gamma ray spectrum (both real plus chance and chance coincidences) when the multichannel pulse height analyser was gated by alpha particles in the range 2 to 13 MeV. After subtraction of the chance coincidences, the intensity of the 560 keV gamma ray relative to the 350 keV gamma ray was determined and the result is shown in table 4-3. The 560 keV gamma ray was due to the decay of the well known first excited state in Pb^{207}. That this state was being fed by a 6.90 MeV alpha particle can be seen in Fig. 4-15. This alpha feed is a well known one (J-1, 1954). From the relative gamma ray intensity and previously determined information (see equations below) the probability of Po^{211} (see Fig. 4-1) decaying via the 6.90 MeV alpha particle to the first excited state of Pb^{207} (560) keV) was calculated. The internal conversion coefficient which was known to be low (α_K = 0.018, R-13, 1951) was neglected in this calculation.

$$\text{Probability of } Po^{211} \text{ emitting a 6.90 MeV alpha particle} \approx \frac{\text{number of 560 keV gamma rays}}{\text{number of Bi-211 beta decays (population of Po-211)}}$$

$$= \frac{\left[\frac{\text{number of 560 keV gamma rays}}{\text{number of 350 keV gamma rays}}\right]\left[\frac{\text{number of 350 keV gamma rays}}{\text{number of Bi-211 decays}}\right]}{\left[\text{number of Bi-211 beta decays/number of Bi-211 decays}\right]}$$

continued,

$$= \frac{(0.00008)(.134)}{(.00287)}$$ (see table 4-3, section 4.5 and section 4.2)

$$= .00^{40} \pm .001 \text{ or } 0.40 \pm .10\%$$

In addition an upper limit of .0007 ± 0.0002 or 0.07 ± 0.02% can be put on the probability of any other alpha particle emission by Po^{211} to an excited non-isomeric state in Pb^{207}. Since prompt coincidences were used, isomeric states could not be investigated. An upper limit of 10^{-6} compared to the 6.28 MeVα-350 keV gamma coincidence can be put on the probability of any other alpha-gamma coincidence.

The alpha gamma angular correlations for the two coincidences seen here could have an effect on their relative intensities. However, the 6.90 MeV alpha- 560 keV gamma ray coincidence was so weak that no angular correlation could be performed on it. Thus angular correlation effects on the relative coincidence rates were ignored.

4.7 Gamma-gamma coincidences and absolute gamma ray intensities.

Using the apparatus described in section 3.4 possible coincidences between gamma rays were investigated. Sources were prepared on aluminum foils and were 3/8 in. diameter in active area. They were exposed to actinon gas for 1 hr., left unexposed for 20 min. to allow for transient equilibrium to be established and then were counted for 1 hr. The single channel counting rate on both sides was approximately 5×10^4 counts/sec. and the coincidence counting rate was approximately 10^3 counts/hr. for the 400-430 keV coincidence. One scalar in addition to those described in section 3.4 was needed to provide normalization for the different source intensities

when the single channel analyser window positions were changed. This additional scaler was connected directly to one of the amplifiers in Fig. 3-4. Figure 4-16 shows the real plus chance and normalized chance coincidence spectra when gated by gamma rays in the range 350-450 keV. Figure 4-17 shows the result of subtraction of the chance coincidences and how the three gamma rays made up the spectrum. The dashed line in the 650 keV region is just consistent with the experimental errors. This makes the intensity determined for the 650 keV gamma ray only an upper limit. The table below shows which gamma rays are in coincidence and how intense they are.

gate (keV)	Gamma rays in coincidence(keV)	(area)	relative area
350-450	430	13.60	1.00
	650	0.24	<0.018
	706	0.78	0.057
650-750	400	0.85	0.063
550-650	400	0.30	0.023
950-1150	None		
800-900	None		
700-800	290	0.20	0.015

(NOTE - because of instrumental limitations only the region below approximately 350 keV was examined when the gate was set at 700-800 keV.)

Figure 4 - 16

Gamma ray spectrum in coincidence with gamma rays in the range 350-450 keV.

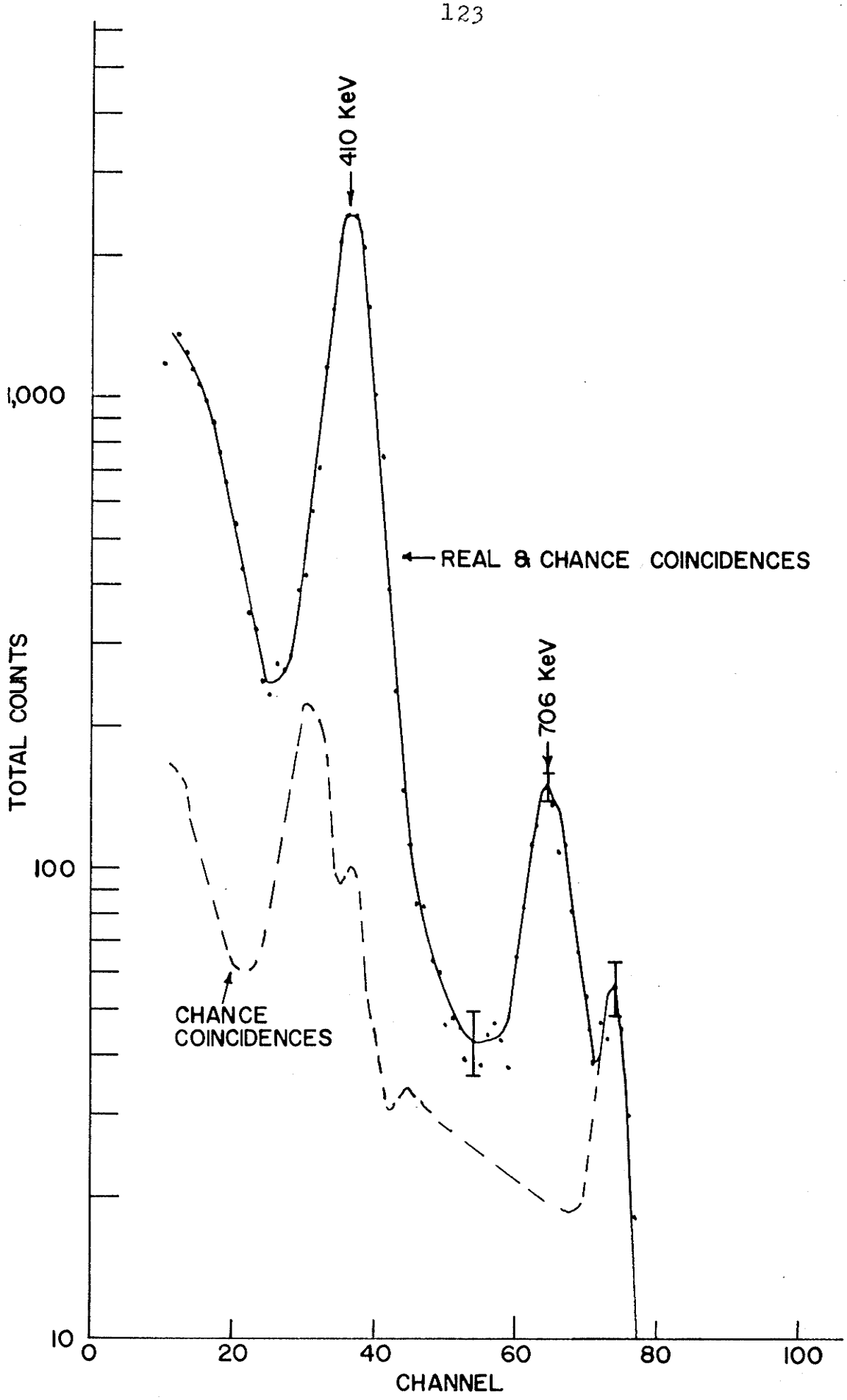
410 KeV
706 KeV
REAL & CHANCE COINCIDENCES
CHANCE COINCIDENCES
TOTAL COUNTS
1,000
100
10
0
20
40
60
80
100
CHANNEL

Figure 4 - 17

Difference between real plus chance coincidences and chance coincidences from Fig. 16.

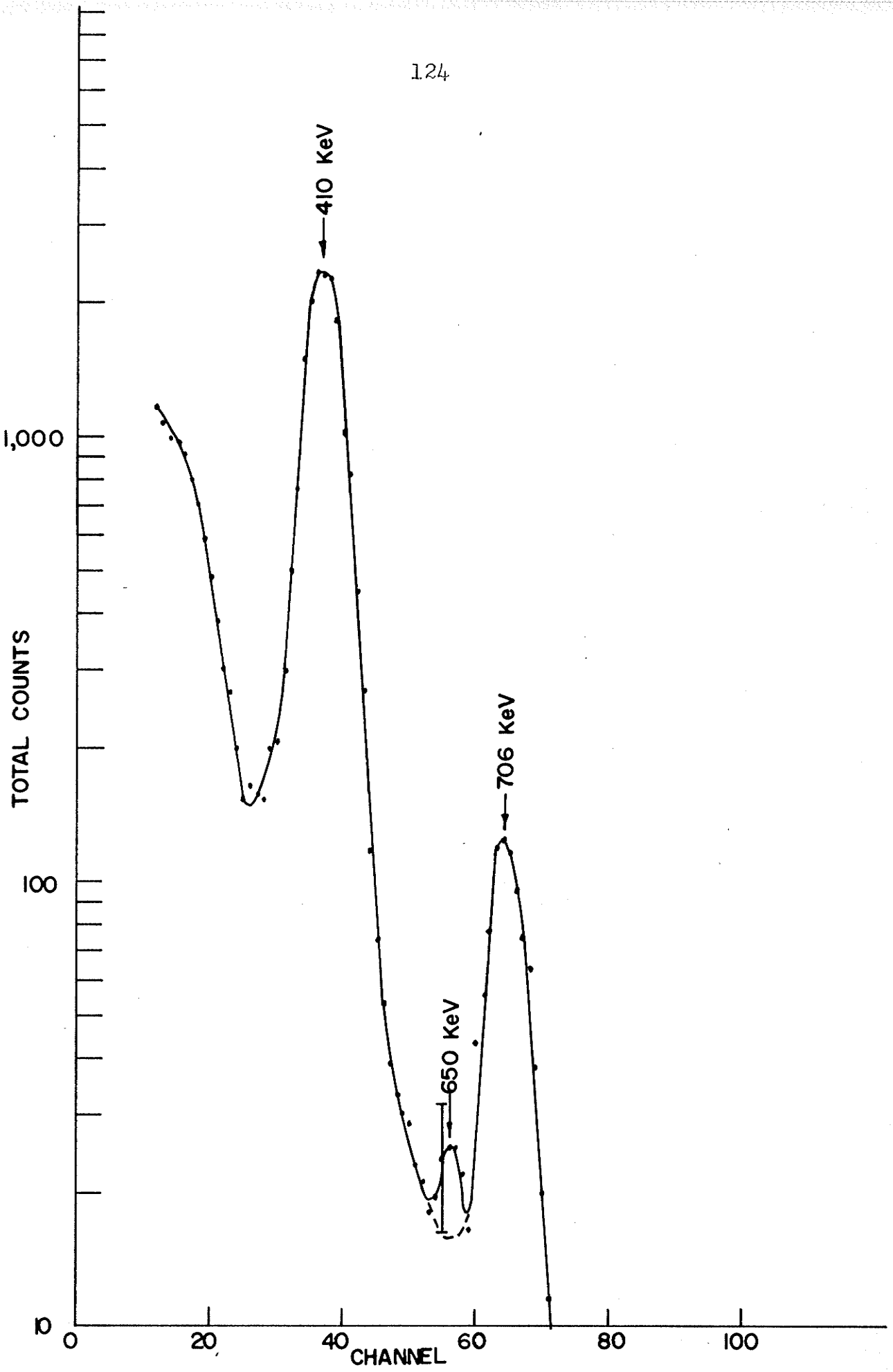
410 KeV
706 KeV
650 KeV
1,000
100
10
TOTAL COUNTS
0
20
40
60
80
100
CHANNEL

The 400 keV gamma ray was in coincidence with the 430, 650 and 706 keV gamma rays and the 758 keV gamma ray (see section 4.1) was in coincidence with the 290 keV gamma ray. No other coincidences were present with intensities greater than one part in 10^2 compared to the 400-430 keV coincidence. Approximately 90 sources were needed for the gamma-gamma coincidence studies.

The gamma-gamma coincidence spectra were analysed in the same way as the gamma ray spectra except that the photopeak areas had to be corrected for crystal efficiency and the peak to total distribution (see section 3.3) for both of the gamma rays involved. The data and analysis can be seen in table 4-3. ϵ was the relative efficiency and r the relative peak to total distribution ratio. The 706-290 keV gamma ray coincidence was normalized to the 400+430 keV gamma ray coincidence by the method described in section 4.7 (using an extra scaler to determine the source intensity). The 400 and 430 keV gamma ray photopeaks could not be resolved, and the single channel pulse height analyser was wide enough that either radiation could enter either counter.

Table 4-3

	350 keV	560 keV
ϵ r	.350	.172
relative area(A_R)	8673.0	0.33
A_R/ϵ r	24780.0	1.92

the relative intensity is

$$\frac{\left(\frac{A_R}{\epsilon r}\right)_{560}}{\left(\frac{A_R}{\epsilon r}\right)_{350}} = 0.00008 \pm 0.00002$$

This essentially meant that the effective solid angle for the coincidence between these radiations was twice as large as for the other coincidences. Thus the relative intensities determined in Table 4-4 for the 650, 706 and 290 keV gamma rays had to be multiplied by two to get the true relative intensities shown below.

energy (keV)	intensity(relative to 430 keV gamma ray)	intensity(relative to 350 keV gamma ray)
430	1.000	0.22
650	$\leq$ 0.06	$<$ 0.013
706	0.24	0.053
290	0.042	0.009

The relative intensity of the 706 keV gamma ray determined by gamma-gamma coincidence work is in good agreement with the relative intensity determined in the unpeeling of the gamma ray spectrum (see section 4.3). The coincidence spectra for the 758-290 keV and 400-430 keV cascades were taken with the counters in the same geometrical positions.

The gamma-gamma angular correlations for the coincidences shown above could have an effect on their relative intensities. However some of the coincidences were so weak that no angular correlations could be performed. Thus angular correlations effects on the relative coincidence rates were ignored. The alpha branching ratio to

Table 4-4

Coincidences (keV) a	b	$K=\frac{(\epsilon r)_a}{(\epsilon r)_b}$ X10	area	$\frac{\text{area}}{K}$	$\frac{\text{rel. area}}{K}$
400	430	0.730	13.6	18.6	1.00
400	650	0.395	$\leq$ 0.24	$\leq$ 0.61	$\leq$ 0.03
400	700	0.349	0.78	2.24	0.12
758	290	0.517	0.20	0.39	0.021

the excited state of Tl^{207} relative to the ground state was 16.2% and there were 6.3% more alpha particles from Bi^{211} than there were beta particles from Pb^{211}. Therefore there were (1.063)(0.162) = 0.172 350 keV transitions (gamma rays and conversion electrons) per Pb^{211} decay. To determine the absolute gamma ray intensities, the number of 350 keV gamma rays per Pb^{211} decay must be determined. There were .0245 350 keV K conversion electrons per Pb^{211} decay (see section 4.5) and using the theoretical K/L and K/M ratios (table 4-2) there were 0.032 K, L, and M 350 keV conversion electrons per Pb^{211} decay. Subtracting the number of conversion electrons from the number of transitions per Pb^{211} decay (0.172) it was found that there were 0.140 350 keV gamma ray photons per Pb^{211} decay. This number, with the relative gamma ray intensities (see section 4.3) gave the absolute gamma ray intensities shown in table 4-5.

energy (keV)	Number of gamma rays per Pb-211 decay
290	0.0013 ± 0.0003
350	0.140 ± 0.021
400	0.044 ± 0.004
430	0.031 ± 0.003
650	$\leq$ 0.0019
706	0.0077 ± 0.0008
758	0.0090 ± 0.0009
830	0.038 ± 0.004
890	0.0066 ±0.0007
1060	0.0007 ± 0.0001
1100	0.0012 ± 0.0002

4.8 The 900 keV Gamma Ray

Benedetti (B-10,1939) and Surugue (S-5,1942) indicated the presence of a gamma ray at 865 keV in Pb^{207} following the β-decay of Tl^{207}. The stronger gamma ray in Pb^{207} was shown by Benedetti to be close to the 830 keV gamma ray in Bi^{211}. Fig. 4-6 shows no indication of a gamma ray at 865 keV. This figure does show a gamma ray of 890 keV whose intensity relative to the 350 keV gamma ray was 0.076.

Alburger and Sunyar (A-2,1955) have shown from the electron capture decay of Bi^{207} that the resulting gamma ray in Pb^{207} is 894 keV. It was thus important to determine if the 890 keV gamma ray seen in the active deposit was due to the decay of the 890 keV level in Pb^{207}. Since the only gamma ray to appear in the spectra of the separated Tl^{207} sources was 900 keV(that is the active deposit spectrum of gamma rays did not appear)(see section 4.3), it must be due to the decay of a level in Pb^{207}. Christensen et al (C-17,1963) using a separated source of Tl^{207} found the energy of this gamma ray to be 900±10 keV. There is no evidence to suggest other than that the 900 keV gamma ray in the decay of Tl^{207} is the same transition as that at 890 keV seen in the spectrum of the active deposit.

Two corrections must be applied to the relative intensity(per Pb^{211} decay) of the 900 keV gamma ray since it is in the decay of Tl^{207}. Firstly it must be corrected for the 30% recoil loss of Tl^{207}(see section 4.5) and secondly it must be corrected for transient equilibrium (see appendix I). The corrected intensity of the 890 keV gamma ray is 0.007 ± 0.001 per Tl^{207} decay. That is 0.7% of the beta decays of Tl^{207} populate the 900 keV level in Pb^{207}.

The absence of the 350 keV Bi^{211} gamma ray in the spectrum of the separated Tl^{207} source indicated that no aggregate recoil was occurring and that the source was pure. This effect is significant for other alpha decays (R-18,1930).

4.9 Excitation probability of levels in Bi^{211} and Pb^{207}

Using the gamma ray information of section 4.4, 4.7, and 4.8 along with the information that the 350 keV transition was in Tl^{207} (section 4.6) and that the 560 and 900 keV transitions were in Pb^{207} (section 4.6 and 4.8) the excitation probabilities (beta feeds) of levels in Bi^{211} were calculated. Table 4-6 includes the $\log_{10}$ft values as well as the % beta feeds. These % feeds agree well with the Fermi plots in section 4.4 obtained from the beta continuum. In the following table t is the half life of Pb^{211} (2166 sec.) and $\log_{10}$ f values were obtained from the tables of Feenberg and Trigg (F-10, 1950).

Table 4-6

level (keV)	W_o(MeV)	$W_o(mc^2)$	$\log_{10} f$	% feed	t/% feed	log(t/% feed)	$\log_{10}$ ft
g.s.	1.378	3.69	2.6	90.2	2.4×10^3	3.4	6.0
400	0.978	2.91	2.1	0.4	5.4×10^5	5.8	7.8
758	0.620	2.21	1.4	0.8	2.7×10^5	5.4	6.8
830	0.548	2.07	1.3	7.3	3.0×10^4	4.5	5.8
1060	0.318	1.62	0.7	0.4	5.4×10^5	5.8	6.4
1100	0.278	1.54	0.3	0.9	2.4×10^5	5.4	5.7

The above table is calculated assuming that there is no 40 keV transition from the 1100 keV level to the 1060 keV level. If there was a 40 keV gamma ray there the beta feed to the 1100 keV level would be higher. This would have made the log ft value of the beta feed to the 1100 keV level lower than 5.7. Since it is already low for a first forbidden transition (parity change required [see section 4.11] and E-3, 1958) the % feed is unlikely be higher and therefore there can be no appreciable 40 keV gamma ray de-exciting the 1100 keV level.

Using the gamma ray information in section 4.8 the following table (table 4-7) of % beta feeds and log ft values in the decay of Tl^{207} was calculated.

Table 4-7

level (keV)	W_o(MeV)	$W_o(mc^2)$	$\log_{10}f$	% feed	t/% feed	log(t/%feed)	$\log_{10}ft$
g.s.	1.431	3.80	2.7	99.30	2.9×10^2	2.5	5.2
900	0.531	2.04	1.1	0.70	4.1×10^4	4.6	5.7

In the above table the half life of Tl^{207} (t) was 288 sec. and the $\log_{10}f$ values were obtained from the tables of Feenberg and Trigg (F-10, 1950).

The shell model predictions for the ground states of the isotopes involved in the active deposit of actinium are shown below (W-6, 1961).

Pb^{211}-$9/2^+$, Bi^{211}-$9/2^-$, Po^{211}-$9/2^+$, Tl^{207}-$1/2^+$ and Pb^{207}-$1/2^-$.

Only the spin of Pb^{207} has actually been measured and it is in agreement with the shell model assignment.

The beta transitions from Pb^{211} to Bi^{211} and from Tl^{207} to Pb^{207} both involve a parity change and thus are described as being first forbidden. The log ft values in tables 4-6 and 4-7 all cluster around 6 and thus are consistent with the interpretation that the transitions are first forbidden following modern views on beta decay. It is not inconsistent with the allowed character described above for there to be a spin change of ± 1 in addition to the parity change. However a spin change of ± 2 would be inconsistent with the given log ft values.

4.10 Alpha-gamma angular correlation

The 6.280 MeV alpha particle in the decay of Bi^{211} was the only alpha particle whose coincidence counting rate with a gamma ray (here the 350 keV gamma ray) was high enough to allow an angular correlation to be performed. The sources used were collected on aluminum foil and were 25 $mm.^2$ in active area. They were exposed to the actinon gas for 1 hr. and immediately counted for 1 hr. The sources used gave counting rates in the alpha and gamma channels of approximately 400 and 500 counts/sec. respectively. The coincidence counting rate was approximately 400 counts/hr. and by removing the delay in one channel in order that genuine coincidences could not occur, the random rate was determined as about 6 per hour. Coincidence counting rates were taken for the angles 108°, 120°, 150°, 180°, 210°, and 240°, and then normalized by the alpha single channel counting rate.

The data was accumulated by moving among the six selected angles at random until a total of 2500 coincidences had been registered for each angle. Since the correlation must be symmetric about 180°, the data collected for angles greater than 180° provides a check on the physical alignment of the counters and source. However the counts at angles beyond 180° can be added to their corresponding angles below 180° (e.g. 150° and 210°) to improve statistics. The angular correlation between the 6.280 Mev alpha particle and the 350 keV gamma ray was isotropic with an overall error of $\pm 1\frac{1}{2}\%$ (see Fig.4-17a) This required approximately 70 sources.

Using the notation of Fig. 4-18 the expression for the angular correlation of an α-particle of unmixed angular momentum λ followed by a γ-ray of unmixed angular momentum L is

$$W(\theta) = A_{\gamma}\ b_{\gamma}(\lambda,\lambda)\ P_{\gamma}(\cos\theta) \qquad 4\text{-}7$$

where $A_{\gamma} = F_{\gamma}(\lambda j_1 j)\ F_{\gamma}(L j_2 j)$

Figure 4 - 17 - a

The 6.280 Mev alpha- 350 keV gamma angular correlation in the decay of Bi^{211}.

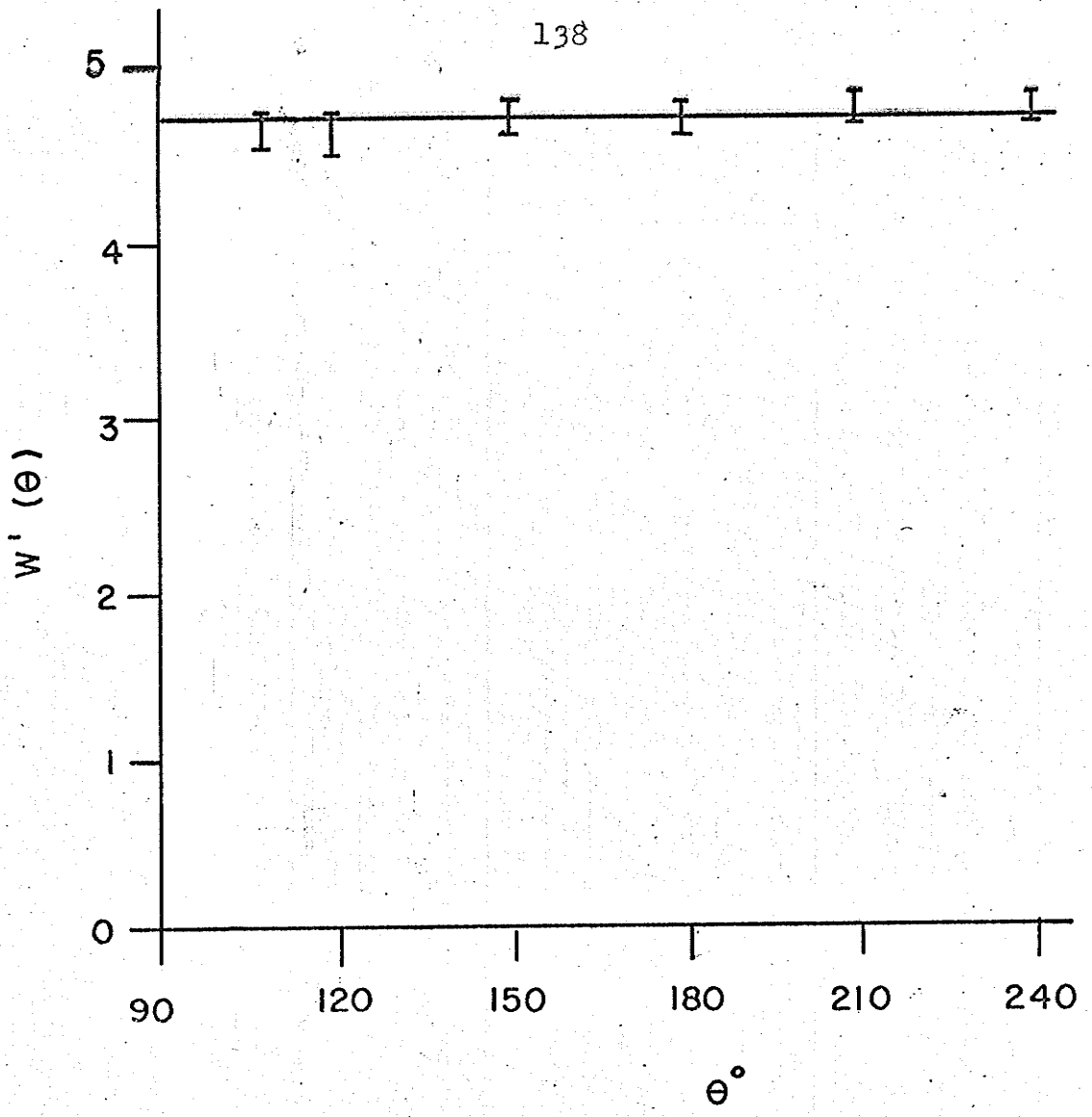
5
4
3
2
1
0
W' (θ)
90
120
150
180
210
240
θ°

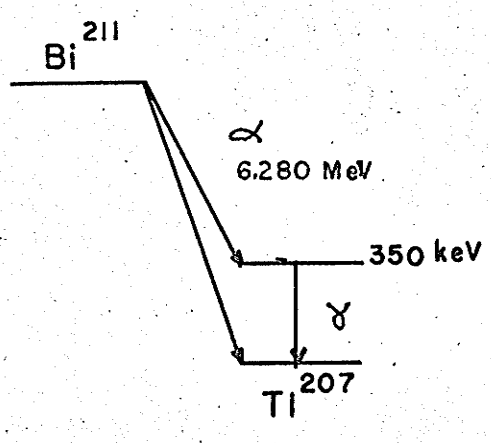
Bi 211
α
6.280 MeV
350 keV
γ
Tl 207

Figure 4 - 18

Notation for equations in section 4.10 (alpha-gamma angular correlation).

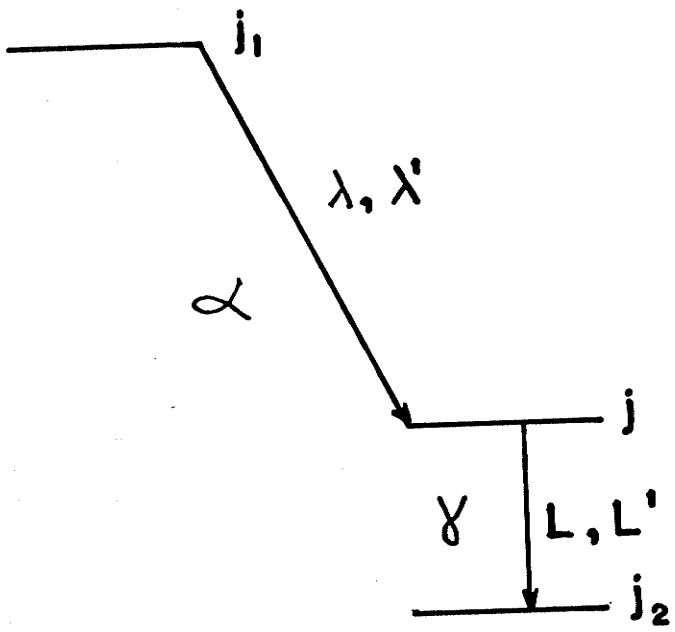
j_1
λ, λ'
α
j
γ
L, L'
j_2

$$\text{and } F_\nu(\lambda j_1 j) = (-1)^{j_1 - j - 1}(2j+1)^{1/2}(2\lambda+1)$$

$$\times C(\lambda\lambda\nu;\ 1\text{-}1)\ W(jj\lambda\lambda;\nu j_1)$$

$$\text{with } b_\nu(\lambda.\lambda) = \frac{2\lambda(\lambda+1)}{2\lambda(\lambda+1) - \nu(\nu+1)}$$

The functions $P_\nu(\cos\theta)$ are the Legendre polynomials. The function C and W are the Clebsh-Gordan and Racah coefficients which are related to Wigner's 3-J and 6-J symbols respectively (see Appendix II). Restrictions on the values of ν are as follows:

$$0 \leq \nu \leq 2j$$
$$0 \leq \nu \leq 2\lambda$$
$$0 \leq \nu \leq 2L$$

If the α-particle angular momentum is mixed (λ and λ') but the γ-ray angular momentum is pure L the angular correlation function becomes

$$W(\theta) = 1 + \frac{1}{1+\delta^2}\sum_\nu [b_\nu(\lambda,\lambda)\ F_\nu(\lambda j_1 j) +$$

$$\delta^2 b_\nu(\lambda',\lambda')\ F_\nu(\lambda' j_1 j) + 2\delta b_\nu(\lambda,\lambda')$$

$$F_\nu(\lambda\lambda' j_1 j)\ ]\ F_\nu(LL j_2 j) \times P_\nu(\cos\theta) \qquad 4\text{-}8$$

where δ^2 is the ratio of the intensities of the α-particles having angular momentum λ' to those having angular momentum λ,

$$\text{and } b_\nu(\lambda,\lambda') = \frac{2[\lambda(\lambda+1)\ \lambda'(\lambda'+1)]^{1/2}}{\lambda(\lambda+1) + \lambda'(\lambda'+1) - \nu(\nu+1)} \times$$

$\times \cos(\sigma_{\lambda'} - \sigma_\lambda)$ and where σ_λ is the Coulomb phase shift for an outgoing α-particle with angular momentum λ.

Parity conservation demands that λ and λ' differ by 2.4 ... etc. Hence if λ is odd (even) λ' is odd (even). The values of $(\sigma_{\lambda'} - \sigma_\lambda)$ may be calculated from (S-23, 1952).

$$\sigma_{\lambda+2} - \sigma_\lambda = \tan^{-1}\left(\frac{\eta}{\lambda+2}\right) + \tan^{-1}\left(\frac{\eta}{\lambda+1}\right)$$

$$\sigma_{\lambda+4} - \sigma_\lambda = \tan^{-1}\left(\frac{\eta}{\lambda+4}\right) + \tan^{-1}\left(\frac{\eta}{\lambda+3}\right) + \tan^{-1}\left(\frac{\eta}{\lambda+2}\right)$$

$$+ \tan^{-1}\left(\frac{\eta}{\lambda+1}\right) \text{ where } \eta = \frac{2Ze^2}{h\, v_\alpha}$$

Here Z is the atomic number of the daughter nucleus and v_α is the α-particle velocity. The function

$$F_\nu(\lambda\lambda'\ j_1 j) = (-1)^{j-j_1-1}\left[(2j+1)(2\lambda+1)(2\lambda'+1)\right]^{1/2}$$

$G_\nu(\lambda\lambda' j_1 j)$ and $G_\nu(\lambda\lambda'\ j_1 j) = C(\lambda\lambda'\nu\ ;\ 1\text{-}1)\ W(jj\ \lambda\lambda', \nu\ j_1)$. The quantities $b_\nu(\lambda,\lambda')$ and $F_\nu(\lambda\lambda'\ j_1 j)$ do not change in value if λ and λ' are interchanged.

When the α-particle angular momentum is pure but the γ-ray angular momentum is a mixture of L and L' we have:

$$W(\theta) = 1 + \frac{1}{1+\epsilon^2} \sum_{\nu} [F_\nu (LL j_2 j) + \epsilon^2 F_\nu (L'L' j_2 j) + 2\epsilon F_\nu (LL' j_2 j)] F_\nu (\lambda j_1 j) \; P_\nu (\cos\theta) \qquad 4\text{-}9$$

where ϵ^2 is the ratio of the intensity of the γ-rays with angular momentum L' to those having angular momentum L.

Finally, the angular correlation function for mixed α-particle and mixed γ-ray angular momenta is

$$W(\theta) = 1 + \frac{1}{(1+\delta^2)(1+\epsilon^2)} \sum_{\nu} [F_\nu (LL j_2 j) + \epsilon^2 \chi F_\nu (L'L' j_2 j) + 2\epsilon F_\nu (LL' j_2 j)] \times [F_\nu (\lambda\lambda j_1 j) b_\nu (\lambda,\lambda) + \delta^2 F_\nu (\lambda'\lambda' j_1 j) b_\nu (\lambda,\lambda') + 2\delta F_\nu (\lambda\lambda' j_1 j) b_\nu (\lambda.\lambda')] \times P_\nu (\cos\theta) \qquad 4\text{-}10$$

These relations have been discussed by Biedenharn and Rose (B-8, 1953), Fraunfelder (F6, 1955), Devons and Goldfarb (D-5, 1957) and by Singer (S-22, 1957).

The experimentally determined correlation between 6.280 MeV alpha particle and the 350 keV gamma ray revealed no angular dependence at all within the limits of the

statistical accuracy (1.5%) of the points at the four angles chosen, viz., 108°, 120°, 150° and 180°.

The half-life of the 350 keV state in Tl^{207} has been found to be 0.6×10^{-10} sec. (V-1, 1963), hence perturbing influences are likely to be negligible and the isotropy a genuine nuclear effect.

The spin and parity of the ground state of Bi^{211} has previously been taken as 9/2-. The evidence for this is less than overwhelming and rests largely on the single particle model prediction (M-14, 1959) that the lowest single particle energy level for the 83rd proton is an h 9/2- level. Support for this view is afforded by the observation that the ground state spin of Bi^{209} is 9/2 (M-15 , 1950) but the spin of Bi^{211} does not appear to have been measured and the possibility of its being 9/2+ should not be overlooked.

Cuperman (C-8, 1961) advances three strong arguments for accepting the spin and parity of the ground state of Tl^{207} as 1/2+, viz,

i) the measured spins and parities of Tl^{197}, Tl^{199}, Tl^{201}, Tl^{203}, and Tl^{205} are all 1/2+,

ii) Tl^{207} decays by β-emission predominantly to the ground state (1/2-) of Pb^{207}, while the 3/2-level is populated only to the extent of 0.5% and the 5/2- level is not populated to any measurable extent.

iii) the $\log_{10}$ft value of the β-decay from the ground state of Tl^{207} to that of Pb^{207} is 5.2 which indicates a $\Delta J = 0$, yes transition.

On the basis of these arguments it will be accepted in what follows that the ground state of Tl^{207} is 1/2+.

It was therefore necessary to determine the possible combinations of spins, parities, α-particle angular momenta (pure and mixed), γ-ray angular momenta (pure and mixed) which could yield the present isotropic correlation to within ±1-1/2%. The possibilities are

	j_1	j	j_2	λ	L
(a)	9/2-	3/2+	1/2+	3 and 5	1 and 2
(b)	9/2+	3/2+	1/2+	4 and 6	1 and 2
(c)	9/2-	5/2+	1/2+	3 and 5 and 7	2 and 3
(d)	9/2+	5/2+	1/2+	2 and 4 and 6	2 and 3

These possibilities yield twenty possible arangements of pure α - pure γ correlations, sixteen mixed α (two angular momenta mixing) -pure γ correlations and ten pure α-mixed γ (two angular momenta mixing) correlations. One combination, (a) above, was examined for a mixed α-mixed γ correlation.

For the 20 unmixed correlations, the Bendix G15-D computer at the University of Manitoba was programmed to calculated $W(\theta)$ from Eq. 4-7 at 3^{o} intervals. Typical correlations are shown in Fig. 4-19. None of the 20 possibilities yielded correlations which were isotropic within $\pm$ 1-1/2%.

In order to compare the experimental correlation to the theoretical correlations with mixed radiations (equations 4-8, 4-9, and 4-10) the computer was programmed to calculate $\Delta W/W$ for various values of δ^2 (or ϵ^2) where

$$\Delta W/W = \frac{W(\theta)\ \max - W(\theta)\ \min}{W(\theta)}$$

Hence $W(\theta)$ max and $W(\theta)$ min refer to the largest and smallest values of the correlation function. The observed correlation $W'(\theta)$ is related to the theoretical correlation $W(\theta)$ through the equation $W(\theta) = K\,W'(\theta)$ where K is a constant. Thus

$$\Delta W/W = \frac{KW'(\theta)\ \max - KW'(\theta)\ \min}{KW'(\theta)}$$

$$= \frac{W'(\theta)\ \max - W'(\theta)\ \min}{W'(\theta)} \leq 0.03, \text{ the}$$

experimental value 4-11

Figure 4 - 19

Typical theoretical angular correlations where both the alpha and gamma radiations are pure.

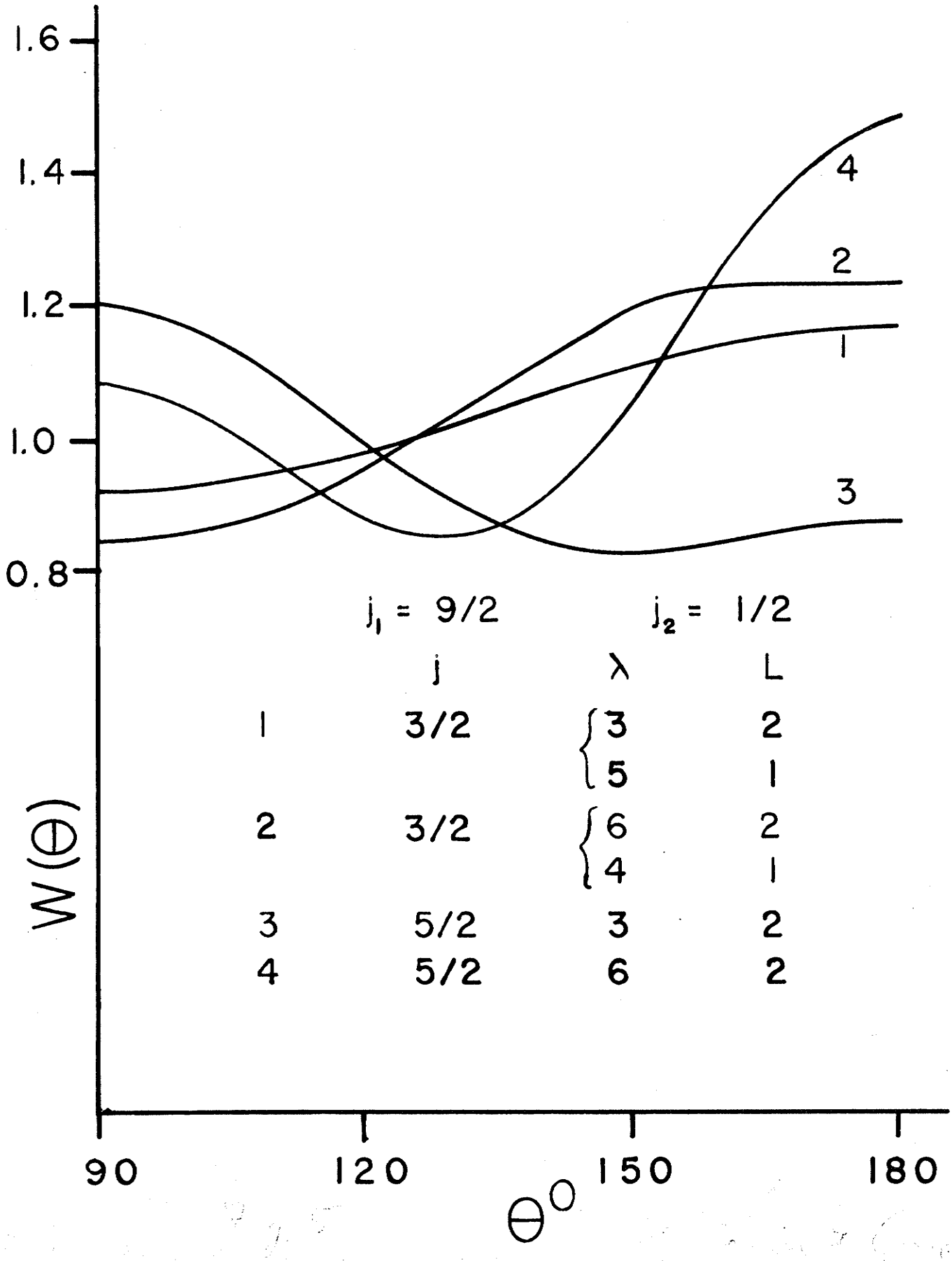

$j_1 = 9/2$ $\quad j_2 = 1/2$

	j	λ	L
1	3/2	3	2
		5	1
2	3/2	6	2
		4	1
3	5/2	3	2
4	5/2	6	2

The values of δ, (ϵ) used were ±1, ±1.5, ±2, ±2.5, ±3, ±3.5, ±4, ±4.5, ±5, ±6, ±7, ±8, ±9, and ±10. The range of mixing was thus approximately 1% to 99%.

In the analysis the choice of angle used in the denominator of Eq. 4-10 seemed to make little difference and 120° was arbitrarily chosen.

Plots were then made of $\Delta W/W$ against δ(or ϵ) and the experimental value of $\Delta W/W$ was drawn on the same plot. The intersection of the theoretical and experimental curves determined the range of mixing possible.

Graphs of $\Delta W/W$ against δ will be asymmetric about $\delta = 1$ because of the invariance of the functions $F_\nu(\lambda\lambda' j_1 j)$ and $b_\nu(\lambda\lambda')$ with respect to an interchange of λ and λ'. Where the value of $\Delta W/W$ fell below the 0.03 level, the correlation was isotropic to within the quoted experimental errors for that range of values of δ or ϵ. Of the sixteen mixed α-pure γ correlations none of the twelve arising from situations (c) and (d) yielded a $\Delta W/W \leq 0.03$ for any δ value. Graphs of the remaining four correlations are shown in Fig.4-20.

Figure 4 - 20

Plots of $\Delta W/W$ vs. δ (see text) for mixed alpha-pure gamma angular correlations.

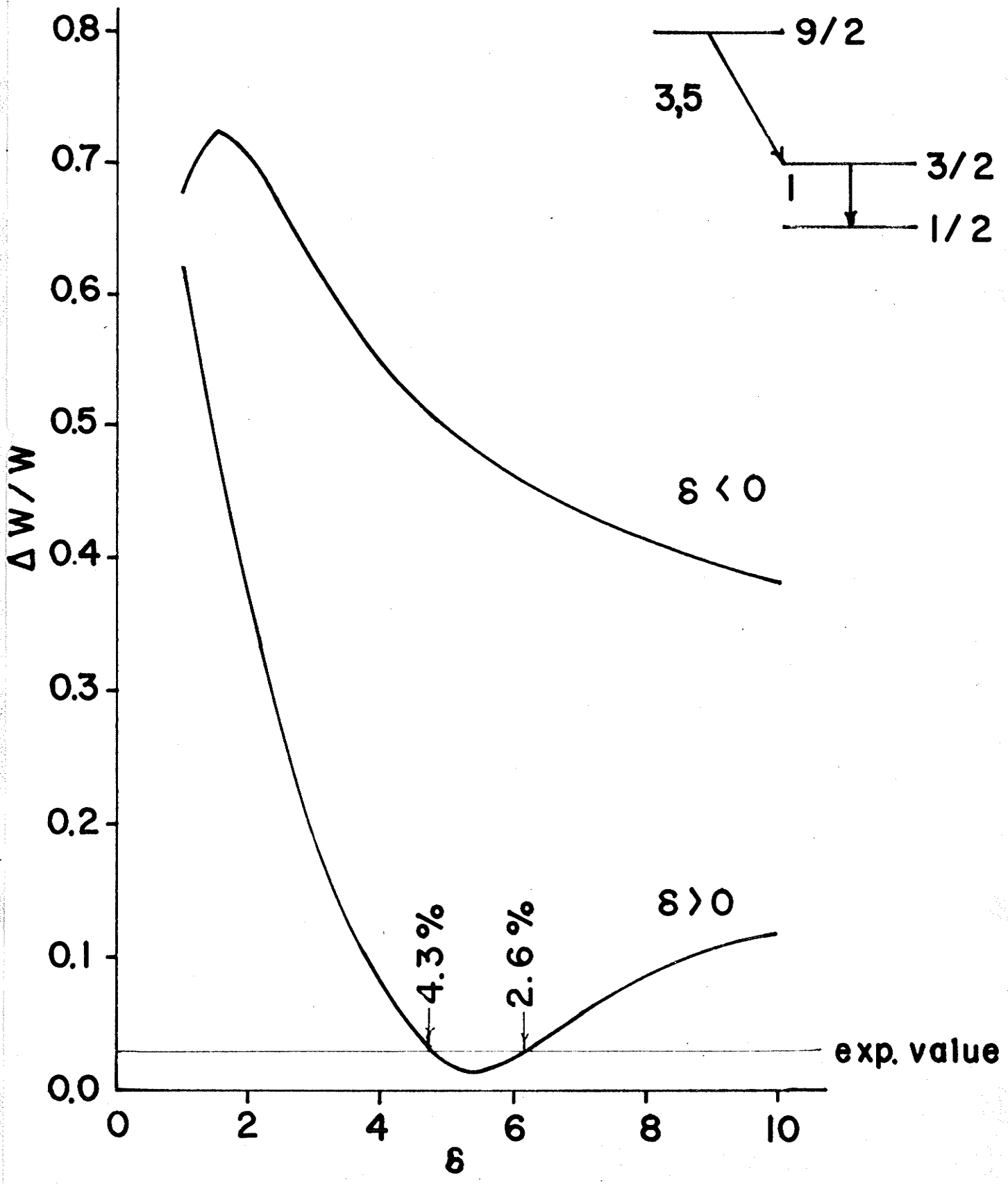
9/2
3,5
3/2
1
1/2
0.8
0.7
0.6
0.5
0.4
0.3
0.2
0.1
0.0
ΔW/W
δ < 0
δ > 0
4.3%
2.6%
exp. value
0
2
4
6
8
10
δ

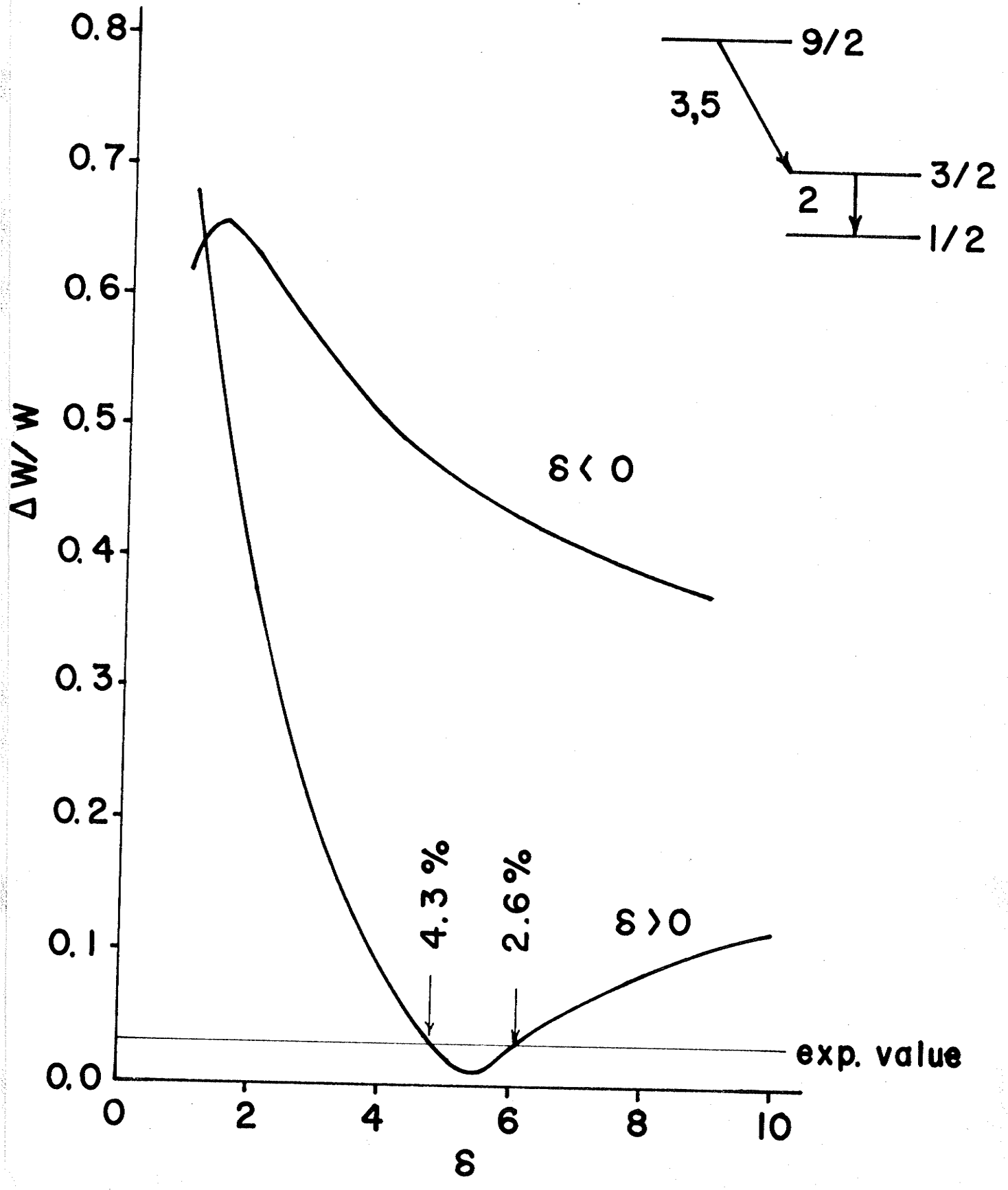
0.8
0.7
0.6
0.5
0.4
0.3
0.2
0.1
0.0
ΔW/W
0
2
4
6
8
10
δ
9/2
3,5
3/2
2
1/2
δ < 0
δ > 0
4.3 %
2.6 %
exp. value

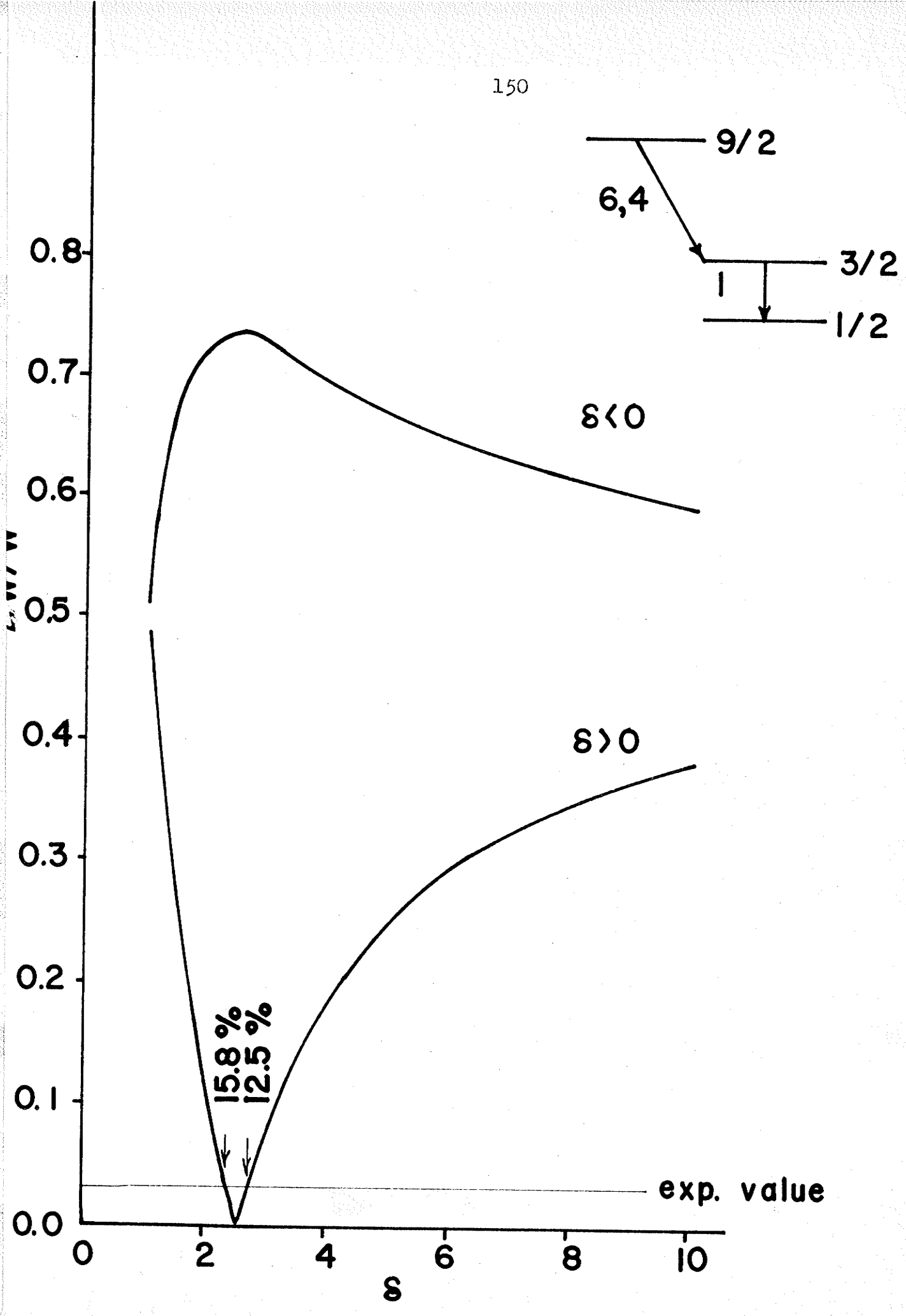
9/2
6,4
3/2
1
1/2
δ<0
δ>0
15.8%
12.5%
exp. value
0.0
0.1
0.2
0.3
0.4
0.5
0.6
0.7
0.8
0
2
4
6
8
10
δ

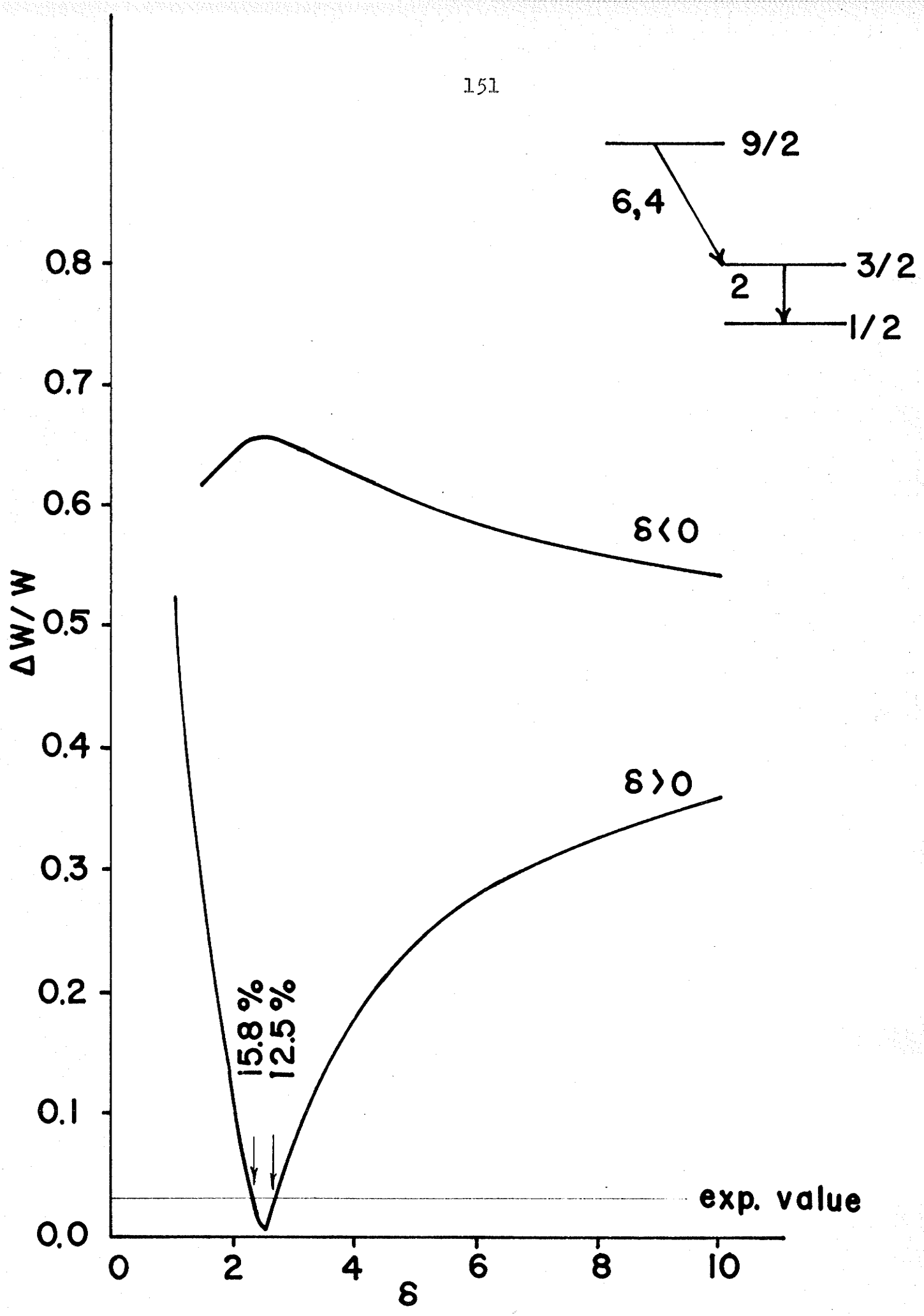
9/2
6,4
3/2
2
1/2
δ<0
δ>0
ΔW/W
0.8
0.7
0.6
0.5
0.4
0.3
0.2
0.1
0.0
15.8%
12.5%
exp. value
0
2
4
6
8
10
δ

Of the ten pure α-mixed γ-correlations, none of the six arising from situations (c) and (d) yielded a $\Delta W/W$ value ≤ 0.03 for any ϵ value. Graphs of the remaining four correlations are shown in Fig.4-21.

These results indicate that the first excited state of Tl^{207} cannot be 5/2+ for no case with j = 5/2 survives this test.

An examination of these eight graphs shows that for mixed α-particle angular momenta the values of δ giving isotropy are the same for both γ-ray angular momenta, and for mixed γ-ray angular momenta the values of ϵ giving isotropy are the same for both α-partcile angular momenta.

Fig.4-22 shows the graph of possible values of δ and ϵ for a mixed α-mixed γ-correlation based on the shell model assignments (situation (a) above), which would give an isotropic angular correlation within the observed accuracy. The shaded areas represent the infinity of points whose coordinates (δ, ϵ) satisfy the isotropy conditions.

Discussion

The results of the preceding section may be summarized as follows:

i) The spin of the first excited state of Tl^{207} cannot be 5/2 so possibilities (c) and (d) above must be discarded and in what follows the shell model

prediction of 3/2+ will be accepted as the only reasonable alternative.

ii) As no pure δ-pure γ cascade represents the observations, one or other or both must be of mixed angular momentum. If one of the radiations is pure the possibilities are,

	Alpha particle	Gamma-Ray
I	Pure = 3	, M1 + (5.4 - 8.4)% E2
II	Pure = 5	M1 + (5.4 - 8.4)% E2
III	Pure = 4	M1 + (6.2 - 7.6)% E2
IV	Pure = 6	M1 + (6.2 - 7.6)% E2
V	(2.6 - 4.3)% = 3, (5)	Pure M1
VI	(2.6 - 4.3)% = 3, (5)	Pure E2
VII	(12.5-15.8)% = 4, (6)	Pure M1
VIII	(12.5-15.8)% = 4, (6)	Pure E2

iii) If both transitions are mixed the possibilities are shown in Fig. 4-22.

In order to determine which of the many possibilities represents the true nature of this decay additional evidence must be brought to bear.

It will be understood that α-transitions involving even angular momentum can arise only if the ground state of Bi^{211} possesses positive parity. There is no

evidence to suggest that this is so and negative parity is predicted by the single particle model. It is proposed to accept this prediction in the absence of any suggestion to the contrary. This leaves possibilities I, II, V and VI and those contained in Fig. 4-22. The conversion coefficient of the 350 keV gamma ray was 0.175 ± 0.017 indicating a 76% M1 + 24% E2 mixture. This indicates that none of the pure-mixed cases are applicable and that both the alpha particle and the gamma ray momenta are mixed.

Figure 4 - 21

Plots of $\Delta W/W$ vs. δ (see text) for pure alpha-mixed gamma angular correlations.

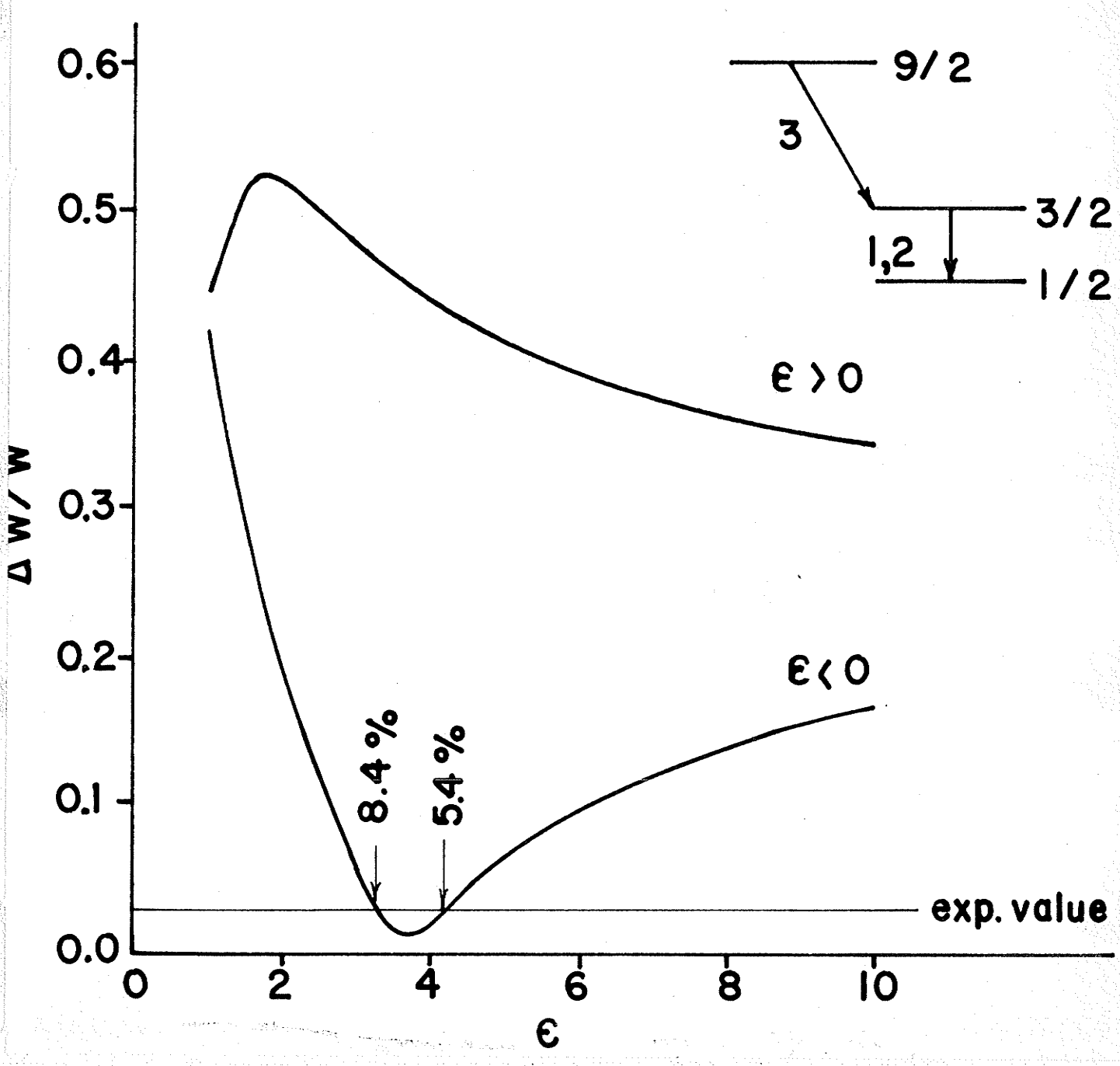
0.6
0.5
0.4
0.3
0.2
0.1
0.0
ΔW/W
0
2
4
6
8
10
ε
9/2
3
3/2
1,2
1/2
ε > 0
ε < 0
8.4 %
5.4 %
exp. value

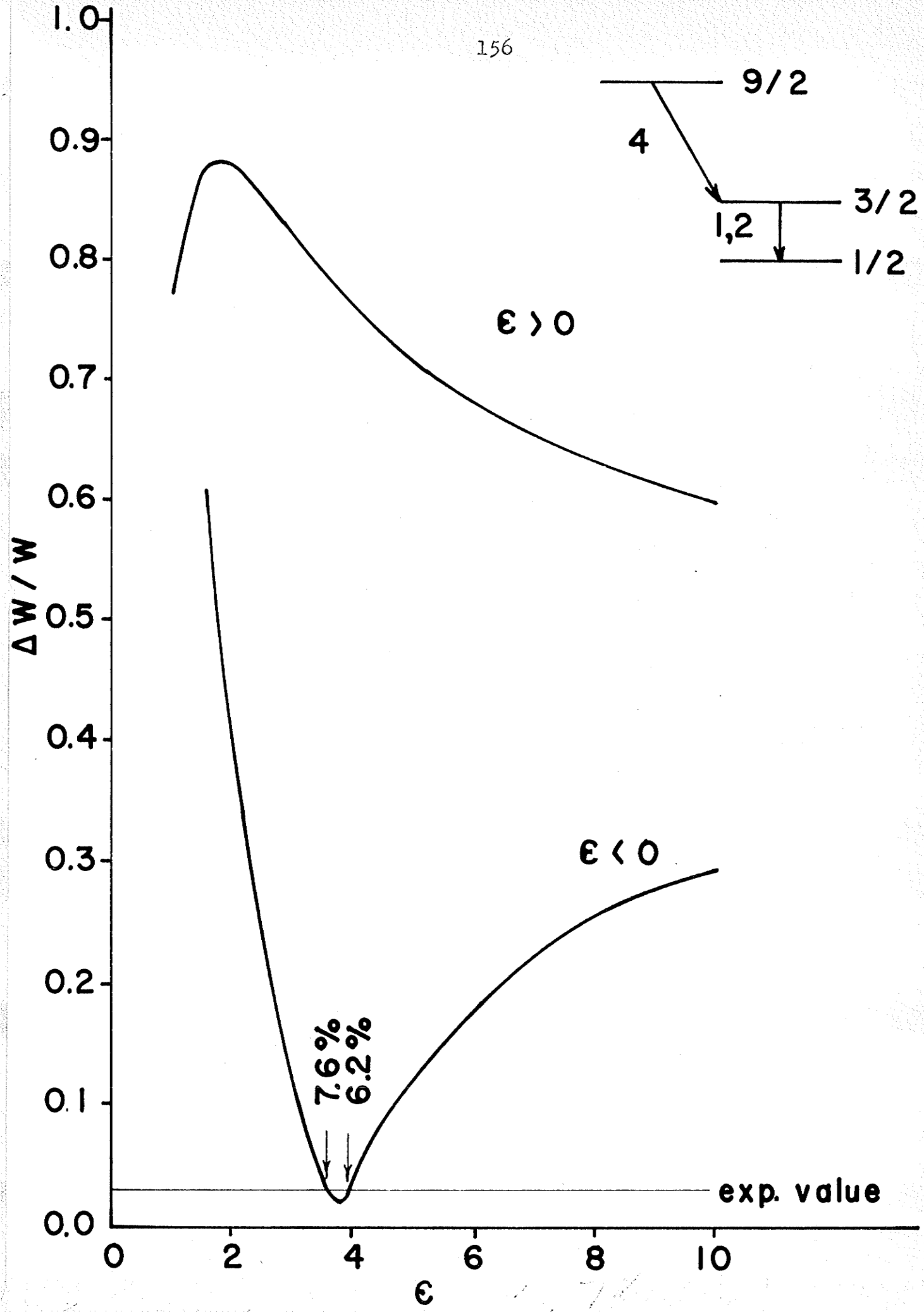
9/2
4
3/2
1,2
1/2
ε > 0
ε < 0
7.6%
6.2%
exp. value
ΔW/W
ε
1.0
0.9
0.8
0.7
0.6
0.5
0.4
0.3
0.2
0.1
0.0
0
2
4
6
8
10

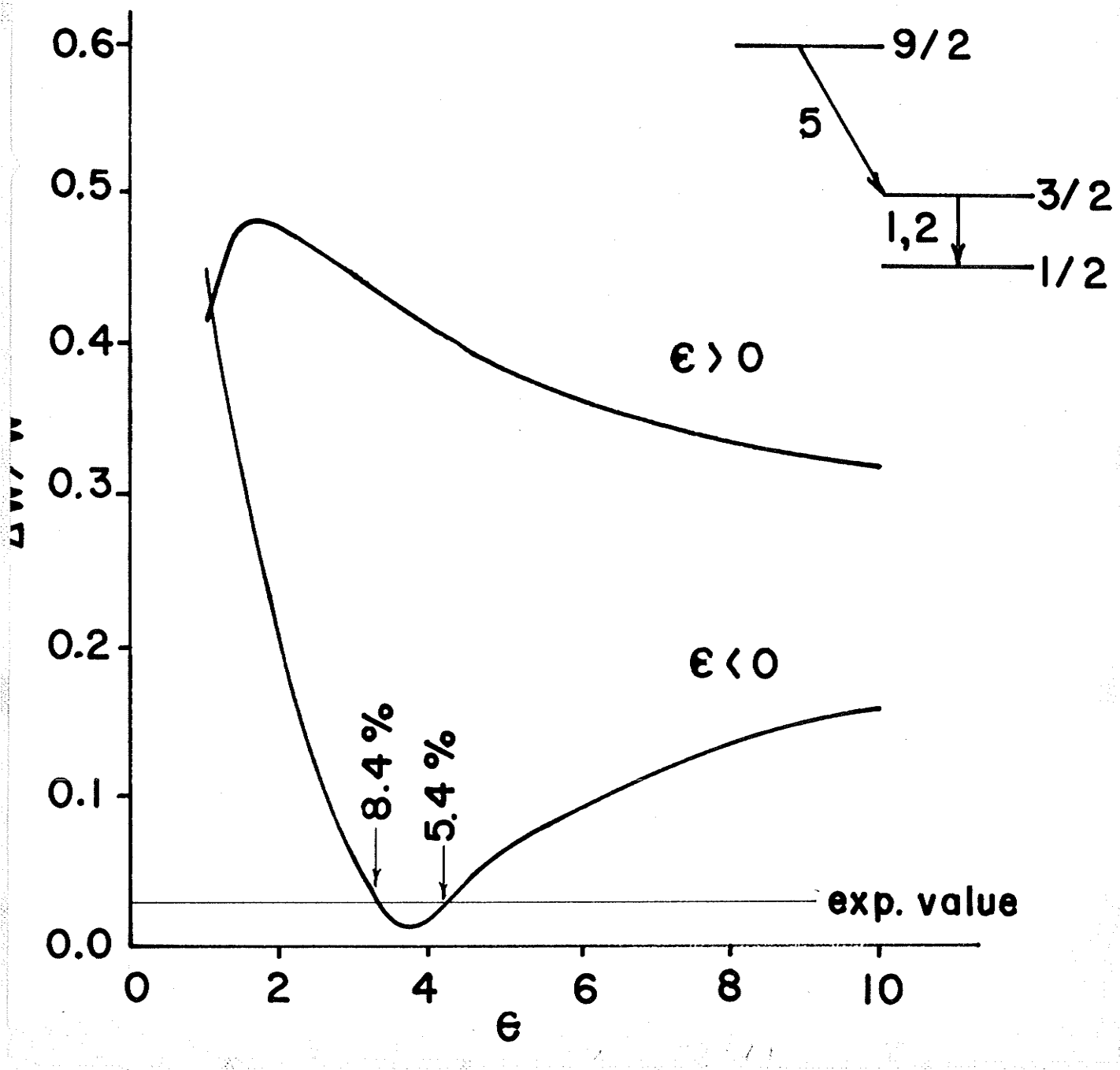
0.6
0.5
0.4
0.3
0.2
0.1
0.0
0
2
4
6
8
10
ε
9/2
5
3/2
1,2
1/2
ε > 0
ε < 0
8.4 %
5.4 %
exp. value

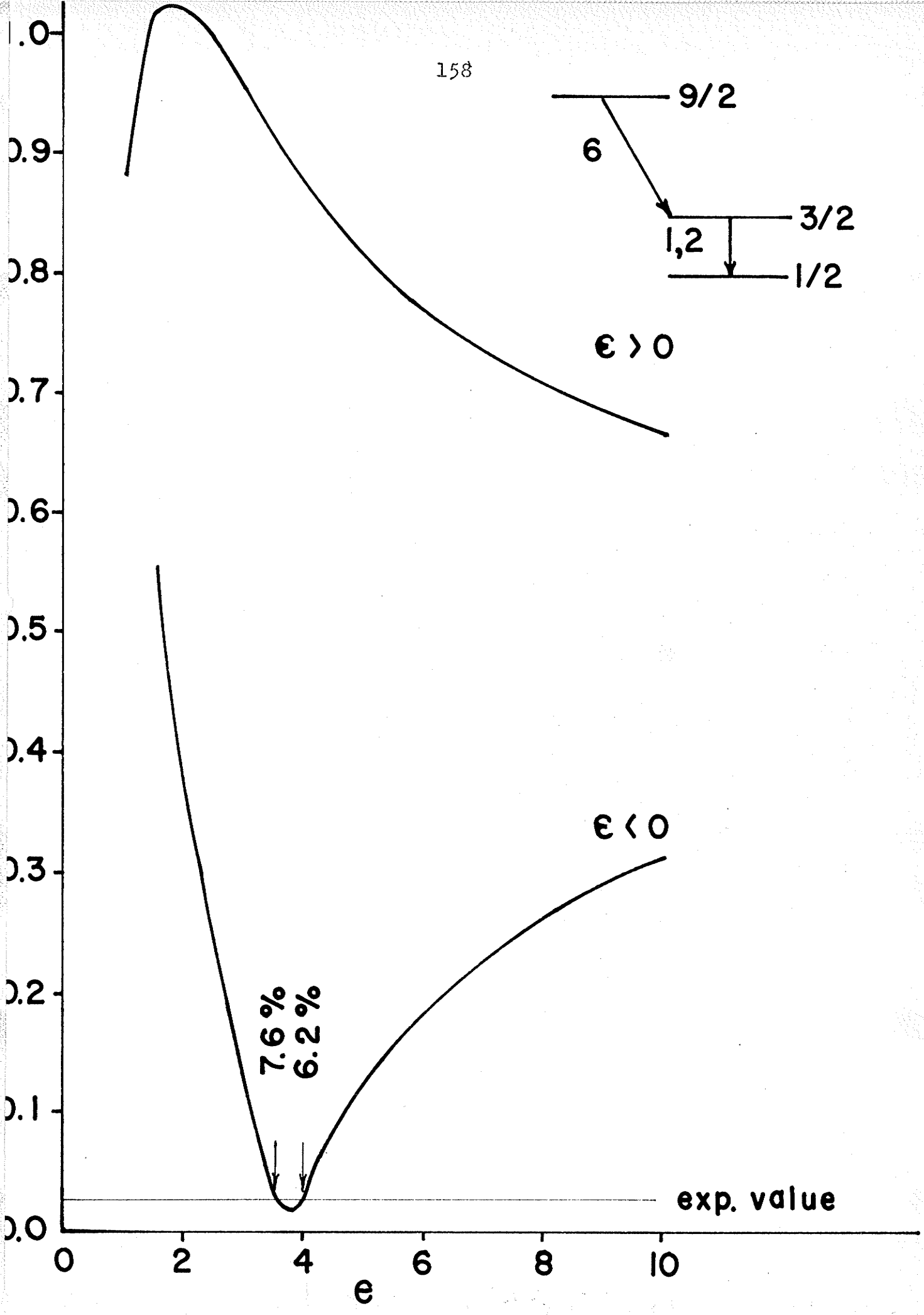
1.0
0.9
0.8
0.7
0.6
0.5
0.4
0.3
0.2
0.1
0.0
9/2
6
3/2
1,2
1/2
ε > 0
ε < 0
7.6%
6.2%
exp. value
0
2
4
6
8
10
e

Figure 4 - 22

Plot of the alpha mixing ratio (δ) against the gamma mixing ratio(ϵ)for shell model spins and parities. The crosses represent the values of Gorodetzky et al (G-8,1962).

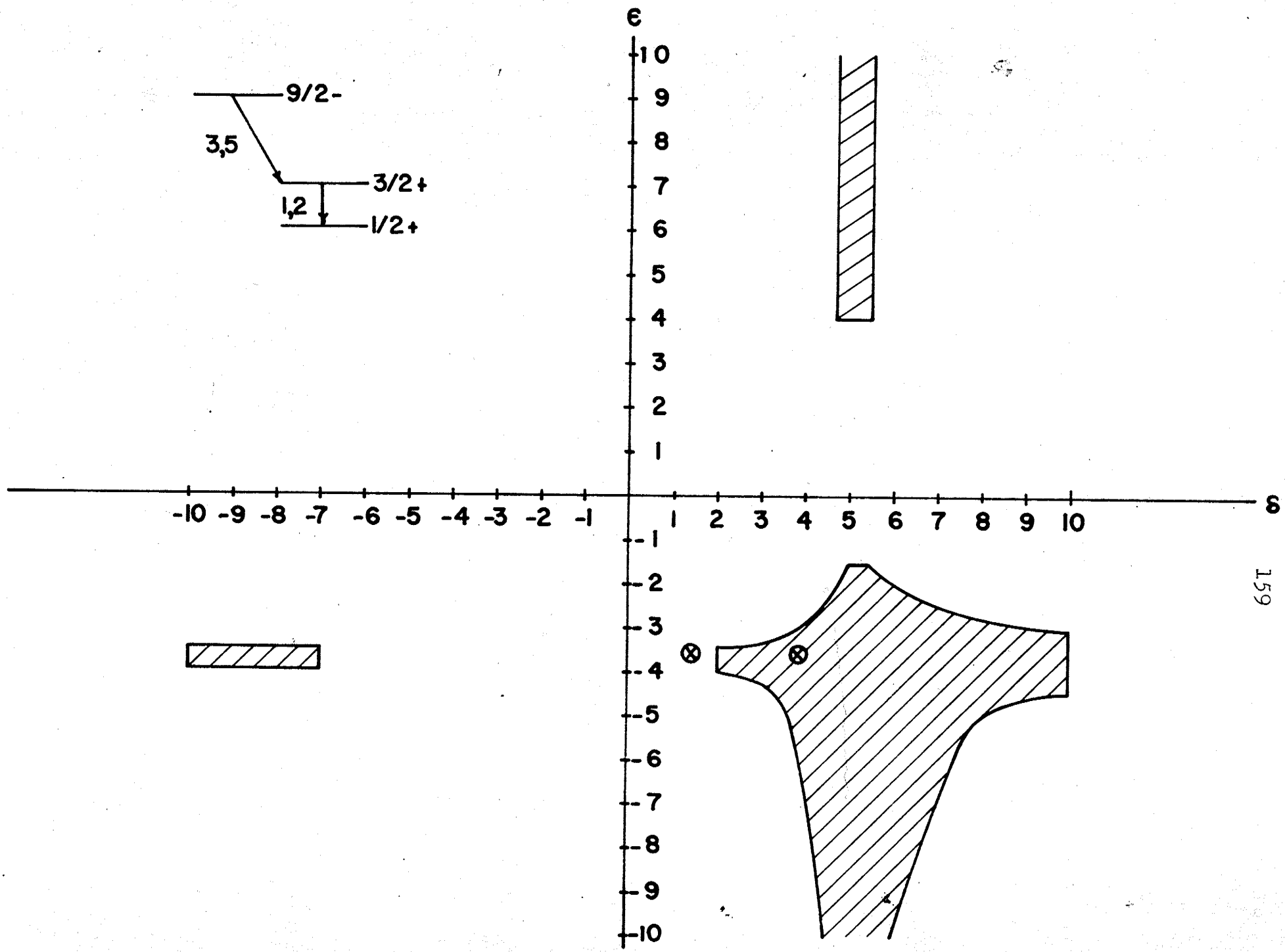
9/2-
3,5
3/2+
1,2
1/2+
ε
δ
10
9
8
7
6
5
4
3
2
1
-1
-2
-3
-4
-5
-6
-7
-8
-9
-10
-10 -9 -8 -7 -6 -5 -4 -3 -2 -1
1 2 3 4 5 6 7 8 9 10

4.11 Gamma-gamma angular correlations

Two gamma ray cascades in the active deposit were strong enough to allow their angular correlations to be measured. Both cascades were in Bi^{211} (430-400 keV and 706-400 keV). The sources used were collected on aluminum foil and were 3/8in. diameter in active area. They were exposed to the actinon gas for 1 hr. and then immediately counted for 1 hr. The counting rates are shown in the table below.

Cascade	Single channel rates(per sec.)	Real coincidence rates (per min.)	Chance coincidence rates (per min.)
430 and 400 keV	5,000	100	25
706 and 430	200 5,000	4	1

Coincidence counting rates were normalized by the single channel counting rates and normalized to the 90° count for both correlations. The data was collected for 90°, 120°, 150°, 180°, 210°, 240°, and 270°. The counts at the angles beyond 180° can be added to their corresponding angle below 180° to improve statistics. The correlations are shown in Fig. 4-23 (430-400 keV-statistical error $\pm 1\%$) and Fig. 4-24 (706-400 keV-statistical error $\pm 1\frac{1}{2}\%$). It will be seen from Fig. 4-23 that the present work agrees well with that of Vandenbosch et al. (V-1, 1963) and Giannini et al. (G-5, 1962) for the 400-430 keV angular correlation but the agreement is not as good with either group for the 400-706 keV angular correlation (see Fig. 4-24). This work required approximately 70 sources.

Figure 4 - 23

Gamma-gamma angular correlation for the 400-430 keV cascade. The X's are from a fitted curve.

x- Vandenbosch et al

o- Giannini et al

•- Present work

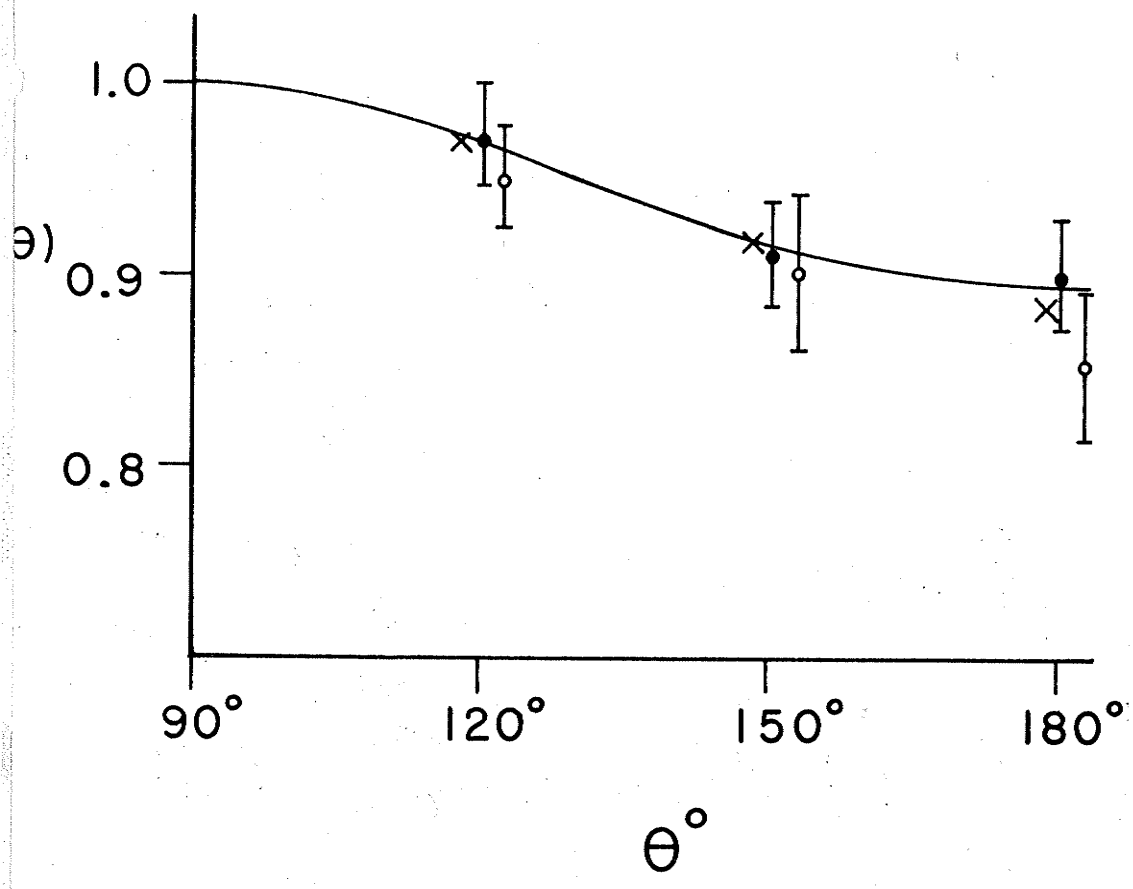

Figure 4 - 24

Gamma-gamma angular correlation for the 400-706 keV cascade. The X's are from a fitted curve.

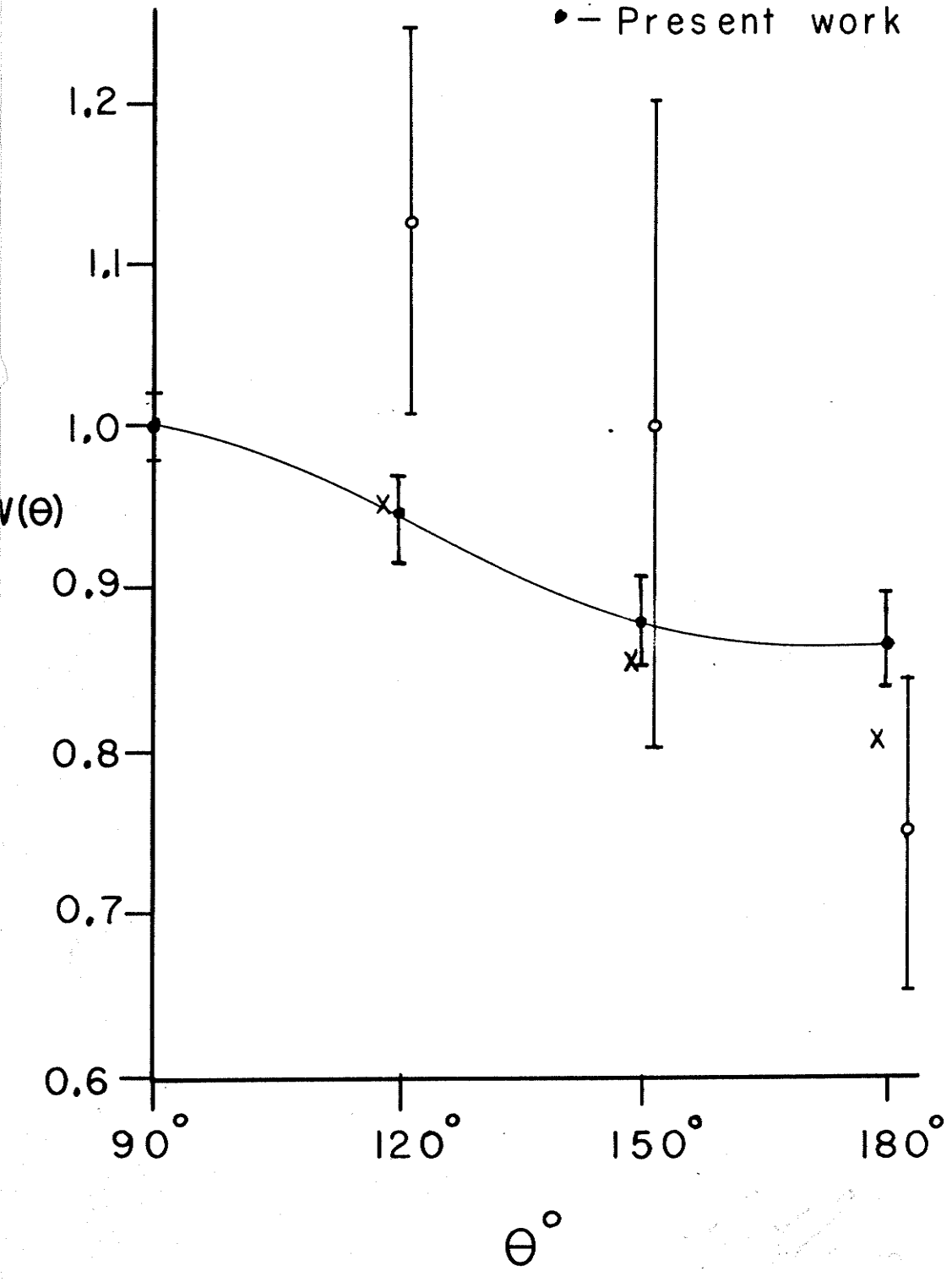
x - Vandenbosch et al
o - Giannini et al
• - Present work
1.2
1.1
1.0
0.9
0.8
0.7
0.6
W(θ)
90°
120°
150°
180°
θ°

Using the notation of Fig. 4-25, the expression for the angular correlation of a gamma ray of unmixed angular momentum L_1 followed by a gamma ray of unmixed angular momentum L_2 is (B-8, 1953; F-6, 1955; D-5, 1957)

$$W(\theta) = \sum_{\nu} A_{\nu} P_{\nu} (\cos\theta) \qquad 4\text{-}12$$

where $A_{\nu} = F_{\nu}(L_1 j_1, j)\ F_{\nu}(L_2 j_2 j)$

and $F_{\nu}(L_1 j_1 j) = (-1)^{j_1 - j - 1} (2j+1)^{1/2} (2L_1+1) C(L_1 L_1 \nu\ ;1\text{-}1)$

$W(jjL_1L_1;\ \nu\ j_1)$

The functions $P_{\nu}(\cos\theta)$ are the Legendre polonomials. The functions C and W are the Clebsh-Gordon and Racah coefficients which are related to Wigner's 3-J and 6-J symbols respectively (R-12, 1959 and Appendix II).

Figure 4 - 25

Notation for equations in section 4.11
(gamma-gamma angular correlations).

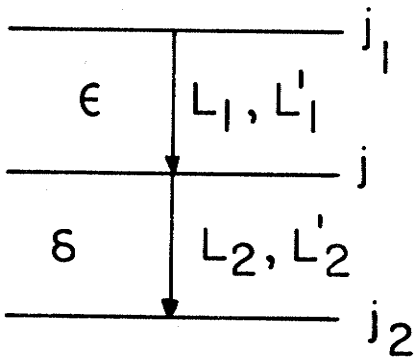
j_1
ϵ
L_1, L_1'
j
δ
L_2, L_2'
j_2

Restrictions on the values of ν are as follows

$$0 \leq \nu \leq 2j$$

$$0 \leq \nu \leq 2L_1$$

$$0 \leq \nu \leq 2L_2$$

If one of the gamma radiations is mixed (L_1 and L'_1) and the other pure L_2 the angular correlation function becomes

$$W(\theta) = 1 + \frac{1}{1+\delta^2} \sum_{\nu} [F_\nu(L_1 j_1 j) + \delta^2 F_\nu(L_1' j_1 j) + 2\delta F_\nu(L_1 L'_1 j_1 j)] \times F_\nu(L_2 L_2 j_2 j) P_\nu(\cos\theta) \qquad 4\text{-}13$$

where δ^2 is the ratio of the intensities of the gamma rays having angular momentum L'_1 to those having angular momentum L_1.

The function

$$F_\nu(L_1 L_1' j_1 j) = (-1)^{j-j_1-1} [(2j+1)(2L_1+1)(2L_1'+1)]^{1/2} G_\nu(L_1 L'_1 j_1 j)$$

and

$$G_\nu(L_1 L_1' j_1 j) = C(L_1 L_1' \nu ; 1-1) W(jj L_1 L'_1; \nu\ j_1)$$

The quantity $F_\nu(L_1 L'_1 j_1 j)$ does not change in value if L_1 and L'_1 are interchanged.

Finally, the angular correlation function for both radiations of mixed angular momentum is

$$W(\theta) = \frac{1}{(1+\delta^2)(1+\epsilon^2)} \sum_{\nu} [F_{\nu}(L_2 L_2 j_2 j) + \delta^2 F_{\nu}(L'_2 L'_2 j_2 j) + 2\delta F_{\nu}(L_2 L'_2 j_2 j)] \times [F_{\nu}(L_1 L_1 j_1 j) + \epsilon^2 F_{\nu}(L'_1 L'_1 j_1 j) + 2\epsilon F_{\nu}(L_1 L'_1 j_1 j)] P_{\nu}(\cos\theta) \qquad 4\text{-}14$$

where ϵ^2 refers to the intensity ratio of the L_1 to L'_1 angular momentum and δ^2 refers to the intensity ratio of the L_2 to L'_2 angular momentum.

The A_{ν}'s were corrected for finite solid angle by the method of Rose (R-11, 1853).

The half-life of the 400 keV state in Bi^{211} has been found to be $3.15 \pm 0.020 \times 10^{-10}$ sec. (V-1, 1963). This half life was borderline for the possibility of perturbing influences (extra nuclear fields, etc, D-6, 1957 and F-9, 1955). That is if the half life were much longer there would definitely be some perturbing influences. However it was here assumed that the correlation observed was a genuine nuclear effect.

The spin and parity of the ground state of Bi^{211} will be taken as $9/2^-$ in the following analysis. The justification for this selection was given in section 4.10.

Since the 400 keV transition contains some M1 radiation (Table 4-2) the spin of the 400 keV level (j) is related to that of the ground state (j_2) through $j = j_2 \pm 1, j_2$. On the basis of shell model predictions the value $j = j_2 = 9/2$ is most unlikely and will not be considered further. As $j_2 = 9/2$ then $j = 7/2$ or $11/2$. Moreover, both states must have the same parity because all three transitions contain some M1. For the second state (j_1), table 4-8 shows the possible spins and gamma ray angular momenta on the basis of the single particle model (P-8, 1962).

Table 4-8

j	j_1	L_1 and L_2
7/2	5/2,7/2,9/2,11/2	All combinations of the two lowest possible angular momenta e.g. (1,1 1,2 2,1 2,2)
11/2	7/2,9/2,11/2,13/2	

This gives rise to thirty possible unmixed correlations, twenty-eight possible correlations where one of the radiations was mixed and eight possible correlations

where both were mixed, which must be compared with the observed correlations.

Now, it will be remembered that the natures of all three gamma rays involved in the two correlations presently under study are known from the present work and it is believed that all three are of mixed angular momenta, yet Vandenbosch et al (V-1, 1963), on the basis of their α_K for the 350 keV transition obtained an α_K for the 430 keV transition (0.154) which implied that it was pure M1. Their angular correlation work was subsequently interpreted on this basis. Giannini et al (1962) interpreted their data as showing both the 400 and 430 keV transition as pure E2. It seemed worthwhile therefore to examine all possible cascades for pure-pure, mixed-pure and mixed-mixed angular momenta in order to see if a theoretical description based on the first two could fit the observations.

For the thirty unmixed correlations the IBM 1620 computer at the University of Manitoba was programmed to calculate $W(\theta)$ from equation 4-12 at 3° intervals. Six correlations are shown in Fig. 4-26 which are those which might be thought to approximate to a fit of the 400-706 keV and 400-430 keV correlations. The values of the spins j_1 and J and the angular momenta involved, L_1 and L_2 are shown in the figure. It will be seen that some of the

Figure 4 - 26

Theoretical angular correlations which are the best of those which might be thought to approximate to a fit of the 400-760 keV and 400-430 keV correlations. The experimental points for the 400-706 keV cascade are shown as open circles and the points representing the 400-430 keV cascade are shown as solid circles.

	j_1	j	L_1	L_2
1	11/2	7/2	2	2
2	7/2	7/2	1	2
3	11/2	11/2	1	1
4	7/2	11/2	2	1
5	7/2	11/2	3	1
6	7/2	7/2	1	1

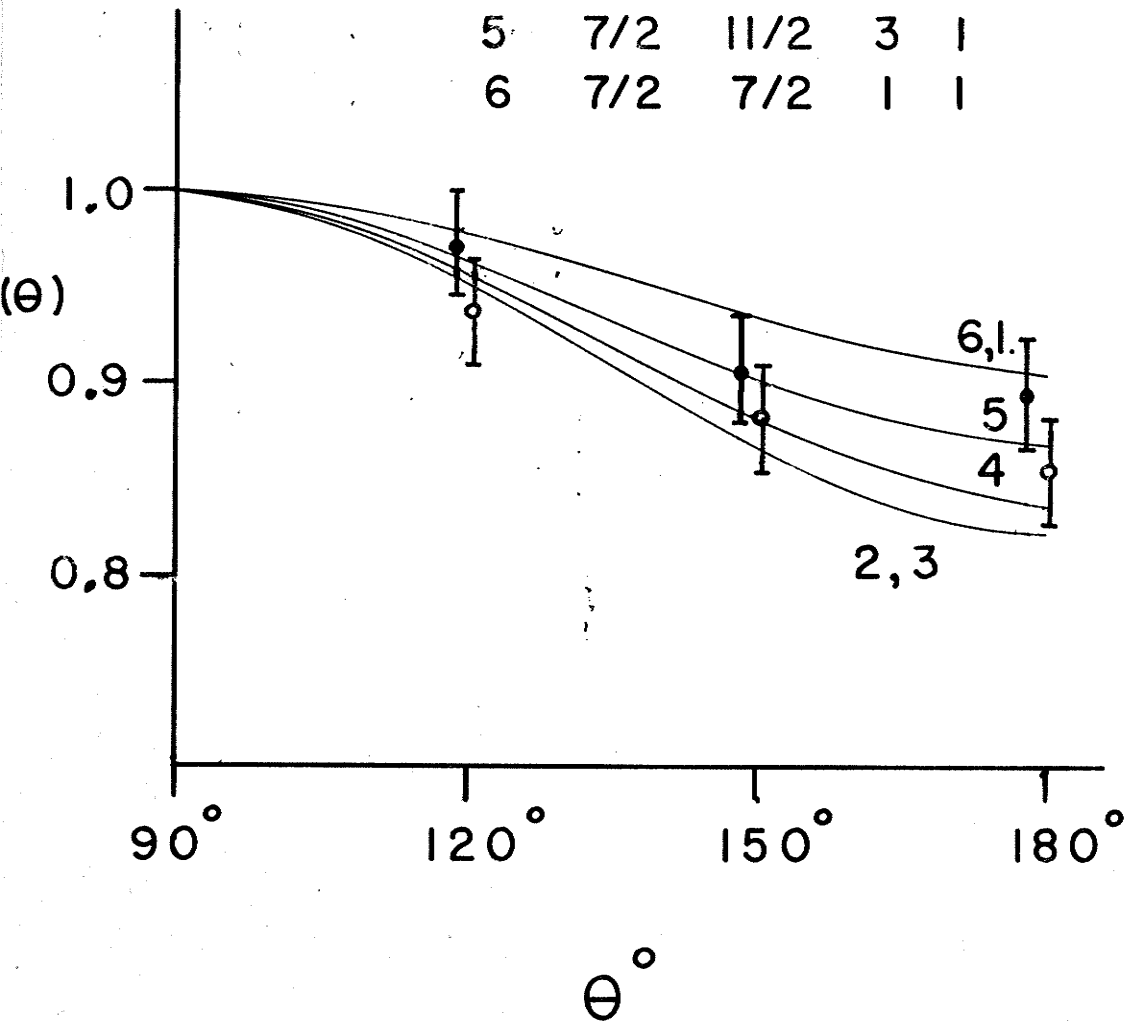

six do fit either the 400-706 keV of the 400-430 keV correlations. However all are rejected since from the internal conversion coefficients all three of the radiations involved are mixed. The experimental points for the 706-400 keV cascase are shown as open circles and the points for the 430-400 keV cascade are shown as solid circles. Both are normalized to unity at 90^{o}, and the error bars correspondingly increased to (1.4 x 2)%.

In order to compare the experimental data to the theoretical correlations for situations where one radiation is mixed and the other pure, the computer was programmed to claculate $W(\theta) / W(90^{o})$ from equation 4-13 for $\theta = 120^{o}$, 150^{o}, and 180^{o}, for the following values of δ; ±1, ±1.5, ±2, ±2.5, ±3, ±3.5, ±4, ±4.5, ±5, ±6, ±7, ±8, ±9, and ±10. This corresponds to a range of mixing of one gamma ray from 99% down to 1%.

Now Vandenbosch et al have indicated the 430 keV gamma ray to be pure and have suggested that the 706 keV gamma ray may be 99% pure M1. Therefore from the twenty-eight possible mixed-pure situations only those for which $L_1 = 1$, $L_2 = 1$ and $L'_2 = 2$ were chosen for examination. There were only six situations which satisfied these conditions. (Internal conversion and beta ray data do not support any $L_2 = 2$, $L'_2 = 3$). The values of $W(120^{o}) / W(90^{o})$, $W(150^{o}) / W(90^{o})$ and $W(180^{o}) / W(90^{0})$ as a function of δ are shown in Fig. 4-27 for these six situations. Superimposed on these

Figure 4 - 27

Plots of (a) $W(120^{\circ})/W(90^{\circ})$

(b) $W(150^{\circ})/W(90^{\circ})$

and (c) $W(180^{\circ})/W(90^{\circ})$

vs. δ (see text).

The experimental values are shown as the range between the solid lines (400-706 keV cascade) and the dashed lines (400-430 keV cascade).

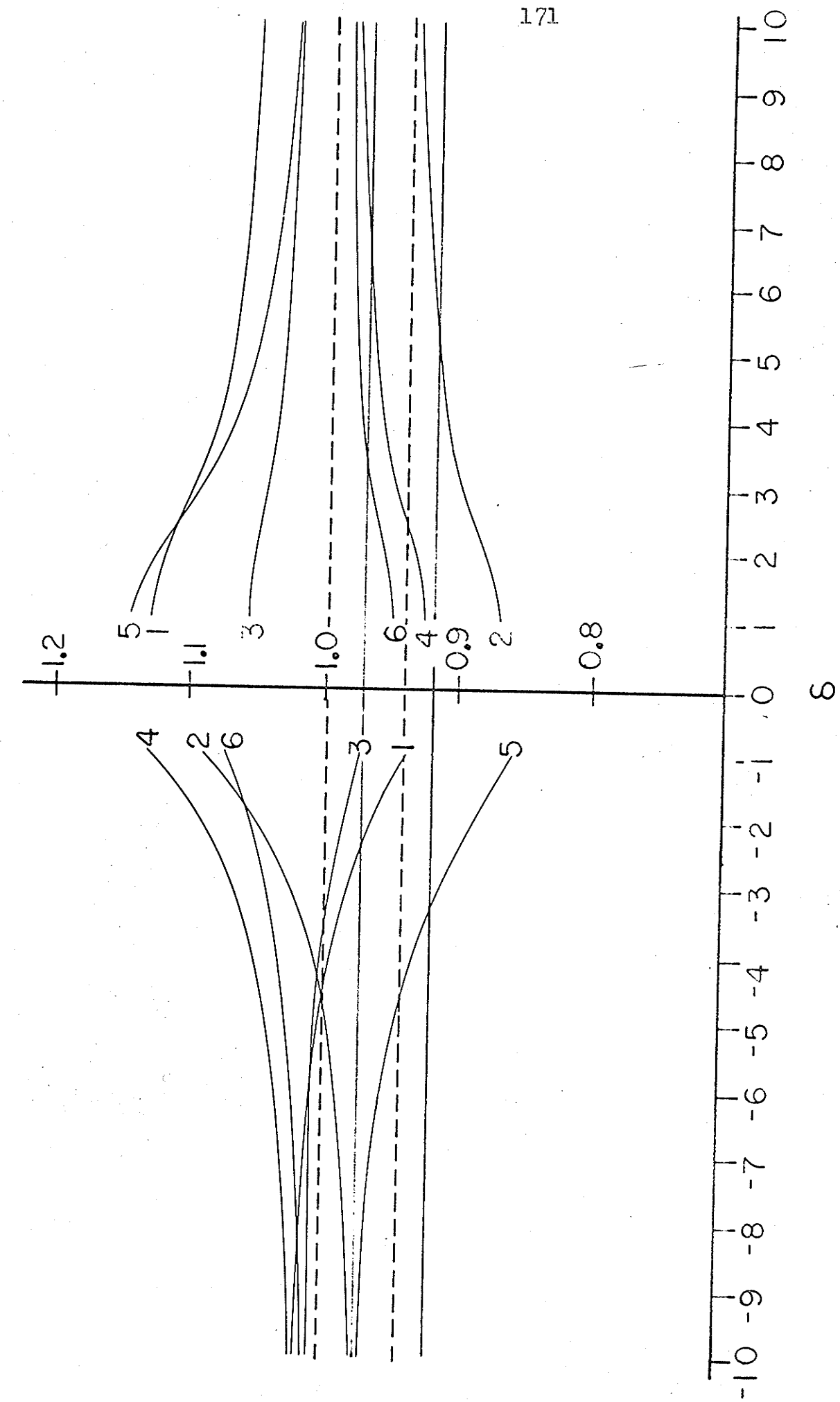
W(120°)/W(90°)
1.2
1.1
1.0
0.9
0.8
5
1
3
6
4
2
4
2
6
3
1
5
θ
10
9
8
7
6
5
4
3
2
1
0
-1
-2
-3
-4
-5
-6
-7
-8
-9
-10

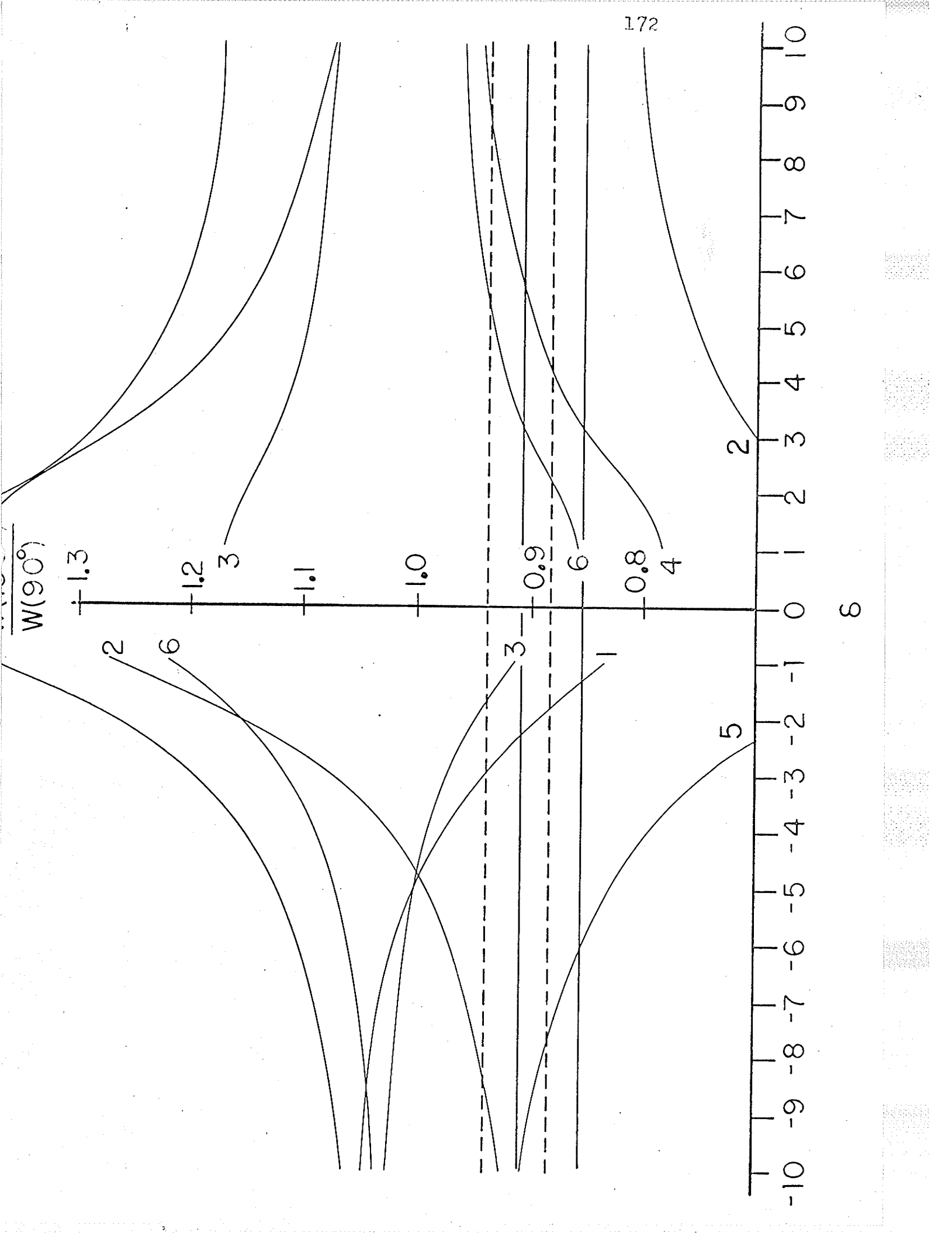
W(90°)
1.3
1.2
1.1
1.0
0.9
0.8
3
6
4
2
2
6
3
1
5
-10 -9 -8 -7 -6 -5 -4 -3 -2 -1 0 1 2 3 4 5 6 7 8 9 10
δ

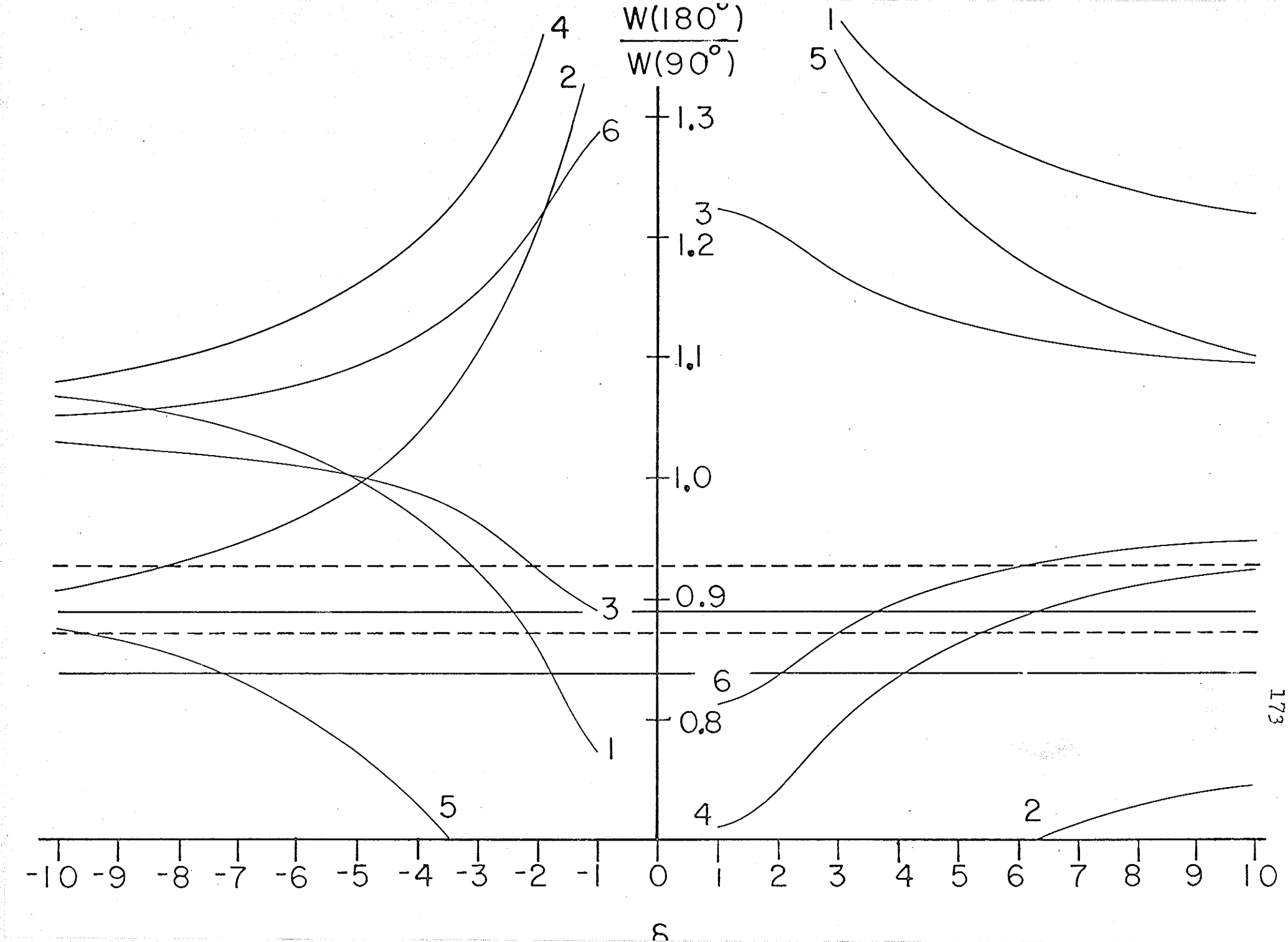
W(180°)
W(90°)
1.3
1.2
1.1
1.0
0.9
0.8
1
2
3
4
5
6
-10 -9 -8 -7 -6 -5 -4 -3 -2 -1 0 1 2 3 4 5 6 7 8 9 10
δ

curves are the experimental values of the two cascades. They are shown as the range of values between two horizontal lines, a solid line for the 706-400 keV cascade and a broken line for the 430-400 keV cascade. The error bars were increased to (1.4 x 1)% because of the normalization at 90°. The six situations are identified in Table 4-9. Table 4-9 also gives the range of the mixing ratio δ which satisfies the observations (i.e., lie between the horizontal lines) for all three values of $W(\theta) / W(90^\circ)$.

Table 4 - 9

Range of δ for mixed-pure cascades

$j_2 = 9/2$ $L_1 = 1$ $L_2 = 1$ $L'_2 = 2$

Situation	j_1	j	Cascade 706-400 keV	Cascade 430-400 keV
1	5/2	7/2	1.8 - 2.3	2.2 - 2.9
2	7/2	7/2	-	8.7 - 10
3	9/2	7/2	-	1.0 - 1.6
4	9/2	11/2	4.0 - 5.2	5.2 - 8.2
5	11/2	11/2	7.6 - 9.5	9.5 - 10
6	13/2	11/2	2.0 - 2.9	3.0 - 5.2

The α_k value of the 400 keV gamma ray given in table 4-2 is 0.091 ± 0.018 which corresponds to a possible range of mixing $1 \leq \delta \leq 2$.

This allows situation 1 and perhaps 6 for the 706-400 keV cascade with situation 3 for the 430-400 keV cascade. But neither 1 nor 6 can be accepted because the log ft value (section 4.9) of the beta transition to this level (1100 keV) is inconsistent with a spin of either 5/2 or 13/2. It is therefore unlikely from this evidence that either the 706 or the 400 keV gamma ray is of unmixed angular momentum. Situation 3 does fit the angular correlation data but is inconsistent with the internal conversion data (see table 4-2).

Next the mixed-mixed cascades will be examined. Since all radiations involved are known to be mixed this is the correlation which is expected to fit the physical situation under review. The eight situations are shown in table 4-10 where all possible values of $\in$ are given for which the mixing ratio of the 400 keV transition (δ) lies between 1 and 2. This information was obtained by programming the computer to calculate $W(\theta)/W(90^{\circ})$ from equation 4-14 for $\theta = 120^{\circ}$, 150° and 180° and for δ and $\in$ each having the range 1-10 as shown in detail earlier and selecting from the readout those ranges of $\in$ which occured for $1 \leq \delta \leq 2$ and which were within the experimentally observed range for all three $W(\theta)/W(90^{\circ})$ values.

Table 4-10

Range of ϵ for mixed-mixed correlations

Situations where $1 \leq \delta \leq 2$

Situation	j_1	j	Cascade 706-400 keV	Cascade 430-400 keV
1	5/2	7/2	6 - 10	8 - 10
2	7/2	7/2	2.5	2.5 - 3, 7 - 10
3	9/2	7/2	3.5	4, 9 - 10
4	11/2	7/2	8 - 10	3, 6 - 10
5	7/2	11/2	2	2, 4 - 4.5
6	9/2	11/2	-	-
7	11/2	11/2	4	2, 3.5
8	13/2	11/2	-	4.5 - 5, 9 - 10

Consider table 4-10 which shows the range of ϵ for mixed-mixed situations where $1 \leq \delta \leq 2$. Situation 1 would make the spin of the 830 keV level 5/2 and situation 8 would make the spin of the 830 keV level 13/2 both of which are inconsistent with the log ft value for the beta feed to that level (see section 4.9). Situations 4 and 5 require a mixed radiation of angular momentum 2 and 3 which is inconsistent with the internal conversion coefficients of both the 430 keV and the 706 keV gamma rays. Situation 6 does not fit the possible range of mixing ($1 \leq \delta \leq 2$) for the 400 keV gamma ray as determined by its internal conversion coefficient.

For the situations where j = 11/2 (5-8)this leaves only situation 7 which would make the spin of the 400, 840, and 1100 keV levels all 11/2. There is no isotope in the Pb^{208} region which has three levels below 2 MeV all with the same spins, and since such an assignment (all three levels 11/2) would be inconsistent with the single particle model, situation 7 is rejected. This leaves situation 2 and 3, both of which are consistent with the internal conversion coefficients of the 430 keV add 706 keV transitions and means that the available spins for the 830 keV and 1100 keV levels are 7/2 and 9/2. Noting that the beta decay of Pb^{211} prefers to decay to the 830 keV level rather than the 400 keV level (see table 4-6) it would not be reasonable to assign to these two states the same spin. Thus since the spin of the 400 keV level has been determined as 7/2, the 830 keV level is assigned the spin 9/2. If the 1100 keV level were assigned spin 9/2 it would make the 1100 keV, 830 keV and ground levels all have spin 9/2 which as pointed out above is not reasonable. Therefore the 1100 keV level is assigned spin 7/2.

Chapter 5

DISCUSSION

5.1 Introduction

The final chapter discusses the active deposit of actinium according to the radiations de-exciting each isotope. The discussion compares the known experimental and theoretical information including the present work. The discussion follows 'chronologically' the decay of the active deposit, i.e., the beta decay of Pb^{211}, levels in Bi^{211}, ..., levels in Pb^{207}. It will be seen that the present experimental results are consistent with each other and are in general consistent with the meagre amount of knowledge previously known. For some measurements (e.g., the internal conversion coefficients) the present work does not agree with other researchers' results; however in all such cases arguments are advanced to explain the discrepancy. In general the agreement with the few theoretical works available is quite good although the applicability of the nuclear shell model to the isotope involved in the active deposit is questionable (see section 5.3).

5.2 The beta decay of Pb^{211}

Hahn and Meitner (H-4, 1908) were the first to examine the beta rays from the decay of Pb^{211}. Two groups were found; one of low intensity which was easily absorbed and a stronger more penetrating group. The former was rather arbitrarily assigned to the decay of Pb^{211} and the latter to the decay of the subsequent product, Tl^{207}.

On the other hand, Sargent, (S-16, 1933) in many careful experiments found a high energy group in the decay of Pb^{211} which had the same penetrating power as the beta rays from Tl^{207}. In later work Sargent (S-15, 1939) found the low energy group of Hahn and Meitner had a range of 0.08 gm./cm.^{2} in aluminum and a maximum energy of 300 keV. The intensity of this group was too small in any case to account for the complete decay of Pb^{211} (if it were to represent the decay of Pb^{211} it should be approximately as intense as the beta rays from Tl^{207} when in equilibrium). Further, the low energy group did not fit the rule enunciated by Sargent (S-25, 1933) between half life and endpoint energy. The energy (300 keV) was not high enough to correspond to the observed half life of 36.1 min. (S-4, 1939) and Sargent pointed out that Sanielevici (S-17, 1936) supported the presence of a high energy beta component

in the decay of Pb^{211} from heating measurements in a micro-calorimeter. Assuming 470 keV to be the average energy of the beta rays from Tl^{207}, Sanielevici found the average energy of the Pb^{211} spectrum to be 370 keV. The value, obtained by Lecoin (L-4, 1938) for this was 360 keV and he further concluded the endpoint of the spectrum to be between 1.00 and 1.25 MeV. Lecoin's description of his spectrum however (L-3, 1936) bears little resemblance to that determined in this work.

Sargent's value of the endpoint from absorption measurements was 1.39 MeV (no error quoted), the maximum range being 6.4 gm./cm.^{2} of aluminium, using the relation

$$R = 0.526E - 0.094 \quad \text{----- (S-4, 1939)}$$

With this extreme endpoint, ''from graphical attemps at breaking up the spectrum into two reasonable components'' the endpoint of the lower energy group emerged as 500 keV as opposed to the 300 keV of earlier work. The intensity of the high energy component relative to the low was placed between 1/2 and 1/5. From this Sargent inferred that the excitation probability of the state fed by the low energy component was between 0.12 and 0.17. Li's value (L-1, 1937) for the excitation probability was 0.195 and also in the same paper he quotes 3.3 secondary beta rays per 100 Pb^{211} decays. The latter number corresponds well to the intensity of the internal conversion lines determined in this work.

Sargent's view of Li's value was 'In view of all the difficulties of measuring beta and gamma intensities the agreement is as good as can be expected'. Sargent (S-4, 1939) comments that the partial decay constants are 0.000040 and 0.00028 sec.$^{-1}$ for the endpoints of 0.50 and 1.39 MeV respectively are in good agreement with the expected half life-energy curves.

Much more recently, Vandenbosch et al (V-1, 1963) used a six-gap beta spectrometer with 1.2% resolution and 10% transmission to measure the beta spectrum. They did not unpeel the partial beta spectra from the composite spectrum but used beta-gamma coincidences to determine the endpoint energies and intensities of the partial spectra. Their coincidence apparatus had a resolving time of 12.5 nanosedonds and the gamma detector was a 7.6 x 7.6 cm. NaI(Tl) crystal. Coincidences were examined between the beta rays and the 830, 400 and 430 keV gamma rays. The present work is the only one to examine the entire beta spectrum in detail and to unpeel the partial beta spectra.

Table 5-1 below sets out the results of all the above work.

Table 5-1

Observer	End Point Energies (keV)			
Sargent (1933)	-	500 (10%)	-	- (90%)
Lecoin (1936)	-	-	-	1000-1250
Li (1937)	-	500 (19.5%)	-	- (80.5%)
Sargent (1939)	-	500 (12-17%)	-	1390(83-88%)
Vandenbosch et al (1963)	251±25(0.7±0.2%)	525±25(5.5±0.8%)	951±25(1.4±0.5%)	1355±25(92.4±1.5%)
Present Work	200±100(2±1%) *248±18(0.9±0.2%)	470±100(6±3%) 548±7(7.3±0.5%)	- 978±7(0.4±0.12%)	1378±8 (92±4%) - (90.2±0.5%)

* Calculated using gamma ray energies and intensities.

5.3 The levels in Bi^{211}

(a) Gamma rays

Until the present work was undertaken the gamma ray spectra of the active deposit of the actinium series had not been investigated with any technique other than by examining the gamma ray attenuation in different absorbers. Rutherford and Richardson (R-10, 1913) found that the mass absorption coefficient for the gamma rays from Ra^{223} (which is the precursor of the active deposit) and its daughters was 0.073 in aluminum of thickness 6 - 9 cm. Curie and Savel (C-11, 1933) found the mass absorption coefficient for the same gamma rays to be 0.076 for lead of thickness between 4.6 and 10.6 cm. That these coefficients are likely to be due to the more penetrating gamma rays of Bi^{211} was suggested by Sargent (S-4, 1939). This conclusion seems reasonable in light of the present day knowledge of the gamma rays of Ra^{223} and its daughters (W-1, 1962); however it is not quantitative enough to determine a level scheme. Using the energies of the internal conversion electrons and their binding energies, the energies of the expected gamma rays were determined by several authors in the 1930's (G-11, 1933; C-2, 1938 and S-19, 1936). The intensities of the gamma rays were estimated by Surugue (S-6, 1941) using his own data and that of Li (L-1, 1937) and are shown in table 5-2 (below). These estimates depend on knowing the relative intensities of the internal conversion lines, the absolute intensity of one of them

(in this case the 350 keV K conversion line) and the internal conversion coefficients. Before the internal conversion tables of Rose (R-17, 1958) and Sliv and Band (S-24, 1958) appeared the knowledge of the internal conversion process was limited and calculations based on earlier tables are open to criticism. As an example Sargent (S-4, 1939) states that the 350 keV gamma ray 'must be electric quadrupole'. It is now known to be mixed M1 and E2 with the M1 admixture the predominant one. Sargent also shows that the intensities Li quotes assuming that the 400 and 430 keV transitions were E2 are close to his intensities. Also he shows agreement with the estimates of Kara-Michailova (K-8, 1938). It is now known (see section 4.5) that the 400 and 430 keV transitions are 42 and 72 M1 respectively. It should be noted that none of the three predominant investigators involved in the early beta and gamma ray work (Sargent, Li and Surugue) quote errors, and neither Li nor Surugue mention transient equilibrium or its effect on their values.

Sargent (S-4, 1939) attempted to determine the intensity of the gamma rays relative to the intensity of the beta rays using the experimentally determined mass absorption coefficients, initial intensities with corrections (how they were determined and what corrections were needed were not explained) and average gamma and beta ray energies.

He reduces the beta intensity by a factor of 1.32 to account for 'reflection from the aluminum disc'. That this determination was crude was recognised by Sargent when he put an error of ±50% on the number determined stating 'the number of gamma quanta from actinium (B and C) (Pb^{211} + Bi^{211}) is about 19 per 100 beta particles from actinium B'(Pb^{211}). He was in agreement with Kara-Michailova but not with Li (L-1, 1937) or Surugue (S-20, 1937). Sargent tries to explain the discrepancy by suggesting that Surugue (S-20, 1937) assumed erronously that the radiation was M1 instead of E2. It seems remarkable that considering the state of the theory and Sargent's techniques, which are crude by today's standards, that he should have seen through the numbers to what we now know is the true situation.

Li (L-1, 1937) using an erronous value for the absolute intensity of the 350 keV K conversion electrons thus gets erronous values for the intensities of the other beta conversion lines he . . . . . measured. (See tables 5-3 and 5-4, and section 5.2). Considering the weak sources he had (a few hundredth of a millicurie) it is not surprising that his work agrees only in general with the present work. The amount of disagreement can be seen in the comparison between the K/L ratios in table 5-4. Furthermore it is surprising in view of the crudeness of Li's experimental method that it should lead to even reasonable intensities for the gamma rays (see table 5-2). Li concludes his paper with the level scheme shown in Fig. 5-1.

Table 5-2

Gamma rays in Bi^{211}

Intensity relative to the 350 keV gamma ray in Tl^{207}

Energy (keV)	Surugue and Li (iF transitions is dipole)	Vandenbosch et al	Giannini et al	Present Work
80	-	-	< .009	-
88	.00019	-	< .018	-
170	-	-	~.006	-
260	-	-	.0076±.0019	-
270	-	-	~.006	-
290	-	-	-	0.009 ± 0.001
350	1.000	1.000	1.000	1.000
400	.236	.258±.052	.34±.05	0.31 ± 0.03
430	.202	.125±.025	.22±.02	0.22 ± 0.02
487	.010	-	-	-
650	-	-	.0076±.0015	<0.014 ± 0.003
706	-	.038±.011	.055±.004	0.055 ± 0.006
758	.067	-	.061±.004	0.064 ± 0.06
830	.400	.248±.025	.34±.02	0.28 ± 0.03
1060	-	-	.0038±.0019	0.0053 ± 0.0005
1100	-	.0107±.0016	.014±.002	0.0088 ± 0.0009

As can be seen from table 5-2 the detail concerning the gamma rays in Bi^{211} is not well defined. The first column shows the energy of the gamma ray and the other columns indicate the relative intensities due to various authors. For Vandenbosch et al (V-1, 1963) and the present work the first several places are left blank in the table because the technique used did not allow investigation of energies below 300 keV. Surugue and Li used internal conversion lines to determine the gamma ray intensities including those in the region below 300 keV. Giannini et al used the sum coincidence method which allowed them to see low energy gamma rays. Vandenbosch et al seems to have identified only the scintillation peaks in the gamma ray spectrum without considering the possibility that the peaks might be due to more than one gamma ray. Giannini et al used the sum coincidence technique throughout. It is now known (S-27, 1963 and S-28, 1964) that some of the peaks in a sum coincidence spectrra may be due to coincidences between a known gamma ray and a compton scattered photon. Because (a) the gamma rays they claim at 80, 170, 260 and 270 keV have not been seen elsewhere,
(b) considering the technique used (sum coincidence) and
(c) because only a few counts (5-10) are shown in these peaks, it seems reasonable to conclude that they were due

to Compton scattered events. The K X Ray for Bi^{211} is 85 keV (S-29, 1955) and this is identified with the gamma ray shown at 88 keV. Walter and Coche (W-2, 1960) using a Th^{227} source (which occurs in the actinium series above the active deposit) found gamma rays at 405, 425, 827 and 1070 keV. They did not quote intensities and in view of the present work failed to resolve the composite spectrum into its constituent gamma rays. The gamma ray shown at 487 keV by Surugue (S-13, 1946) and Li has not been seen since and is probably spurious. The present work affords the first confirmation of the 1060 and 1100 keV levels first suggested by Giannini et al (G-5, 1962). The works of Giannini et al and Vandenvosch et al were published after the present work had been started and in fact after the present work had shown the presence of the 1060 and 1100 keV levels.

Vandenbosch et al (V-1, 1963) found by gamma-gamma coincidence that the 706 keV and 430 keV gamma rays are in cascade with the 400 keV gamma ray. The present work confirms this and also shows the 758 keV gamma ray to be in cascade with the 290 keV gamma ray and that the 650 keV gamma ray is in cascade with the 400 keV gamma ray. This provides evidence that the 830 keV, 1060 keV and 1100 keV levels are in Bi^{211}.

Figure 5 - 1

Level diagram of Bi^{211} due to Li(1-1,1937).

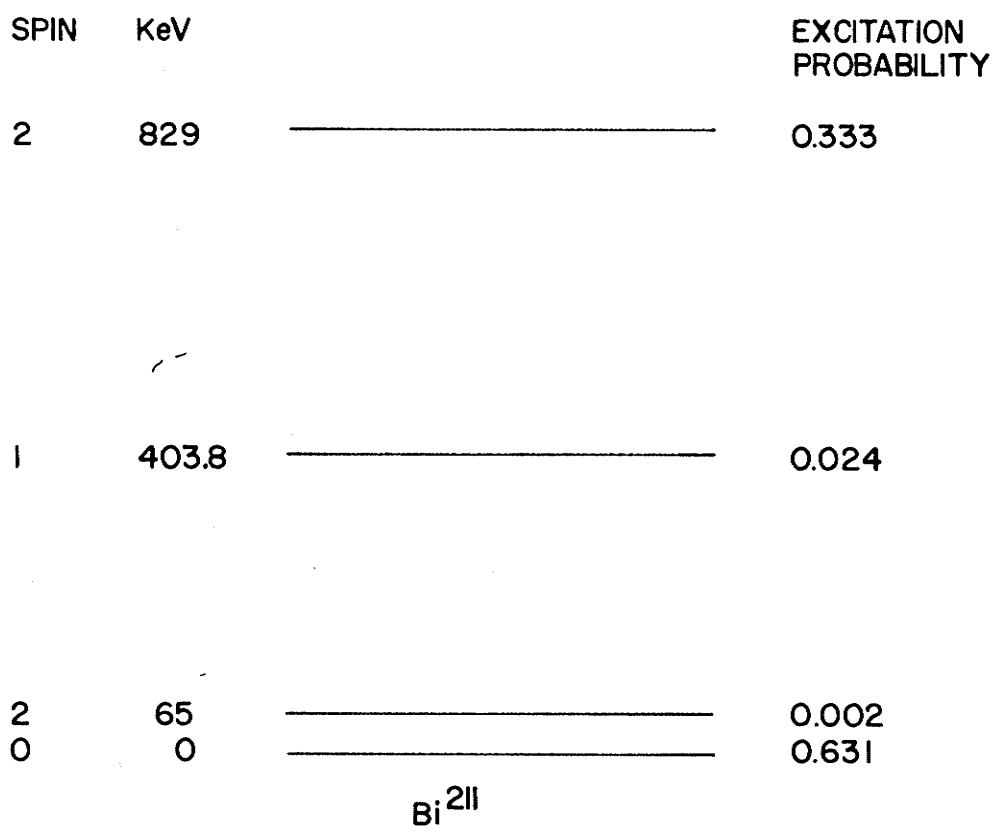
SPIN
KeV
EXCITATION PROBABILITY
2
829
0.333
1
403.8
0.024
2
65
0.002
0
0
0.631
Bi 211

Line	Hρ	II Energy in e-volts	III Energy of γ-ray in e-volts	IV Shell	V Intensity Rel.	V Intensity Abs. (electron/disint.)	VI Experimental internal conversion coeff. for K shell Quadripole	VI Experimental internal conversion coeff. for K shell Dipole	VII γ-ray intensity (calc. from cols. V & VI) If Quadripole	VII γ-ray intensity (calc. from cols. V & VI) If Dipole
AcB . C										
γ A	763·2	48·90	65·22	L_I	20	0·0032	—	—	—	—
A_a	768·5	49·56	65·22	L_{II}	2	0·0003	—	—	—	—
A_b	858·8	61·22	65·23	M_I	5	0·0008	—	—	—	—
A_c	881·3	64·29	65·23	N_I	1	0·0002	—	—	—	—
γ C	2157	313·4	403·8	K	25	0·0041	0·062	0·017	0·065	0·236
D_c	2522	387·5	403·8	L_I	3	0·0005	—	—	—	—
γ D_2	2250	335·2	425·6	K	20	0·0032	0·052	0·016	0·062	0·202
D_d	2544	409·4	425·7	L_I	5	0·0008	—	—	—	—
D_e	2602	421·7	425·7	M_I	5	0·0008	—	—	—	—
γ E	3805	739·0	829·4	K	10	0·0016	0·012	0·004	0·135	0·400
E_a	4075	813·2	829·4	L_I	2	0·0003	—	—	—	—
AcC . C″										
γ B	1946	264·6	349·7	K	100	0·0162	0·100	0·025	—	—
D_1	2247	334·4	349·7	L_I	40	0·0065	—	—	—	—
D_a	2295	346·0	349·7	M_I	5	0·0008	—	—	—	—
D_b	2306	348·8	349·7	N_I	1	0·0002	—	—	—	—

Table 5-3 Li's(L-1,1937) internal conversion results and analysis.(AcB is Pb^{211}, AcC is Bi^{211} and AcC'' is Tl^{207})

(b) Internal Conversion Lines and
Level Excitation Probability

As can be seen from table 5-4 the agreement between Vandenbosch et al and the present work is reasonably good. The K/L ratios of Li (see table 5-3) do not correspond to the values determined in the present work. No other experimenter (except Li) has been able to resolve the 430 K line from the 350 L line although Vandenbosch et al determined the intensity of the 430 keV K line relative to the 400 keV K line by measuring both of these lines in coincidence with K X Rays. There is good agreement between their value and the value calculated in the present work (see Section 4.5). Vandenbosch et al had a spectrometer with a 10% transmission and were still unable to see the 706 keV K and 830 keV K lines on the beta continuum. Vandenbosch et al improved their signal to noise ratio by a factor of ten by recording only events in coincidence with K X Rays. Neither of these lines were seen in the present work which combined with Vandenbosch's findings leads one to suspect that Li's observation is spurious since Li had weaker sources and cruder techniques.

Pilger (P-3, 1957) gives a beta continuum with internal conversion lines for Ra^{223} and daughters but the isotopes above the active deposit in the actinium series are so rich in conversion lines that it is not clear which

Table 5-4

		400 keV	430 keV	700 keV
α_K	Giannini et al	.033±.006	.039±.010	-
	Vandenbosch et al	.108±.026	.154±.039	.035±.012
	Present Work	.091 ± .018	.117 ± .024	.025±.010*
	Giannini et al	100% E2	10% E2	-
	Vandenbosch et al	50%M1+45%E2	100%M1	82%M1
	Present Work	42%M1+58%E2	72%M1+28%E2	45%M1+55%E2
K/L	Li	8.2	4.0	-
	Present Work	4±1	7±2	-

lines are due to the active deposit. Pilger's work was concentrated on the isotopes above the active deposit.

The determination of internal conversion coefficients depends, among other things, on a knowledge of the number of 350 keV K electrons per Pb^{211} beta decay. Vandenbosch et al quotes this number as 0.0314, the number from the present work being 0.0245 ± 0.0024 (see section 4.5). Since Vandenbosch et al's number is higher than that of the present work it would introduce a calculable systematic error in the internal conversion coefficients which depend on it. The internal conversion coefficients shown as starred (*) in the present column (table 5-4) result from a normalization to the values of Vandenbosch et al. As was pointed out in section 4.4, the source was covered to prevent the loss of Tl^{207} by alpha recoil for the internal conversion measurements. If Tl^{207} was lost the resulting beta continuum would be smaller than its true value and thus any internal conversion coefficient determined by the peak to continuum method would be high. It should be noted from table 5-7 that all the other values for α_K (350 keV) are higher than that of the present work. Only Falk-Variant mentions the effect of alpha recoil (although he did not comment on whether he covered his source) and his value is the closest to the value determined here. Since all the other α_K's depend on α_K (350 keV) (see section 4.5) it is

Table 5-5

Excitation Probability

level	Li	Vandenbosch et al	Giannini et al	Present Work
1100 keV	-	.007	.012±.001	0.009±0.001
1060	-		.004	0.004±0.0005
830	.333	.055	.087±.006	0.073±0.001
758	-	-	.009±.001	0.008±0.001
400	.024	.014	~.009	0.004±0.0005
0	.637	.924	.879±.01	0.902±0.001

$\log_{10}$ ft

β transition to level at	Vandenbosch et al	Giannini et al	Present Work
1100 keV	5.9	5.5	5.7
1060		6.7	6.4
830	5.9	5.5	5.8
758	-	6.8	6.8
400	7.3	7.5	7.8
0	5.9	6.1	6.0

not surprising that they are all higher than the present values also. Giannini et al did not explain how they calculated their α_K's and they infer E2 which is in violent disagreement with the present work and that of Vandenbosch et al.

From the absolute gamma intensities and the internal conversion coefficients the excitation probability for the levels in Bi^{211} and the corresponding $\log_{10}$ft values for the beta feeds to these levels were determined and are shown in table 5-5. As can be seen the $\log_{10}$ft values cluster around 6 which is consistent with the interpretation that the transitions are first forbidden following modern views on beta decay (W-5, 1961).

(a) Spins and Parities

As was pointed out in Section 4.11 two other determinations of the gamma-gamma angular correlation have been made and there was some agreement between them and the present work. However the interpretation and analysis by the previous workers (Vandenbosch et al, V-1, 1963 and Giannini et al G-5, 1962) were far from complete. Giannini used α_K values different from those used in the present work and assigned to the 430 and 706 keV transitions a 100% E2 nature. They thus suggest a mixed-pure correlation

giving the 830 keV level spin 11/2 and the 400 keV level spin 7/2. They claim that the 1100 keV level must be 7/2 but do not explain this. Vandenbosch et al using their seemingly high α_K values assign a 100% M1 nature to the 430 keV gamma ray and a large (82%) M1 nature to the 706 keV gamma ray. From this they suggest spin 9/2 for the 830 keV level, 7/2 for the 400 keV level but cannot find agreement between their angular correlation and α_K value for the spin of the 1100 keV level. The present work agrees with the above two in that the spin of the 400 keV level is 7/2 but since the α_K values determined here indicate that both the 430 and 706 keV gamma rays are mixed both angular correlations should involve mixed radiations. As was pointed out in section 4.11 the only set of spins and parities consistent with the present angular correlation, the gamma ray intensities and the internal conversion coefficients are: ground level ($9/2^-$), 400 keV level ($7/2^-$), 830 keV level ($9/2^-$) and 1100 keV level ($7/2^-$).

The decay scheme of Pb^{211} and the level scheme of Bi^{211} resulting from the present work is shown in Fig.5-2.

It seems somewhat surprising to find so many low lying excited levels (five) in a nucleus which has only three nucleons outside the closed shells.

Figure 5 - 2

The decay scheme of Pb^{211} and the level scheme of Bi^{211} resulting from the present work. The $\log_{10}$ ft values are shown in parenthseis.

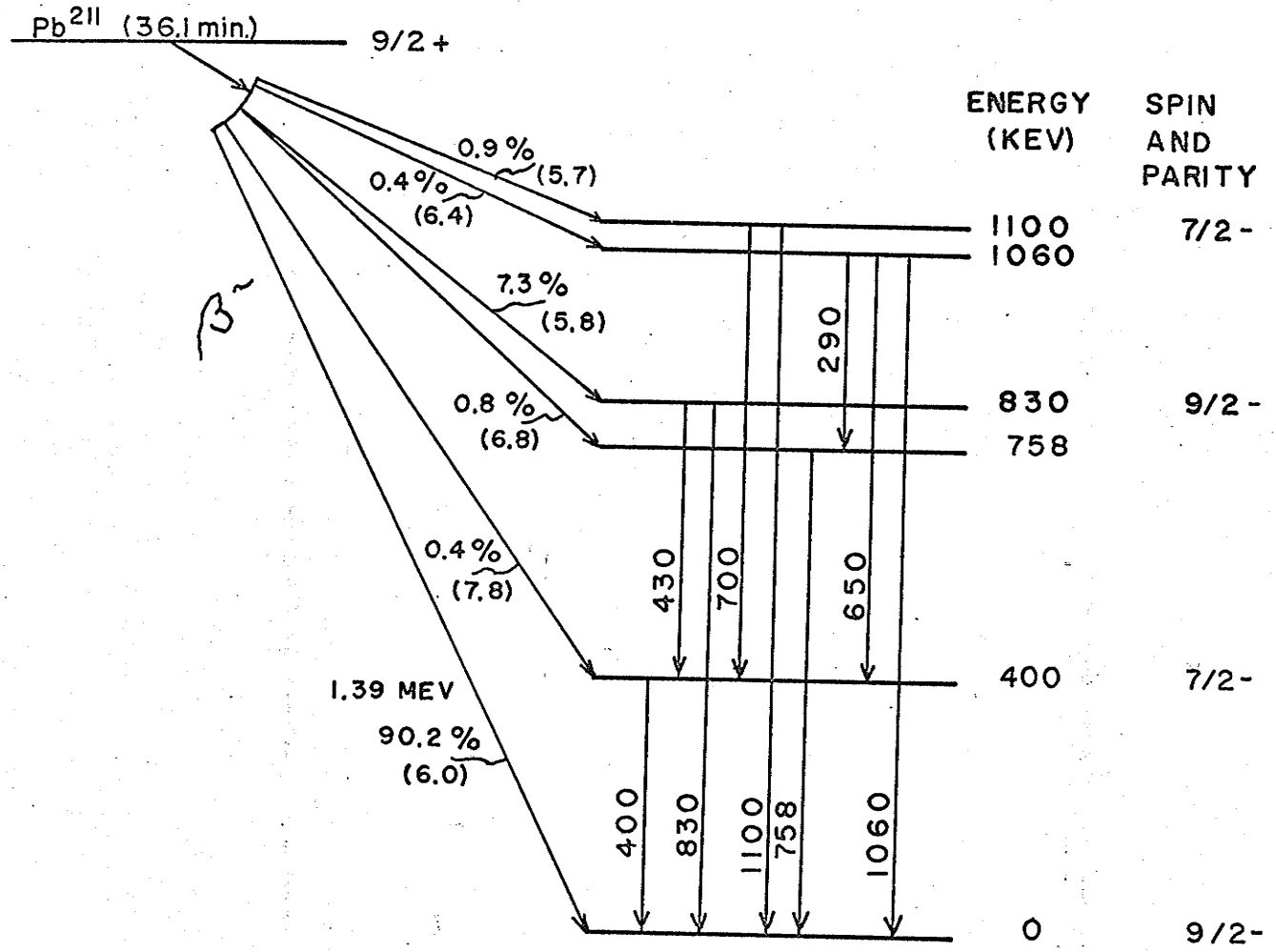
Pb211 (36.1 min.)
9/2+
ENERGY (KEV)
SPIN AND PARITY
0.9 %
(5.7)
0.4 %
(6.4)
β⁻
7.3 %
(5.8)
0.8 %
(6.8)
0.4 %
(7.8)
1.39 MEV
90.2 %
(6.0)
1100
1060
830
758
400
0
7/2-
9/2-
7/2-
9/2-
290
430
700
650
400
830
1100
758
1060

In passing, it should be noted that Zeh and Mang (Z-1, 1962) had some success in describing Po^{211} (also three nucleons outside the closed shells) with shell model wave functions. However in light of the many levels of Bi^{211} the applicability of the shell model to such systems is questionable.

5.4 Alpha Decay of Bi^{211}

The alpha decay of Bi^{211} involves the assembly of the alpha particle from two protons, one inside and one outside the closed shell at Z = 82.

As mentioned in section 4.2 there were two alpha particles involved in the decay of Bi^{211}. The table below (Table 5-6) shows the energies and relative intensities of these two due to various authors.

Table 5-6

Worker	energy (MeV)	intensity (%)	energy (MeV)	intensity (%)
Rutherford (1931)	6.597	84	6.254	16
Falk-Variant (1954)	6.621	82.6	6.274	17.4
Pilger (1957)	6.617±0.002	83.3±0.7	6.273±0.002	16.7±0.7
Rytz (1961)	6.62219±0.00069	-	6.27752±0.00068	-
Walen et al (1962)	6.6218	84	6.2781	15.8
Giannini et al (1962)	-	-	-	15.8
Present work	6.618±0.005	83.3±0.2	6.280±0.005	16.2±0.2

Walen et al saw a 5.9464 MeV group in the alpha particle spectrum of Ra^{223} along with 45 other alpha groups. They contended the 5.9464 MeV alpha group was in the decay of Bi^{211} to Tl^{207} and quote an intensity of 3.7×10^{-5} alpha particles/Bi^{211} decay. Their attempt to assign a spin to the resulting 675 keV level in Tl^{207} is not conclusive and their assignment of the alpha particle to Bi^{211} is dubious since the present work puts an upper limit of 10^{-5} alpha particles/Bi^{211} decay on an alpha particle of 5.946 MeV (see section 4.6).

Rutherford et al (R-9, 1931) searched for alpha particles in the range 7.1 cm. to 12 cm. ($\sim$7.7 MeV to $\sim$10.7 MeV) for the actinium active deposit and put an upper limit of any possible alphas of less than 1 in 300,000 of the two main alpha feeds (per Bi^{211} decay). This was further confirmed by Curie and Rosenblum (C-10, 1931). As shown in section 4.4 and 4.6 no other alpha particles exist in the region 7.6 - 13 MeV with intensity greater than 1 part in 10^6 compared to the two main alpha feeds. Also there are no alpha particles in the energy range 7.0 - 7.6 with intensity greater than 1 part in 10^4. Pilger (P-3, 1957) puts an upper limit of 2 parts in 10^3 compared to the main alpha feeds of any other alpha particles within 100 keV of the main alpha feeds.

Discussions of the present state of alpha decay theory are available in the literature (W-3, 1952-5, H-10, 1959), and in particular theoretical calculations have been performed for the alpha decay of Bi^{211} (R-5, 1959, H-10, 1959). However the latter two authors make contradictory predictions concerning the alpha decay of Bi^{211} which allow little meaningful interpretation of experimental work in terms of theoretical predictions. It should be pointed out that there are two major difficulties with present alpha decay theories; (1) they ignore the preformation factor, i.e., the probability of two neutrons and two protons getting together at the nuclear surface with the proper energy to escape (for further discussion of this point see P-7, 1949), and (2) the calculations are very sensitive to small changes in the nuclear radius, a parameter whose value is not precisely known.

Zeh and Mang (Z-1, 1962) used shell model calculations and obtained a value for the ratio of the intensity of the 6.280 MeV alpha particle to the 6.618 MeV alpha particle of 0.15 using a shell model radial function and including configuration mixing. The experimental value

from the present work is 0.193 ± 0.002. Zeh and Mang also predicted that the ratio of the intensity of the L = 5 to the L = 3 transitions for the 6.280 MeV alpha particle as 0.12. The experimental value determined here (see Fig. 4-22) is 0.04 ± 0.01 if the shell model spins and parities are assumed. Considering the large uncertainties encountered in alpha decay theory this agreement can be considered good.

5.5 The Levels in Tl^{207}

Tl^{207} having one proton less than doubly magic Pb^{208} would be the most likely of the isotopes in the active deposit of actinium to be described by the shell model.

Since the 350 keV gamma ray is by far the most intense one in the active deposit, it is well known (Pilger P-3, 1957, Vandenbosch et al V-1, 1963, Gorodetzky et al G-7, 1953, Falk Variant F-7, 1954). From alpha particle and alpha-gamma coincidence studies in the present work there are no other levels with intensity greater than 0.0002% of all the Bi^{211} decays.

The theoretical level scheme of Bloomquist and Wahlborn (B-2, 1960) is shown in Fig. 5-3. The energy separation of the two lowest levels corresponds well to the experimental value (350 keV) but the zero energy levels disagree by about 0.7 MeV between experimental and

theory. Pryce in a theoretical calculation using the independent particle model puts the separation of the levels in Tl^{207} at 350 keV and suggests that the ground state spin is $1/2^+$ and the excited state spin $3/2^+$.

The α_K and K/L ratios of the 350 keV transition are shown in table 5-7. The present α_K value is lower than any of the previous ones which as suggested in section 5.3 may be due at least in part to other workers neglecting to cover the source to prevent the loss of Tl^{207}.

Using the theoretically calculated alpha decay intensities, Zeh and Mang (Z-1, 1962) predicted the ratio of E2/M1 for the 350 keV transition to be 0.27 ± 0.02. The experimental value determined here was 0.31 ± 0.10 which is in excellent agreement and lends support to the interpretation of the alpha transition to the excited state being predominantly $\lambda = 3$ (see discussion of Mang's calculation in section 5.4).

Table 5-7

Worker	α_K	Multipolarity
Falk-Variant	0.18 ± 0.03	-
Gorodetzky et al	0.195 ± 0.015	M1 with 7-12% E2
Vandenbosch et al	0.239	100% M1
Mead	0.24 ± 0.01	100% M1
Present work	0.175 ± 0.017	M1 with 24 ± 10% E2

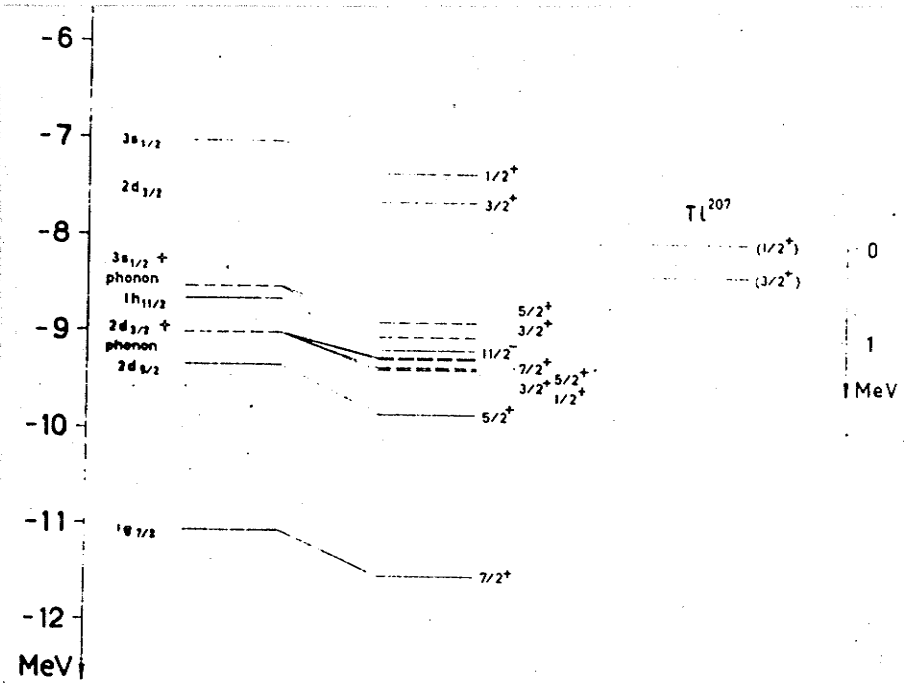

Theoretical unperturbed (to the left) and perturbed energies for proton states, and experimental levels of the nuclei $Pb^{208} \pm$ one proton. Dotted lines denote the lowest quadrupole vibrational states. Arrows indicate energies used for the choice of parameters.

Fig. 5-3 (from Bloomqvist and Wahlborn, B-2, 1960)

Table 5-7 continued,

Worker	K/L
Li	2.5
Falk-Variant	5.5 ± 0.5
Present work	5.0 ± 0.5*

As shown in section 4.10 the most plausable interpretation of the alpha gamma angular correlation is to assign a spin $1/2^+$ to the ground state and spin $3/2^+$ to the 350 keV level.

Gorodetzky et al had measured the alpha-gamma angular correlation of Bi^{211} previously (G-7, 1953) and also got an isotropic correlation. However their interpretation of this result was to invert the spins of the ground and 1st excited state suggested above. With spin 1/2 assigned to the first excited state the theoretical angular correlation is always isotoropic regardless of the ground state spin, the spin of the parent level (the ground state of Bi^{211}) or any of the transitional angular momenta involved. Theoretically, this arises because of a failure of the triangulation requirements of the angular momenta involved in the F functions (B-8, 1953) which are themselves contained in the coefficients of the Legendre polonomials in the angular correlation function.

---

* Calculated for the observed M1, E2 mixture

An alternative suggestion by Perlman and Rasmussen (P-4, 1956) retained the shell model spin assignments (Fig. 5-2) but has postulated mixed alpha particle angular momentum (λ = 3 and 5 in the proportion 87% and 13% with a pure M1 gamma transition). A further suggestion (Gorodetzky et al (G-8, 1962)) has been that the alpha transition is pure λ = 3 but that the gamma transition is mixed (M1 with 12% E2). They (Gorodetzky et al) performed a polarization correlation experiment and accepting an α_K of 0.195 suggested that the cascade could also be described by alpha particles of mixed angular momentum (λ = 3 with either 6.8 or 64.8% λ = 5) and a gamma ray of mixed nature (M1 with 12% E2). These two points are shown in Fig. 4-22 as crosses and it will be seen that only one (6.8% λ = 5) is consistent with the angular correlation, however neither cross is consistent with the present internal conversion value (M1 with 24% E2).

Gil and Petit (G-6, 1961) have also measured the alpha gamma angular correlation of Bi^{211} and report that their findings are consistent with the following spins: Bi^{211} (9/2), Tl^{207*} (3-2) and Tl^{207} (1/2). The present work shows (section 4.10) that none of theprevious intepretations are complete representations of the experimental evidence. In fact from the α_K of the 350 keV transition the gamma ray is mixed (M1 with 24% E2) and since the ranges of gamma ray mixing allowed by the pure alpha-mixed gamma theoretical correlations (see section 4.1) do not include the possiblity

of a 24% E2 component both radiations must be mixed. The most probable spins, parities and angular momenta are shown in Fig. 5-5.

It will be clear from this work that it is not sufficient to determine a single set of spins, parities, angular momenta and mixing ratios from the angular correlation work in order to arrive at the physical pattern being studied. Far from being unique, any one result which is consistent with the data may be only one of an infinity of equally good theoretical interpretations, and an appeal to other information may be required to narrow down the range of possibilities.

Further, it should be noted that even though the parameters predicted by a certain nuclear model fit a correlation, they may not be the only parameters to do so, hence the fit cannot be taken as confirming evidence for this model. The present results accommodate among others the shell model spins and parities but this cannot be interpreted as a confirmation of the applicability of the model to the levels in question. It is no more than plausible that this is so.

It is somewhat surprising to find an isotope which has seemingly only one excited state. Although there may be other excited levels their intensity would be more than five orders of magnitude down from that of the 350 keV level (see section 4.2).

Figure 5 - 5

The alpha decay scheme of Bi^{211} and the levels in Tl^{207} resulting from the present work.

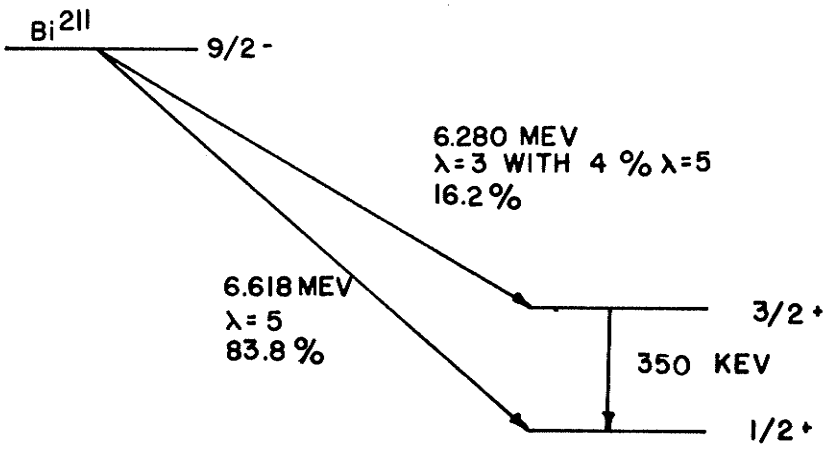
Bi211
9/2-
6.280 MEV
λ=3 WITH 4 % λ=5
16.2 %
6.618 MEV
λ=5
83.8 %
3/2+
350 KEV
1/2+

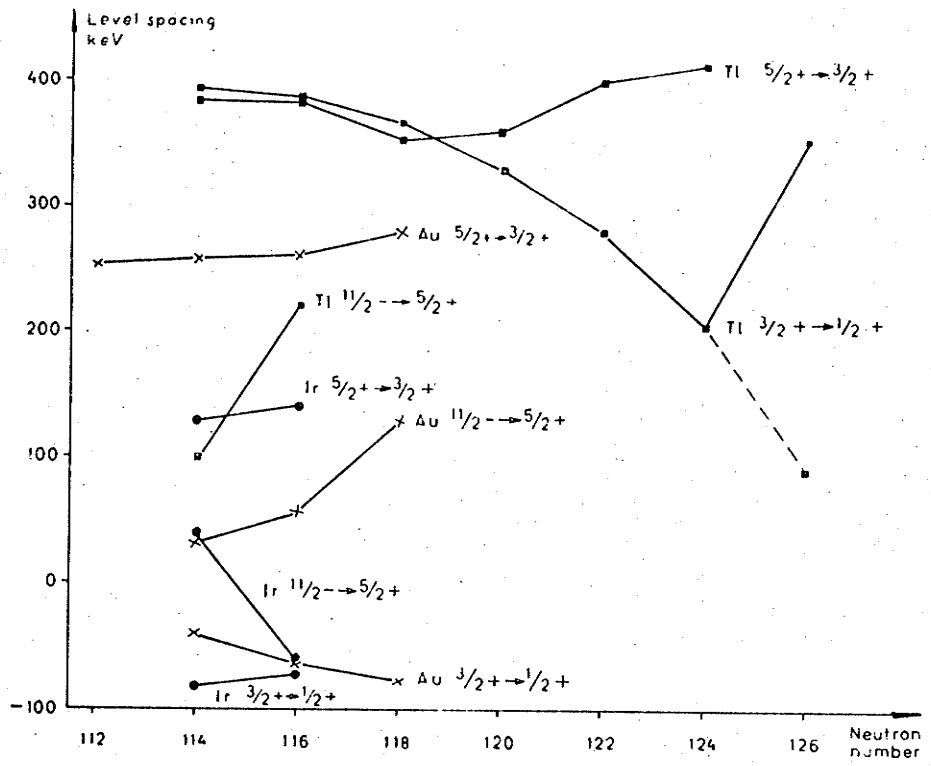

Level separations in odd mass isotopes of Tl, Au and Ir as functions of neutron number.

Fig. 5-4 Level spacings for the odd A thalium isotopes(top two curves) due to Bergstrom and Anderson(B-3,1957).

Fig. 5.4 (B-3, 1957) shows the level spacings for the odd A isotopes of thalium (top two curves) and it is seen that the 350 keV level in Tl^{207} is a definite break in the trend. This effect may be due to the closed neutron shell and may also explain why the other excited states in Tl^{207} are so weak.

The final alpha decay of Bi^{211} and level scheme of Tl^{207} is shown in Fig. 5.5.

5.6 Beta Decay of Bi^{211}

As was pointed out in section 4.2 very few of the Bi^{211} decays go via beta decay to Po^{211}. Table 5-8 shows the actual percentages due to various workers.

Table 5-8

Worker	% of Bi^{211} beta decays
Rutherford	0.32
Walen et al	0.29
Way et al	0.28
Present work	0.287 ± 0.005

Figure 5 - 6

The alpha-beta branching of Bi^{211}.

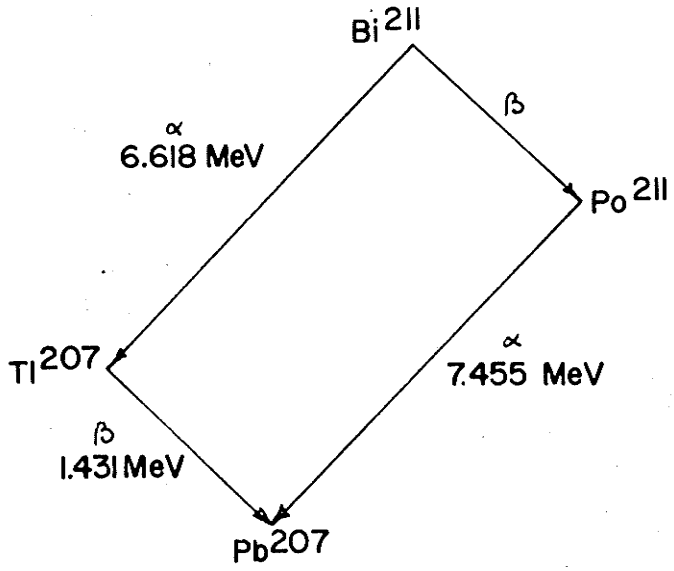
Bi 211
α
6.618 MeV
β
Po 211
Tl 207
α
7.455 MeV
β
1.431 MeV
Pb 207

This beta decay was too weak to be seen in the continuum of the active deposit and the above percentage was determined by comparing the intensities of the Bi^{211} and Po^{211} alpha particles (see section 4.2). The energy of the beta decay of Bi^{211} can be calculated by deduction. Consider Fig. 5-6 in which are noted the transition energy between ground states as determined in the present work. It is seen that the energy between the ground states of Po^{211} and Bi^{211} (energy of the beta decay) is 7.455 MeV - (6.618 + 1.431 MeV) = 0.594 ± 0.008 MeV.

5.7 Beta Decay of Tl^{207}

Lecoin (L-4, 1938) using a Knonpinski-Uhlenbeck plot quoted two endpoints for the beta decay of Tl^{207} at 1.50 and 1.85 MeV. Sargent (S-4, 1939) performed the first accurate measurement of the endpoint using absorbers and put the value at 1.44 MeV. Evans (E-1, 1950) using a separated source whose strength was 1.6 microcuries put the endpoint at 1.442 ± 0.008 MeV. Vandenbosch et al (V-1, 1963) give 1400 ± 20 keV as the endpoint of the composite beta spectrum of the active deposit. The present work gives an endpoint of 1.431 ± 0.008 MeV.

The beta decay from the ground level of $Tl^{207}(1/2^+)$ to the ground level of $Pb^{207}(1/2^-)$ having a parity change and no spin change is first forbidden but displays the statistical shape and a low $\log_{10}$ ft value.

Choong and Surugue (C-2, 1938) searched for internal conversion lines in the decay of Tl^{207} and were unable to find any. Surugue (S-6, 1941) found an 870 keV gamma ray with intensity of 1 in 200 Tl^{207} disintegrations. Christensen et al (C-17, 1963) quote a 900 keV gamma ray but as noted in section 4.8 the energy determination of Surugue may have been in error.

Table 5-9 shows the % feeds and $\log_{10}$ ft values for the beta decay of Tl^{207} as determined from a knowledge of the gamma rays involved.

Table 5-9

Beta energy (MeV)	percentage feed		$\log_{10}$ ft	
	Surugue	Present Work	King and Peaslee	Present Work
1.431	99.5	99.30	5.2	5.2
0.531	0.5	0.70	---	5.5

The tables of Feenberg and Trigg (F-10, 1956) were used in the calculation of the $\log_{10}$ ft values.

5.8 Alpha Decay of Po^{211}

Po^{211} alpha decay involves crossing the closed neutron shell at N = 126.

The alpha groups found in past work de-exciting the ground state of Po^{211} (the excited state at 1.3 MeV cannot be fed in the actinium series - see Fig. 4-1) are shown in table 5-10. It will be noted that there are four groups which when viewed through the actinium series are very weak compared to the Bi^{211} alpha groups (6.280 and 6.618 MeV). Since Po^{211} is produced in the actinium series by an 0.287% beta feed from Bi^{211} and since the 6.90 and 6.56 MeV alpha groups are 1/2% of the decay of Po^{211} (see table 5-10) these two alpha groups are very weak compared to the Bi^{211} alpha groups. Thus since the 6.56 and 6.90 MeV alpha groups are so weak and are so close in energy to the Bi^{211} alpha groups they are not seen in the ordinary alpha single spectrum (see Fig. 4-2). One of these two weak groups in Po^{211} were revealed by alpha-gamma coincidences in the present work. The 6.90 MeV alpha group feeds the 560 keV level in Pb^{207} and the 6.56 MeV alpha group feeds the 890 keV level in Pb^{207} (see Fig. 4-1). When alpha particles were displayed on the multi-channel analyser (see Fig. 4-15) only the 6.90 MeV alpha

group was revealed. However because of the large number of 6.618 MeV chance coincidences in Fig. 4-15 a peak at 6.56 MeV comparable to that of 6.90 MeV would be inside the statistical accuracy and thus would not be seen. When gamma rays are displayed on the multichannel analyser (see Fig. 4-13) one might well expect to see the 890 keV gamma ray since the 560 keV gamma ray is so easily visible. No peak is seen at 890 keV and the upper limit of 0.07% shown on table 5-10 was determined from Fig. 4-13.

Table 5-10

Alpha energy (MeV)	Jentschke et al	Walen et al	Neuman and Perlman	Present Work	Zeh and Mang (theoretical)
7.455	99.0%	99%	99.88%	99.60±0.10 %	99.72%
6.90	0.50%	0.7%	0.57%	0.40±0.10%	0.80%
6.56	0.53%	-	0.48%	*<0.07±0.02%	0.48%
6.34	-	-	0.07%	*<0.07±0.02%	-

* not observed in the present work, upper limits of intensity quoted.

Because the present work disagrees with that of Jentschke et al and Neuman and Perlman it seems worthwhile to comment on their work. It should be noted that both Jentschke et al and Newman and Perlman used At^{211} sources

which decay to Po^{211} by electron capture and hence their spectra were not complicated by the presence of the intense Bi^{211} alpha groups (6.618 and 6.280 MeV) as was the present work. Jentschke et al published only a letter which contained no alpha particle spectra. However the 6.58 MeV alpha group they report is very weak and they are uncertain of its origin. Since no actual spectra were shown it is impossible to advance any comment on the work itself. Neuman and Perlman saw a 6.59 MeV alpha group of very low intensity but their detection of the 6.90 MeV alpha group rests on one experimental point which is less than completely satisfactory. Neuman and Perlman also report a 6.34 MeV alpha group whose intensity is consistent with the upper limit determined in the present work (see table 5-10). Having regard to the meagreness of the existing information it seems important to keep an open mind on the intensity of any 6.59 MeV alpha feed. The present result is advanced as a new determination of this intensity and should be considered with the earlier data.

Zeh and Mang (Z-1, 1962) use shell model wave functions in their calculations and it is interesting to note how close they come to the experimental values.

Long range alpha particles have been reported in Po^{211} by several workers. Curie and Lub (C-3, 1933) reported alpha particles in the range 9.1 - 9.7 MeV in abundance 3×10^{-7} per Bi^{211} disintegration (i.e., $10^{-5}/Po^{211}$ disintegration). Avignon (A-5, 1950) and Ader (A-4, 1955) also

reported alpha particles in this range for Po^{211}. The present work puts an upper limit of $10^{-5}/Po^{211}$ disintegration on any alpha particles in this region which is not in disagreement with Curie and Lub but does not confirm their findings. However it should be noted that such alpha particles could only arise due to the decay of an excited state of Po^{211} between 1.6 and 2.2 MeV. No beta particle from the Bi^{211} ground state could feed either of these levels and the excited state in Bi^{211} required to feed these levels would be above 1 MeV. This high energy level in Bi^{211} would have to be an isomeric state to allow beta decay to compete reasonably well with the gamma decay and thus would be expected to have a high spin. The spin of the 1100 keV level in Bi^{211} has been determined as 7/2 which is not consistent with an isomeric level. Therefore the only possible explanation of these long range alpha particles would be an isomeric level in Bi^{211} higher than 1 MeV and de-exciting only by beta decay to an isomeric level in Po^{211}. However the only known exicted state in Po^{211} is an isomeric level but its energy (1.3 MeV) is not consistent with an alpha particle of 9.1 - 9.7 MeV. Thus it is here suggested that the long range alpha particles mentioned above are not due to the active deposit of actinium. An additional piece of evidence for this contention comes from Hanna (H-11, 1959) who comments that because of the very low beta to alpha branching ratio (0.287%)of Bi^{211}, long range alpha particles would not be expected in the decay of Po^{211}.

Chang (C-56, 1946,8) saw several alpha particles in Po^{214} (which is in the active deposit of the radium or uranium series). Their energies were in the range 3-5 MeV and their intensities were in the range 1 part in 10^4 to 2 parts in 10^5 compared to the main alpha groups. He believed the alpha particles had nuclear or atomic origin although there was no obvious explanation. He suggested two possible explanations:

1) vibrating nucleus

2) nucleus in a state of pre-fission

Similar alpha particles were looked for in the active deposit of actinium (see section 4.2) and a limit of 1 part in 5×10^5 put on their possible existence. Therefore it can be concluded that if such alpha particles exist in the alpha decay of Po^{211} they are much weaker than those in Po^{214}.

These kind of peaks have been seen before in alpha spectra and are usually ascribed to backscattering in the source or adsorbed material on the source backing (F-11, 1929 and F-12, 1963).

The theoretical predictions for the alpha decay of Po^{211} (R-5, 1959, H-10, 1959) are contradictory in the same way as for Bi^{211} (see section 5.4). Thus no interpretation of the experimental results in terms of theoretical predictions is possible.

If one considers the two protons outside the Z = 82 closed shell to be paired there is left a $g_{9/2}$ neutron in Po^{211}. Also the spins of the levels (from shell model (P-2, 1952) in Pb^{207} are shown in Fig. 5-7 along with the decay information from the present work. It might therefore be expected that the alpha feed to the 560 keV level involving the assembly of $g_{9/2}$ and $f_{5/2}$ neutrons would be less hindered than the other feeds ($g_{9/2}$ with $p_{1/2}$ and $p_{3/2}$ neutrons) because of the better overlap of the wave functions. This suggestion is in agreement with the experimental result that the alpha feed to the 560 keV level (0.50%) was larger than the alpha feed to the 900 keV level (<0.07%).

Figure 5 - 7

The alpha decay scheme of Po^{211} and the levels in Pb^{207} resulting from the present work.

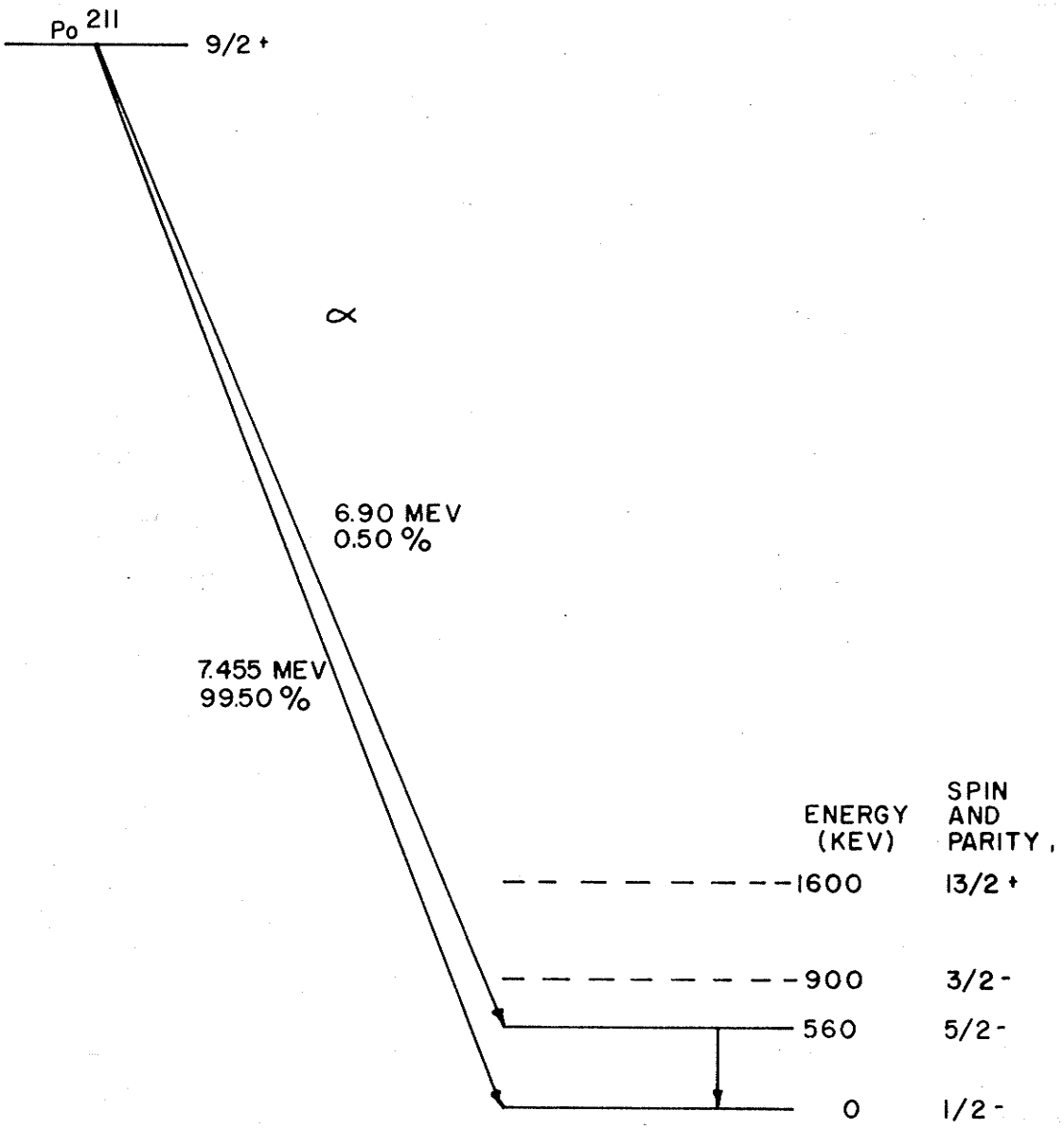
Po 211
9/2 +
α
6.90 MEV
0.50 %
7.455 MEV
99.50 %
ENERGY (KEV)
SPIN AND PARITY ,
1600
13/2 +
900
3/2 -
560
5/2 -
0
1/2 -

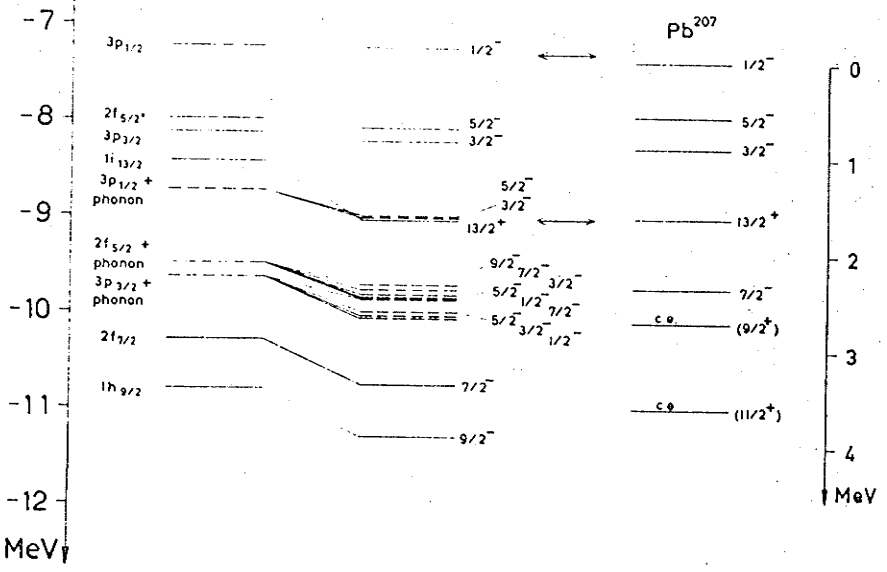

Theoretical unpertubed (to the left) and perturbed energies for neutron states, and experimental levels of the nuclei $Pb^{208} \pm$ one neutron. Dotted lines denote the lowest quadrupole vibrational states. Arrows indicate energies used for the choice of parameters. "c.e." means core-excited state.

Fig. 5-8 (from Bloomqvist and Wahlborn, B-2, 1960)

5.9 The Levels in Pb^{207}

The level scheme of Pb^{207} has been examined by experiments involving:

1) electron capture from Bi^{207} (Alburger and Sunyar, A-2, 1955; Neuman and Perlman, N-3, 1951; Grace and Prescott, G-13, 1951).

2) the alpha decay of Po^{211} (Spiess, S-10, 1954 and S-11, 1951; Walen et al, W-1, 1962; Jentschke et al, J-1, 1954).

3) (d,p) and (d,t) nuclear reactions using Pb^{206} and Pb^{208} targets (Harvey, H-6, 1953 and H-7, 1951).

4) neutron spectroscopy (Newson et al, N-8, 1961).

The levels indicated by these experiments along with the suggested shell model spins are shown in Fig. 5-8. The isomeric level (13/2) gives rise to a 1060 keV gamma ray whose internal conversion electron line is a standard in beta ray spectroscopy (A-3, 1953).

Pryce was the first to make theoretical calculations for Pb^{207} (P-2, 1952). He used the independent particle model and ignored non-central forces and assumed rigorous jj coupling. He disagreed with the level diagram shown in Fig. 5-8 only by including a level at 1110 keV. This level was in good agreement with a 6.34 MeV alpha particle reported in the alpha decay of Po^{211} (N-3, 1951 and S-10, 1954 and S-11, 1951). Pryce quotes a note from Prescott confirming

the presence of the 1110 keV level. Prescott (P-5, 1954) then reported from coincidence data that the 1060 keV gamma ray may actually be double, 6% of it being in prompt coincidence with electron capture electrons and in fact did not support the 1110 keV level. He suggested from his results that instead of an additional level at 1110 keV there was an additional one in the neighbourhood of the isomeric level at 1600 keV giving rise to the prompt 1060 keV gamma ray. However he does not seem to rule out a level in the neighbourhood of 1100 keV since he suggests the possibility of two gamma rays in the 500 keV region. Reid and McNeil (R-7, 1954) support such a level and suggest that its spin is 11/2. Prescott had assigned spin $f_{7/2}$ to this level but found this assignment 'embarassing'. He pointed out that according to the shell model the $(f_{5/2} - f_{7/2})$ doublet spacing should be three times that of the $(p_{3/2} - p_{1/2})$ doublet, whereas it would only be 1.2 for this if Prescott's suggestion were accepted. Further, analogy with other doublets suggests that the $f_{7/2}$ level should be located at about 2 to 2.5 MeV (H-6, 1953) (it has since been assigned to a level at 2.4 MeV). The support for Prescott's 7/2 assignment is seen in Fig. 5-9 (B-3, 1957) which suggests a 7/2 level between the 3/2 level (900 keV) and the 13/2 level (1600 keV). Montalbetti however (M-11, 1952) points out that any level around

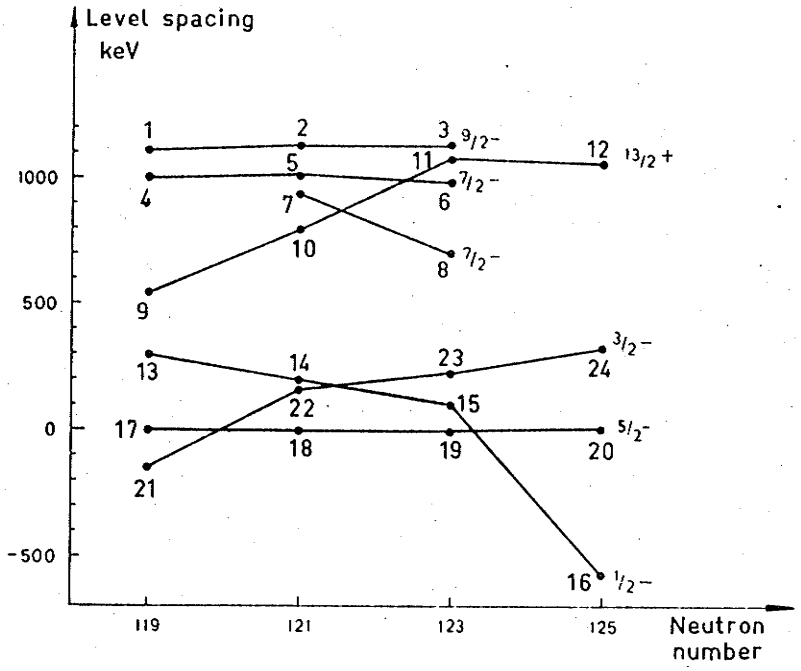

Energies of single-particle states 1/2 , 3/2 , 5/2 and 13/2 + and low-lying complex states 7/2 − and 9/2 − in Pb isotopes

Fig.5 -9 Level spacings for the odd A lead isotopes due to Bergstrom and Anderson(B-3,1957) (calculated by M.H.L. Pryce).

1.11 MeV with a spin 7/2 would by shell model decay preferentially to the 560 keV level (spin 5/2) by a probability exceeding 10^5 to 1 compared to the ground state transition.

It should be also noted that the 6.34 MeV alpha particle quoted by Neuman and Perlman could be from the 1.3 MeV level in Po^{211} (J-1, 1953) to the 2.4 MeV level in Pb^{207} (H-6, 1953). It should be noted that it is not energetically possible to excite the 1.3 MeV level in Po^{211} in the actinium series. Lazar and Klema (L-2, 1955) took Prescott's suggestion of two closely spaced levels and re-examined the Pb^{207} gamma ray spectrum. They found no evidence of close levels (i.e., prompt gamma rays) near the 1600 keV level. Gupta and Lawson (G-10, 1959) in examining the 1060 keV transition conclude that weak configuration mixing (which is very small near closed shells) is not capable of bringing the theoretical M4 lifetime (0.32 sec.) into agreement with the experimental lifetime (1.3 sec.). They also contend that this is not due to spin-orbit effects but suggest that it is due to meson currents. Hoff and Asaro (private communication to H-9, 1953) did not find any evidence for the 1110 keV level. Yavin and Schmidt (Y-1, 1955) say that no gamma ray exists in the region of 80 keV to either side of the 1060 keV keV gamma ray with intensity greater than 10% of the 1060 keV gamma ray and differing more than 10 keV from it in energy. Alburger (A-2,,1955)

searched carefully in the 1060 keV region for internal conversion electrons. He put an upper limit of 1.5% compared to the 1060 keV K line of any other transition unless it fell on one of the 1060 keV conversion lines. True (T-2, 1956) in a theoretical calculation supports the levels as shown in Fig. 5-9 and does not include a level at 1110 keV. True's calculation is supported by one due to Sliv and Volchok(S-9,1959) in which they used experimental information in the Pb^{208} region to determine an average nuclear potential. Blomqvist and Wahlborn (B-2,1960) in yet another theoretical calculation,(see Fig. 5-8) show no level at 1110 keV. The spin of the ground level, the 560 keV level and the 1600 keV level have been confirmed by gamma-gamma angular correlation as the shell model spins(see Fig. 5-8; M-6,1953).

One gamma ray of 900 keV exists in the decay of Tl^{207} in the present work, i.e., is due to excited levels in Pb^{207}. Christensen et al (C-17,1963) report the gamma ray from a separated source of Tl^{207} to be 900±10 keV. They quote a $\log_{10}$ ft value for the ground state beta transition of 5.07 (the present value is 5.2). The suggested decay scheme of Tl^{207} and corresponding levels in Pb^{207} due to the present work are shown in Fig. 5-10 (an upper limit of 0.02% was

put on the possibility of the 560 keV level being excited by the beta decay of Tl^{207}). Sargent(S--4,1939) found that the gamma rays due to the decay of Tl^{207} are 1/4 as intense as those due to the decay of Pb^{211}. Surugue (S-6,1941) finds a 0.5% feed to the 900 keV level(he calls it the 870 keV level) which agrees reasonably well with the present work.

The final decay and level scheme for the isotopes in the active deposit of actinium are shown in Fig. 5-11.

Figure 5 - 10

The beta decay scheme of Tl^{207} and the levels in Pb^{207} resulting from the present work.

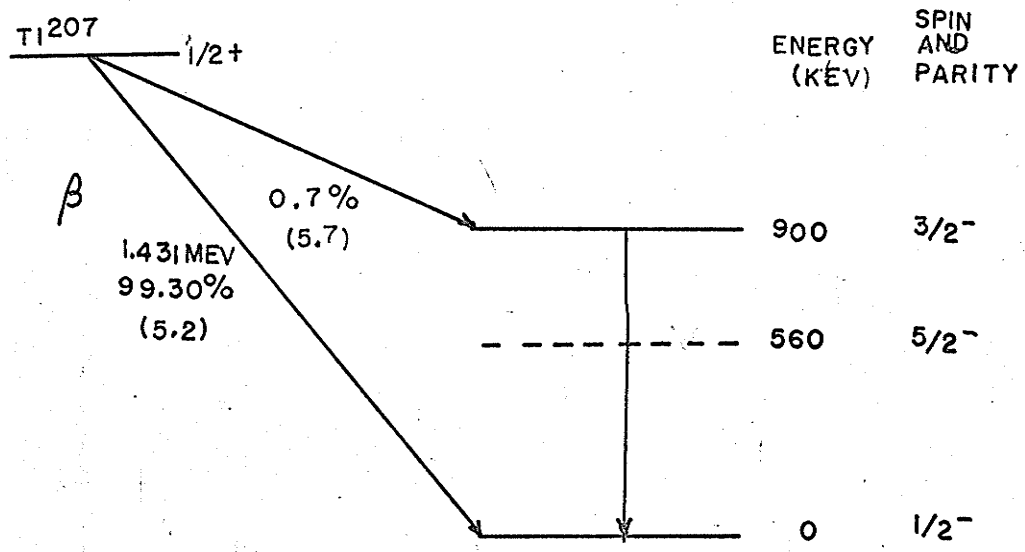
Tl207
1/2+
ENERGY (KEV)
SPIN AND PARITY
β
0.7%
(5.7)
1.431 MEV
99.30%
(5.2)
900
3/2⁻
560
5/2⁻
0
1/2⁻

Figure 5 - 11

Decay and level scheme for the isotopes in the active deposit of actinium resulting from the present work.

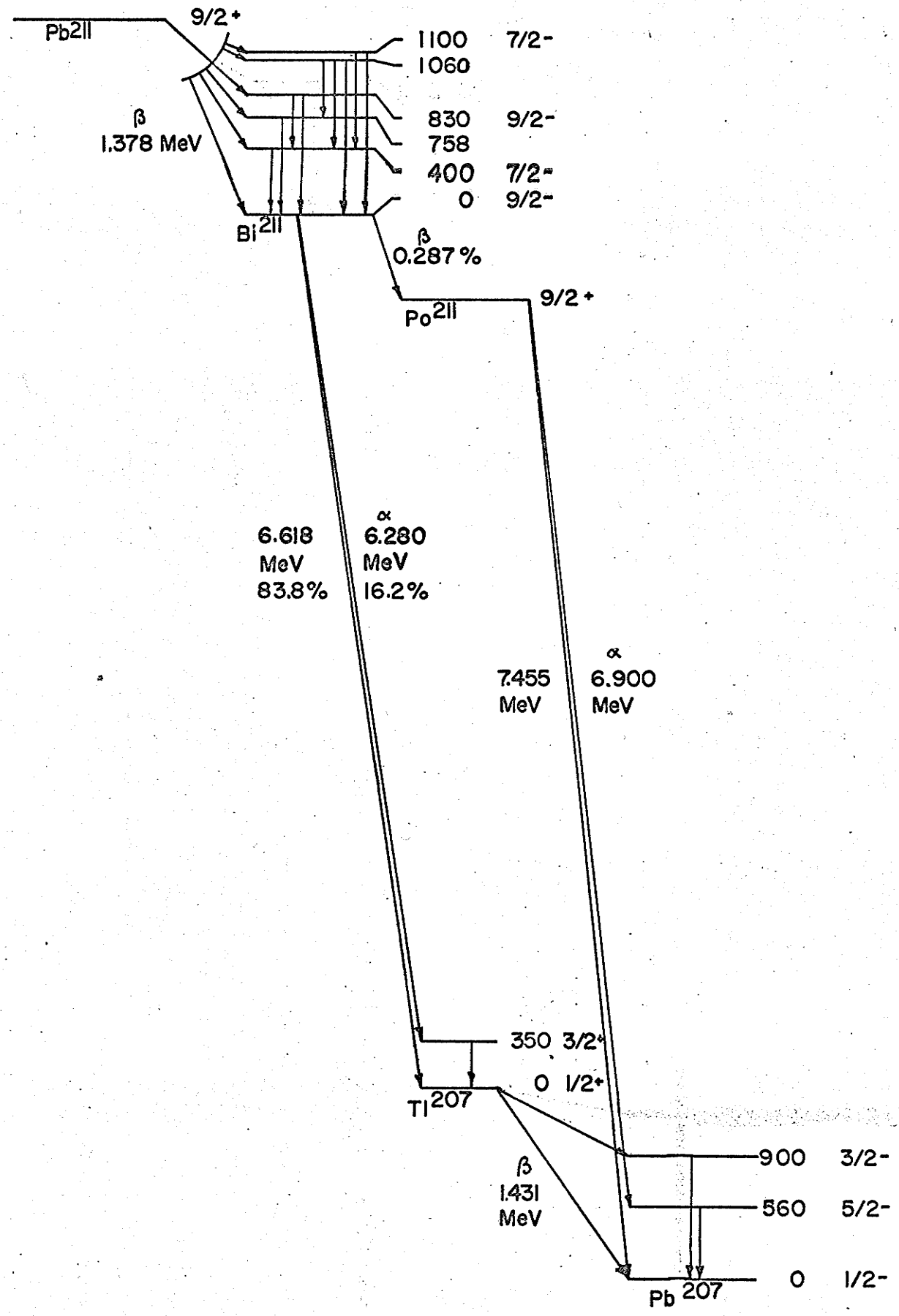
Pb211
9/2+
1100 7/2-
1060
830 9/2-
758
400 7/2-
0 9/2-
β
1.378 MeV
Bi211
β
0.287%
Po211
9/2+
6.618
MeV
83.8%
α
6.280
MeV
16.2%
7.455
MeV
α
6.900
MeV
350 3/2+
0 1/2+
Tl207
β
1.431
MeV
900 3/2-
560 5/2-
0 1/2-
Pb 207

REFERENCES

A-1 D. E. Alburger and M. H. L. Pryce, Phy. Rev. 95. 1482, (1954).

A-2 D. E. Alburger and A. W. Sunyar, Phys. Rev. 99, 695, (1955).

A-3 D. E. Alburger, Phys. Rev. 92, 1257, (1953).

A-4 M. Ader, Compt. Rend. 240, 2138, (1955).

A-5 P. Avignon, J. phys. et radium 11, 521, (1950).

B-2 J. Blomquist and S. Wahlborn, Arkiv for Fysik 16, 545, (1960).

B-3 I. Bergstrom and G. Anderson, Arkiv for Fysik 12, 415, (1957).

B-4 Miss Brooks Phil. Mag. Sept. (1904).

B-5 K. Bleuler and C. Terreaux,Helv. Phys. Acta 30, 183, (1957).

B-6 H. Bethe, Rev. Mod. Phys. 9, 161, (1937).

B-7 G. H. Briggs, Rev. Mod. Phys. 26, 1, (1959).

B-8 L. C. Biedenharn and M. E. Rose, Rev. Mod. Phys. 25, 729, (1953).

B-9 R. E. Bell, R. L. Graham and H. E. Petch, Can. J. Phys. 30, 35 (1952).

B-10 S. Benedetti, J. de Phys. 10, 294, (1939).

C-1 J. C. Carter, W. T. Pinkston and W. W. True, Phys. Rev. 120, 504 , (1960).

C-2 S. P. Choong and J. Surugue , J. De Physique et le Radium 9, 437, (1938).

C-3 P. Curie and W. Lub, J. Phys. et Rad. 4, 513, (1933).

C-4 E. C. Campbell and F. Nelson, J. Inorg. Nuc. Chem. 3, 233, (1956).

C-5 W. Y. Chang, Phys. Rev. 69, 60, (1946).

C-6 W. Y. Chang, Phys. Rev. 70, 632, (1948).

C-7 B. L. Cohen, P. Mukherjee, R. H. Fulmer and A. L. McCarthy, Phys. Rev. 127, 1675, (1962).

C-8 S. Cupermen, Nuc. Phys. 28, 84, (1961).

C-9 S. Cuperman, Nuc. Pnys. 30, 568, (1962).

C-10 P. Curie and S. Rosenblum, Compt. Rend. 193, 33, (1931).

C-11 P. Curie and S. Savel, J. Phys. Rad. 4, 457, (1933).

C-12 C. Campbell and M. Goodrich, Phys. Rev. 78, 640, (1950).

C-14 S. Cuperman, Nuc. Phys. 28, 84, (1961).

C-15 R. D. Connor, Thesis, University of Edinburgh, (1949).

C-16 R. D. Connor and M. K. Husain, Nuc. Instr. and Methods 6, 337, (1960).

C-17 P. R. Christensen, B. B. Nielsen and H. Nordby, Phys. Letts. 4, 318, (1963).

D-1 A. Debierne, C. R. 129, 593, (1899).
C. R. 130, 306, (1900).

D-2 A. Debierne, C. R. 139, 538, (1904).

D-3 A. Debierne, C. R. 136, 146, (1903).

D-4 A. J. Dempster, Proc. Am. Phil. Soc. 75, 755, (1935).

D-5 S. Devons and L. J. B. Goldfarb, Handbuch der Physik (Springer-Verlag, 1957), Vol. 42, Pg. 362.

D-6 S. Devons and L. J. B. Goldfarb, Handbuch der Physik (Springer-Verlag, 1957), Vol. 42, Pgs. 513-517.

E-1 H. D. Evans, Proc. Phys. Soc. 63A, 575, (1950).

E-2 R. Evans, ''The Atomic Nucleus'', McGraw-Hill, New York, 1958.

E-3 R. Evans, ''The Atomic Nucleus'', McGraw-Hill, New York, 1958, Pg. 208.

F-1 B. M. Foreman, Jr. and G. T. Seaborg, J. Inorg. Nucl. Chem. 7, 305, (1958).

F-2 J. Frilley, J. Phys. et Rad. 1, 34, (1940).

F-3 P. O. Froman, Mat Fys Skr Dan Vid Selsk 1, no. 3, (1957).

F-4 P. Falk-Vairant, J. Teillac and C. Victor, J. Phys. Rad. 13, 313, (1952).

F-5 P. Falk-Variant, Ann. Phys. 9, 524, (1954).

F-6 H. Frauenfelder, Beta and Gamma Ray Spectroscopy (North-Holland Publishing Company, 1955), Chapter 19.

F-7 P. Falk-Vairant, Ann. Phys. (Paris), 9, 524, (1954).

F-8 J. S.Fraser and R. B. Tomlinson, ''Transistor Circuits with Nanosecond Resolution'', an invited paper delivered at the Hamilton meeting of the Canadian Association of Physicists, June 6-9, 1962.

F-9 H. Frauenfelder, Beta and Gamma Ray Spectroscopy (North-Holland Publishing Company, 1955), Chapter 19, Pgs. 572-576.

F-10 E. Feenberg and G. Trigg, Rev. Mod. Phys. 4, 399, (1950).

F-11 N. Feather and R. R. Nimmo, Proc. Camb. Phil. Soc. 25, 198, (1929).

F-12 N. Feather, private communication.

G-1 F. Giesel, Ber. d. D.Chem. Ges., 3608, (1902).
342, (1903).

G-2 F. Giesel, Phys. Zeit. 5, 882, (1904).
Jahrbuch d. Radiocktivitat, 4, 345, (1904).

G-3 S. Glasstone, ''Source book on Atomic Energy'', D. Van Nostrand, Princeton, New Jersey, 1958, Pg. 132.

G-4 F. S. Goulding, UCRL 11302, (1964).

G-5 M. Giannini, D. Prosperi and S. Sciuti, Nuovo Cimento 25, 1227, (1962).

G-6 F. B. Gil and G. Y. Petit, J. Phys. Rad. 22, 680, (1961).

G-7 S. Gorodetzky, A. Knipper and R. Armbruster, Comp. Rend. 237, 245, (1953).

G-8 S. Gorodetzky, F. Beck, A. Knipper, R. Marquenouille, and R. Richert, Comp. Rend. 254, 2319, (1962).

G-9 V. N. Gunmon, JETP 14, 574, (1962).

G-10 K. K. Gupta and R. D. Lawson, Phys. Rev. 114, 326, (1959).

G-11 H. Graf, Comp. Rend. 197, 238, (1933).

G-12 M. Goldhaber and A. W. Sunyar, Phys. Rev. 83, 906, (1951).

G-13 M. A. Grace and J. R. Prescott, Phys. Rev. 84, 1059, (1951).

G-14 M. Goldhaber, Phys. Rev. 89, 1146, (1953).

H-1 O. Haxel, J. H. D. Jensen and H. E. Suess, Phys. Rev. 75, 1766, (1949).

O. Haxel, J. H. D. Jensen and H. E. Suess, Z. Physik 128, 295, (1950).

H-2 J.M. Hollander, W.G. Smith and J.W. Mihelich, Phys. Rev. 102, 740, (1956).

H-3 O. Hahn and L. Meitner, Zeit. Physik 9, 649, (1908).

O. Hahn, Chem. Ber. 39, 1605, (1904).

F. Giesel, Chem. Ber. 38, 1775, (1905).

H-4 O. Hahn and L. Meitner, Zeit. Physik 9, 697, (1908).

H-5 G. C. Hanna, ''Experimental Nuclear Physics'', Vol. III, Wiley, New York, (1959), Pg. 236.

H-6 J. A. Harvey, Can. J. Phys. 31, 278, (1953).

H-7 J. A. Harvey, Phys. Rev. 81, 353, (1951).

H-8 J. W. Horton, Phys. Rev. 101, 717, (1956).

H-9 J. M. Hollander, I. Perlman and G. T. Seaborg, Rev. Mod. Phys. 25, 469, (1953).

H-10 G. C. Hanna, ''Experimental Nuclear Physics'', Vol. III, Wiley, New York, (1959), Pgs. 129-136.

H-11 G. C. Hanna, ''Experimental Nuclear Physics'', Vol. III, Wiley, New York, (1959), Pg. 139.

J-1 W. Jentschke, A. C. Juveland and G. H. Kinsey, Phys. Rev. 96, 231, (1954).

K-3 L. S. Kisslinger and R. A. Sorensen, Mat. Fys. Medd. Dan Vid Selsk 32, #9, (1960).
L. S. Kisslinger and R. A. Sorensen, Carnegie Institute of Technology, Pittsburgh, Contract NONR-760(15), NRO 12-202, UC-34, Apr. 16, 1963.

K-4 M. J. Kearsly, Nuc. Phys. 4, 157, (1957).

K-5 F. Konopasek and R. D. Connor, Nuc. Instr. and Meth. 24, 66, (1963).

K-6 P. F. A. Klinkenberg, Rev. Mod. Phys. 24, 63, (1952).

K-7 R. W. King and D. C. Peaslee, Phys. Rev. 94, 1284, (1954).

K-8 E. Kara-Michailova, Proc. Camb. Phil. Soc. 34, 429, (1938).

L-1 K. T. Li, Proc. Roy. Soc. 158A, 571, (1937).

L-2 N. H. Lazar and E. D. Klema, Phys. Rev. 98, 710, (1955).

L-3 M. Lecoin, Compt. Rend. 202, 1057, (1936).

L-4 M. Lecoin, J. Phys. Rad. 9, 81, (1938).

M-1 M. G. Mayer, Phys. Rev. 75, 1969, (1949).
M. G. Mayer, Phys. Rev. 78, 16, (1950).

M-2 H. J. Mang, Phys. Rev. 119, 1069, (1960).

M-3 H. J. Mang, Z. Phys. 148, 572, (1957).

M-4 H. J. Mang, UCRL 8931.

M-5 R. Manquenouille, Ann. Phys. (Paris) 6, 1121, (1961).

M-6 F. K. McGowan and E. C. Cambell, Phys. Rev. 92, 523, (1953).

M-7 F. K. McGowan and E. C. Cambell, Phys. Rev. 92, 524, (1953).

M-8 J. W.Michelich,A. W. Schandt and E. Segre, Phys. Rev. 95, 1508, (1954).

M-9 P. Mukherjee and B. L. Cohen, Phys. Rev. 127, 1284, (1962).

M-10 B. Mottelson and S. G. Nilsson, Phys. Rev. 99, 1615, (1955).

M-11 R. Montalbetti, Can. J. Phys. 30, 660, (1952).

M-12 E. Marsden and P. B. Perkins, Phil. Mag. 27, 690, (1914).

M-13 W. E. Mott and R. B. Sutton, Handbuch der Physik, Vol. XLV, (Springer-Verlag), Pgs. 124-128, 1958.

M-14 B. R. Mottelson and S. G. Nilsson, Kgl. Danske Videnskab. Selskab. Mat. Fys. Medd. 1,#8, (1959).

M-15 J. E. Mack, Rev. Mod. Phys. 22, 64, (1950).

M-16 R. Mead, private communication (1964).

N-1 Nuclear Enterprises, 550 Berry St., Winnipeg, Manitoba.

N-2 O. Nathan, Nuc. Phys. 30, 332, (1962).

N-3 H. M. Neumann and I. Perlman, Phys. Rev. 81, 958, (1951).

N-4 R. V. Nussbaum, Rev. Mod. Phys. 28, 423, (1956).

N-5 S. G. Nilsson, Kgl. Danske Vid Selskr. Mat Fys. Medd 29,#16, (1955).

N-6 NBS, 583 (X-Ray Attenuation Coefficients).

N-7 NBS, Applied Math series 13, (1952).

N-8 H. W. Newson, J. H. Gibbons, H. Marshak, E. G. Bilpuch, R. H. Rohrer and P. Capp, Ann. Phys. (USA) 14, 346, (1961).

P-1 M. A. Preston, ''The Physics of the Nucleus'', Addison-Wesley, Reading, Mass. 1962, Pg. 69.

P-2 M. H. L. Pryce, Proc. Phys. Soc. (Lon.) A65, 773, (1952).

P-3 R. C. Pilger, UCRL 3877, (1957).

P-4 I. Perlman and J. O. Rasmussen, UCRL 3424, (1956).

P-5 J. R. Prescott, Proc. Phys. Soc. 67A, 540, (1954).

P-6 M. H. L. Pryce, Proc. Phys. Soc. 63A, 692, (1950).

P-7 I. Perlman, Phys. Rev. 75, 1096, (1949).

P-8 M. A. Preston, ''The Physics of the Nucleus'', Addison-Wesley, Reading, Mass. 1962, Chp. 10, Pgs. 269-270.

R-1 E. Rutherford, J. Chadwick and C. D. Ellis, Cambridge University Press, 1913.

R-2 E. Rutherford, ''Radio-Activity'', Cambridge at the University Press, 1904, page 20.

R-3 E. Rutherford, J. Chadwick and C. D. Ellis, Cambridge University Press, 1913.

R-4 E. Rutherford, ''Radioactive Substances and their Radiations'', Cambridge University Press, London, (1913).

R-5 J. O. Rasmussen, Phys. Rev. 115, 1675, (1959).

R-6 M. G. Redlich, Phys. Rev. 127, 555, (1962).

R-7 J. M. Reid and K. G. McNeil, Phil. Mag. 45, 957, (1954).

R-8 S. Russ and W. Makower, Proc. Roy. Soc. 82A, 205, (1909).

R-9 E. Rutherford and C. E. Wynn-Williams, Proc. Roy. Soc. 133A, 351, (1931).

R-10 E. Rutherford and H. Richardson, Phil Mag. 26, 937, (1913).

R-11 M. E. Rose, Phys. Rev. 91, 610, (1953).

R-12 M. Rotenberg, R. Bivins, N. Metropolis and S. K. Wooten, Sr., ''The 3j and 6j Symbols'', (The Technology Press, M.I.T., 1959).

R-13 R. A. Ricci, Physica 23, 693, (1957).

R-14 K. I. Roulston, private communication.

R-15 M. E. Rose, C. L. Perry and N. M. Dismake, ORNL-1459, (1953).

R-16 S. Rosenblum, M. Guillot and M. Perry, Compt. Rend. 202, 1274, (1934).

R-17 M. E. Rose, ''Internal Conversion Coefficient'', (North-Holland 1958).

R-18 E. Rutherford, ''Radio-Activity'', Cambridge at the University Press, 1904, page 557.

R-19 A. Rytz, Helv. Phys. Acta 34, 240, (1961).

S-1 L. J. Schiff, ''Quantum Mechanics'', McGraw-Hill, New York, 1949, Section 22.

S-2 F. Stephens, J.P. Hummel, F. Asaro and I. Perlman, Phys. Rev. 98, 261, (1955).

S-3 B. W. Sargent, LP-16, Chalk River, 1947.

S-4 B. W. Sargent, Can. J. Research 17, 82, (1939).

S-5 J. Surugue, J. Phys. Rad. 32, 71, (1942).

S-6 J. Surugue, Compt. Rend. 212, 337, (1941).

S-7 H. Slatis and K. Siegbahn, Ark. f. Fysik 1, #17, 399, (1949).

S-8 B. W. Sargent, Can. J. Phys. 31, 235, (1953).

S-9 L. A. Sliv and B. A. Volchuk, JETP 36, 539, (1959).

S-10 F. N. Spies, Phys. Rev. 94, 1292, (1954).

S-11 F. N. Spies, UCRL-1494, (1951).

S-12 P. H. Stelson, W. G. Smith, and F. K. McGowan, Phys. Rev. 116, 167, (1959).

S-13 J. Surugue, J. Phys. Rad. 7, 145, (1946).

S-14 J. Surugue, Compt. Rend. 212, 337, (1941).

S-15 B. W. Sargent, Proc. Camb. Phil. Soc. 25, 514, (1929).

S-16 B. W. Sargent, Proc. Camb. Phil. Soc. 29, 156, (1933).

S-17 A. Sanielevici, Compt. Rend. 202, 1055, (1936).

S-18 J. Surugue, Compt. Rend. 202, 410, (1939).

S-19 J. Surugue, J. Phys. Rad. 7, 337, (1936).

S-20 J. Surugue, Ann. Phys. (Paris), 8, 484, (1937).

S-21 D. Strominger, J. M. Hollander and G. T. Seaborg, UCRL 1928, (1958), 2nd edition.

S-22 S. Singer, Thesis, University of Illinois, (1957).

S-23 J. Seed and A. P. French, Phys. Rev. 88, 1007, (1952).

S-24 L. A. Sliv and I. M. Band, Report 57ICCK1, University of Illinois, 1958.

S-25 B. W. Sargent, Proc. Roy. Soc. (Lon.) A139, 659, (1933).

S-26 R. M. Steffen, Advances in Physics 4, 293, (1955).

S-27 S. O. Schriber and B. G. Hogg, Nuc. Phys. 48, 647, (1963).

S-28 S. O. Schriber and B. G. Hogg, Nuc. Instr. and Meth. 26, 141, (1964).

S-29 K. Siegbahn, ''Beta and Gamma Ray Spectroscopy'', (North-Holland, 1958), Pg. 918.

T-1 W. W. True and K. W. Ford, Phys. Rev. 109, 1675, (1958).

T-2 W. W. True, Phys. Rev. 101, 1342, (1956).

T-3 W. W. True, Bull. Am. Phys. Soc. 2, 228, (1957).

T-4 H. A. Tolheok and P. J. Brussard, Phys. Rev. 109, 1675, (1958).

V-1 S. E. Vandenbosch, C.V.K. Baba, P. R. Christensen, O. B. Nielsen and H. Nordby, Nuc. Phys. 41, 482, (1963).

W-1 R. J. Walen , V. Nedovessov and G. Bastin-Scoffier, Nuc. Phys. 35, 232, (1962).

W-2 G. Walter and A. Coche, J. Phys. Rad. 21, 477, (1960).

W-3 G. H. Winslow and O. Simpson, ANL 4841, Pt. I. 1952.
ANL 4901, Pt. IIa. 1952.
ANL 4910, Pt. IIb. 1953.
ANL 5277, Pt. III. 1954.
ANL 5381, Pt. IV. 1955.

W-4 A. H. Wapstra, Arkiv for Fysik 7, 279, (1954).

W-5 H. A. Weidenmuller, Rev. Mod. Phys. 33, 574, (1961).

W-6 K. Way et al., Nuclear Data Sheets.

Y-1 A. I. Yavin and F. H. Schmidt, Phys. Rev. 100, 171, (1955).

Z-1 H. D. Zeh and H. J. Mang, Nuc. Phys. 29, 529, (1962).

APPENDIX I

a) Consider the following decay scheme (S-1)

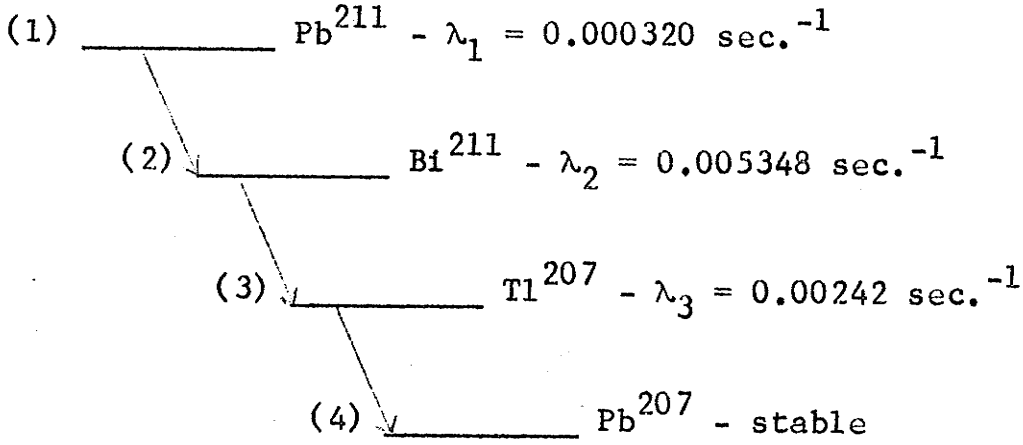

where isotope (1) has the longest half life and isotope (4) is stable.

The equations governing the decay are (R-1)

$$dN_1/dt = -\lambda_1 N_1 \qquad \text{I-1}$$

$$dN_2/dt = \lambda_1 N_1 - \lambda_2 N_2 \qquad \text{I-2}$$

$$dN_3/dt = \lambda_2 N_2 - \lambda_3 N_3 \qquad \text{I-3}$$

where Ni and λi are the populations and decay constants of isotope i where i = 1, 2, 3.

The solution to eq. I-1 is

$$N_1 = N_{10}\, e^{-\lambda_1 t} \qquad \text{I-4}$$

where N_{10} is the number of atoms of isotope 1 initially.

Substituting eq. I-4 into eq. I-2

$$dN_2/dt = \lambda_1 N_{10} e^{-\lambda_1 t} - \lambda_2 N_2$$

The solution of this equation is of the form

$$N_2 = N_{10}(a\, e^{-\lambda_1 t} + b\, e^{-\lambda_2 t})$$

By substitution it is found that

$$a = \lambda_1/(\lambda_2-\lambda_1)$$

and since $N_2 = 0$ when $t = 0$, $b = -\lambda_1/(\lambda_2-\lambda_1)$

Thus

$$N_2 = \frac{N_{10}\,\lambda_1}{(\lambda_2-\lambda_1)}\,(e^{-\lambda_1 t} - e^{-\lambda_2 t}) \qquad \text{I-5}$$

Substituting this value of N_2 in eq. I-3, it can readily be shown that

$$N_3 = N_{10}(\alpha\, e^{-\lambda_1 t} + \beta\, e^{-\lambda_2 t} + \gamma\, e^{-\lambda_3 t}) \qquad \text{I-6}$$

where

$$\alpha = \frac{\lambda_1\,\lambda_2}{(\lambda_2-\lambda_1)(\lambda_3-\lambda_1)}$$

$$\beta = \frac{\lambda_1 \lambda_2}{(\lambda_1 - \lambda_2)(\lambda_3 - \lambda_2)}$$

$$\gamma = \frac{\lambda_1 \lambda_2}{(\lambda_1 - \lambda_3)(\lambda_2 - \lambda_3)}$$

b) Suppose that n_o atoms of isotope 1 are deposited each second (from the emanation). After a time of exposure T, the number of particles N_{1T} of isotope 1 present is given by

$$N_{1T} = n_o \int_o^T e^{-\lambda_1 t}\, dt = \frac{n_o}{\lambda_1} (1 - e^{-\lambda_1 T})$$

At any time t, after removal of the source, the number of atoms N_1 is given by

$$N_1 = N_{1T}\, e^{-\lambda_1 t} = \frac{n_o}{\lambda_1} (1 - e^{-\lambda_1 T})\, e^{-\lambda_1 t} \qquad \text{I-7}$$

Consider the number of atoms $n_o dt$ of isotope 1 produced during the interval dt. At a later time t, the number of atoms dN_2 of isotope 2, which result from the change in N_1, is given by (see eq. I-5)

$$dN_2 = \frac{n_o \lambda_1}{\lambda_1 - \lambda_2} (e^{-\lambda_2 t} - e^{-\lambda_1 t}) dt = n_o f(t) dt \qquad \text{I-8}$$

Ater a time of exposure T, the number of atoms N_{2T} of isotope 2 present is given by

$$N_{2T} = n_o \int_o^T f(t)d\ t.$$

If the source is removed from the emanation after an exposure T, at any later time t the number of particles of isotope 2 is given by

$$N_2 = n_o \int_o^{t+T} f(t)\ dt - n_o \int_o^t f(t)\ dt$$

where the second term is present because isotope 1 is no longer being fed from the emanation after time T.

Since $\int_A^B + \int_B^C = \int_A^C$

then $\int_A^C - \int_A^B = \int_B^C$

and thus

$$N_2 = n_o \int_t^{t+T} f(t)dt$$

it should be noted that this expression is independent of the expression used for f(t).

Substituting the particular value of f(t) given in eq. I-8 and integrating it can readily be deduced that

$$N_2 = n_o \left[\frac{e^{-\lambda_1 t}(1-e^{-\lambda_1 T})}{\lambda_2 - \lambda_1} - \frac{\lambda_1}{\lambda_2} \frac{e^{-\lambda_2 t}(1-e^{-\lambda_2 T})}{\lambda_2 - \lambda_1} \right] \qquad \text{I-9}$$

Similarly N_3 may be found by using the value of f(t) from eq. I-6 in the equation

$$N_3 = n_o \int_t^{T+t} f(t)\, dt$$

$$= n_o \left[\alpha(1-e^{-\lambda_1 T})e^{-\lambda_1 t} + \beta(1-e^{-\lambda_2 T})\, e^{-\lambda_2 t} + \gamma(1-e^{-\lambda_3 T})e^{-\lambda_3 t}\right] \qquad \text{I-10}$$

where $$\alpha = \frac{\lambda_2}{(\lambda_2-\lambda_1)(\lambda_3-\lambda_1)}$$

$$\beta = \frac{\lambda_1}{(\lambda_1-\lambda_2)(\lambda_3-\lambda_2)}$$

$$= \frac{\lambda_1\, \lambda_2}{\lambda_3(\lambda_1-\lambda_3)(\lambda_2-\lambda_3)}$$

Using the values for λ from part a

$$N_1 = 3125\ (1 - e^{-\lambda_1 T})\ e^{-\lambda_1 t}$$

$$N_2 = 198.9\ (1-e^{-\lambda_1 T})\ e^{-\lambda_1 t} - 11.90(1-e^{-\lambda_2 T})e^{-\lambda_1 t}$$

$$N_3 = 508.5\ (1-e^{-\lambda_1 T})\ e^{-\lambda_1 t} + 21.7(1-e^{-\lambda_2 T})e^{-\lambda_2 t} - 115.5(1-e^{-\lambda_3 T})e^{-\lambda_3 t} \qquad \text{I-11}$$

c) If, as we have with Pb^{211} being isotope 1, the decay constant of isotope 1 is small compared to the others ($\lambda_1 < \lambda_2$ or λ_3), the term containing $e^{-\lambda_1 T}$ will be the dominant one.

Thus after a long time t equations I-5 and I-6 reduce to

$$N_2 = \frac{N_{10}\ \lambda_1}{\lambda_2 - \lambda_1}\ e^{-\lambda_1 t} \qquad \text{I-12}$$

$$N_3 = N_{10}\ \frac{\lambda_1\ \lambda_2}{(\lambda_2-\lambda_1)(\lambda_3-\lambda_1)}\ e^{-\lambda_1 t}$$

The rate of emission for levels 1, 2 and 3 are $\lambda_1 N_1$, $\lambda_2 N_2$ and $\lambda_3 N_3$ respectively. If $\lambda_1 N_1 = \lambda_2 N_2 = \lambda_3 N_3$ secular equilibrium exists. If the daughter is radiating at a constant rate which is faster than the parent, transient

equiibrium exists. It is important to examine how these two equilibrium conditions are related. The relationship can be investigated by the ratio of the rate of emission of the daughter to the rate of the parent, which by substitution can be shown to be

$$\frac{\lambda_2 N_2}{\lambda_1 N_1} = \frac{\lambda_2}{\lambda_2 - \lambda_1}$$

and

$$\frac{\lambda_3 N_3}{\lambda_1 N_1} = \frac{\lambda_2 \lambda_3}{(\lambda_2 - \lambda_1)(\lambda_3 - \lambda_1)}$$

The result of the above ratios has the form of the Bateman solutions (B-1) to the radioactive decay equations and are tabulated for all the radioactive series (K-1). Also useful are the tables of growth and decay for the naturally occuring radioactive series calculated by Kirby (K-2).

Using the values of λ from part c

$$\frac{N_2 \lambda_2}{N_1 \lambda_1} = 1.063 \qquad \text{I-13}$$

$$\frac{N_3 \lambda_3}{N_1 \lambda_1} = 1.226$$

That is Bi^{211} (isotope 2)is emitting alpha particles 6.370 % faster than Pb^{211} (isotope 1) is emitting beta particles and Tl^{207} (isotope 3) is emitting beta particles 22.6% faster than Pb^{211} is emitting beta particles.

APPENDIX II

Some values of the F functions (for $L > 4$) were not listed in the literature and had to be calculated from tables of Clebsh-Gordan and Racah coefficients. However there are some differences in notation in the available literature. In the theoretical part of this paper (Sec. 5.8 and 5.9) the Clebsh-Gordan coefficient is written in the form $C(j_1 j_2 \nu ; M_1 M_2)$. This is exactly equivalent with another common notation $C(j_1 M_1 j_2 M_2; jM)$. For our case $M_1 = 1$, $N_2 = -1$ and thus $M = 0$. Therefore our coefficients will look like

$$C(j_1 j_2 \nu \; ; \; 1\text{-}1) = C(j_1 1 j_2 \text{-}1; \; j0)$$

$$= (-1)^{j_2 - j_1 - M} (2j+1)^{1/2} \begin{pmatrix} j_1 & j_2 & j \\ M_1 & M_2 & -M \end{pmatrix}$$

where $\begin{pmatrix} j_1 & j_2 & j \\ M_1 & M_2 & -M \end{pmatrix}$ is a 3-j Wigner symbol and is tabulated (R-12, 1959). The Racah coefficient $W(j_1 j_2 j_3 j; \; j_{12} j_{13})$ in our expressions is simply related to the 6-j coefficient by

$$W(j_1 j_2 j_3 j; \; j_{12} j_{13}) = (-1)^{j_1 + j_2 + j_3 + j} \begin{pmatrix} j_1 & j_2 & j_{12} \\ j & j_3 & j_{13} \end{pmatrix}$$

The following are tables of values for the functions F, G and b which were needed in this analysis and were not available in the literature.

$$F_2\ (5\ 9/2\ 3/2) = 0.300$$

$$F_2\ (6\ 9/2\ 3/2) = -0.591$$

F_ν(L 9/2 5/2)

ν \ L	5	6	7
2	0.259	-0.181	-0.781
4	-0.0554	-0.467	0.288

$$G_2\ (5\ 3\ 9/2\ 3/2) = 0.051$$

$$G_2\ (6\ 4\ 9/2\ 3/2) = 0.0345$$

G_2(LL' 9/2 5/2)

L' \ L	4	5	6	7
2	0.0472	--	0	-
3	-	-0.0384	-	0
4	-	-	-0.0263	-
5	-	-	-	0

$G_4(LL'\ 9/2\ 5/2)$

L'/L	4	5	6	7
2	-0.00445	-	-0.0458	
3	-	-0.0175	-	-0.0253
4	-	-	0	-
5	-	-	-	0.0184

$b_2(\lambda,\lambda')$

λ'/λ =	2	3	4	5
4	-1.04	-	-	-
5	-	-0.958	-	-
6	0.494	-	-0.896	-
7	-	0.422	-	-0.840

$b_4(\lambda,\lambda')$

λ'/λ =	2	3	4	5
4	-3.44	-	-	-
5	-	-1.565	-	-
6	0.742	-	-1.195	-
7	-	0.545	-	-1.02